UNIVERSITEIT VAN PRETORIA
UNIVERSITY OF PRETORIA
YUNIBESITHI YA PRETORIA

University of Pretoria

PREPARATION AND PROPERTIES CHARACTERIZATION OF POLYAMIDE/CLAY BIO-NANOCOMPOSITES

By

Afonso Daniel Macheca

Submitted in partial fulfilment of the requirements for the degree of

Doctor of Philosophy in Chemical Technology

in the

Faculty of Engineering, Built Environment and Information Technology

University of Pretoria

Pretoria

July 2016

DECLARATION

I, Afonso Daniel Macheca, the undersigned, declare that the thesis that I hereby submit for the degree Ph.D. in Chemical Technology at the University of Pretoria is my own work, and has not previously been submitted by me for a degree or examination at this or any other university.

Pretoria, July 2016

_____

Afonso Daniel Macheca

Preparation and Properties Characterization of Polyamide/Clay Bio-nanocomposites

Student: Afonso Daniel Macheca

Supervisor: Prof. Walter W. Focke

Department: Chemical Engineering

University: University of Pretoria

Degree: Ph.D. (Chemical Technology)

SYNOPSIS

A novel method for polyamide/clay bio-nanocomposites fabrication was developed in an attempt to facilitate "extensive delamination" of clay stacks in polyamide matrices. The method, the so-called "surfactant-free organo-modification approach" did not employ any surfactants for the matrix-clay compatibilisation. The idea was to exploit the use of dimer fatty acid polyamides with protonated amine end groups as clay surface modifiers of the clay previously dispersed in a liquid medium. The clays of choice in the study were the standard smectite clays commonly used to prepare polymer-clay nanocomposites and vermiculite. They were ultimately chosen on the basis of their ability to exfoliate into nano-thick sheets.

Dimer fatty acid polyamide/clay bio-nanocomposites containing either montmorillonite or vermiculite were successfully prepared using the "surfactant-free organo-modification approach". Bio-nanocomposites containing as much as 28 wt.% montmorillonite and 30 wt.% vermiculite were obtained. In both cases, the composites featured a mixed morphology containing some exfoliated clay sheets together with nano-sized clay tactoids. At these filler loadings, the melt viscosity, tensile strength and Young's modulus increased. Dynamic mechanical analysis showed that the glass transition temperature of the polymer increased by as much as 5 °C when 27.5 wt.% montmorillonite was added and 10 °C when 30 wt.% vermiculite was added. This indicates that the high interfacial surface area, presented by the clay platelets dispersed in the matrix, significantly impaired the polymer chain mobility.

A further goal of the research was to extend the application of organo-modified vermiculite to the semi-crystalline polyamide-11. In this particular case, organomodified- and unmodified vermiculite and commercial sepiolite (Pangel S9) were considered. The clays were melt-compounded into the polyamide-11 to form products that contained either no filler, i.e. neat polyamide-11 or 10 wt.% clay. The aspects that were addressed included the effect of vermiculite organomodification, the effect of the shape of the clays, the aspect ratio of the particles, and the degree of dispersion that was achieved on properties of the generated polyamide-11/bio-nanocomposites. The emphasis was given to the mechanical and flame retardant properties.

Polyamide-11/clay bio-nanocomposites were successfully prepared. Tensile properties results showed improvements in tensile strength and Young's modulus increased with the presence of the nano-fillers. Young's modulus of the bio-nanocomposites was almost the double of that of the neat polymer. Thermo-mechanical results also showed improvements in storage modulus with the addition of all particles, especially in the temperature range corresponding to the rubbery plateau (above the glass transition temperature). Cone calorimeter test results showed that the peak heat release rate and smoke production rate values of the polyamide-11/clays significantly decreased compared with those of neat polymer. This indicates that the addition of clays not only decreased the flammability of polyamide but also effectively reduced smoke production.

The key findings of the thesis are:

- The "surfactant-free organo-modification approach" offers an alternative to conventional clay modification routes based on cationic surfactants. It provides additives suitable for the improvement of the properties of amorphous polyamide matrices.
- The solution casting route allows the preparation of amorphous polyamide/clay nanocomposites with a very high clay content, i.e. approaching 30 wt.%.
- There are at least three stiffening mechanisms operating in amorphous polyamide/clay bio-nanocomposites. The reinforcing effect of the high stiffness inorganic flakes is the primary contributor. Together with the chain confinement effect, that expresses itself in an apparent increase in the glass transition temperature, this provided an adequate rationalisation of the stiffness variation below the glass transition temperature. However, an additional stiffening effect is indicated at temperatures above the glass

transition temperature. The mechanism may involve dynamic network formation based on fluctuating hydrogen bonding interactions between the matrix polymer chains and the filler particles.

- From an engineering viewpoint, the good mechanical and fire retardant properties obtained with the vermiculite samples are very encouraging considering the inexpensive nature of this filler.
- The organo-modification of vermiculite and sepiolite is not necessary for the preparation of polyamide-11/clay bio-nanocomposites with excellent mechanical and thermal properties.

Keywords: Polyamide bio-nanocomposites, solution intercalation, exfoliation, thermo-mechanical properties, fire retardancy

ACKNOWLEDGEMENTS

My sincere acknowledgements and gratitude go to the following for making this thesis a success:

- Prof. Walter W Focke, my supervisor for his rigorous approach to science he tried to teach me, for the many discussions we had and for his never-ending patience in correcting reports, papers and, of course, this thesis.
- Gnanasekaran Dhorali, who accompanied me along the first steps of the present work, is strongly acknowledged. I really appreciated his collaboration and assistance during this period of time, thank you very much.
- My tutor at University Eduardo Mondlane, Prof. António José Cumbane for his support and encouragement to continue with my studies.
- Ollie Del Fabbro and Rainer Ohland-Schumacher are acknowledged for their technical help in assisting with the operation of equipment, maintenance, extensive discussions and practical advice.
- Isbe van der Westhuizen for her assistance in operating thermal characterisation equipment.
- Suzette Seymore for her efficient administrative assistance particularly for the purchase of consumables.
- Past and present students of Institute of Applied Materials (IAM) an the University of Pretoria, especially Herminio Muiambo, Shepherd Tichapondwa, Mthokozisi Sibanda, Shatish Ramjee, Washington Mhike, Lumbi Moyo, Pedro Massinga Jr, Dan Molefe, Homa Izady, Refilwe Mphahlele, for the very good work environment they created. The will of helping each other and sharing their knowledge makes IAM a very nice place to work.
- Our Algerian collaborators and friends at Laboratoire des Matériaux Polymères Avancés, Faculté de Technologie, Université Abderrahmane Mira, Bejaia, especially Prof. Mustapha Kaci and Dr Aida Benhamida. Thank you for your friendship and collaboration.

- Prof Joseph Kwaku Ofori Asante who assisted in carrying out the cone calorimeter experiments is acknowledged.
- My parents Geraldo Macheca and Josefina Mariano for their trust and love. To my younger brother Sorinho and sisters Dorteia and Merina and to my daughter Telma for their affection and love.
- My wife Izilda Macheca for the love, compassion and patience through these long years of study and sacrifices.
- Financial support for this research from the National Research Foundation (NRF) via the South African/Mozambique Collaboration Programme and Algeria research partnership programme under Grant 87453.
- Financial support from Ministry of Science and Technology of Mozambique

PREFACE

Polymer nanocomposites are high-performance materials promising to meet new application requirements and to replace existing materials. The addition of clay-based nanoparticles can significantly improve properties of polymers. However, the vast majority of matrices used for this purpose are oil-based polymers. But, environmental concerns and sustainability issues are driving the adoption of biopolymers. Biopolymers are either fully biodegradable polymers or polymers derived from renewable resources such as plant oils and agro-industrial waste.

Biopolymers are already offering promising properties for a variety of industrial applications. However, compared to equivalent petroleum-based polymers, they tend to be more expensive and often feature relatively poor mechanical, physical or processing properties. These drawbacks make them less competitive and limit their straightforward use in many applications. Some of these problems can be alleviated by incorporation of suitable inorganic fillers.

The extent of polymer property enhancement with clay-based fillers depends strongly on factors such as particle size and aspect ratio. This implies the need for extensive exfoliation (favoured by strong interfacial adhesion) together with homogeneous dispersion (achieved by an appropriate mixing process) in the matrix. Ideally, the dispersed particles should correspond to stacks comprising only a few clay mineral layers or individual fibres.

Conventional polymer nanocomposites are prepared using cationic surfactant-modified clays. Unfortunately, the use of cationic surfactant molecules introduces two main problems. They need to be chosen very carefully. Interactions between the polymer chains and the matrix must be preferred above surfactant-clay and surfactant-surfactant interactions so that exfoliation will be favoured in the thermodynamic sense. They also have limitations with respect to thermal stability. The lower degradation onset temperatures of organoclays limit the processing temperatures of the polymer nanocomposites. Alkylammonium surfactants chemically degrade from about 180 °C, i.e. at temperatures well below conventional polymer processing temperatures. Therefore, the surfactant molecules may degrade even when melt intercalation is performed at temperatures in excess of 200 °C.

The present study exploited an alternative route for polyamide/clay bio-nanocomposites fabrication to the conventional polymer nanocomposites preparation route outlined above. The goal was to achieve high degrees of clay sheet delamination in the polyamide matrices. The method did not employ any surfactants for the matrix-clay compatibilisation. The idea was to exploit the use of dimer fatty acid based polyamides with protonated amine end groups as clay surface modifiers of the clay previously dispersed in a liquid medium.

The first phase of the project involved the preparation and full characterization of clay (montmorillonite and vermiculite) nanoparticles as described in Chapter 3. This was followed by the preparation of polyamide nanocomposites by either a solution casting route or extrusion compounding. In the third phase of the study the morphology, thermal, rheological, flammability, and mechanical properties of the various bio-nanocomposite samples were investigated using techniques such as wide angle X-ray scattering, electron microscopic analysis, thermogravimetric analysis, dynamic mechanical analysis, tensile measurements, cone calorimeter, etc.

Thesis outline

In total, the thesis comprises five chapters and references. Appendices are also included.

An introduction to the study, description of the novel method and methodology used in the present work are given in **Chapter 1**.

Chapter 2 provides a review of clays and clay minerals (with emphasis to bentonite and vermiculite clays) and their use as additives in polymer matrices is given. The chapter introduces the reader to the conventional way for clay surface modification and polymer clay nanocomposites preparation methods. A description of the principle of the new route that was followed in the present study is presented. Definition of polymer and biopolymers and polymer composites and a distinction between nanocomposites and micro-composites is given. The chapter also reviews the properties observed for nanocomposites. An overview of the common analytical techniques that are used for the characterization of clays and PA-bio-nanocomposites is also given.

Chapter 3 outlines the experimental design and presents the raw materials and the instruments that were available for laboratory work. The methods and procedures followed in the laboratory are also described in this chapter.

The results of the investigation of dimer fatty acid based polyamide/(montmorillonite or vermiculite) bio-nanocomposites produced by solution casting method as well as polyamide-11/(vermiculite or sepiolite) bio-nanocomposites are presented in **Chapter 4.** The chapter discusses the morphology, thermal, rheological, flammability, and mechanical properties of the generated bio-nanocomposite. The relationships between the structure and the physical properties of dimer fatty acid based polyamide and polyamide-11 bio-nanocomposites were studied.

Chapter 5 summarises the study and the key findings.

Additional and relevant information data are given in the appendices.

TABLE OF CONTENTS

LIST OF FIGURES

LIST OF TABLES

LIST OF ABREVIATIONS

AFM	Atomic force microscopy
ASTM	American Society for Testing and Materials
CEC	Cation exchange capacity
DMA	Dynamic mechanical analysis
DSC	Differential scanning calorimetry
FESEM	Field emission scanning electron microscope
FTIR	Fourier transform infrared
HRR	Heat release rate
GHG	Greenhouse gas
LOI	Loss on ignition
LALLS	Low angle laser light scattering
Mt	Metric tons
MLR	Mass loss rate
PA	Polyamide
PGS9	Pangel S9
PMLR	Peak mass loss rate
PVC	Polyvinyl chloride
RH	Relative humidity
RT	Room temperature
SEM	Scanning electron microscopy
SPR	Smoke production rate
TEM	Transmission electron microscopy
TGA	Thermogravimetric analysis
T_g	Glass transition temperature
TTI	Time to ignition
VMT	Vermiculite
UV	Ultraviolet
UVMT	Unmodified vermiculite
WAXS	Wide-angle X-ray scattering
XRD	X-ray diffraction
XRF	X-ray fluorescence

CHAPTER 1

1. GENERAL INTRODUCTION

1.1. Background

Polymer nanocomposites are high performance materials promising to meet new application requirements and to replace existing materials (Fu et al., 2008, Yeh et al., 2012, Mago et al., 2011). Adding clay-based nanoparticles such as exfoliated clay sheets can significantly improve properties such as heat resistance, stiffness, strength, dimensional stability, adhesive strength, toughness, impact resistance, barrier properties, rheological properties, flame retardancy, UV stability, etc. (Kiliaris and Papaspyrides, 2010, de Sousa Rodrigues et al., 2013, Arora and Padua, 2010, Utracki, 2008, de Paiva et al., 2008, LeBaron et al., 1999, Ahmadi et al., 2005, Alexandre and Dubois, 2000, Fischer, 2003, Lee and Lee, 2004, Ray and Okamoto, 2003, Wang et al., 2004).

The vast majority of matrices used for this purpose are oil-based polymers. However, environmental concerns and sustainability issues are driving the development of bio-polymers. When incinerated or degrade naturally oil-based polymers release the greenhouse gas CO_2, thus contributing to global warming. Biopolymers are either fully biodegradable polymers or polymers derived from renewable resources such as plant oils and agro-industrial waste (Hablot et al., 2010a, de Espinosa and Meier, 2011, Matadi et al., 2011, Petersson and Oksman, 2006, Babu et al., 2013, Lunt, 1998, Mohanty et al., 2002, Satyanarayana et al., 2009, Storz and Vorlop, 2013).

Biopolymers are already offering promising properties for a variety of industrial applications. However, compared to equivalent petroleum-based polymers, they often feature relatively poor mechanical, physical and processing properties. These drawbacks make them less competitive and limit their straightforward use in most applications. Addition of inorganic fillers has been shown to improve significantly these properties, allowing these polymers to be used for a number of applications (Bhattacharya et al., 2008, de Espinosa and Meier, 2011, Fu et al., 2008, Hablot et al., 2010a, Matadi et al., 2011, Petersson and Oksman, 2006, Satyanarayana et al., 2009).

The extent of polymer property enhancement depends strongly on factors such as size and particle aspect ratio, extensive exfoliation (favoured by strong interfacial adhesion) together with a homogeneous dispersion (achieved by an appropriate mixing process). Ideally, the dispersed particles should correspond to stacks comprising only a few clay mineral layers or individual fibres (Pavlidou and Papaspyrides, 2008, Chaiko and Leyva, 2005, Gopakumar et al., 2002, LeBaron et al., 1999, Powell and Beall, 2007, Yang et al., 1999).

Conventional polymer nanocomposites are prepared using surfactant-modified clays. The nature of the surfactant plays an important role as it determines the degree of clay exfoliation that can be achieved. Unfortunately, the use of cationic surfactant molecules introduces two main problems namely: (1) they need to be chosen very carefully such that interaction with the polymer chains in the matrix is favoured above surfactant-clay and surfactant-surfactant interactions (LeBaron et al., 1999, de Paiva et al., 2008); otherwise, exfoliation will not be favoured in the thermodynamic sense; (2) limitations with respect to thermal stability. The lower degradation onset temperatures of organoclays limit the processing temperatures of the polymer nanocomposites. Alkylammonium surfactants chemically degrade around 180 °C. When using melt intercalation, for example (a process commonly carried out in excess of 200 °C), the surfactant molecules may degrade (Tjong, 2006). These observations imply that new or alternative routes to facilitate “extensive delamination” of clay stacks in polymer matrices need to be found. This was the main objective of the present research.

Instead of conventional surfactants, the present study focused on a new way of clay surface modification, the so-called “surfactant-free organo-modification approach”. In essence, the goal was to use polyamides with protonated amine end groups as clay modifiers of the clay previously dispersed in the liquid medium. A primary objective of the study was to prepare polyamide (PA)/clay bio-nanocomposites with “extensive delamination” of clay stacks in PA matrices. This “novel” technique is of great interest because it allows organo-modification of the external surfaces of nano-sized clay sheets suspended in an acidic solution. This may facilitate clay dispersion and to prevent restacking when they are ultimately compounded into the polymer matrix. In addition, the solution route should enable the preparation of nanocomposites with relatively high clay contents (Macheca et al., 2016, Macheca et al., 2014, Nicolosi et al., 2013).

The principle was as follows: In some polyamides, it is possible for the polymer chains themselves to provide the required organo-modification when amine functional groups are

present e.g. at the chain ends. Dimer fatty acid-based polyamides (DAPA) (the polyamide of choice as clay surface modifiers in this study) are of this type and they are soluble in lower carboxylic acids, e.g. formic acid or acetic acid (Fan et al., 1997). When dissolved in these acidic solvents, the amine functional groups at the ends of some chains become protonated. Thus, it should be possible for these cationic molecules to ion exchange with the intercalated cations present in the clay galleries. In this case, exfoliation may be favoured owing to the strong hydrogen bonding interactions that occur in DAPA polymers. This means that organo-modification of the clays should be possible via solution intercalation of the polymer chains *per se* provided that suitable exchangeable ions are present in the clay. The choice fell on ammonium ions as, after exchanging, they can be removed by volatilisation as ammonia gas. Therefore, it was proposed to first prepare ammonium-loaded clays by exhaustive ion exchange. Then to contact such ammonium-loaded clays dispersed in acetic acid with DAPA solutions in the same solvent. These clay surface modifier polyamides may be identical with the matrix PA or it may be a different PA. These are the ideas that were explored in the present work.

The clay modification route outlined above was applied to vermiculite (VMT) and the standard smectite clays commonly used to prepare polymer clay nanocomposites. Keep in mind that a primary objective of the study was to achieve high degrees of clay sheet delamination in the PA matrices. Smectite clays swell and, with monovalent exchangeable cations, exfoliate spontaneously in water giving stable colloidal dispersions (Norrish, 1954, Walker, 1960). On the other hand, vermiculite exfoliates easily when heated or treated with hydrogen peroxide (H_2O_2) and further delamination can be effected by sonication using high power ultrasound (Walker and Garrett, 1967, Muiambo et al., 2010, Muiambo et al., 2015, Justo et al., 1989, Hillier et al., 2013, Kehal et al., 2010, Obut and Girgin, 2002, Wiewiora et al., 2003, Poyato et al., 2009, Pérez-Maqueda et al., 2001, Pérez-Rodríguez et al., 2002, Ali et al., 2014). Exploring these abilities was considered to be at least a good starting point in the preparation of polymer/clay nanocomposites with extensive delaminated clay stacks. Obviously, this assumes that “all” synergistic factors required are properly modulated in order to obtain the desired final properties of the polymer/clay nanocomposites.

The polyamides of choice in the study to prepare PA-clay bio-nanocomposites were PA-11 and DAPA. They are polyamides derived from renewable resources. Both polyamides already offer promising properties for a variety of industrial applications. PA-11 is

manufactured from castor or canola oil while DAPA are derived from plant oils such as soybean or sunflower oils (Hablot et al., 2010a, Türünç et al., 2012, Maisonneuve et al., 2013, La Scala et al., 2004). Both polyamides are used in high technology applications. PA-11is used as a barrier material in fuel lines (Zhang et al., 2001, Zhang et al., 2012, Hu et al., 2006). DAPA find application as thermoplastic hot melt adhesives and as injection mouldable polymeric encapsulants for electronics packaging (Fan et al., 1997, Yao et al., 2015). These applications, however, may benefit from improvements in their properties.

1.2. Research objectives

As previously stated, the extent of polymer property enhancement depends strongly on factors such as size and particle aspect ratio, extensive exfoliation together with a homogeneous dispersion of clay mineral layers or fibres. The primary objective of the present work was to prepare and characterize PA/cay bio-nanocomposites with "extensive delamination" of clay stacks in PA matrices (with emphasis to DAPA and PA-11) via a novel approach. For this purpose the following specific objectives were set:

- Prepare and characterize the modified clays using the new approach outlined above;
- Prepare bio-nanocomposite samples by solution casting method and/or melt blending method varying both the types and the nature/concentration of the polymer matrix and the modified clays;
- Characterize the morphology, thermal, rheological, flammability, and mechanical properties of the various bio-nanocomposite samples using techniques such as wide angle X-ray scattering (XRD), electron microscopic analysis (SEM, AFM and TEM), thermogravimetric analysis (TGA), dynamic mechanical analysis (DMA), tensile measurements, cone calorimeter, etc.;
- Understand the relationships between the structure and the physical properties of DAPA and PA-11 bio-nanocomposites. Here the aspects that were addressed include the clay content, the effects of the nature of the clay, the aspect ratio of the platelets, and the degree of dispersion that is achieved;
- Compare the functional properties of these clays and to seek scientific explanations for the observed behaviours.

1.3. Methodology

Three main phases were followed in the present study:

(1) Preparation and full characterization of clay nanoparticles. In one approach the clays modification was carried out by loading them with ammonium cations via exhaustive ion exchange. In the case of VMT clay, the submicron nanoflakes were obtained by ultrasound dispersion in the liquid phase of VMT that was first exfoliated by either thermal shock or chemical treatment with hydrogen peroxide. The ammonium-loaded clays (MMT or VMT dispersed in acetic) were then contacted with DAPA solutions in the same solvent;

(2) Preparation of PA (DAPA and PA-11)-clay bio-nanocomposites. This particular phase was divided into three steps:

(a) In this step, MMT clay was used to prepare the polymer clay nanocomposites. DAPA (amorphous PA) was used as a clay surface modifier and it also served as the polymeric matrix. The polymer nanocomposites were produced by solution casting method. The main focus here was to understand the relationships between the new processing method and structure as well as to understand the relationships between the structure and the properties of the generated nanocomposites;

(b) Instead of smectite clay in the second step submicron VMT nanoflakes obtained by ultrasound dispersion in the liquid phase of VMT that was first exfoliated by either thermal shock or chemical treatment with hydrogen peroxide were used. Here again, DAPA was used as a clay surface modifier as well as a polymeric matrix. The study compared the effect of the two different exfoliated submicron VMT flakes on the mechanical properties of such DAPA/bio-nanocomposites. The primary objective was to gain an understanding of the stiffening mechanisms operating in amorphous DAPA–VMT bio-nanocomposites;

(c) In the third step, a similar technique to the one was applied in the second step to exfoliate the VMT clay was used except that only the thermal exfoliation route was followed instead of the chemical exfoliation one. In this particular step part of the resulting thermally expanded and ultrasonicated VMT was used for the organic modification process outlined above while the remaining part was used as unmodified VMT (i.e. no organic modification). Here PA-11was used as a polymeric matrix while the DAPA was kept as a clay surface modifier. The organic modified (OVMT) and the unmodified one (UVMT) were melt compounded into the PA-11 to form products

that contained either no filler, i.e. neat PA-11 or 10 wt.% clay. The main goal was to compare the effect of the organic modification on properties of the generated PA-11 bio-nanocomposites, with emphasis on the mechanical and flame retardant properties. The performance of OVMT and UVMT samples with the commercial sepiolite (PGS9) was also studied. In this particular case, the aspects that were addressed included the effect of the shape of the clay, the aspect ratio of the particles, and the degree of dispersion that was achieved.

(3) Full characterization of the elaborated polymer bio-nanocomposites by SEM and TEM, TGA, XRD, DMA, rheological, cone calorimeter and tensile properties.

CHAPTER 2

2. LITERATURE SURVEY

2.1. Clays and clay minerals

The term “clay”, refers to naturally occurring materials (i.e., non-synthetic) composed of very fine-grained minerals that show some plasticity when mixed with appropriate amounts of water and that will harden with dried or fired (Guggenheim and Martin, 1995). It is, therefore, applicable to all small-sized particles, normally < 2 μm, found in soils, sediments or as alteration products of rocks, including, apart from the phyllosilicates, lesser quantities of other minerals and/or organic products such as quartz, feldspars, carbonates, sulphates, Fe and/or Al oxides, humus, etc. “Clay mineral” is a mineralogical term referring to the part of a family (the phyllosilicates) consisting of hydrated aluminosilicates containing considerable amounts of Mg, Ca, Na, K, and Fe and, occasionally, fewer communions such as Ti, Mn, or Li. Despite their varied chemical composition, they can be classified in just a few major groups - smectites, vermiculites, micas, kaolin, talcum, chlorites, fibrous and interstratified (López-Galindo et al., 2007).

Clays and clay minerals find use in a wide range of applications and the diversity of uses is still increasing. Millions of tons are utilized annually in a large variety of applications. These applications include uses in geology, the process industries, agriculture, environmental remediation and construction. The reasons are simple, as native materials, clays and clay minerals are available in immense reserves all around the world and their processing or modification is neither difficult nor expensive. This is useful for applications in industry. On the other hand, their colloidal size and crystalline structure imparts peculiar properties which are translated into the high specific surface area, interesting rheological properties and/or excellent adsorptive capacity. This makes clays very useful for a wide range of applications (Murray, 1999, Murray, 2000, Bergaya and Lagaly, 2001, Del Hoyo, 2007).

Nowadays an application of great interest for clays, which is also the interest of present study, is to disperse them as nanometer-sized particles in a polymer phase, forming novel nanocomposite materials with improved properties (Bergaya et al., 2006). Clays suitable for polymer nanocomposites technology include smectite, VMT, kaolin, mica, palygorskite and sepiolite. However, in the family of phyllosilicates, 2:1 type silicates are most popular among

industries and academia (Kumar et al., 2009). The clays of choice in the present study were the standard smectite clays commonly used to prepare polymer clay nanocomposites and VMT.

2.2. Smectites

Smectite is a group name for platy phyllosilicates of 2:1 layer with a layer charge between 0.2 and 0.6 per formula unit (pfu). The interlayer separation (*d*(001) spacing) will vary depending on H_2O retention and interlayer occupancy, but generally for natural samples, the separation is approximately 14.4-15.6 Å. The smectite group consists of several clay minerals such as montmorillonite (MMT), saponite, hectorite, beidellite and nontronite. However, montmorillonite (Na-MMT and calcium Ca-MMT) are the two most important industrially. MMT it is a hydrated alumina-silicate layered clay mineral consisting of an edge-shared octahedral sheet of aluminium hydroxide between two silica tetrahedral layers. Na^+ and Ca^{2+} cations are the typically interchangeable cations giving the MMT a high ion exchange capacity. The most common occurrences of these two smectite minerals are in bentonite. Mineralogically, bentonite is a soft, plastic, light-coloured rock, which typically forms from chemical alteration of glassy volcanic ash deposits or tuff under marine or hydrothermal conditions. Bentonite may contain accessory crystal grains that were originally phenocrysts in the parent rock as well as secondary authigenic mineral phases such as K-rich feldspar (Alexandre and Dubois, 2000, Guggenheim et al. 2006, Weiss et al., 2006, Murray, 2002, Murray, 2000, Utracki, 2004, Inglethorpe et al., 1993, Bailey, 1980).

MMT has a 2:1 layered structure with the inner layer composed of an octahedral sheet that shares oxygen atoms between two tetrahedral sheets located on either side. In smectites, the substitution of Al^{3+} for Si^{4+} in tetrahedral sheets and substitution of divalent cations such as Mg^{2+} and Fe^{2+} for trivalent cations such as Al^{3+} and Fe^{3+} in octahedral sheets lead to a negative charge at the basal surface. This charge is balanced by monovalent and divalent cations (usually Na^+, K^+, Ca^{2+} and Mg^{2+}) present in the interlayers. Their amount is usually expressed as the cation exchange capacity (CEC) (Annabi-Bergaya, 2008, Daković et al., 2008, LeBaron et al., 1999).

The sheet (octahedral and tetrahedral) thickness of smectites is about 2.2-2.3 Å and the lateral dimensions (*a* and *b* parameters) are less greater than 5 and 9 Å, respectively. These layers organize themselves to form stacks with a regular van der Waals gap in between them called

the interlayer or the gallery. A model presentation of smectite clay mineral structure is shown in Figure 2.1. MMT has a generic chemical formula as shown below (Alexandre and Dubois, 2000).

$$M_x(Al_{4-x}Mg_x)Si_8O_{20}(OH)_4$$

where M = monovalent cation and x = degree of isomorphous substitution (between 0.5 and 1.3).

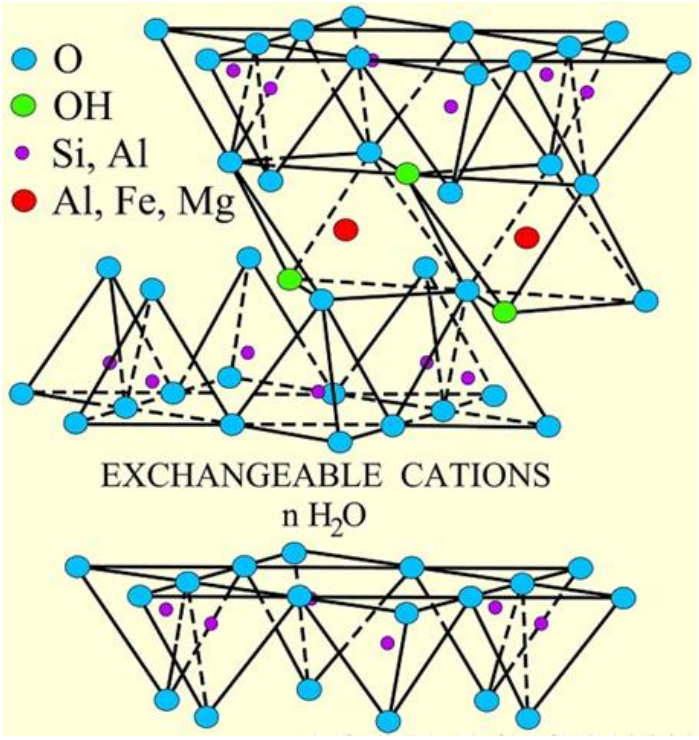

Figure 2.1. The structure of smectite (Adapted from Grim, 1962).

The high layer charge, the very fine particle size, the thin flakes, the high cation exchange capacity, the high surface area and the large aspect ratio (50–1000) of MMT (specially the Na-MMT) result in the physical and chemical properties that make it the most preferred material for its intercalation in polymer as an effective reinforcement filler (Murray, 2000, De Azeredo, 2009). Other important applications of smectites are shown in Table 2.1.

Table 2.1. Industrial uses of smectites (Adapted from Murray, 2000).

Drilling mud	Bleaching clay	Emulsions stabilizers
Foundry binder clay	Agricultural carriers	Desiccants
Pelletizing iron ores	Cat litter absorbents	Catalysts
Sealants	Adhesives	Cosmetics
Animal feeds binders	Pharmaceuticals	Paint

2.2.1. Location and geology setting of Boane bentonite used in the study

The main smectite bearing deposit investigated in this study is found in Boane District, Maputo Province, in the South of Mozambique. The deposit is located at about 40 km SW of Maputo (capital city of Mozambique) in the Boane area on the slope of the Montes Pequenos Libombos and about 9 km from the town of Boane district.

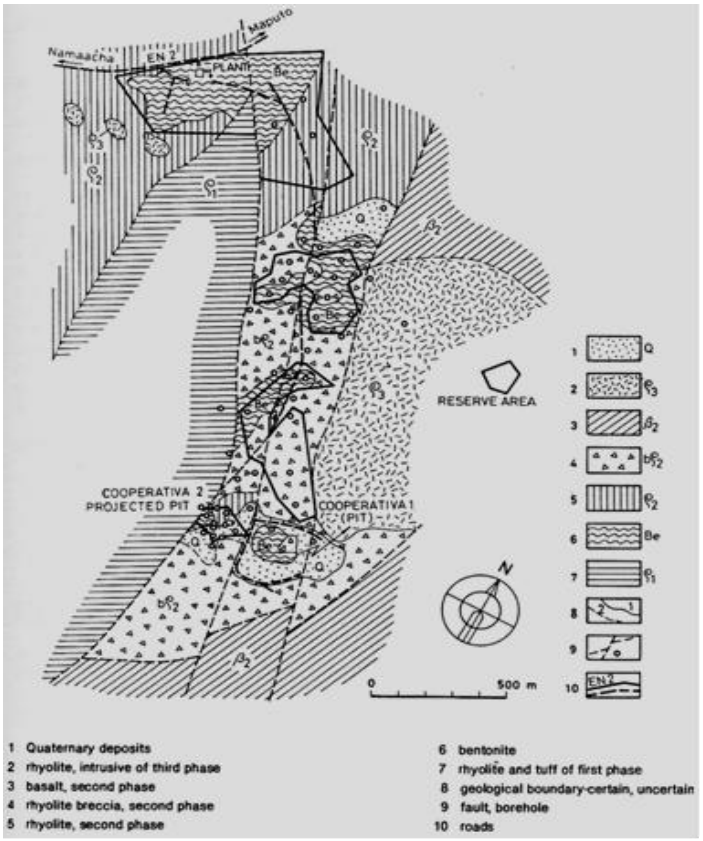

Figure 2.2. Geological map of the bentonite deposit near Boane District (Adapted from Cílek and Duda, 1989).

The study area is accessible by both the Maputo-Namaacha and Maputo-Ressano Garcia roads and by footpaths. The main river in the area is the Umbeluzi, fed mostly by perennial tributaries. During the rainy season, the phreatic water table rises considerably and floods the low-lying parts. Raw bentonite is extracted from an open pit. One of the well-studied deposits, with an area of about 40,000 m^2 is called *Depósito Cooperativa* 1 and 2 (see Figure 2.2). This bentonite occurs as a weathering product of rhyolites and rhyolitic tuffs of the Karoo volcanic distributed in the Pequenos Libombos range. The thickness of bentonite varies from a few metres to up to 20 m, depending on the intensity of weathering (Cílek and Duda, 1989, Lehto and Goncalves, 2008). Previous studies (Massinga et al., 2010,

Muchangos, 2000, Cílek and Duda, 1989, Grim and Guven, 1978) on Boane bentonites suggested that these bentonites are composed mainly of MMT, with cristobalite being the major impurity. Chemically, Boane bentonite is characterized by high silica (SiO_2) and generally low contents in Al_2O_3 and MgO (Massinga et al., 2010, Macheca et al., 2014) features which are strictly related to the parent rocks of dominantly rhyolitic composition.

2.3. Vermiculite

As a traded commodity, the term "Vermiculite" is used to describe commercially exploited deposits of micaceous minerals which can be exfoliated when heated rapidly to high temperatures (Kogel, 2006). However, in the mineralogical sense, VMT is a 2:1 phyllosilicate, in which the negatively charged aluminosilicate layer is composed of one central magnesium octahedral sheet sandwiched between two hydrated silica tetrahedral sheets. Magnesium and iron sites are also present within the sheets of typical vermiculites. VMT, like the well-known MMT clay is characterized by substitution in the tetrahedral sheet (Si^{4+} by Al^{3+} and Fe^{3+}) and in the octahedral sheet (Mg^{2+} by Al^{3+}, Fe^{3+} and Fe^{2+}. The substitutions of Si^{4+} by trivalent cations in tetrahedral positions are responsible for the negative layer charge of vermiculites. This charge is compensated by exchangeable cations, mainly Mg^{2+} or Ca^{2+} (Maqueda et al., 2009, Ramírez-Valle et al., 2006, Xu et al., 2003, , Pérez-Rodríguez et al., 2002, Lagaly, 1982, Shirozu and Bailey, 1966, Walker and Garrett, 1967).

Vermiculites are generally trioctahedral clay minerals. They are termed on the basis of a negative layer charge, which is between 0.6 to 0.9 per $Si_4O_{10}(OH)_2$ formula unity (pfu) (de Haro et al., 2005, Guggenheim et al., 2006, Bailey, 1980, Brindley and Pedro, 1975, Guggenheim et al., 1997). Vermiculites are mostly formed by weathering of micas, mainly from biotite, phlogopite or muscovite by the release of interlayer K^+ and the oxidation of Fe^{2+} (Bergaya and Lagaly, 2013, Martin et al., 1991, Norrish, 1972). That is why the VMT chemistry from this perspective is closely linked to that of mica (Valášková and Martynkova, 2012, Brown, 1972, Grim, 1968). Vermiculites can also be obtained by the decomposition of the interlayer hydroxide sheet in chlorite (Bergaya and Lagaly, 2013). In reality, many existing vermiculites are a mixture of VMT, VMT/mica interstratification and mica (de Haro et al., 2005, Justo et al., 1993). The thickness of the structural unit (2:1 layer and interlayer space) is about 1.4 nm, depending on the water interlamellar layers and the interlayer cations (Valášková and Martynkova, 2012).

The characteristic properties of VMT, such as high cation exchange capacity (100-150 cmol/Kg), the ability to form complexes with organic substances, and a variable interlamellar distance depending on the exchangeable cations present and the humidity of the sample are very similar to those of MMT (Walker, 1947, Walker, 1949, Walker, 1950, Walker, 1951, Barshad, 1948, Barshad, 1949, Barshad, 1952, Walker and Milne, 1950, Xu et al., 2005). The similarity of their structures which consist of complex silicate layers interleaved with layers of water molecules carrying exchangeable cations it is the main reason for the similarity in the properties (Mathieson and Walker, 1954). A model presentation of VMT clay mineral structure is shown in Figure 2.3.

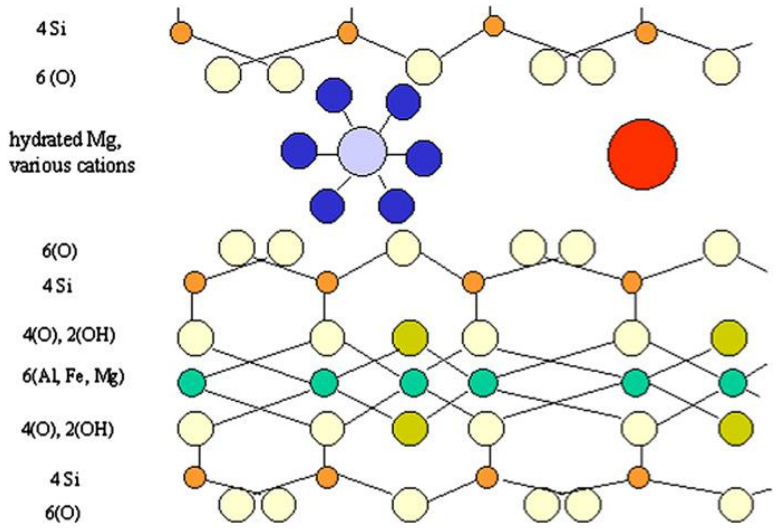

Figure 2.3. The structure of VMT (Adapted from Zhang et al., 2009).

The structural formula of vermiculites is often reported on the basis of the structure unit (half unit-cell content). The general formula can be written as (Valášková and Martynkova, 2012):

$$X_4(Y_{2\text{-}3})O_{10}(OH)_2\ M{\cdot}nH_2O$$

where M is exchangeable (Mg^{2+}, Ca^{2+}, Ba^{2+}, Na^{+}, K^{+}) cations positioned in the interlayer space, that compensates the negative layer charge, Y is octahedral Mg^{2+}, Fe^{2+} or Fe^{3+}, Al^{3+}, and X is tetrahedral Si, Al. Valášková and Martynkova (2012) provide a summary of the half unit cell compositions of vermiculites from different countries for comparison and the list is given below:

Llano: $(Si_{2.86}Al_{1.14})(Mg_{2.83}Al_{0.15}Fe^{3+}_{0.02})O_{10}(OH)_2\ Mg_{0.41}{\cdot}3.72H_2O$

Kenya: $(Si_{2.72}Al_{1.28})(Mg_{2.36}Al_{0.16}Fe_{0.58})O_{10}(OH)_2Mg_{0.32}{\cdot}4.32H_2O$

Santa Olalla, Spain: $(Si_{2.72}Al_{1.28})(Mg_{2.59}Fe^{2+}_{0.03}Al_{0.06}Fe^{3+}_{0.24}Ti_{0.08})O_{10}(OH)_2Mg_{0.39}Ca_{0.02}{\cdot}4.7H_2O$

Ojen, Spain: $(Si_{2.83}Al_{1.17})(Mg_{2.01}Al_{0.2}Fe^{2+}_{0.16}Fe^{3+}_{0.40}Ti_{0.14})O_{10}(OH)_2Mg_{0.235}$

Letovice, Czech Republic: $(Si_{2.64}Al_{1.36})(Mg_{2.38}Fe^{2+}_{0.02}Al_{0.06}Fe^{3+}_{0.51}Ti_{0.03})O_{10}(OH)_2Mg_{0.35}Ca_{0.01}Na_{0.01}\cdot 4.9H_2O$

West China: $(Si_{3.02}Al_{0.98})(Mg_{2.27}Al_{0.12}Fe^{3+}_{0.28}Fe^{2+}_{0.05}Ti_{0.07})O_{10}(OH)_2Mg_{0.35}Ca_{0.09}Na_{0.21}K_{0.50}$

Palabora, South Africa : $(Si_{3.02}Al_{0.79}Ti_{0.05}Fe^{3+}_{0.14})(Mg_{2.50}Fe^{2+}_{0.38}Fe^{3+}_{0.09})O_{10}(OH,F)_2Ba_{0.29}Ca_{0.09}K_{0.14}Ca_{0.08}$

Brazil: $(Si_{3.43}Al_{0.57})(Al_{0.26}Fe_{0.32}Mg_{2.34})O_{10}(OH)_2Ca_{0.64}Na_{0.16}K_{0.047}$

2.3.1. Exfoliation and delamination of vermiculite

Exfoliation and *delamination* of clay mineral particles are often confusing terms in the literature. However, clear definitions of them were most recently given by Bergaya et al. (2012). According to these authors, in aqueous dispersion, intercalated water molecules lead to increasing separation between two successive layers. As long as there is no significant interaction between the two successive layers with some crystallographic orientation maintained, this separation is called *delamination*. When at some point, no further interaction occurs between the two delaminated units (isolated layers or stacking of few layers) which become independently mobile in the liquid phase, this phenomenon is called *exfoliation*.

In particular case of vermiculite, however, the term *exfoliation* can also be used to describe the process of separation of its layers when heated thermally or by chemical treatment.

In fact, the "VMT" of commerce features the desirable property that it expands up to 20-30 times in volume when heated rapidly to elevated temperatures (Walker and Garrett, 1967, Muiambo et al., 2010, Muiambo et al., 2015, Macheca et al., 2016, Justo et al., 1989, Hillier et al., 2013) or by treating it with H_2O_2 (Kehal et al., 2010, Obut and Girgin, 2002, Macheca et al., 2016). Exfoliation into submicronic and even nanoflakes can be accomplished by subsequent sonication using high power ultrasound (Kehal et al., 2010, Wiewiora et al., 2003, Poyato et al., 2009, Pérez-Maqueda et al., 2001, Pérez-Rodríguez et al., 2002, Ali et al., 2014, Macheca et al., 2016).

Exfoliation of VMT involves a volume expansion with individual platey particles expanding perpendicular to the cleavage planes, bloating in an accordion- or concertina-like fashion (Macheca et al., 2016) to up to 20-30 times their original volume. When exfoliated the VMT accordions become curved, which together with their segmented appearance evokes the vermiform resemblance to worms. This explains the origin of the name "vermiculite" (Walker, 1951).

In its exfoliated state, VMT has the following important qualities (Hall, 2010): low density, moderately low thermal conductivity, high-temperature resistance, high absorbency, high specific surface area and cation exchange property.

a) Exfoliation of vermiculite using thermal treatment

The most well-known method of exfoliating VMT is by short-lived rapid so-called 'shock' or 'flash' heating. Commercially, this is usually achieved by heating to temperatures of around 900 ºC for a few minutes or more in a vertical or rotary furnace (Kogel, 2006). Heating rapidly a VMT flake to elevated temperatures (≈ 900 ºC), results in the rapid transformation of the interlayer water into steam. This generates high pressure that causes the flakes to separate and to expand in a worm-like manner. As a consequence, a highly porous expanded material, which is an efficient thermal insulator, is formed. This expansion, that can reach 30 times the original flake thickness, is conventionally called as exfoliation although the individual sheets that make up the original flake remain attached to each other (Justo et al., 1989, Kehal et al., 2010, Marwa et al., 2009, Walker, 1961).

The exfoliation property of VMT is related to the explosive release of water molecules from between the silicate layers and causes the flakes to separate and to expand. Midgley and Midgley (1960), Couderc and Douillet (1973), Justo et al. (1989) and Hillier et al. (2013) found that samples that are poly-phase and/or rich in mica-VMT mixed layers exfoliate more readily compared to samples that are rich in true VMT. Couderc and Douillet (1973) attributed this phenomenon to the fact that during the thermal shock, the water molecules from the VMT layers hit the mica layers, producing the large gap between them. Later, Justo et al. (1989) suggested that the sudden release of interlayer water is not the only factor influencing the thermal expansion of VMT samples. The mechanism differs from one sample to another, depending on chemical composition, loss of OH groups, and mineralogical composition.

Very recently, Hillier et al. (2013) offered what appears to be a satisfactory and convincing explanation for the exfoliation mechanism of thermal exfoliation of VMT. An intra-particle mosaic-like intergrowth of VMT, mica and mica-VMT mixed layers in most commercial vermiculites seems to be the key point to explain the mechanism of thermal exfoliation. According to authors, exfoliation is related to the mosaic distribution of the different mineral phases within the particles. Lateral phase boundaries between VMT and mica layers or VMT

and chlorite layers are postulated to prevent or impede the escape of gas from a particle, resulting in exfoliation when the pressure exceeds the interlayer bonding forces that hold the layers together. The model developed by these authors explains also the commonly observed particle size dependence of exfoliation and the tendency for poly-phase VMT samples to show the largest coefficients of expansion.

At laboratory scale, the onset of exfoliation of some VMTs (e.g. the well known Palabora VMT from Phalaborwa, South Africa and the industrial interstratified VMT from China) can be observed at temperatures as low as 300 ºC. This can be achieved by cation exchange treatments with Na^+, K^+ or NH_4^+ (Muiambo and Focke, 2012, Huo et al., 2012).

Another thermal exfoliation technique of VMT, but seldom used, is heating VMT with microwaves (Marcos and Rodríguez, 2010, Marcos and Rodríguez, 2011, Marcos and Rodríguez, 2014, Folorunso et al., 2012). It was shown recently by Marcos and Rodríguez (2011) that microwave irradiation reduced the time and energy required for the preparation of expanded VMT particles. However, the method is still not commercially popular because, to date, most of the published investigations of microwave exfoliation of VMT have been carried out on the laboratory scale using the domestic microwave. The disadvantages of using domestic microwave are first, the spatial non-uniform distribution of the electric field which causes uneven heating of materials, secondly, the creation of multiple hotspots within the cavity and the low power density (Meredith, 1998). These drawbacks make domestic microwave ovens unsuitable for scientific investigations as the distribution of the electric field may vary considerably between the discrete treatment of different samples and it is subsequently impossible to predict the distribution of the electric field in the workload (Folorunso et al., 2012).

b) Exfoliation of vermiculite using chemical treatment with hydrogen peroxide

In addition to thermal methods, VMT may also be exfoliated chemically. By far the most effective and most gentle chemical method known (to date used only in laboratory scale) is that of using hydrogen peroxide (H_2O_2) (Baumeister and Hahn, 1976, Obut and Girgin, 2002, Kehal et al., 2010, Hillier et al., 2013, Marcos and Rodríguez, 2011). The technique is based on the observation that the decomposition of H_2O_2, which obviously is catalysed by the interlayer cations of the clay and the concomitant evolution of oxygen, separates the layers. Oxygen atoms also attack the hydroxide groups of the silicate structure causing the vigorous

release of the hydroxides from the silicate structure. The interactions between H_2O_2 and hydroxide groups of the silicate structure and interlayer water molecules disrupt the electrostatic equilibrium between the layers and the interlayer cations, causing dissolution of the interlayer cations and separation of the layers (Groves, 1939, Obut and Girgin, 2002).

Since exfoliation occurs due to the decomposition of H_2O_2 in the interlayers of the samples, it is reasonable to think that decomposition of H_2O_2 by the evolution of oxygen gas may be accelerated by the presence of fluoride and iron ions in the solution phase (Obut and Girgin, 2002).

The advantages of this method are first, the much better yield of very thin (2-3 nm) flakes, secondly, the maintenance of the full ion-exchange capacity (Baumeister and Hahn, 1976) and finally, the decomposition of H_2O_2 into gaseous oxygen and water, subsequent to its intercalation between the layers, generates a much greater expansion rate than that obtained by thermal exfoliation (Muromtsev et al., 1990, Obut and Girgin, 2002).

The exfoliation mechanism postulated above for thermal exfoliation is also valid for chemical treatment with H_2O_2. The mechanisms of both thermal and H_2O_2 chemical exfoliation share one or more common factors.

c) Exfoliation and delamination of vermiculite using high power ultrasound

Particle size reduction of VMT can significantly affect the commercial interest of this material. The milling methods (wet or dry) represent one of the most popular approaches to produce the required clay particles by the mechanical way. The clay particles are normally carried out in the energy intensive grinding mills such as planetary ball mill, vibratory mill and jet mill (De Haro et al., 2004, Maqueda et al., 2009, Wang et al., 2011, Barabaszová and Valášková, 2013). Among the industrial mills currently employed for producing high-quality fine materials, the jet mill now occupies an important place (Palaniandy and Azizli, 2009). Milling in a jet mill seems to be the suitable technique for obtaining ultrafine materials with an average size of around a few microns. The disadvantage of using jet milling is relatively the high energy consumption (Palaniandy et al., 2008). On the other hand, when milling VMT for example the agglomeration of VMT particles takes place and the layered structure of the material is destroyed when the grinding time increases (Perez-Rodrlguez, 2003, Pérez-Maqueda et al., 2004, Barabaszová and Valášková, 2013). Barabaszová and Valášková (2013) for instance, examined the influence of different milling techniques on the structure of

natural Mg-VMT from Brazil and its sodium form and obtained that the destruction of the layered structure of VMT took place after 15 min grinding in a vibration mill. This was confirmed by the disappearance of the basal reflections on the XRD patterns.

Recently sonication was proposed as a feasible alternative to grinding for reducing the particle size of clays. Using ultrasonic treatment of VMT submicronic and nanometric particles were obtained (Pérez-Maqueda et al., 2001, Pérez-Rodríguez et al., 2002, Wiewiora et al., 2003, De Haro et al., 2004, Pérez-Maqueda et al., 2004, de Haro et al., 2005, Poyato et al., 2009, Kehal et al., 2010, Poyato et al., 2012, Reinholdt et al., 2013, Barabaszová and Valášková, 2013, Ali et al., 2014, Macheca et al., 2016, Nguyen et al., 2013). The method is preferred because it does not modify the crystal structure and prevents amorphisation when compared with grinding technique (Wiewiora et al., 2003, Pérez-Maqueda et al., 2004).

During the ultrasound process, vapour cavities are formed which act as microjets. Their shockwaves impact and interact with the particles. The ultrasound process allows reduction of submicron and nanometric VMT particles with a relatively narrow particle size distribution. Ultrasound produces an increase of the surface area while the micropore surface area remains almost unchanged (Peters, 1996, Pérez-Maqueda et al., 2005, de Haro et al., 2005).

The higher charge density of the VMT sheets (a key parameter facilitating the incorporation of cationic organic modifiers to generate larger interlayer spacings), the formation of porous and highly fire resistant foams as a result of its spontaneous exfoliation at elevated temperatures (better fire retardancy effect to polymer composites), the formation of macroscopic crystals (that are potentially suitable for producing high-aspect-ratio nanofillers), the high absorbency and cation exchange property make VMT a great candidate to be used for polymer nanocomposites technology. On other hand, by exploring the great ability to exfoliate is, at least, a good starting point in the preparation of clay mineral-polymer composites with extensive delaminated clay stacks, assuming obviously that “all” synergistic factors needed are properly modulated in order to obtain the desired final properties of the polymer clay based nanocomposites.

2.3.2. Location and geology setting of Palabora vermiculite

The main deposit of VMT investigated in this work is located in Palabora Complex. This Proterozoic Complex lies in the Archaean of the north-eastern Transvaal. It resulted from

alkaline intrusive activity in which there was emplaced in successive stages pyroxenite, syenite and ultrabasic pegmatoid.

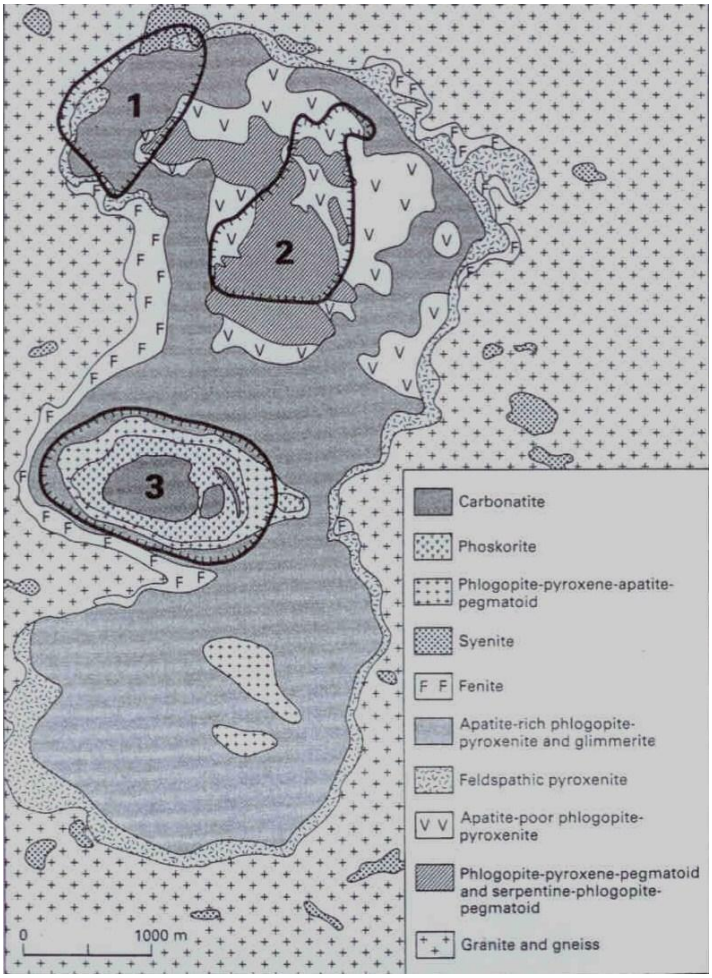

Figure 2.4. Simplified geological map of the Palabora igneous complex, Limpopo, South Africa (Adapted from Evans, 1993): (1) Open pit operation of Foskor which produces phosphate; (2) The VMT open pit; (3) The Palabora open pit at, which produces mainly copper and magnetite.

The Palabora VMT open pit mine (marked by 2 in Figure 2.4) is the second largest VMT mine in the world. The mining operations and concentration were started in 1946 by Dr Hans Merensky. In 1990, it has been calculated to contain 46 metric ton (Mt) of VMT, which makes it the world's largest ore body of this type (Schoeman, 1989).

The Palabora VMT resulted from the hydration of phlogopite (and biotite) by the loss of alkali and the addition of water. VMT is therefore essentially a complex hydrous silicate of magnesium and aluminium with varying amounts of iron, possibly of isomorphous

replacement. The surface weathering, under the influence of percolating meteoric water, it is seen to be the main cause of the conversion of phlogopite to VMT (Schoeman, 1989).

Palabora VMT is not a pure VMT, the mineral is a trioctahedral VMT intermediate between a mica (biotite) and a VMT. It is composed of sequences of mica layers, sequences of VMT layers and a seemingly regular interstratification between these two kinds of layers. However, the mica content is low compared to the content of VMT layers or the interstratified mica VMT layers (Le Dred, 1968, Muiambo et al., 2010).

2.4. Sepiolite

Sepiolite is a natural hydrated magnesium silicate clay mineral. Sepiolite structural formula can be written as $Mg_8Si_{12}O_{30}(OH)_4(OH_2)_4.xH_2O$, ($x$=6-8). From the formula, (OH) indicates the hydroxyl group, (OH_2) group denotes crystal water and H_2O as zeolitic water. The unit cell parameters (a, b, c and β) determined for sepiolite are a=0.528 nm, b=2.695 nm, c=1.33 nm and β=90°). Sepiolite shows a microfibrous morphology with channels running parallel to the fibre length and a particular texture that provides a high specific surface area (200–300 m^2/g) and porous volume (0.4 cm^3/g) (Bergaya and Lagaly, 2013, Perraki and Orfanoudaki, 2008, Preisinger, 1963, Galan, 1996, Aranda et al., 2007, Choudhury et al., 2010, Volle et al., 2011, Bilotti et al., 2008, Nagata et al., 1974).

Like MMT and VMT, sepiolite is a 2:1 phyllosilicate. Sepiolite structure is composed of blocks of two tetrahedral silica sheets sandwiching an octahedral sheet of magnesium oxide hydroxide. The tetrahedral sheets are extended to a considerable distance in the ‘‘*a*’’ and ‘‘*b*’’ directions. The blocks are linked by an inverted Si-O-Si bond forming an open channel (0.36 nm x 1.1 nm) similar to that of zeolites. The periodic inversion of the SiO_4 tetrahedral determines a regular discontinuity of the sheets, which is the origin of the structural cavities (*tunnels*) extending along the c-axis. Due to the discontinuity of the external silica sheet, a significant number of silanol (Si–OH) groups are present at the surface of the sepiolite, generating a microporous structure with a large surface area, which is responsible for its adsorption properties. In addition, the isomorphous substitution of Al^{3+} for Si^{4+} in the tetrahedral sheets of the lattice of sepiolite forms negatively charged adsorption sites. Such sites are occupied by exchangeable cations (Na^+, Ca^{2+}, etc.) that compensate for the electrical charge at the sepiolite surface, resulting hydrophilic environment at the surface (Choudhury et al., 2010, García-López et al., 2010, Brauner and Preisinger, 1956, Ahlrichs et al., 1975,

Casal et al., 2001, Rytwo et al., 2002, Grim, 1968, Özcan and Özcan, 2005). A schematic presentation of sepiolite clay mineral structure is shown in Figure 2.5.

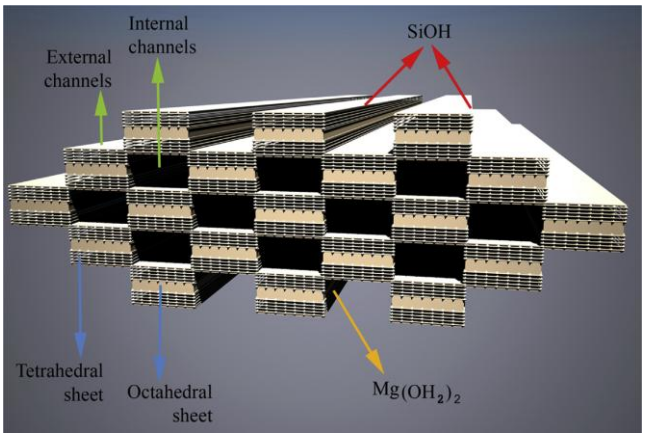

Figure 2.5. The structure of sepiolite (Adapted from Soheilmoghaddam et al., 2014).

The essential features of the sepiolite are: (a) the continuous tetrahedral basal oxygen planes, (b) the inverted tetrahedral arrangement that forms ribbons of joined pyroxene-like chains, and (c) the discontinuous tetrahedral sheet (Bergaya and Lagaly, 2013). Compared with layered MMT for example, the morphology of fibre-like sepiolite provides a higher specific surface area and the smaller contact surface between the nanoclay particles. This is what also makes this interesting and attractive material for nanocomposites technology. With these characteristics, polymer chains have a better chance not only of interacting with the external surface of the sepiolite but also of penetrating into the structure, which facilitates a dispersion of the clay in the polymer matrix more uniformly than those plate-like clays. The better dispersion of the clay will further improve the mechanical and thermal properties of nanocomposites (Lu et al., 2005, García-López et al., 2010, Xie et al., 2007, Liu et al., 2012).

The adsorption properties presented by these fibres, along with the elongate habit of the minerals, make them particularly useful in many industrial applications (Murray, 2000). Table 2.2 summarizes the important industrial uses of sepiolite.

Table 2.1. Industrial uses of sepiolite (Adapted from Murray, 2000).

Drilling mud	Cat box absorbents	Paper
Paint	Suspension fertilizers	Pharmaceuticals
Agricultural carriers	Animal feeds bondants	Anti-caking agent
Industrial floor absorbents	Catalyst supports	Reinforcing fillers
Tape joint compounds	Adhesives	Environmental absorbent

2.5. Clay surface modification

Surface modification of clay minerals has become important for improving the practical applications of clays and clay minerals. Traditional applications of modified clays are numerous. Some of the more important applications include their use in polymer nanocomposite technology; as adsorbents of organic pollutants in soil, water and air; rheological control agents; paints; cosmetics; refractory varnish; thixotropic fluids, etc. (Carrado, 2000, Van Oss and Giese, 2003, de Paiva et al., 2008).

The different approaches used to modify 2:1 clay minerals are listed by Bergaya and Lagaly (2001):

- Adsorption;
- ion exchange with inorganic cations and cationic complexes;
- ion exchange with organic cations;
- binding of inorganic and organic anions, mainly at the edges;
- grafting of organic compounds;
- reaction with acids;
- pillaring by different types of poly(hydroxy metal) cations;
- interlamellar or intraparticle and interparticle polymerization;
- dehydroxylation and calcination;
- delamination and reaggregation of smectitic clay minerals, and;
- physical treatments such as lyophilisation, ultrasound, and plasma.

2.5.1. Organomodified clays for polymer nanocomposite technology

Most of the polymer/clay nanocomposites have been prepared using organomodified clays as raw materials.

In polymer nanocomposite technology the surface modification aims to make the surface of the clay compatible with a polymer of interest. Layered silicates in their pristine state exhibit a hydrophilic nature and are only miscible with hydrophilic polymers, such as poly(ethylene oxide) and poly(vinyl alcohol) (Aranda and Ruiz-Hitzky, 1992, Greenland, 1963). However, most polymers are hydrophobic. To allow them to be miscible with hydrophobic polymers, the surface layers should be modified through an ion exchange reaction with an inorganic or organic onium ion. The process of such substitution is called intercalation. It lowers the

surface energy of the clay layers and makes it possible for organic species to diffuse into the gallery between the clay sheets. The replacement of inorganic exchange cations by organic onium ions on the gallery surfaces of clays not only serves to match the clay surface polarity with the polarity of the polymer, but it also expands the clay galleries. This facilitates the penetration of the gallery space by either the polymer precursors or preformed polymer (Alexandre and Dubois, 2000, LeBaron et al., 1999).

Ion exchange reaction with cationic surfactants including primary, secondary, tertiary, and quaternary alkylammonium or alkyl phosphonium cations (Ray and Okamoto, 2003) is well-known and the preferential method to modify the surface of the clay. In this reaction (Figure 2.6), the inorganic, relatively small (sodium) ions are exchanged against more voluminous organic onium cations. The ion-exchange reaction has two fundamental consequences: firstly, the gap between the single sheets is widened enabling polymer chains to move in between them and secondly, the surface properties of each single sheet are changed from being hydrophilic to hydrophobic (Fischer, 2003).

The capability of the clay to exchange ions is quantified by a specific property known as the cation exchange capacity (CEC) and it is determined by the nature and extent of the isomorphous substitutions in the tetrahedral and octahedral layers and therefore on the nature of the soil where the clay was formed (Kornmann et al., 2001, Manias et al., 2001). A typical ion-exchange reaction is illustrated schematically in Figure 2.6.

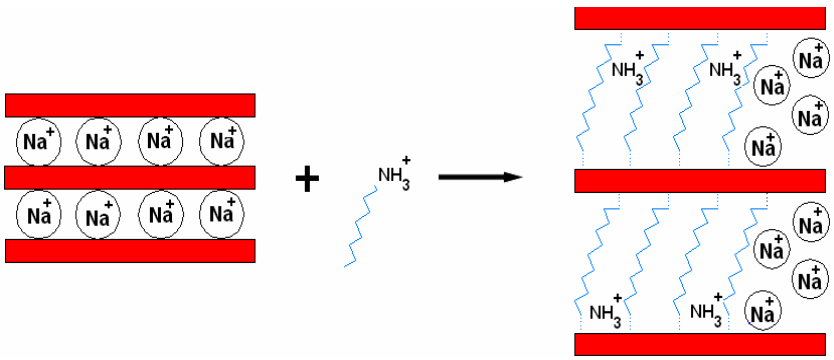

Figure 2.6. Surface modification of clay by ion exchange reaction (intercalation), where Na cations are replaced by cations of the surfactant (Adapted from Kaya, 2006).

2.5.2. Organomodified clay structure

In order to describe the structure of the interlayer in organoclays, it is believed that to counter the negative charge on the surface, the cationic head group of the alkylammonium molecule

preferentially resides at the layer surface, leaving the organic tail radiating away from the surface. Two parameters then define the equilibrium layer spacing in a given temperature range: the cation exchange capacity of the layered silicate driving the packing of the chains and the chain length of organic tails (Alexandre and Dubois, 2000, Zanetti et al., 2000).

The orientation of the chains in the organic silicate was initially inferred from measurements of XRD and FTIR. Depending on the layer charge of the clay mineral and the chain length of the organic ion, different arrangements of organic molecules between the layers can be formed (Figure 2.7). The geometry of the surface and the degree of exchange can also influence. The organic ions may lie flat on the silicate surface as a monolayer or bilayer, or depending on the packing density and the chain length an inclined paraffin-type structure, with the chains radiating away from the silicate surface can be formed. In the pseudotrimolecular layers, some chain ends are shifted above one another, so that the spacing is determined by the thickness of three alkyl chains (Lagaly, 1981, Lagaly, 1986, Brown and Brindley, 1980, Weiss, 1963, Bergaya et al., 2006, Vaia et al., 1994).

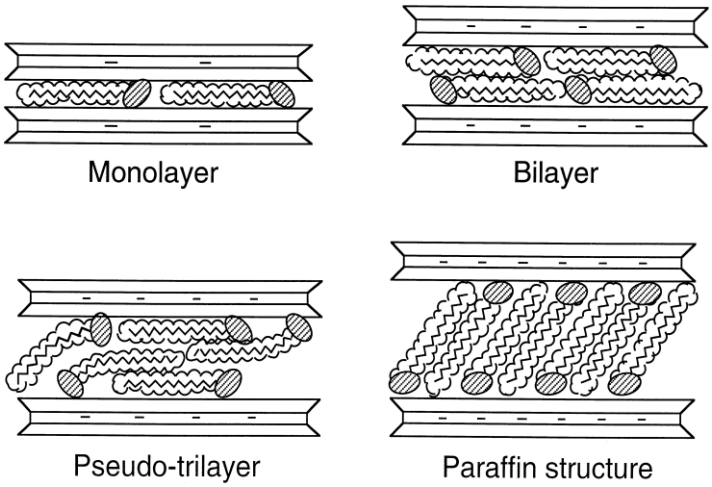

Figure 2.7. Orientations of alkylammonium ions in the galleries of layered silicates with different layer charge densities (Adapted from Lagaly, 1986).

The distance between the layers is strongly dependent on two parameters namely, the surfactant chain length and charge density of the clay. In general, the longer the surfactant chain length, and the higher the charge density of the clay, the further apart the clay layers will be forced. This is expected since both of these parameters contribute to increasing the volume occupied by the intragallery surfactant (LeBaron et al., 1999). The interlayer spacing increases with the increase in the size of alkylamine chain length. However, the interlayer

distance also depends on the way the onium ion chains organize themselves in the organoclay (Pavlidou and Papaspyrides, 2008).

The wet method, involving the contact of a dilute aqueous dispersion of layered silicates with ammonium salt solutions or melts of the guest compounds seems to be the best for preparing organophilic clays (Breakwell et al., 1995). The alkylammonium compounds may be adsorbed in excess of the cation exchange capacity of the clay implying the intercalation of ion pairs, although the extent to which this happens depends on factors such as alkyl chain length, layer charge and pH. Usually, the ion pairs are labile with respect to washing, although some material may be more tenaciously held. Alternatively the wet method, a "dry" method may be employed which involves the reaction of the clay and the surfactant at 60 °C in a high shear mixer. The "wet" process can aid the removal of non-clay impurities from the natural bentonites, but the product of the "dry" process will retain such material (Breakwell et al., 1995, Bergaya and Lagaly, 2001). Many organo-montmorillonites and vermiculites reported in the literature are produced using the above-described methods (Massinga and Focke, 2012, Merckel et al., 2012, Massinga et al., 2010, He et al., 2010, Breakwell et al., 1995, Zhu et al., 2008, Xu et al., 2005, Pérez Rodríguez et al., 1988).

The above-mentioned methods can also be applied successfully to the organophilization of sepiolite. However, some changes in methods should be introduced. For instance, if on the one hand the swelling capacity of bentonite is one of the determining factors for the success of the organophilization process, the same cannot be said for the sepiolite. The nano-rods of sepiolite are naturally aggregated together in raw minerals because of the presence of impurities such as carbonates, silicates, quartz, and so on. Unlike layered clays, sepiolite does not swell and exfoliate spontaneously in water. The sepiolite fibre dispersion requires mechanical mixing at the high shear rate for a relatively long time and at relatively high sepiolite concentrations as the higher density of fibre bundles produces an internal shear and friction that drags the individual particles from the bundles and produces an extensive disentanglement of fibres (García et al., 2011).

The number of sorption/modification sites available for each of these clays is one of the characteristics that mark the difference between them. The structure of the sepiolite presents three sorption/modification sites: (a) oxygen ions on tetrahedral sheets, (b) a small amount of cation-exchange sites, and (c) Si–OH groups along the fibre axis. Neither large molecules nor those of low polarity can penetrate the channels though they can be adsorbed on the external

surface, which accounts for 40–50% of the total specific surface area (Galan, 1996). The specific organic modifier can be introduced onto the sepiolite based on the surface reactive silanol groups, which it is a fundamental difference between sepiolite and laminar silicates such as MMT (García-López et al., 2010).

Although theoretically the organic modification of layered and fibre silicates can render them miscible with polymers, the process presents serious disadvantages. First of all, the use of cationic surfactants has limitations with respect to thermal stability. Alkylammonium surfactants chemically degrade around 180 °C. When using melt intercalation, for example (a process commonly carried out in excess of 200 °C), the surfactant molecules may degrade (Tjong, 2006). Another problem is that the surfactant molecules need to be chosen very carefully such that interaction with the polymer chains in the matrix is favoured above surfactant-clay and surfactant-surfactant interactions (LeBaron et al., 1999, de Paiva et al., 2008); otherwise, exfoliation will not be favoured in the thermodynamic sense. These observations imply that new routes of clay surface modification must be found. This was the main objective of the present research.

2.5.3. Characterization of modified clays

The first piece of information obtained on every new synthetic sample is an XRD pattern. The technique allows monitoring the effective intercalation of quaternary ammonium salts between the layers of clay minerals, observing the increase of interplanar distance $d(001)$, passing from values which are generally between 1.2 and 1.6 nm (depending on the humidity of the sample) to values located generally between 2.0 and 4.0 nm. The basal spacing value (determined from the Bragg's relation: $\lambda=2d\sin\theta$, where λ corresponds to the wave length of the X-ray radiation used in the diffraction experiment, d the spacing between diffractional lattice planes and θ is the measured diffraction angle or glancing angle) obtained varies according to the type, concentration and orientation of the surfactant used and preparation methodology. Changes in basal spacings are often an indication that organic has been incorporated within the interlayers during clay crystallization. However, to confirm the supposition based on basal spacings, more direct evidence of organic uptake is needed. This is done by TGA, microanalysis (CHN composition), and Fourier transform infrared (FTIR) spectroscopy. The FTIR spectrum of organoclays can provide detailed information on the interlayer structure and alkylammonium phase between the clay galleries. The results reveal

the frequency variations in strains and angular deformations of CH_2 and CH_3 groups of organic salts as a function of packing density, chain length and temperature. Thermogravimetric methods are used in order to study the thermal stability or behaviour of neat clay and their modified derivatives. Since weight loss between 200 and 600 °C is very low for the inorganic clay, any peak in a derivative plot of this region is indicative of the presence of organics (Carrado, 2000, Ray and Okamoto, 2003, Vaia et al., 1994, Breakwell et al., 1995). The other characterization techniques include scanning electron microscopy (SEM) and transmission electron microscopy (TEM).

2.6. Generalities about polymers

Polymers are made from organic, synthetic or natural macromolecules. Plastics and rubber are examples of synthetic polymers while the leather, silk, horn, cotton, wool, wood and natural rubber are made of natural organic macromolecules (Padilha, 1997). The polymers are organic compounds chemically based on carbon, hydrogen and the other non-metallic elements (such as oxygen, nitrogen and silicon). They are chemical compounds of high molecular weights, formed by the association of many small molecules (*monomers*), of the same or several different types, connected to each other by consecutive covalent bonds resulting from various addition reactions or condensation (Junior, 2002). The monomers are almost exclusively produced from fossil raw materials, especially oil, gas and coal occasionally (Piringer and Baner, 2008). Young and Lovell (2011) define a polymer as “a substance composed of molecules which have long sequences of one or more species of atoms or groups of atoms linked to each other by primary, usually covalent, bonds”. The emphasis upon substance in this definition is to highlight that although the words polymer and macromolecule are used interchangeably, the letter strictly defines de molecules of which the former is composed.

2.6.1. Macromolecule polymer chains

A polymer is prepared by stringing together a series of low molecular weight species (such as ethylene) into an extremely long chain (polyethylene) much as one would string together a series of beads to make a necklace. The chemical characteristics of the starting low molecular weight species will determine the properties of the final polymer (Barry et al., 2006). The formal definition of a *homopolymer* is a polymer derived from one species of monomer. However, the word *homopolymer* often is used more broadly to describe polymers whose

structure can be represented by multiple repletion of a single type of repeat unit which may contain one or more species of monomer unit. When a polymer is derived from more than one species of monomer the polymer is called *copolymer*. However, in accordance with the use of the word *homopolymer*, it is common practice to use a structure-based definition. Thus, the word *copolymer* more commonly is used to describe polymers whose molecules contain two or more different types of the repeat unit. The reaction for the formation of a *homopolymer* is called *homopolymerization* and the reaction for the formation of a *copolymer* is called *copolymerization*. The *copolymers* may have more than two types of chemical units in its chain. If the *copolymer* is formed by three different units, the resulting *copolymer* is called *terpolymer*. Acrylonitrile-butadiene-styrene is an example of a *terpolymer* (Young and Lovell, 2011, Junior, 2002).

2.6.2. Skeletal structure of polymers

The physical characteristics of a polymer depend not only on its molecular weight and form but also differences in the structure of the molecular chains. The modern techniques of synthesis of polymers allow considerable control over various structural possibilities. Several structures can be found, some of them are *linear*, *branched*, *crosslinked* and *network* structures. The linear polymers are those in which the repeating units are joined together at their ends into a single chain. In linear polymers, there may be large amounts of van der Waals bonds and hydrogen between the chains. Polymers, where branched side chains are linked to the main chain, can be synthesized; these polymers are called appropriately branched polymers. The branches, considered as part of the backbone molecule may result from parallel reactions occurring during the polymer synthesis. In crosslinked polymers, adjacent linear chains are joined to each other in various positions by means of covalent bonds. The process of crosslinking is achieved, or during the synthesis or by an irreversible chemical reaction. Often, this crosslinking reaction is obtained from atoms or molecules by covalent bonds into chains. The multifunctional monomers containing three or more active covalent bonds form three-dimensional networks and are called network polymers. Indeed, a polymer that possesses many crosslinkings can also be classified as a polymer network (Junior, 2002).

2.6.3. Classification of polymers

The response of a polymer to the application of mechanical forces in temperatures is related to its molecular structure. A classification of these materials is made according to their behaviour with increasing temperature during processing. This is the basis for their classification in thermoplastics, thermosets and elastomers. Thermoplastics are composed of thread-like chain molecules tangled together. This group of plastics takes its name from the properties resulting from such structures. Thermoplastics soften with increasing temperature, which allows them to be formed and then becomes hard again as they cool. Thermosets normally are rigid materials and are network polymers in which chain motion is greatly restricted by a high degree of crosslinking. Thermosets have all chains linked by covalent bonds in a network. Once crosslinked, thermosets cannot be reprocessed. A crosslinked network of covalent bonds polymer chains leads to the formation of elastomers which is another class of polymers. Elastomers are crosslinked rubbery polymers (i.e. rubbery networks) that can be stretched easily to high extensions (e.g. 3x to 10x their original dimensions) and which rapidly recover their original dimensions when the applied stress is released. This extremely important property is a reflection of their molecular structure in which the network is of low crosslinking density (Junior, 2002, Young and Lovell, 2011, Padilha, 1997, Piringer and Baner, 2008, Barry et al., 2006).

2.6.4. Biopolymers

Polymeric materials are gradually replacing the traditional inorganic materials such as metals and ceramic. The massive use of polymers in everyday life is driven by its remarkable combination of properties, low weight and ease of processing. However, the vast majority of polymers are derived from oil but the diminishing fossil resources, environmental and economical concerns are driving the development of bioplastics. Oil-based polymers are associated with environmental concerns and sustainability issues. When incinerated or degrade naturally they release the greenhouse gas (GHG), thus contributing to global warming. Bioplastics are either fully biodegradable polymers or polymers derived from renewable resources such as plant oils and agro-industrial waste (Hablot et al., 2010a, de Espinosa and Meier, 2011, Matadi et al., 2011, Petersson and Oksman, 2006, Satyanarayana et al., 2009, Mohanty et al., 2002, Lunt, 1998, Patel et al., 2005, Storz and Vorlop, 2013, Babu et al., 2013). Although biodegradability is important in some niche applications, the prevailing view in European countries is that it is more important for materials to be bio-

derived. PA-11 (manufactured from castor oil) and DAPA derived from other plant oils, e.g. sunflower oil are important examples (Hablot et al., 2010a).

The key difference between bio-based polymers and biodegradable polymers is presented by Babu et al. (2013): Biodegradable polymers are defined as materials whose physical and chemical properties undergo deterioration and completely degrade when exposed to microorganisms, via carbon dioxide (aerobic) processes, methane (anaerobic processes), or water (aerobic and anaerobic processes). Bio-based polymers can be biodegradable (e.g., poly(lactic acid) or nondegradable (e.g., biopolyethylene). Similarly, while many bio-based polymers are biodegradable (e.g., starch and poly(hydroxyalkanoates)), not all biodegradable polymers are bio-based (e.g., polycaprolactone).

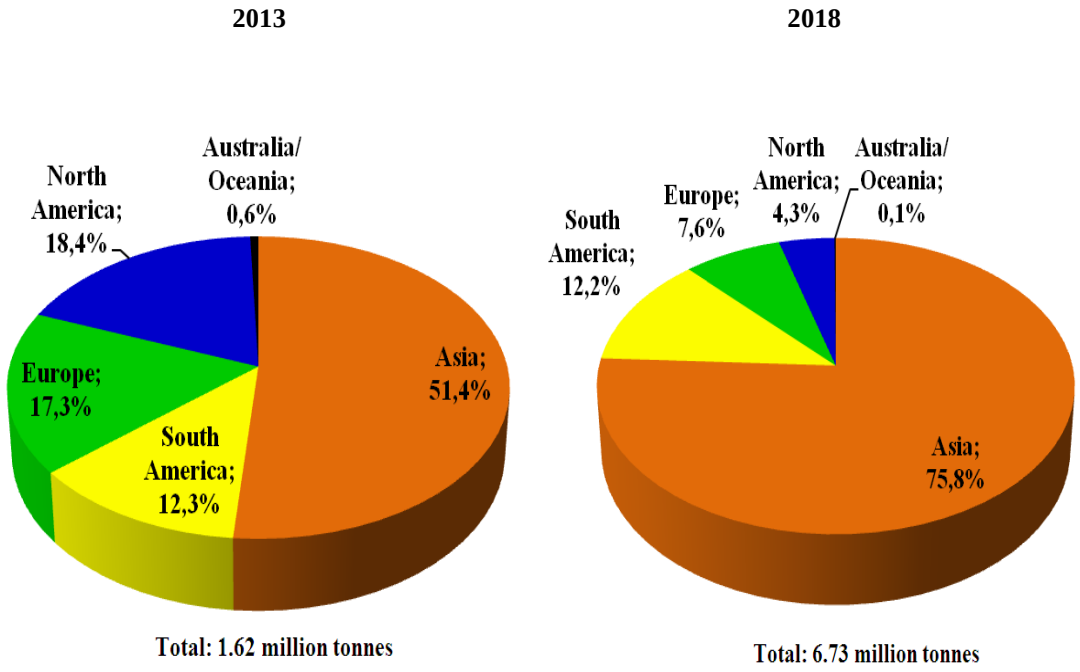

Figure 2.8. Evolution of the shares of bio-based polymers production capacities in different regions (Adapted from Aeschelmann and Carus, 2015).

Today bioplastics are becoming increasingly popular and they are seen as an environmentally-friendly material, with terms such as “renewable”, “recyclable” and “sustainable” becoming buzzwords (Hablot et al., 2010a, de Espinosa and Meier, 2011, Matadi et al., 2011, Lunt, 1998, Satyanarayana et al., 2009). The global bioplastics production capacity (Figure 2.8) is set to grow 400% from 2013 to 2018 (Aeschelmann and Carus, 2015), showing a clear indication of the industry's interest in replacing step by step the

oil-based polymers. Among the various environmental benefits of bioplastics as a result of using renewable resources to produce them are:

- Increasing resource efficiency:
  - Resources can be (at least) annually cultivated;
  - Principle of cascade use, (biomass first, then energy generation)
- A reduction of the carbon footprint and green house gases (GHG)
- Saving fossil resources, and for substituting them step by step
- Efficient Waste management:
  - Biodegradable plastics offer an additional end-of-life solution (composting);
  - Non-biodegradable plastics can be recycled or used for energy recovery.

2.6.5. Dimer fatty acid-based polyamides - Preparation routes and main applications

DAPA are a special class of biopolymers derived from plant oils (Hablot et al., 2010a, Türünç et al., 2012, Maisonneuve et al., 2013) such as soybean oil, which are composed of over 99% triglyceride molecules (La Scala et al., 2004). DAPA are made by a dimerisation process of unsaturated vegetable fatty acids. Such dimer acids together with other diacids and certain aliphatic diamines result in the desired polyamides by a polycondensation (Matadi et al., 2011).

Dimers of fatty acids, issued from vegetable oils and shown in Figure 2.9, are well-known and commercially available. With two reactive functions *per* molecule, they are good candidates to elaborate thermoplastic polyamides by polycondensation. Dimers of fatty acids are obtained by condensation of two unsaturated fatty acids such as oleic and linoleic acids, for example. They are valuable renewable building blocks for the synthesis of designed monomers in the search for specific polymer properties that do not require extensive chemical modification prior to their application. The wide chemistry that can be applied to fatty acids is reflected in a large amount of publications dealing with the use of fatty acids in the synthesis of valuable derivatives. With regard to polymer science, recent contributions show a growing interest in the use of fatty acids as precursors of monomers; not only because of their renewability but also because of the properties they can provide to the final polymers. Dimers of fatty acids are environmentally friendly chemicals, liquid at room temperature, noncrystalline, and have high molecular weights. The fatty acids commonly used in polymer chemistry are as follows: (i) oleic acid, (ii) linoleic acid, (iii) linolenic acid, (iv) erucic acid,

(v) petroselinic acid, (vi) ricinoleic acid, (vii) vernolic acid, (viii) 10-undecenoic acid. Compared to conventional polyamides, DAPA are less crystalline, more flexible and they feature lower water uptake and ease of processing (owing to a lower melt viscosity). These characteristics make these materials find application in the wood, furniture, shoe, electrical, automotive, textile, packaging and other industries as adhesives or sealants for joining, sealing or fixing (Hablot et al., 2010a, de Espinosa and Meier, 2011).

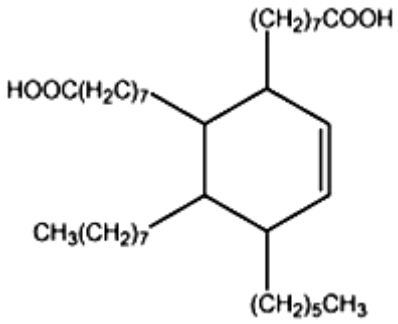

Figure 2.9. Dimer acid structure (Adapted from Hablot et al., 2010b).

Several syntheses based on dimers of fatty acids have been reported in the literature. Reaction kinetics, properties and structure of condensation between rapeseed oil-based dimer acid and tree aliphatic diamines, 1,2-diaminoethane, 1,6-diaminohexane or 1,8-diaminooctane was investigated by Hablot et al. (2010a). The reaction was studied in the temperature range of 50 to 180 °C. In a reactor equipped with mechanical stirrer, a thermometer, a nitrogen inlet and a Dean-Stark apparatus dimer acid and diamines were charged at 50 °C. For kinetics measurements, the aliphatic diamines (previously heated over its melting temperature) were added with a dropping funnel over a period of 3 min directly at 180 °C. After the addition of the diamine, samples were taken out of the reactor and then titrated for the analysis of acid and amine end groups. The reaction was carried out within 3 h (corresponding to the consumption of more than 99% of the acid groups). The final DAPA were found to be of yellowish colour, transparent and flexible at ambient temperature with a molecular weight of 14000 g/mol, a glass transition temperature as low as -10 °C and a fusion temperature exceeding 81 °C. They are considered as “bio-polyamides” since they contain around 85% wt of renewable resources. An investigation of the chemical reaction kinetics, thermal, physical and mechanical properties of the corresponding products allowed the authors to conclude that the chain length of the diamine has a great influence on the final properties of the materials. Biopolymers with greater chain length showed better properties than those with smaller chain length. More details about the method, structure and characterization properties are given in

the respective work (Hablot et al., 2010a). A similar route was performed with success by Hablot et al. (2010b), Hablot et al. (2010c) and Matadi et al. (2011).

2.6.6. Polyamide 11 - Preparation routes and main applications

PA-11 $[C_{11}H_{21}ON]_n$, one of the promising engineering plastics is a semicrystalline polymer that can be produced from renewable resources, such as castor oil or canola oil. Recently, although its impact properties, tensile strength, and thermal properties are somewhat poor PA-11 has attracted much attention due to its good oil and water resistance, as well as, excellent piezoelectric, cryogenic, electromechanical and ferroelectric properties (Hablot et al., 2010a, Wu et al., 1999, Takase et al., 1991, Yang et al., 2011, Spiccia et al., 2013).

Because of the excellent properties mentioned above PA-11 is widely used in industrial fields from automotive to offshore oilfield applications. The excellent oil resistance property makes PA-11 a prime candidate to be used as a barrier material in fuel lines (Zhang et al., 2012, Zhang et al., 2001, Hu et al., 2006).

PA-11 (Rilsan®), is synthesised by the condensation polymerization of the monomer 11-aminoundecanoic acid, which in turn is products from chemical conversion of ricinoleic acid, the major fatty acid component of castor oil (Spiccia et al., 2013, Ogunniyi, 2006). In this process, castor oil is hydrolyzed to give ricinoleic acid and glycerol, which are separated. High temperature treatment of the methyl ester of ricinoleic acid produces 11-undecanelic acid and heptanal (Dubois, 2012). Bromination of the double bond of 11-undecalenic acid followed by reaction with ammonia gives 11-aminoundecanoic acid (Polymer Innovation Blog). All the steps involved in the process are shown in Figure 2.10.

On the other hand, synthesis of nylon-11 monomer from an alternative renewable feedstock, namely canola oil is also reported (Spiccia et al., 2013). The main nylon-11 monomer in this process is the methyl 11-aminoundecanoate hydrochloride (11). This was generated by using a mild, multi-catalytic sequence, prepared in a three-step sequence from renewable, canola oil derived methyl undec-9-enoate (1) in 69% yield or 58% yield without the use of column chromatography. Canola oil is derived from rapeseed and possesses a high proportion of the mono-unsaturated C18 fatty acid oleic acid (Castor Oil Report, 2013).

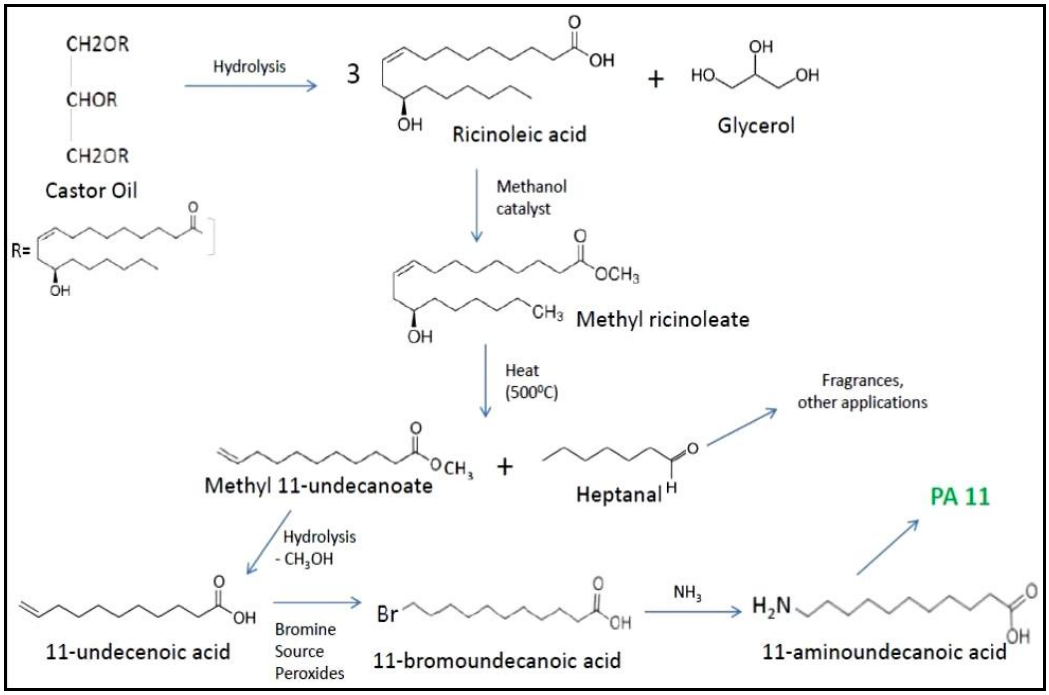

Figure 2.10. PA-11production steps from castor oil (Adapted from Polymer Innovation Blog, http://polymerinnovationblog.com/bio-polyamides-where-do-they-come-from/)

2.7. Polymer composites and nanocomposites

2.7.1. Polymer composites

Although polymers are being employed more and more as structural materials, their use is often limited by their relatively low levels of stiffness and strength compared, for example, with metals. Because of the need for light, stiff and strong materials for applications as diverse as aerospace structures and sporting goods, polymer composites with a specific combination of properties beyond those obtainable from a single material have been developed over recent years. Junior (2002) defines a composite as "a multiphase material made artificially in contrast with material that occurs or is formed naturally. In addition, the constituent phases must be chemically different and must be separated by a distinct interface". Also according to Junior (2002), in general, a composite may be considered as any multiphase material that exhibits a significant proportion of the properties of the constitute phases.

Polymer composites can be obtained through the use of copolymers or blends, but the specific aspect that characterizes composite materials is that they are made up of distinct phases with very different physical properties. They are often, but not exclusively, found to

consist of a relatively soft flexible matrix reinforced by a stiffer component. Sometimes, however, a softer phase is used to improve impact properties. An example is the addition of rubber particles to a rigid polymer to yield a rubber-toughened material. In some cases, a second phase is added to a polymer to improve properties other than just mechanical behaviour. The need for property improvement is not the only reason for the development of composite materials. For instance, polymers are often employed in low-cost high-volume applications where the addition of an inexpensive inert mineral filler may reduce the quantity of relatively expensive of the polymer used with no sacrifice in mechanical properties. Historically, the first type of synthetic polymer composites developed were formaldehyde-based resins filled with mineral particles or sawdust (Young and Lovell, 2011).

The most well-known polymer composites in industry are those filled with synthetic or natural inorganic compounds (commonly called conventional fillers). Conventional fillers are materials in the form of particles (e.g. calcium carbonate), fibres (e.g. glass fibres) or plate-shaped particles (e.g. mica). However, although conventionally filled or reinforced polymeric materials are widely used in various fields, it is often reported that the addition of these fillers imparts drawbacks to the resulting materials. The disadvantages include weight increase, brittleness and opacity.

2.7.2. Polymer nanocomposites

“A nanocomposite refers to every material that combines one or more separate components in order to improve performance properties, for which at least one dimension of the dispersed particles is in the nanometer range” (Kumar et al., 2009). Alexandre and Dubois (2000) defined it more narrowly stating that polymer nanocomposites are a new class of composites that are particle-filled polymers for which at least one dimension of the dispersed particles is in the nanometer range.

Fillers with at least one nanoscale dimension (nanoparticles) have proportionally larger surface area than their microscale counterparts, which favours the filler–matrix interactions and the performance of the resulting material. A uniform dispersion of nanoparticles leads to a very large matrix/filler interfacial area, which changes the molecular mobility, the relaxation behaviour and the consequent thermal and mechanical properties of the material. The interest of scientists in applying nanoscale fillers with a high aspect ratio (i.e., high specific surface area) into polymer matrices is the attainment of potentially unique properties.

In addition, to the effects of the nano-reinforcements themselves, an interphase region of altered mobility surrounding each nanoparticle is induced by the well-dispersed nanoparticles. This results in a percolating interphase network in the composite that plays an important role in improving the polymer nanocomposite properties (Kumar et al., 2009, Tjong, 2006, De Azeredo, 2009).

In fact, it is well established that dramatic improvements in physical properties, such as heat resistance, stiffness, strength, toughness, impact resistance, barrier properties, rheological properties, flame retardancy, etc., can be achieved by adding just a small fraction of clay nanoparticles to a polymer matrix, without impairing the optical homogeneity of the material. Since the weight fraction of the inorganic additive is typically well below 10%, the materials are also lighter than most conventional composites (Kiliaris and Papaspyrides, 2010, de Sousa Rodrigues et al., 2013, Arora and Padua, 2010, Utracki, 2008, de Paiva et al., 2008, LeBaron et al., 1999). The unique properties pointed out here make polymer nanocomposites ideal materials for products ranging from high-barrier packaging for food and electronics to strong, heat-resistant automotive components.

Among the various applications of polymer nanocomposites, automotive parts, packaging and electronics are the main nanocomposite applications on a worldwide basis. In 2013 for example, the automotive industry absorbed 51.4%, packaging industry with 22.5% and finally electronics with 13.8% of the market. By 2019, automotive parts' share is expected to drop to 40.6%, while electronics' share may drop to 8% (BCC Research).

The question arises how polymer nanocomposites differ from traditional composites and how they improve the properties so drastically? The distinguishing characteristics between conventional fillers and nanoscale particles have been explained by Vaia and Wagner (2004). Over the conventional micro-composites, the nanoscopic dimensions and inherent extreme aspect ratios of the nanofillers result in six interrelated characteristics, which distinguish the obtained nanocomposites:

- Low-percolation threshold;
- Particle–particle correlation (orientation and position) arising at low-volume fractions;
- Large number density of particles *per* particle volume;
- Extensive interfacial area *per* volume of particles;
- Short distances between particles; and

- Comparable size scales among the rigid nanoparticles inclusion, the distance between particles, and the relaxation volume of polymer chains.

2.7.3. Polyamide bio-nanocomposites

As previously stated, biopolymers originate from renewable resources such as plant oils and agro-industrial waste. However, compared to equivalent petroleum-based polymers, biopolymers often feature relatively poor properties. The brittle nature and a lack in toughness, poor thermal stability, and melt strength, for instance, are disadvantageous in practical processing especially in the film extrusion industry. These drawbacks plus higher costs make them less competitive and limit their use in most applications. The preparation of PA bio-nanocomposites by addition of inorganic fillers can significantly contribute towards improving biopolymer properties, allowing them to be used in a variety of applications.

It is well known that the first successful and the most studied polyamide system is PA-6/clay nanocomposite which has been well documented in the literature (Fornes et al., 2004, Fornes and Paul, 2003a, Fornes and Paul, 2003b, Fornes et al., 2002, Fornes et al., 2001, Cho and Paul, 2001, Shah and Paul, 2004, Chavarria and Paul, 2004, Vlasveld et al., 2005a, Vlasveld et al., 2005b, Vlasveld et al., 2005c, Vlasveld et al., 2005d, Touchaleaume et al., 2011). Since the first studies on PA-6/MMT nanocomposites obtained via in situ intercalative polymerization (Usuki et al., 1993), and probably the most important study in pioneering the polymer/clay field, a considerable range of other polyamides has been studied as hosting matrices for fabrication of polyamide nanocomposites. This include polyamides such as PA-66, PA-11, PA-12 and the emerging dimer fatty acid-based polyamides (Macheca et al., 2016, Gnanasekaran et al., 2015, Macheca et al., 2014, Zhang et al., 2012, Wang et al., 2012, Aldousiri et al., 2012, Mago et al., 2011, Yang et al., 2011, Lecouvet et al., 2011, Lao et al., 2011, Lao et al., 2010, Li et al., 2010, Lao et al., 2009, Chung and Das, 2008, Alexandre et al., 2006, Yu et al., 2004, Matadi et al., 2011, Hablot et al., 2010b, Hablot et al., 2010c, Song et al., 2008, Tarameshlou et al., 2007, Kalkan and Goettler, 2009, Liu et al., 2002).

Nevertheless, PA-6 remains a particularly successful choice for nanoclay nanocomposites preparation using either direct melt compounding or in situ polymerization or even solution casting method. The reason of the success of PA-6 lies essentially in the ease in obtaining efficient nanoclay dispersions due to the polarity of the matrix and the formation of strong

interactions (H-bonds) between polymer and nanofiller (Bilotti et al., 2009, Shen et al., 2005).

There is a vast array of both natural and synthetic layered crystalline fillers that are able, under specific conditions, to intercalate a polymer. Nanoparticles such as carbon nanotubes, carbon nanofibers and graphene have attracted enormous attention in recent years due to their remarkable physical characteristics, such as magnetic properties, extremely high Young's modulus and rupture strength, conductivity, and thermal stability, low mass density, high aspect ratio and diameters in the nanometer range. These properties make them an ideal reinforcing agent for high strength polymer composites (Arash et al., 2014, Spitalsky et al., 2010, Sahoo et al., 2010, Kuilla et al., 2010, Al-Saleh and Sundararaj, 2011, Coleman et al., 2006).

Presumably, incorporation of uniformly dispersed of carbon nanotubes, carbon nanofibers and graphene in polymer matrices can provide polymer nanocomposites with significantly improved strength and modulus, thermal, gas barrier, electrical and flame retardant properties compared to the neat polymer (Arash et al., 2014, Song et al., 2013, Liu and Kumar, 2014, Wang et al., 2008, Stankovich et al., 2006, Ansari and Giannelis, 2009, Ramanathan et al., 2008, Lee et al., 2009, Xu et al., 2009, Quan et al., 2009, Eda and Chhowalla, 2009, Liang et al., 2009, Kim and Macosko, 2009, Iijima, 1991, Fu et al., 2008).

However, significant agglomeration, difficult surface-modification, difficult processing and dispersion, inconvenience in large-scale syntheses and their relatively high cost obstruct their wide-ranging applications. Researchers in both academia and industry are looking for promising alternatives to take the place of such nanofillers in some applications (Gao et al., 2012, Wang et al., 2008). Clay minerals based on phyllosilicates have extensively been researched for last few decades. Economic and environmental aspects can be among the reasons for the large interest in clays. As native materials, clays are not expensive materials and are widespread in all countries. Even after the adequate required treatments, their price is still acceptable in view of the vast improvement in the properties of the unfilled polymer nanocomposites or as compared to the polymer nanocomposites filled with other conventional materials (Wang et al., 2008).

According to BCC Research, the global consumption of polymer nanocomposites has increased significantly, reaching 190,562 metric tons (Mt) in 2013. The global consumption

of polymer nanocomposites is expected to reach close to 585,000 Mt by 2019. The market share for the clay nanocomposite category is expected to increase to 60.2% by 2019 while the carbon nanotube nanocomposites' share should drop to 13.5%, and metal/metal oxide nanocomposites' share is expected to reach 7.7% of the market. The expected significant growth in the consumption of clay polymer nanocomposites clearly shows that the use of nanoparticulate clays for polymer nanocomposites technology is really a promising alternative to other nanofillers.

Among all clay mineral phyllosilicates, 2:1 type layered silicates are most popular for polymer nanocomposites technology. The crystal structure of the 2:1 type layered silicates consists of stacked layers made of two silica tetrahedrons fused to an edge-shared octahedral sheet of alumina (Figures 2.1 and 2.3). The large aspect ratios of layered silicates are believed to be mainly responsible for the enhanced properties of particulate–polymer nanocomposites when compared with a virgin polymer or conventional micro and macro-composites. Two particular characteristics of layered silicates that are generally considered for polymer layered silicate nanocomposites are: (1) the ability of the silicate particles to disperse into individual layers and (2) the ability to fine-tune their surface chemistry through ion exchange reactions with organic and inorganic cations. These two characteristics are, of course, interrelated since the degree of dispersion of layered silicate in a particular polymer matrix depends on the interlayer cation (Kiliaris and Papaspyrides, 2010, Fu et al., 2008, Ray and Okamoto, 2003).

MMT is the most commonly used layered silicate. Indeed, originally, the vast majority of the studies in polymer–clay nanocomposites concerned composites in which the inorganic component was an organically modified MMT (Lambert and Bergaya, 2013, Theng, 2012). As stated above, high particle aspect ratio is one of the most important parameters for the success in the preparation of clay-polymer composite. In the case of smectite, the aspect ratio is very high, close to 1000 (1 nm/µm). The BET specific surface area of a smectite powder lies between 30 and 130 m^2/g. The total specific surface area reaches 700-850 m^2/g when all the layers are accessible to interfacial contact with the polymer (Annabi-Bergaya, 2008). This can explain why smectites are the most preferred.

Although less frequently used than MMT, VMT has also been proved to be a nice reinforcement for the preparation of nanocomposites (Ballard and Rideal, 1983, Liu et al., 2003, Macheca et al., 2016, Nigam et al., 2012, Qian et al., 2011, Tjong and Meng, 2003a, Tjong and Meng, 2003b, Tjong et al., 2002, Xu et al., 2003, Valášková and Martynkova,

2012, Wang et al., 2009, Xu et al., 2003). As previously described, the higher charge density of the VMT sheets (a key parameter facilitating the incorporation of cationic organic modifiers to generate larger interlayer spacings), the formation of porous and highly fire resistant foams as a result of its spontaneous exfoliation at elevated temperatures (better fire retardancy effect to polymer composites), the formation of macroscopic crystals (that are potentially suitable for producing high-aspect-ratio nanofillers), the high absorbency and cation exchange property make VMT a great candidate to be used for polymer nanocomposites technology.

On other hand, much research work on polymer nanocomposites has been done based on sepiolite clay using a variety of polymer matrices (including the bio-based biodegradable polymers) (Basurto et al., 2013, Basurto et al., 2012, Bilotti et al., 2009, Chen et al., 2012, Chen et al., 2011, Choudhury et al., 2010, Franchini et al., 2009, Fukushima et al., 2012, García-López et al., 2010, González et al., 2012, Huang et al., 2012, Lee et al., 2002, Liu et al., 2012, Roy and Bhowmick, 2010, Soheilmoghaddam et al., 2014, Tartaglione et al., 2008, Torró-Palau et al., 1997, Xie et al., 2007, Yu et al., 2011). Improvements in mechanical and dynamic mechanical, fire retardancy, biodegradation, rheological, crystallization, viscoelastic, adhesion, thermal and barrier properties have been achieved by incorporation of fibrous sepiolite nanoparticles in polymer matrices. These improvements are even more than conventional macro- and micro-scale composites due to the strong interaction between the inorganic particles and organic polymer matrix, which plays an important role in improving the compatibility between polymer matrix and fillers. The strong interaction between the inorganic particles and the organic polymer matrix is mainly attributed to the large concentration of surface silanols (present as a result of discontinuity of the silica sheets) that are easily available for coupling reactions with local polarity on polymer chains.

The present section will highlight (where applicable) the major developments of PA-11 and DAPA/clay (or other fillers) nanocomposites. Because MMT and VMT are the two main chosen clays for the study, the content of the section will be based mainly on these two clays. However, sepiolite based polyamide bio-nanocomposites or composites will be briefly discussed where appropriate. The different prepared PA-11 and DAPA/clay (or other fillers) nanocomposites and their properties will be discussed. However, given that developments on nanocomposites of VMT and sepiolite using PA-11 and DAPA as host matrices are limited or almost non-existent, the discussions will be made based on other polymer matrices. This will

also include other polyamides and/or other biopolymers. On other hand, other fillers-based polyamide bio-nanocomposites or composites will be briefly discussed where appropriate.

a) Dimer fatty acid-based polyamide bio-(nano)composites

As previously stated, DAPA are a special class of biopolymers derived from plant oils. Compared to other polyamides, they are less crystalline, more flexible and they feature lower water uptake and ease of processing they feature lower water uptake and ease of processing (owing to a lower melt viscosity). These characteristics make these materials find application in the wood, furniture, shoe, electrical, automotive, textile, packaging and other industries as adhesives or sealants for joining, sealing or fixing. These properties can be enhanced by adding clay nanoparticles.

However, almost all the DAPA/composites reported so far were prepared using cellulose fibres. For instance, Hablot et al. (2010b) and Hablot et al. (2010c) have reported the synthesis of bio-composites of DAPA with cellulose fibres using melt processing method. Morphological observations of the corresponding bio-composites revealed a moderate interfacial adhesion between the fibres and the matrix. Dynamic mechanical spectra of these bio-composites showed an increase in the stiffness and higher thermal–mechanical stability. With the increase of the fibre content, tensile tests showed a high increase in Young modulus and yield stress, and a decrease in elongation at break. The resulting material exhibited a high increase in T_g and a decrease in the crystallization temperature and crystallinity degree.

Biocomposites based on DAPA with pure cellulose short fibres were also synthesized by Matadi et al. (2011) via melt processing method. The dynamic property results showed an enhancement of the Young's modulus, the yield stress, and the flow stress with increasing cellulose fibres content. It was also found that both systems, neat polymer and its composites were highly thermo-dependent and mechanically sensitive. According to the authors, the increase in strain rate led to the increase of polymer flow, with a very significant increase of strain hardening, indicating that the addition of cellulose fibres did not change the ability of the neat polymer to plastically deform. The addition of cellulose fibres showed no remarkable effect on the strain rate sensitivity.

The structure-gas transport properties in DAPA/Polyhedral oligomeric silsesquiloxane (POSS) nanocomposite were studied by Gnanasekaran and co-workers (2015). The DAPA/POSS nanocomposites were prepared by solution casting method. TEM images

revealed good dispersion of POSS into the membranes. The POSS particles were found to be in the range of 10 to 20 nm in size. Considerable influence of POSS on the T_g of the bio-nanocomposite membranes was observed. The free volume and density of the membranes decreased and increased, respectively with increasing POSS content.

The very first study on bio-nanocomposites based on DAPA with MMT as nanofiller was reported by Macheca and co-workers (2014). The bio-nanocomposites were prepared using a surfactant-free approach described in this work. DMA results showed an enhancement of the Young's modulus and a high increase in T_g.

Most recently, bio-nanocomposites based on DAPA with VMT (presumably the first report for DAPA/VMT nanocomposites) were also successfully prepared using a surfactant-free approach (Macheca et al., 2016). The content of VMT was varied from 5 to 30 wt %. At the loading level of 30 wt%, the tensile strength doubled, the modulus increased five-fold but the elongation-at-break decreased by a factor of ten. Dynamic mechanical analysis suggests three stiffening mechanisms namely, the reinforcing effect of the high stiffness inorganic flakes (found as the primary contributor), the chain confinement effect (that expresses itself in an apparent increase in the *Tg*), and the dynamic network formation based on fluctuating hydrogen bonding interactions between the matrix polymer chains and the filler particles.

These two pioneering studies (Macheca et al., 2014 and Macheca et al., 2016) were published as a result of the present PhD work. More details can be found in sections 4.3 and 4.4.

b) Polyamide-11 bio-nanocomposites

PA-11 possesses excellent piezoelectric behaviour, plus good cryogenic, oil resistance, and water resistance properties, although its impact properties, tensile strength, and thermal properties are somewhat poor. PA-11 is an important commercial PA used in a large range of industrial fields from automotive to offshore applications. These properties, however, can benefit from intercalation of clay nanoparticles. The pioneering work on PA-11 based clay nanocomposites obtained via melt-compounding was first developed by Liu and co-workers (2003). The results showed that the clay sheets were completely exfoliated at low clay loading (4 wt%). Thermal stability recorded by TGA of the nanocomposites was improved by about 20 °C when the clay loading was lower than 4 wt%. At higher clay concentrations the thermal stability significantly decreases. This behaviour was related to the relatively poor clay dispersion. With the clay loading of 8 wt% the storage modulus was increased by about

100% in comparison to PA-11. T_g steadily decreases by more than 10 °C as a function of clay loading and according to the authors, this was due to a plasticizing effect from the presence of organic surfactants within organoclay. Compared with neat polymer, the elastic modulus and yield strength of PA-11/organoclay nanocomposites were significantly enhanced.

Since this first work on PA-11/organoclay nanocomposites, a wide range of works on PA-11/clay nanocomposites has been carried out. Hu and co-workers (2006) have successfully employed nanoindentation technique to study mechanical properties (i.e. hardness and elastic modulus) of PA-11 and its nanocomposites with different clay loadings. The nanocomposite samples, with clay loading of 0, 1, 2 and 5 wt% were prepared by melt compounding using a Brabender twin-screw extruder at 220 °C with a screw speed of 80 rpm. Amorphous thin sheets with thickness of 1 mm for nanoindentation tests were prepared by compression molding in a press at a temperature of 220 °C with a pressure of 150 bar, quickly followed by quenching in an ice/water bath. The results revealed that the hardness and modulus of the nanocomposites steadily increased with increasing clay content. At clay loading level of 5wt%, both the hardness and elastic modulus were improved by about 30% in comparison to PA-11. PA-11/organoclay nanocomposites with improved mechanical and thermal stability properties have also been successfully prepared by melt-compounding or via in-situ intercalative polymerization (Fornes and Paul, 2004, Yu et al., 2004).

The presence of dispersed MMT clay in PA-11 matrix was also reported to increase the storage modulus and loss modulus and show stronger shear thinning behaviour than neat PA-11 (He et al., 2006, Zhang et al., 2006a). For instance, Zhang et al. (2006b) studied the rheology and morphology of PA-11/layered silicate nanocomposites. PA-11/organoclay nanocomposites samples were prepared via in situ polymerization. The results show that the clay was uniformly distributed in nylon-11 matrix during in situ polymerization of clay with 4 wt % or less. The presence of clay in nylon-11 matrix increased the crystallization temperature and the thermal stability of the nanocomposites. Rheological properties such as storage modulus, loss modulus, and relative viscosity have close relationship with the dispersion favorably compatible with the organically modified clay. Comparing with neat nylon-11, the nanocomposites showed much higher dynamic modulus and stronger shear thinning behaviour.

Zhang et al. (2004b) on other hand investigated the crystal morphology and crystallization kinetics of PA-11/MMT nanocomposites using polarized light microscopy, small-angle laser

scattering, and differential scanning calorimetry. The authors reported an increased crystallization rate with the addition of clay, while the Avrami exponent showed a reverse tendency to the increase in clay. The changes in crystal morphology and crystallization kinetics were attributed to the supernucleating effect of the nanodispersed clay layers.

The polymorphism behaviour in PA-11/MMT nanocomposites was studied by Zhang et al. (2004a) using a wide-angle X-ray diffraction (WAXD) and variable-temperature infrared spectroscopy. The PA-11/MMT nanocomposites were prepared by intercalating polymerization. First, 11-amin-oundecanoic acid was mixed with MMT modified by 11-aminoundecanoic acid, and then the mixture was polymerized by melt polycondensation. The content of MMT was 5 wt %. The results of WAXD and IR confirmed the presence of the γ-crystalline form of PA-11, which is induced and stabilized by MMT. However, the hydrogen bonds of PA-11 were found to be weak. This was attributed to the addition of MMT that restricts the formation of hydrogen bonding sheets by forcing the amide groups of nylon out of the hydrogen-bonding sheet.

In some applications require PA-11 grades with better fire performance, higher strength and improved heat resistance. The introduction of organomodified MMT clay, combined with conventional intumescent flame retardant additives has resulted in partial achievement of these requirements (Lao et al., 2011, Lao et al., 2010, Lao et al., 2009).

Most recently, Jariyavidyanont et al. (2016) studied the effect of sepiolite nanofiller on the crystallization kinetics of PA-11 nanocomposites. They found that at low cooling rates the presence of sepiolite has no effect on crystallization temperature of PA-11/sepiolite nanocomposites. However, at rapid cooling rates a distinct nucleating effect of sepiolite was detected. The critical cooling rate to suppress crystallization was found to increase from 600 K s^{-1} to about 1000 K s^{-1}. The crystallinity of PA-11/sepiolite nanocomposites was 5-10 % higher than in neat PA-11 when the cooling rate of solidification of the melt was applied. All measurement proved a saturation of the nucleation efficiency at the nanofiller loading of 2.5 wt%.

c) Other polymer nanocomposites based on vermiculite and sepiolite

VMT-based polymer nanocomposite coatings with improved gas barrier properties are reported in the literature (Mittal, 2013, Priolo et al., 2012, Qian et al., 2011, Takahashi et al., 2006, Ward et al., 1991). The gas permeability of the nanocomposite materials was decreased

remarkably by the presence of VMT. The permeability mechanism can be explained in terms of the tortuosity effect caused by the fact that diffusing species must migrate around the clay platelets (Nielsen, 1967). This forces the gas permeant to travel a longer path to diffuse through the film. The increase in path length is a function of the aspect ratio of the clay filler and the volume fraction filler in the composite.

VMT exfoliates spontaneously at elevated temperatures to form porous and highly fire resistant foams. Suitable inorganic and organic modification can even lower the onset temperature to fit polymer degradation temperatures (Muiambo et al., 2010). The fire retardancy effect arises from the exfoliating VMT forming a heat shield on the surface of a plastic part that is exposed to high temperature. With these heat-resistant characteristics, VMT has been proven to be an effective flame-retardant material (Chen et al., 2013, Cheong et al., 2015, Kozlowski et al., 1999).

Fukushima et al. (2010) studied the effect of sepiolite on the biodegradation of poly(lactic acid) (PLA) nanocomposites. They found that PLA and PLA/sepiolite nanocomposites seem to be mainly degraded by a bulk mechanism, showing a significant level of polymer degradation. The presence of sepiolite particles partially delayed the degradation. This behaviour was attributed to the preventing effect of sepiolite particles on polymer chain mobility and/or PLA/enzymes miscibility.

Two years latter Fukushima and co-workers (2012) again evaluated the effect of nature and content of clay on morphology, thermal and thermo-mechanical properties of PLA. Nanocomposites were prepared by melt blending at 5 and 7 wt% loading of an organically modified MMT or an organically modified magnesium sodium fluoro-hectorite or unmodified sepiolite. All nanocomposites showed good level of clay dispersion into the polymer matrix as well as a considerable thermal and thermo-mechanical properties improvement. According to thermal analysis, the clays seem to act as nucleating agents inducing a higher degree of crystallinity of the polymer and rate of crystallization. Similar increases in the thermal stability of PLA were obtained for all clays. However, needle like sepiolite shows thermo-mechanical improvements comparable to the layered silicates and an interesting ability to maintain high storage modulus values at increasing temperatures, due to its good dispersion within the polymer without the need of organic modifiers as instead necessary for layered clays used in that study.

Unmodified sepiolite was also used by Liu et al. (2012) to evaluate the structure and thermal properties of PLA-based nanocomposites that were prepared through a solution casting method. However, PLA-based nanocomposites containing organic modified sepiolite were also prepared using same conditions. Results showed that the bundles of sepiolite were dispersed into small aggregates containing several nanorods without destroying the crystal structure. Sepiolite nanofibers were well dispersed in the PLA matrix, exhibiting a randomly orientation with the contact among them in all cases. However, the thermal stability of nanocomposites was found to be improved more by introducing unmodified sepiolite than that with organic modified sepiolite. Molecular dynamics simulation results revealed that hydrophobic parts of organic modifiers seem to prevent the interaction between PLA molecules and sepiolite surface.

The structure and thermo-mechanical properties of PA-6 nanocomposites with lamella-type and fiber-type sepiolite were studied by Xie et al. (2007). The nanocomposite samples were prepared by the simple melt-compounding approach and compared with the common PA-6/MMT nanocomposites. The results suggested that sepiolite facilitates the formation of a-phase crystals of PA-6, which was quite different from the case observed in MMT-filled nanocomposites. Thermo-mechanical tests showed that heat distortion temperature and Young's modulus of sepiolite-filled nanocomposites were obviously improved compared with neat PA-6. Interestingly, sepiolite-filled nanocomposites exhibited the highest level of reinforcement on the Young's modulus, which may stem from the more efficient interfacial stress transfer. Bilotti et al. (2009) working on PA-6/sepiolite clay nanocomposites, that were obtained by melt compounding demonstrated that sepiolite has a higher reinforcing efficiency (higher effective aspect ratio) than MMT in PA-6 and a good filler-matrix interface, due to strong hydrogen bonds between silanol groups on the sepiolite surface and amide groups of PA-6.

2.8. Clay-polymer composite - Preparation methods

Property improvement of the clay nanocomposites are achieved through conventional processing techniques. There are three main methods used for this purpose according to the starting materials and processing techniques: (i) in situ polymerization; (ii) melt intercalation process; and (iii) solvent intercalation.

2.8.1. In situ polymerization process

In situ polymerization was the first method used to synthesize polymer-silicate nanocomposites based on PA-6 layers produced by the research group of Toyota. In this method, the layered silicates are swollen within the liquid monomer or a monomer solution so the polymer formation can occur between the intercalated sheets. Polymerization can be initiated either by heat or radiation, by the diffusion of a suitable initiator, or by an organic initiator or catalyst fixed through cation exchange inside the interlayer before the swelling step by the monomer. Polymerization produces long-chain polymers within the clay galleries. Under conditions in which intra- and extra-gallery polymerization rates are properly balanced, the clay layers are delaminated and the resulting material possesses a disordered structure. Under conditions where rates of intra-and extra-gallery polymerization are properly balanced the macromolecules molecular weight increases, leading to a *d*(001) increase and sometimes the clay layers are delaminated and the material acquires a disordered structure (Alexandre and Dubois, 2000, Beyer, 2002, Oriakhi, 1998, Pavlidou and Papaspyrides, 2008, Ray and Okamoto, 2003, Solomon et al., 2001).

It is believed that the polymerization is the indirect driving force for exfoliation. The clay, due to its high surface energy, attracts polar monomer molecules to their galleries until equilibrium is reached. The polymerization reactions occur between the layers of the lower polarity of intercalated molecules and shift the equilibrium. This allows new polar species to diffuse between the layers to gradually exfoliate the clay (Souza et al., 2006).

However, it is important to point out that although in situ polymerisation has proven success in the preparation of various layered-silicate nanocomposites disadvantages of this method have been reported: (1) the preparation route is very time consuming (a polymerization reaction may take more than 24 h); (2) exfoliation is not always thermodynamically stable, and platelets can reassemble during subsequent processing steps; (3) the process is only available to the manufactures of resin which are able to devote a production line to this purpose (Sepehr et al., 2005). The other disadvantage is that the method cannot be used to prepare nanocomposites based on biopolymers matrices such as polysaccharides (Chivrac et al., 2009). Despite the disadvantages outlined above in relation to in situ polymerization, this is the only viable technique for the preparation of nanocomposites based on thermosetting polymers.

2.8.2. Melt intercalation process

The preparation of nanocomposites via melt intercalation processes involves annealing, typically under shear of a mixture of polymers and layered silicates above the softening point of the polymer. During the annealing, the polymer chains diffuse from the polymer melt in the galleries between the layers of the silicate. And, if the surfaces of the layers are sufficiently compatible with the chosen polymer, or an intercalated nanocomposites or exfoliated nanocomposites can be formed. The driving force involved in this process is the enthalpic contribution of interactions between polymer and organoclay (Souza et al., 2006).

The process of intercalation of the polymer in the molten state is a flexible cost-effective commercial process. It is capable of generating a variety of products on a large scale because of its compatibility with the existing polymer processes such as extrusion. The melt processing is the most versatile and environmentally friendly among all the methods of preparation of polymer/layered-silicate nanocomposites since no solvents are needed and using this method it is possible to modify the nanocomposite structure by playing around with the melt-blending conditions. The melt intercalation method allows the use of polymers which were previously not suitable for in situ polymerization or solution intercalation (Alexandre et al., 2009, Giannelis, 1996, Liu and Wu, 2002, Pavlidou and Papaspyrides, 2008, Ray and Okamoto, 2003, Tjong, 2006).

However, with the melt blending method it generally becomes very difficult to obtain a good dispersion/complete exfoliated structures. The difficulty in dispersing the clay platelets comes from the facts that the silicate layers have lateral dimensions ranging from 100 to 1000 nm, and the incompatibility between silicate layers and polymer matrix, that even when delaminated cannot be placed completely randomly in the polymer (Baniasadi et al., 2010). Moreover, it is hard for polymer long chains to crawl into the interlayer space even after modification of layers surface. Other disadvantages of melt intercalation are related to a low thermal stability of the onium modifiers and sometimes of the matrix (Chivrac et al., 2009, Xie et al., 2001). The high residence times needed to enhance the clay exfoliation process favour the matrix degradation. In addition and as stated previously, alkylammonium surfactants chemically degraded around 180 °C. Melt intercalation process commonly occurs above 200 °C, leading to the degradation of organic surfactants.

2.8.3. Solvent intercalation process

Solution-blending is a two-stage process and is based on a solvent system in which the polymer is soluble and the clay (with van der Waals forces) is swellable, such as water or *N*, *N*-dimethylformamide, acetone, benzene, or toluene for pristine clay or organoclay. The clay is first swollen in a solvent, and then the polymer is added to the clay solution, and the polymer chains diffuse, intercalate, and displace the solvent molecules previously accommodated within the galleries. The second and final step is the removal of the solvent. This can be done or by vaporization, usually under vacuum, or by precipitation. After removal of the solvent, sheets return to join, compressing the polymer to form a nanocomposite structure. The structure of the nanocomposites obtained depends on molecular factors such as surface energy and interactions between the intermolecular and kinetic factors, including the solvent evaporation rate and shear mixing (Alexandre and Dubois, 2000, Pavlidou and Papaspyrides, 2008).

For the occurrence of the two steps, a negative change in Gibbs free energy is required. It is thought that the diminished entropy due to the confinement of the polymer is compensated by an increase due to desorption of intercalated solvent molecules. In other words, the entropy gained by desorption of solvent molecules is the driving force for polymer intercalation from solution (Aranda and Ruiz-Hitzky, 1992, Fischer et al., 1999, Ruiz-Hitzky and Aranda, 1990, Souza et al., 2006, Theng, 2012, Tunney and Detellier, 1996, Vaia and Giannelis, 1997).

Many polymer-layered silicate nanocomposites have been prepared using this technique. According to Pavlidou and Papaspyrides (2008), the first attempts involved the dissolution of the polymer in hot chloroform, in the presence of organomodified bentonites. But TEM and WAXS analysis did not show any intercalated morphology and much less an exfoliated structure. In the case of polymeric materials which are infusible and insoluble, even in organic solvents, the only possible route to produce nanocomposites with this method is the use of precursor polymers that can be intercalated into layered silicates and then thermally or chemically converted to the desired polymer.

However, despite a large number of nanocomposites have been produced by intercalation of the polymer in solution, the method has its disadvantages. For a given polymer a perfect combination of clay, the organic modifier and solvents are the key issue; otherwise, exfoliation will not be favoured in the thermodynamic sense. It is clear however that to

achieve the desired exfoliation of clays in the polymer the correct selection of the solvent is the first and important criterion. Furthermore, in the industrial point of view, this method can involve the use of large amounts of organic solvents, which are usually environmentally unfriendly, and economically prohibitive (Alexandre and Dubois, 2000, Ho and Glinka, 2003, Ray and Bousmina, 2005, Zanetti et al., 2000). The biggest advantage of this method is that intercalated nanocomposites based on polymers, with low or no polarity, may be synthesized.

2.9. Clay-polymer nanocomposite structure

For true nanocomposites, the clay nanolayers must be uniformly exfoliated and dispersed in the polymer matrix, as opposed to being aggregated as tactoids or simply intercalated. Depending on the nature of the components used (layered silicate, organic cation and polymer matrix) and the method of preparation, four types of composites may be obtained when a layered clay is associated with a polymer (Figure 2.11). When the polymer is unable to intercalate between the silicate layers, a phase separated composite, with the filler assuming a so-called tactoid structure (Figure 2.11A) is obtained. In this case, the properties fall in the same range as traditional microcomposites. The clay interlayer spacing is fixed in an intercalated nanocomposite (Figure 2.11B). The term intercalation describes the movement of atoms, ions or molecules into a layered host structure, often causing the swelling clay mineral. On the other hand, in an exfoliated nanocomposites, the average gallery height is determined by clay silicate loading. The difference between ordered (Figure 2.11C) and disordered (Figure 2.11D) exfoliated nanocomposites is that the former can be detected by X-ray diffraction and the latter is X-ray amorphous. Once nanolayer exfoliation has been achieved, the improvement in properties can be manifested as an increase in tensile properties, as well as enhanced barrier properties, decreased solvent uptake, increased thermal stability and flame retardancy (Alexandre and Dubois, 2000, LeBaron et al., 1999, Tjong, 2006).

Exfoliation involves a degree of separation of the layers of a host structure where individual layers or stacking of several layers, are dispersed in a solvent or polymer matrix. Exfoliation implies that the orientation between the layers of the host structure is lost and that interlayer cohesive forces are overcome (Bergaya and Lagaly, 2011, Bergaya and Lagaly, 2013).

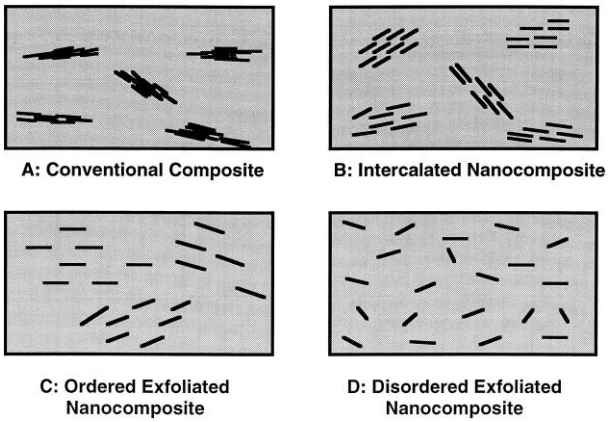

Figure 2.11. Scheme of different types of structures resulting from the interaction of layered silicates and polymers (Adapted from LeBaron et al., 1999).

A more realistic description of requirements that the system must satisfy in order to be qualified as a nanocomposite, which exhibits the useful properties describe previously has been proposed by Bhattacharya et al. (2008):

- The final state of the polymer/clay system must represent a thermodynamic equilibrium state. Otherwise, if it is not an equilibrium state, any change during a possible transition to an equilibrium or more probable state should not have a significant negative influence on the performance of the material during application in the field;
- In both intercalated and exfoliated nanocomposites, there must be sufficient adhesive or other interaction forces between the clay or organoclay and the matrix, so that the product can withstand the stresses and strain encountered under application conditions;
- The clay agglomerates, tactoids, or platelets must be distributed uniformly within the polymer matrix. This is achieved by distributive mixing. In exfoliated systems, the clay agglomerates must be separated into individual clay platelets distributed uniformly in the system;
- In intercalated systems, the polymer matrix must diffuse into the gallery space between the clay platelets. The rate of intercalation or exfoliation should be such that the process could be completed within the range of the acceptable overall processing time;
- While the matrix and/or the clay might undergo some changes during the nanocomposite synthesis process, these changes must not compromise the integrity of

the nanocomposites. Various chemical and physical changes normally occur during nanocomposite synthesis. This includes, for example, chemical degradation of the polymer and/or surfactant crystallization, phase and morphological changes, etc.

All of the above factors should be taken into consideration in nanocomposite synthesis and product and process design while taking into account the relevant fundamental principles of physics, chemistry, thermodynamics, kinetics, and mechanics.

2.10. Clay-polymer composite - Properties and characterization

Property improvements of the polymers in which layered silicate nanofillers are dispersed have been reported. This includes a large increase in Young's modulus of nanocomposites, their increased thermal stability, their unique ability to promote flame retardancy through the formation of insulating and incombustible char and their superior barrier properties against gas and vapour transmission have drawn attention (Alexandre and Dubois, 2000). Some of the properties discussed in the following sections are those that were also investigated in the present study.

There is a vast array of characterization techniques available for the analysis of polymer nanocomposite properties. X-Ray diffraction (XRD), transmission electron microscopy (TEM), scanning electron microscopy (SEM), atomic force microscopy (AFM), thermogravimetric analysis (TGA), differential scanning calorimetry (DSC), Fourier transforms infrared (FTIR) represent the most used techniques to characterize the physical properties of nanocomposites. Mechanical properties are frequently investigated by tensile and impact testing and dynamic mechanical analysis (DMA). Chemical properties of the polymer nanocomposites are examined through rheology, infrared (IR) and UV spectroscopy, gel permeation chromatography among others.

2.10.1. Physical properties

a) Morphology

WAXS analysis and TEM observation are the two techniques commonly used to characterize the structures of the nanocomposites and occasionally to study the kinetics of intercalation of the polymer melt. WAXS analysis allows the determination of the spaces between the structural layer silicates using Bragg's law, represented mathematically by $n\lambda = 2d\ sin\theta$ where λ corresponds to the wavelength of the radiation used in XRD experiment, d is the spacing

between the planes of diffractional network, θ is the diffraction measured angle and n is the order of diffraction (Pavlidou and Papaspyrides, 2008, Ray and Okamoto, 2003). By monitoring the position, shape and intensity of the basal reflections from the distributed silicate layers, the structure of nanocomposites can be identified. For an intercalated structure, the characteristic peak (001) tends to a regime of lower angle due to increased basal spacing. Although the spacing between silicate layers increases, there is an attractive force between them to stack them in an ordered structure. In contrast, there are no diffraction peaks observed in an exfoliated polymer nanocomposite structure due to loss of the layer silicate structure. The absence of Bragg diffraction peaks in nanocomposite may indicate that the clay has been completely delaminated or exfoliated (Tjong, 2006).

Although WAXS offers a convenient method for determining the interlayer spacing of the silicate layers in the original layered silicates and in the intercalated nanocomposites (within 1-4 nm), little can be said about the spatial distribution of the silicate layers or structural heterogeneities in nanocomposites. Clay dilution, preferred orientation, peak broadening, and mixed-layered morphology are factors that complicate the interpretation of the XRD patterns. When mixed structures of the composite are obtained, the pattern of the basal reflexions observed are more complicated and there will be uncertainties about the interlayer distance measured. In addition, some layered silicates initially do not exhibit well-defined basal reflections. Thus, owing to the peak broadening and the decrease in intensity the diffraction patterns become very difficult to study systematically. Some intercalated nanocomposites may even show a decrease in the interlayer spacing. Also, the absence of a characteristic peak does not necessarily mean that an exfoliated nanocomposite structure was obtained. Therefore, conclusions about the mechanism of formation of nanocomposites and structure based solely on WAXS diffraction are provisional at best (Ray and Okamoto, 2003, Samyn et al., 2008). Furthermore, TEM allows a qualitative understanding of the internal structure and can directly provide information in real space in a localized area on the morphology, structure and spatial distribution of the dispersed phase of the nanocomposite. Thus, WAXS and TEM techniques are considered to be complementary techniques for structural characterization of nanocomposite materials (Baniasadi et al., 2010, Horrocks and Price, 2001, Pavlidou and Papaspyrides, 2008, Tjong, 2006).

b) Thermal stability

Under normal conditions, thermal degradation derives from random chain scission events initiated by UV light and thermal energy and leads to oxidative degradation (Tyler, 2004). The thermal stability of polymers is usually studied by TGA, although DSC can also be used for this purpose. The sample mass loss due to volatilization of degraded by-products at high temperature is monitored as a function of temperature ramp (and/or time). When heating occurs under an inert gas flow, a non-oxidative degradation occurs, i.e. simple pyrolysis, while the use of air or oxygen allows one to follow the oxidative degradation of the samples (Bhattacharya et al., 2008).

The incorporation of clay into the polymer matrix was found to significantly affect the thermal stability of polymers including altering the structure and concentration of decomposition products both in the evolved gases and in the condensed phase (Baniasadi et al., 2010, Liu et al., 2003, Macheca et al., 2014, Macheca et al., 2016, Thellen et al., 2005, Wang et al., 2012, Zhao et al., 2005, Wu et al., 2010). The advantageous influence of clay on thermal stability of polymers clearly depends on the degree of intercalation/exfoliation of clay layers - the better dispersion of nanofiller is achieved, the more significant the enhancement of thermal resistance could be expected (Leszczyńska et al., 2007b, Liu et al., 2003). The layered silicates are thought to act as superior insulators and mass transport barrier to the volatile products generated during decomposition. This means that both intercalated and exfoliated structure create a labyrinth for gas penetrating the polymer bulk. This limits the oxygen diffusion into the nanocomposite sample. The increased thermal stability is particularly linked with flame retardancy properties. When nanocomposite samples are exposed to heat they exhibit more intensive char formation on the surface of the sample. The char protects the bulk of sample from heat and decreases the rate of mass loss during thermal decomposition of polymeric nanocomposite materials (Alexandre and Dubois, 2000, Leszczyńska et al., 2007a).

As mentioned before, the advantageous influence of clay on thermal stability of polymers clearly depends on the degree of exfoliation of clay layers in the polymer matrix, but in turn, the degree of exfoliation is related to the clay content. Several studies suggest that only exfoliated polymer nanocomposites exhibit improved thermal stability and lower clay loadings seem to favour the dispersion/exfoliation of clay since high clay loadings tend to lead to agglomerate formation within the polymer matrix. For instance, Liu et al. (2003)

studied the thermal stability of PA-11/organoclay nanocomposites. The thermal stability of the nanocomposites measured by TGA was found to be improved by about 20 °C when the clay loading was lower than 4 wt.%. However, the stabilization significantly decreased at higher clay concentrations (such as 8 wt.%).

Thermal degradation behaviour of PA-6/clay nanocomposites was studied by Pramoda et al. (2003). The onset temperature for degradation was found to be 12 °C higher for nanocomposite with 2.5 wt.% clay compared to the neat PA-6, indicating that the nanocomposite had a greater thermal stability than pure PA-6. However, the onset temperature for degradation remained almost unchanged for samples with loadings of 5, 7.5 and 10 wt.%. The findings were related to morphological observations that showed exfoliated structure only for 2.5 wt.% clay, and distinct clay agglomeration in nanocomposites with higher clay loadings.

c) Heat distortion temperature

Distortion or heat deflection temperature is the temperature at which a polymer sample deforms under a specific load. Thus, heat resistance is an index of a polymeric material to the applied load and is evaluated by the method described in ASTM D-648. In general, the improvements in heat distortion temperature are reported when clay-polymer nanocomposites are formed (Liu and Wu, 2002, Ray and Okamoto, 2003).

d) Barrier properties

In many applications such as food packaging industry the gas barrier properties of polymers are critical since the oxygen ingress determines the shelf life of the food in the package (Powell and Beall, 2007). Compared to metallic materials, polymers are quite stable in liquid media such as water, inorganic acidic or basic solutions, as well as in aggressive atmospheres. However, most polymers (thermoplastics and thermosets) absorb small amounts of water. On the other hand, many polymers are attacked and even dissolved by some organic solvents. Sometimes, the polymer does not become fully dissolved, but the penetration or diffusion of liquid to regions of the solute between the chains increases the separation between them and cause swelling. Furthermore, the material becomes softer and more ductile (Padilha, 1997).

Piringer and Baner (2008) described the process of diffusion or permeation of a substance through a polymer matrix in four basic steps:

- Adsorption of the substance on the surface of the polymeric substrate, in larger amounts on the liquid side where the concentration of the substance in the vicinity of the environment is highest;
- A solution of the substance in the first region near the surface;
- Diffusion trough the bulk of the polymeric substrate under the effect of a concentration gradient;
- Desorption of the polymeric substrate, in larger amounts from the side where the concentration of the substance in the vicinity environment is lower.

The permeability can be measured directly using a permeation cell, or indirectly in sorption/desorption experiments. More details about the procedures for the measurement of the permeability and the diffusivity, as well as the dominant mechanisms for the transport of small molecules in polymers and polymer nanocomposites, are given by Choudalakis and Gotsis (2009).

The barrier properties of polymers can be significantly altered by inclusion of inorganic platelets (clay layers). They alter the diffusion path of the penetrant molecules (Paul and Robeson, 2008). Since clay layers constitute a barrier to gases and water, this forces them to follow a tortuous path (Bharadwaj et al., 2002, Cabedo et al., 2004, Koh et al., 2008, Lagaron et al., 2005, Lotti et al., 2008, Mittal, 2013, Petersson and Oksman, 2006, Priolo et al., 2012, Qian et al., 2011, Takahashi et al., 2006, Ward et al., 1991). The improvement in the barrier properties is good news for biopolymer films since this minimizes one of their main limitations (Adame and Beall, 2009, De Azeredo, 2009). Through polymer films, for example, gas permeability can be reduced by 50–500 times even with low loadings of nanoclays (Choudalakis and Gotsis, 2009). The high aspect ratio characteristic of silicate nanolayers (obtained by an effective dispersion and exfoliation of the platelets into the polymer matrix) has been pointed out as the key factor for highly reduced gas permeability in films prepared from such nanomaterials (Alexandre and Dubois, 2000, Powell and Beall, 2007).

The improvement of barrier properties can be explained based on a theory developed by Nielsen (1967). It is commonly referred to as the tortuous path model. That is, when

impermeable nanoparticles are incorporated into a polymer, the permeating molecules are forced to wiggle around them in a random walk (Figure 2.12), and hence, diffuse by a tortuous pathway (Alexandre and Dubois, 2000, Pavlidou and Papaspyrides, 2008, Powell and Beall, 2007).

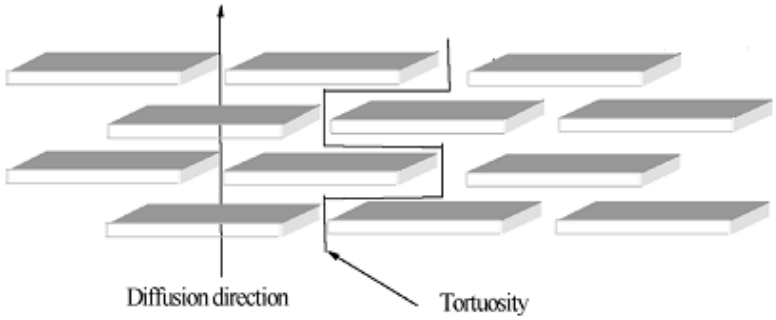

Figure 2.12. Tortuous path of a permeant in a clay nanocomposite (Adapted from Choudalakis and Gotsis, 2009).

On the other hand, there is a belief that improvement in the mechanical properties of composites automatically leads to enhancement in the barrier performance of the polymers. But this is not always true because barrier properties are more strongly affected by the changes at the organic-inorganic interface and by the increase in path length, which in turn the latter is a function of the high aspect ratio of the clay filler and the volume% of the filler in the composite. According to observations from studies of barrier properties, they appear to be most favoured by lower clay loadings (owing to the ease of exfoliation/dispersion of clay) than higher clay loadings (due to its tendency to agglomerate within the polymer matrix). For instance, Nielsen's model allows predicting permeability of systems at clay loading rates of less than 1%, but experimental data deviates significantly from predicted values at higher loading rates (and even more extensively in certain polymers) (De Azeredo, 2009, Mittal, 2009). Therefore, looking for the factors mentioned above is a clear indication that separate studies are required to completely understand the barrier performance of the systems.

However, although barrier properties of the polymer–clay nanocomposites are of immense importance for a number of applications, the relevant research concerns mostly oxygen, carbon dioxide and nitrogen barrier films for food packaging and carbonated drinks. Other applications include gas tanks and coatings (Choudalakis and Gotsis, 2009).

e) Flame Retardancy properties

Fire resistance of a material defines the ability of the material or structure to retard the spread of fire and maintain its mechanical integrity. In other words, fire resistance defines the ability of a construction to decrease the rate of a fire spreading from one room to adjacent rooms. Fire-resistance also describes the ability of a construction to retain the structural integrity (i.e., its shape and its load bearing properties) in a fire (Mouritz and Gibson, 2006).

f) Flame retardant systems

Polymeric matrices have been increasingly used in applications where flame retardancy behaviour is of fundamental importance. Flame retardant systems are designed to inhibit or interrupt the polymers combustion process described in the sections below. Depending on its nature, the flame retardant systems can act physically (for cooling, forming a protective layer or dilution of the fuel) or chemically (reaction in the condensed or gas phase). They can interfere with different processes involved in combustion polymers (heating, pyrolysis, ignition, propagation of thermal degradation) (Laoutid et al., 2009).

Flame retardants are classified as active or reactive compounds. Additive compounds are intimately mixed with the polymer during processing but do not chemically react with the polymer. The chemical composition of many of these compounds is based on the following elements: antimony, aluminium, boron, phosphorus, bromine or chlorine, where all confer a high level of flame retardants. It is estimated that about 90% of all additives are compounds based on these elements, and are used in the form of antimony oxide, alumina trihydrate oxides and boron oxides. Many additives exist as hydrated metal salts which endothermically decompose into a flame, and thus reduces the overall rate of heat release of the polymer. Some additive compounds also release water vapour during the decomposition which dilutes the concentration of combustible gases released in the flame. Reactive compounds are polymerized with a resin during processing to become integrated into the molecular network structure. Reactive flame retardants are mostly based on halogens (bromine and chlorine), inorganic phosphorus and melamine compounds. Until very recently, bromine and chlorine were the most common retarders because of its capacity to eliminate flame. Halogenated compounds flammability resistance conferred by the release of reactive bromine or chlorine species to which interfere with the free radical combustion reactions in the flame (Mouritz and Gibson, 2006).

g) Fundamentals of polymer combustion

When exposed to sufficient heat, polymer decomposes generating flammable gases that mix with the ambient air oxygen to form a flammable mixture. Ignition can occur both due to the presence of an external source or impulse, or if the temperature is suitable for self-ignition.

After ignition heat is released, which in part is fed to the pyrolysis region causing additional substrate decomposition. If the heat evolution is sufficient to keep the decomposition rate of the polymer higher than necessary to keep the concentration of volatiles within the flammability limits, then a cycle of self-sustaining combustion is established. The lifetime of the combustion cycle depends on the amount of heat released during the combustion of the fuel. That is, when the amount of heat released reaches a certain level, new decomposition reactions are induced in the solid phase and, therefore, more fuels are produced. The combustion cycle is well maintained, and called a fire triangle (Figure 2.13). Therefore, it is clear that the development of self-sustaining fire, three elements are essential: the fuel, heat and oxygen.

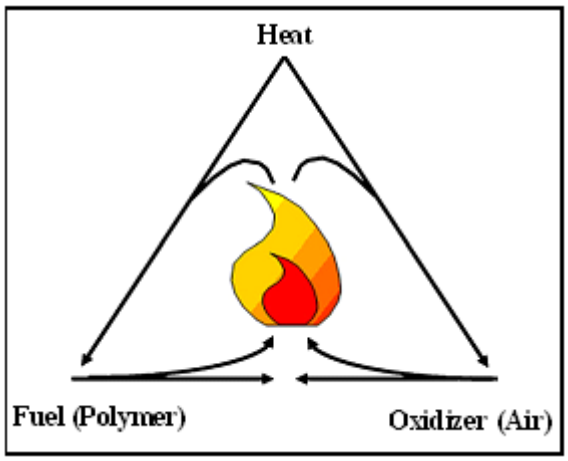

Figure 2.13. The principle of the combustion cycle (Adapted from Laoutid et al., 2009).

The nature of the combustion products is highly dependent on the chemical composition of the polymer and the conditions under which the burning process will occur. Smoke, in particular, is a combination of complete combustion species (CO_2, H_2O and acid gases) and incomplete (CO, soot and partially oxidized fuel gases), while the solid residue is mainly carbon and ash (oxidized metals) (Kiliaris and Papaspyrides, 2010, Laoutid et al., 2009).

h) Flame retardancy in clay-polymer nanocomposites

Plastics find many uses and contribute greatly to the quality of modern life. However, a major problem arises because many polymers in which plastics are based are organic and, therefore, inflammable. Most deaths in building fires are caused by inhalation of smoke and toxic combustion gases with CO the most common cause. Injuries typically result from exposure to the heat involved in these fires. In addition, the annual cost of damage to buildings and property loss are very high. Thus, there is great economic, sociological and legislative pressure on polymer industries for the production of materials with greatly reduced fire risk, i.e. materials with high fire resistance level (Horrocks and Price, 2001).

Traditionally, the flame retardancy has been achieved by using inherently flame retardant polymers, such as fluoropolymers or PVC, or by incorporation into the polymer flame retardants as mentioned above. However, these retardants have significant disadvantages. For example, for aluminium trihydrate ($Al_2O_3 \cdot 3H_2O$) and magnesium hydroxide ($Mg(OH)_2$) the application of very high loadings to be effective it is necessary. This results in high density and low flexibility of the end products as well as low mechanical properties and problems in the composition. On the other hand, the health concerns and the environmental impact caused by the compounds of bromine and chlorine released in vapour form made the halogenated additive unpopular in many countries. Furthermore, the addition of many flame retardants increases the production of soot and CO during combustion. Finally, the intumescent systems are relatively expensive and electrical needs may restrict their application (Pavlidou and Papaspyrides, 2008).

However, contrary to traditional flame retardants, the incorporation of layered silicates (e.g. MMT) in the polymer matrix produces nanocomposites with excellent fire resistance performance. The clearest evidence for the fire resistant character of the layered silicate-polymer nanocomposites was obtained from cone calorimetry experiments (Kiliaris and Papaspyrides, 2010).

i) Nanocomposite structure and fire retardant

There is strong evidence that the fire retardant properties do not depend on the nanocomposite structure, i.e., exfoliated or intercalated. The cone calorimetry technique is used to determine the fire retardancy of a material by evaluating the peak heat release. Through the peak heat release, it is also possible to assess whether or not there was a

dispersion of clay nanoparticles throughout the polymer matrix, which is only valid if the magnitude of the expected reduction is known. This is because the reduction in the peak heat release is different for each polymer. However, an interesting observation is that although the clay should be nanodispersed to affect the flammability of the polymer nanocomposites, it is not necessary that the clay layers are completely delaminated (exfoliated). In fact, excellent performance was observed in a nanocomposite material in which the clay layers were separated by only about 3 nm, which is regarded as being in the intercalation zone (Mouritz and Gibson, 2006, Pavlidou and Papaspyrides, 2008).

A qualitative interpretation of the effect of clay minerals is based on a very rapid formation of a durable carbon-silicate char layer at the surface as observed in the burn tests. Protective flocs are formed at the sample surface and as a consequence of the degradation of the resin to the sample surface (Galimberti et al., 2013).

2.10.2. Chemical properties

a) Rheology

In polymer research rheology has become a powerful tool, being envisaged as a technique that is complementary to traditional methods of materials characterization (e.g., XRD, SEM and TEM) and also considered as an important link in correlation chain from the catalyst over polymerization and chain structure to processing behaviour and final properties. Rheological properties are used to evaluate polymer resins properties for their suitability in processing operations. Rheological properties can also be used to gauge and predict the product quality during polymer converting processes (by injection moulding, extrusion, spinning, blowing, etc.) and the molecular orientations that are formed in these materials while in the molten stage during processing and when frozen to final products. In the thermoplastic polymers, for instance, the knowledge and moreover the design of flow behaviour is essential for all forms of production and processing, as big parts of this occur in the molten state (Gahleitner, 2001, He et al., 2006, Ramkumar and Bhattacharya, 1998, Wang et al., 2012).

With respect to polymer/layered silicate nanocomposites, the measurements of rheological properties are not only important to understand the knowledge of the processability of these materials, but is also helpful to determine the strength of polymer-layered silicate interactions and the structure–property relationship in nanocomposites (Ray and Okamoto, 2003). Viscoelastic properties in the molten state are generally useful to determine the structure and

properties relationships of these materials. The inter-particle and polymer-filler interactions can strongly influence both linear and nonlinear viscoelastic responses. Consequently, rheology appears to be a unique technique for the study of polymer nanocomposites (Cassagnau, 2008).

Pavlidou and Papaspyrides (2008) cited two reasons why, in the case of polymer–layered silicate nanocomposites, the study of rheological properties is instructive and why rheology can be envisaged as a tool that is complementary to traditional methods of materials characterization:

- These properties are indicative of melt processing behaviour in unit operations, such as injection moulding.
- Since the rheological properties of particle-filled materials are sensitive to the structure, particle size, shape and surface characteristics of the dispersed phase, rheology potentially offers a means to assess the state of dispersion in nanocomposites, directly in the melt state.

The rheological properties of composites provide important information on processing parameters, such as the viscosity and possible effects of deformation on the microstructure, including the extent to which the reinforcement has been distributed in the matrix (Satyanarayana et al., 2009). The rheological behaviour of nanocomposites depends on the degree of dispersion of organoclay aggregates, which in turn depends on the degree of compatibility between the polymer matrix and layered silicate, as is the case for polymer applications (Zhang et al., 2006b).

The extent of clay exfoliation can be estimated from the shear thinning behaviour of polymer composites (Szép et al., 2006). Steady shear viscosities for nanocomposites at low shear rates have been found to diverge from Newtonian plateau. The higher the filler concentration the larger is the divergence. At the low shear rate, the nanocomposites with very low amounts of silicates result in a high zero-shear viscosity value. However, above the percolation threshold, the zero-shear viscosity is not observed. Yield stress can be expected in the presence of small sized mesoscopic structures and also due to a decrease in the interparticle distance. The high viscosity at low shear rates points to strong interactions between the delaminated clay platelets and the polymer chains or, alternatively, the formation of network structures by clay

particle interactions. Pronounced shear thinning indicates extensive clay exfoliation in a given system. The nanocomposites internal structure is retained at low shear rates but at high shear rates the clay network structures break down and the platelets tend to orient in the flow direction. The resulting platelet alignment decreases the apparent viscosity so that it approaches that of the neat polymer melt. This ability to re-orient the silicates layers or tactoids in response to externally applied flows also controls the viscoelastic properties of the composites (Bhattacharya et al., 2008, Galimberti et al., 2013, Gupta et al., 2005, Szép et al., 2006, Wagener and Reisinger, 2003, Wang et al., 2012).

The measurement of the rheological properties of any polymeric material is usually conducted by dynamic oscillatory shear, steady shear and extensional flow measurements (Pavlidou and Papaspyrides, 2008). However, dynamic oscillatory shear and steady shear measurements as a function of the nanofiller concentrations (mainly between 0 and 10 wt.%) are the most commonly used. Steady shear measurements provide information such as apparent viscosity, shear thinning properties and first normal stress behaviour. Functions such as storage modulus (G'), the loss modulus (G") and dynamic viscosity (η^*) are estimated by dynamic oscillatory measurements (Bhattacharya et al., 2008).

Most of the steady shear measurements for nanocomposites are carried out using the rotational parallel plate and cone and plate geometries. Viscometric flow is assumed to have been generated in the fluid layer of an applied rate of shear. Most of the measurements are performed at or near the melting point of the matrix polymer and so, temperature control is necessary to avoid the effect of viscous heating. Rotational rheometers are suitable for low to medium range shear rate measurements of nanocomposites. In a rotational plate rheometer measurements above a shear rate range of approximately 10 s^{-1} are not appropriate since the material tends to extrude from the small gaps of the installed plate assembly, leading an inaccurate reading. The information regarding the extent and dynamics of a structure formed by particles in viscoelastic fluids is generated by dynamic measurements. When tested in the molten state, a parallel plate or a cone and plate assembly is normally used. Most dynamic tests are performed in the linear viscoelastic range of the material. In this range, the structure of the viscoelastic material remains unbroken throughout the measurements. The viscoelastic range is frequently tested by (i) dynamic strain sweep test (at different frequencies ranging from 0.1-100 rad/s); (ii) dynamic time sweep test; and (iii) dynamic frequency sweep test (Bhattacharya et al., 2008, Mezger, 2006).

b) Mechanical properties

Mechanical properties include all properties that determine the responses of polymers to external mechanical influences. They are manifested by the ability of these materials to develop reversible and irreversible deformations when subjected to these external mechanical influences (Lima, 2007). As mentioned before, mechanical properties are investigated by tensile testing, impact testing and dynamic mechanical analysis (DMA). In the tensile test, a specimen with standardized forms and dimensions is subjected to a uniaxial tensile force that tends to stretch it (Padilha, 1997). The tensile tests for polymers are based on ISO 527 or ASTM D-638, consisting of the application of a force in a longitudinal direction, stretching the material until the breakup of the same. Using this technique important information regarding the mechanical properties of a material is obtained. This includes maximum force of rupture, plastic and elastic deformation, modulus, cold flow, etc. DMA measures the response of the material to cyclic deformation (usually shear, tension or bending) as a function of temperature. When cyclical variations in stress and strain are involved, DMA properties are taken into account. It is a very useful technique for the characterization of the viscoelastic nature of polymers. There are three important parameters for the DMA (Bhattacharya et al., 2008, Khan et al., 2009), (i) the dynamic storage modulus - a measure of the energy stored in elastic deformation, (ii) loss modulus - a measure of damping material under dynamic loading, and (iii) tan δ - which is the ratio of the dynamic storage modulus and the loss modulus, useful to determine the occurrence of molecular mobility transitions, such as T_g.

Mechanical properties of polymer–clay nanocomposites are highly related to their microstructure which in turn is directly related to the exfoliation and dispersion of clay minerals consisting of layered silicates in the polymer matrix. Dramatic improvements in stiffness or Young's modulus can be achieved by adding either micro- or nano-particles since rigid inorganic particles generally have a much higher stiffness than polymer matrices. The large aspect ratios of layered silicates are thought to be mainly responsible for the enhanced mechanical properties of particulate–polymer nanocomposites (Fu et al., 2008, Tjong, 2006). In fact, the addition of layered silicates in the polymer matrix, assuming of course that the phases are compatible results in significant improvements in the modulus and tensile strength and impact when compared to the pure polymer material. In addition, the modulus tends to

increase as the particle size decreases because particles of small size have a higher possibility of dispersion in the polymer matrix (Khan et al., 2009).

DMA has also been extensively used for the polymer nanocomposites. The main conclusion derived from dynamic mechanical studies for nanocomposites is that the storage modulus and T_g increase upon dispersion of a layered silicate of high aspect ratio in a polymer. T_g improvement is generally attributed to restricted segmental motions near the organic-inorganic interface. The storage modulus increase is generally larger above the T_g, and for exfoliated polymer layered silicate nanocomposite structures is probably due to the creation of a three-dimensional network of interconnected long silicate layers, strengthening the material through mechanical percolation. Above the T_g, when materials become soft, the reinforcement effect of the clay particles becomes more prominent, due to the restricted movement of the polymer chains. This results in the observed enhancement of storage modulus (Alexandre and Dubois, 2000, Mittal, 2009, Pavlidou and Papaspyrides, 2008).

c) The reinforcing mechanism of layered silicates

Rigid fillers such as layered silicates are naturally resistant to straining due to their high moduli. Therefore, when a relatively softer matrix is reinforced with such fillers, the polymer, particularly that adjacent to the filler particles, becomes highly restrained mechanically. This enables a significant portion of an applied load to be carried by the filler, assuming, of course, that the bonding between the two phases is adequate. From this mechanism, it becomes obvious that the larger the surface of the filler in contact with the polymer, the greater the reinforcing effect will be. This could partly explain why layered silicates, having an extremely high specific surface area (on the order of 800 m^2/g) impart dramatic improvements of modulus even when present in very small amounts in a polymer (Affdl and Kardos, 1976, Pavlidou and Papaspyrides, 2008, Ray and Okamoto, 2003, Százdi et al., 2007).

d) Composite mechanics theories of conventional reinforcements

Composite mechanics theories of conventional reinforcements, such as flakes and fibres can be applied to explain the mechanical and fracture toughness properties of polymer–clay nanocomposites. For polymer manufacturing processes such as injection moulding, compression moulding, etc., many micromechanical models have been developed to predict the tensile moduli and tensile strengths of the particulate reinforced polymers. Table 2.3

provides a summary of the different theoretical models developed to predict the Young's modulus and tensile strengths of the particulate reinforced polymers.

Table 2.2. Summary of the different theoretical models developed to predict the Young's modulus and tensile strengths of the particulate reinforced polymers (Adapted from Yan et al., 2006).

Name	Models	Nomenclature
Guth model	For spherical particles $E_c = E_P\left(1 + K_E V_f + 14.1 V_f^2\right)$ For non-spherical particles $E_c = E_P\left(1 + 0.67\alpha V_f + 1.62\alpha V_f^2\right)$	*Ec* = Tensile modulus of the reinforced polymer *Ep* = Tensile modulus of the matrix K_E = Einstein coefficient V_f = Reinforcement volume fraction α = Reinforcement aspect ratio *A* = A constant which takes into account such factors as geometry of the reinforcing phase and Poisson's ratio of the matrix *B* = A constant which takes into account the relative modulus of the reinforcing and matrix phases *Em* = Tensile modulus of the reinforcement φ = A factor which depends on the maximum packing fraction ϕ_m of the reinforcement ϕ_m =Maximum packing fraction of reinforcement ν_1 = Poisson's ratio of matrix ϕ = Void content of composite V_p = Volume fraction of polymeric matrix (associated with zero void) χ = Modified void content (void relative to polymer phase) MRF = Modulus reduction factor G_p = Shear modulus of the polymer σ_c = Tensile strength of the composite
Halpin–Tsai–Nielsen model	$E_c = \frac{1 + ABV_f}{1 - B\varphi V_f} E_P$ where $B = \frac{\frac{E_m}{E_p} - 1}{\frac{E_m}{E_p} + A} \quad \varphi \cong 1 + \frac{1 - \phi_m}{\phi_m^2} ABV_f V_f$ with spherical reinforcements: $A = \frac{7 - 5\nu_1}{8 - 10\nu_1}$ with nearly spherical shaped reinforcements: $A = K_E - 1$	
Verbeek model for tensile modulus	$\phi = \frac{(1 - V_p)^2 \phi_m}{1 - V_p \phi_m}$ $\chi = \frac{\phi}{V_p(1 - \phi) + \phi}$ $\varphi = \alpha \sqrt{\frac{(1 - \chi)^3 G_p}{E_m} \frac{V_f}{1 - V_f}}$ $\mathrm{MRF} = 1 - \frac{\tanh(\varphi)}{\varphi}$ $E_c = V_f E_m MRF + V_p E_p$	
Verbeek model for tensile strength	$u = \alpha \left(\frac{G_p V_f}{E_m (1 - V_f)} \right)^{1/2}$ $\mathrm{MRF} = V_f \left(\frac{\alpha}{u} \right) \left(\frac{1}{\tanh(u)} - \frac{1}{u} \right)$ $\sigma_c = V_p \sigma_p + K_3 \tau_p MPF$	

Nielsen model	$\sigma_c = \sigma_P\left(1 - V_f^{2/3}\right)K$	τ_p = Shear strength of the polymer K_3 = Correction factor MPF = Strength reduction factor σ_p = Tensile strength of the polymer K = Stress concentration factor
Nicolais–Narkis model	$\sigma_c = \sigma_P\left(1 - 1.21V_f^{2/3}\right)$	

e) Modelling the Young's modulus of polymer composites

One of the important utilization properties of any solid material is the Young's modulus. Young's modulus is the stiffness (the ratio between stress and strain) of a material at the elastic stage of a tensile test. It is markedly improved by adding micro- and nanoparticles to a polymer matrix since hard particles have much higher stiffness values than the matrix. For polymer composites, the stiffness depends significantly on particle loading, not particle/matrix adhesion, since the fillers have much larger modulus than the matrix. There is also a critical particle size, usually in nanoscale, below which the composite stiffness is greatly enhanced due to the significant effect of the particle size, probably caused by the much larger surface areas imparting a ''nano"-effect (Fu et al., 2008).

The Halpin–Tsai model (Equation 2.1) is the most widely used to predict the modulus of composites. The models generally include parameters such as the aspect ratio, volume fraction and the orientation of the reinforcement. However, the direct use of such micromechanical models for polymer–clay nanocomposites without taking into account the intrinsic hierarchical morphology of intercalated nanoclay with large surface area and expanded gallery spacing it appears to be inappropriate (Fornes and Paul, 2003b, Tjong, 2006, Tucker III and Liang, 1999).

The Halpin-Tsai equation mentioned above has the form:

$$\frac{E}{E_p} = \frac{(1 + \xi\eta V_f)}{(1 - \eta V_f)} \qquad (2.1)$$

where E is the composite tensile modulus in the longitudinal or transverse direction with respect to the alignment of particles, E_p is the tensile modulus of the matrix, V_f is the volume fraction filler and ξ is a shape factor that depends on the geometry of the filler particles and their relative orientation with respect to the load direction. The parameter η is given by

$$\eta = \frac{(E_f / E_p - 1)}{(E_f / E_p + \xi)} \tag{2.2}$$

where E_f is the tensile modulus of the filler. Van Es (2001) proposed corrected shape factor for platelet reinforcements for the longitudinal E_{CL} and transverse E_{CT} composite modulus as $\xi_L = \frac{2}{3}\frac{w}{t}$ and $\xi_T = 2$ respectively. Van Es (2001) also approximated the composite modulus of a matrix containing randomly oriented platelets using an averaging scheme as follow

$$E_C = 0.49E_{CL} + 0.51E_{CT} \tag{2.3}$$

where E_C is the composite modulus, E_{CL} and E_{CT} are evaluated from Halpin-Tsai equations using the respective shape factor ξ_L and ξ_T.

Halpin-Tsai equation was successfully used by Hablot et al. (2010b) and Macheca et al. (2016) to predict or correlate the modulus of DAPA/cellulose fibres composites and DAPA/VMT bio-nanocomposites respectively. For cellulose fibres, the model provided a good fit to experimental data for ξ value given by the fibre dimensions. However, the best fit of experimental results suggested that the enhancement of the Young's modulus was more related to good fibres dispersion than to strong interactions between the fibres and DAPA matrix since in such study a perfect adhesion was not achieved. The analysis of the variation in Young's modulus with VMT content supported the high aspect ratio nature of the flake reinforcement.

CHAPTER 3

3. EXPERIMENTAL

3.1. Materials

3.1.1. Clay samples

G & W Base and Industrial Minerals supplied Boane bentonite in purified form as a soda ash-activated dispersion. The pH of the bentonite slurry was 7.4, and the solids content was 19.2 wt.%. The cation exchange capacity (CEC) of this clay was 0.70 mEq/g. Vermiculite grade Superfine (1 mm) from Palabora mining (South Africa) was obtained from Mandoval Vermiculite. Commercial sepiolite (Pangel S9) was supplied by Tolsa, S.A, Madrid, Spain.

3.1.2. Chemicals

Acetic acid 100% (glacial), ammonium chloride, silver nitrate, acetone and deionized water were obtained from Merck Chemicals and used as received.

3.1.3. Polymer matrices

The amorphous co-polyamide (Euremelt 2138) was supplied by Huntsman Advanced Materials. According to the supplier, this grade of DAPA has a softening point in the range of 138–148 °C and an amine value of *ca*. 4 mg KOH g^{-1} polymer. The semi-crystalline polyamides (PA-11), Rilsan® Atofina BESNO TL and Rilsan® Atofina BESNO P20 TL were supplied by Arkema, France. The latter is a plasticized natural grade of PA-11containing 20 wt.% plasticizer and it was used to lower the viscosity of the former one.

3.2. Methods

3.2.1. General description of the "novel method" used in the present study

The main and "novel" point of the study is to get a "very" good compatibilization of the clay and the polymer matrix by organo-modifying the clay, "not" by surfactants, but by protonated polymer chains via solution route. This is what was called the "surfactant-free organomodification approach". The preparation procedure begins with the step of clay surface modification schematically represented in Figure 3.1. This clay surface modification route is basically an ion-exchange process. The composites are made by mixing an acetic acid

dispersion of partially delaminated clay particles with a solution of the polyamide in the same solvent.

The underlying principle for the success of the method is based on the following: bio-based polyamides are of low molecular mass and are soluble in a variety of organic solvents. They have amine end groups that are protonated when these polymers are dissolved in suitable carboxylic acids, e.g. acetic acid. This means that organomodification of the clays should be possible via solution intercalation of the polymer chains *per se* (Macheca et al., 2016, Macheca et al., 2014). The composites can be recovered via precipitation by adding water. More details about the preparation route are given in section 3.3.4.

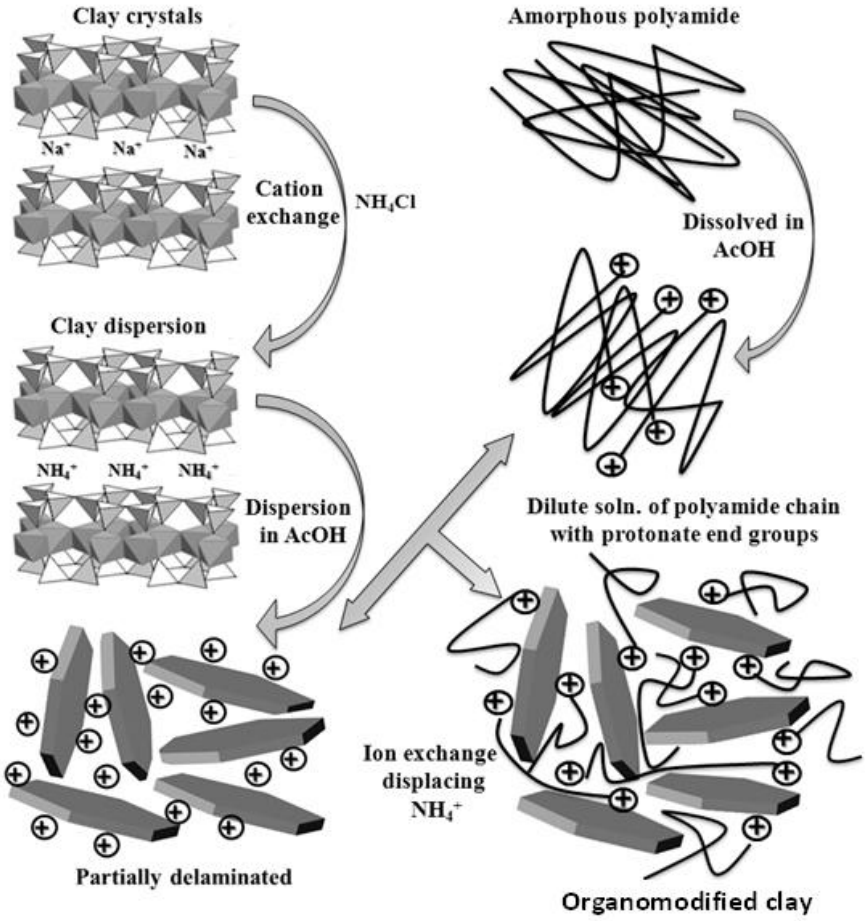

Figure 3.1. Schematic representation of the route to clay organomodification via solution intercalation of the polymer chains.

The clays of choice in the study were the standard smectite clays commonly used to prepare polymer-clay nanocomposites and vermiculite. They were ultimately chosen on the basis of

their ability to exfoliate into nano-thick sheets. The polyamides of choice as clay modifiers are DAPA. They were chosen for the reasons pointed out in Chapter 1.

As has been stated, this "novel" technique is of interest because it also allows organo-modification of the external surfaces of nano-sized clay sheets suspended in an acidic solution. This may facilitate clay dispersion and to prevent restacking when they are ultimately compounded into the polymer matrix. In addition, the solution route should enable the preparation of nanocomposites with relatively high clay contents (Macheca et al., 2016, Macheca et al., 2014, Nicolosi et al., 2013).

3.3. Samples preparation

3.3.1. Ammonium modification of clays

The ammonium exchanged MMT was prepared as follows: about 200 g of the bentonite slurry was suspended in 500 mL of a 1 M solution of NH_4Cl at a pH = 5. The suspension was stirred for 2 h at room temperature (RT) and centrifuged for 1 h. The supernatant was decanted and replaced with fresh ammonium chloride solution. This procedure was repeated four times. The ammonium exchanged MMT was washed with a large volume of deionized water until all Cl^- was removed (checked with $AgNO_3$ solution).

A similar procedure was used to prepare the ammonium exchanged VMT that was first washed with de-ionized water. The washing of VMT was carried out in order to remove soluble compounds and organic impurities by flotation. After the ammonium modification process, the flakes were dried in an air circulating oven at 60 °C for 48 h. The resulting product was then exfoliated using either thermal shock or by suspension in an 30% H_2O_2 aqueous solution and finally delaminated by sonication.

3.3.2. Exfoliation and delamination of vermiculite using thermal shock, chemical treatment with H_2O_2 and high power ultrasound.

Thermal exfoliation was achieved by exposing the material for 5 min to a temperature of 700 °C in a convection oven. The thermally exfoliated VMT flakes were then delaminated using a high power ultrasound. This was carried out at 20 kHz and 375W using an ultrasound probe (Sonics & Materials Inc., Model Vibracell VC375, 12.15 mm probe diameter). Typically, 2 g of clay were suspended in 300 mL of deionized water and sonicated for 2 h. The slurry was

allowed to settle for 2 h. Thereafter the supernatant was decanted. Water was added to the residue and the sonication proceeded for another 2 h. This process was repeated for a third time at which stage the remaining residue was discarded. Afterwards, all samples obtained in this way were combined to obtain the sonicated thermally-exfoliated VMT filler.

A similar procedure was used to prepare the sonicated H_2O_2-exfoliated VMT filler. However, instead of de-ionized water, 30% H_2O_2 solution was initially used as a medium. The chemical exfoliation was first performed by suspending 100 g amounts in 500 mL of 30% H_2O_2 solution at RT for 48 h. After the first sonication, the process used for the thermal-exfoliated VMT was followed. The combined H_2O_2 exfoliated and sonicated VMT samples were then washed with a large amount of de-ionized water to remove any residual H_2O_2.

3.3.3. Dispersion of clays using acetic acid as medium

The ammonium exchanged MMT and the sonicated VMT flakes were recovered by filtration and heated at 150 °C for 48 h to remove residual water. The filler powders were then re-dispersed in acetic acid at a solids content of 5 wt.%. Part of these dispersions was used to prepare DAPA based polyamide bio-nanocomposites via solution route. All the remaining dispersions were again washed several times with de-ionized water, dried in an air circulating oven set at 60 °C for 24 h and then crushed by milling to a powder for further analysis.

3.3.4. Preparation of MMT and VMT/bio-nanocomposites based on DAPA via solution route

In this step, DAPA was used as a clay surface modifier as well as a polymeric matrix. A typical preparation procedure for the DAPA clay composites was as follows: A weighed amount of the DAPA was first dissolved in acetic acid, corresponding to 10 wt.% of DAPA solution. In an 800-mL stainless steel container, a predetermined amount of 10 wt.% NH_4^+-MMT or NH_4^+-VMT (exfoliated by thermal shock and H_2O_2 treatment and/or sonication) dispersion in acetic acid was mixed at RT in a high shear mixer for 2 min. Then, 10 wt.% of DAPA solution was added drop by drop. After completion, mixing was continued for another 10 min. Then, deionized water was added during the mixing process in order to precipitate the polymer bio-nanocomposites. The precipitate was separated from the solution by decantation. The generated composites corresponded to targeted loads of ca. 7.5, 15 and 30 wt.% clay for NH_4^+-MMT and 5, 10, 20 and 30 wt.% clay for NH_4^+-VMT. The precipitates

were washed with deionized water. They were then immersed in a large amount of deionized water for 6 days. The deionized water was replaced with fresh water on a daily basis. Following these steps, the composites were allowed to dry at ambient conditions. Finally, they were dried in a convection oven at 60 °C for 24 h. Neat DAPA polymer was also subjected to the same procedure to prepare the sample used for property comparisons. Finally, thin polymer test sheets were made by hot pressing at temperatures between 160 and 180 °C for 15 min.

3.3.5. Preparation of VMT and PGS9/bio-nanocomposites based on PA-11 via melt compounding

In this step, PA-11 was used as a polymeric matrix while DAPA was kept as a clay surface modifier. Here again, the clay polymer bio-nanocomposites preparation begins with the step of clay surface modification and, this was done according to the procedures described in sections 3.3.1, 3.3.2 and 3.3.3. However, this was done only for vermiculite sample that was previously exfoliated by thermal shock and/or sonication. The resulting organomodified vermiculite (OVMT) corresponded to a load of *ca*. 74.6 wt.% DAPA. This sample was finally dried at RT for 6 days and then milled to a powder. Part of this powder was used to prepare PA-11 bio-nanocomposites via melt compounding process and the remaining one was kept for further analysis.

A typical preparation procedure for the final PA-11/Clay bio-nanocomposites was as follows: The OVMT and PGS9 (used as received) were melt compounded into the PA-11 to form products that contained either no filler, i.e. neat PA-11or 10% clay. The neat PA-11 considered in this study was a mixture of Rilsan® Atofina BESNO TL and Rilsan® Atofina BESNO P20 TL in the proportion, respectively of 25 and 75 wt.%. The Rilsan® Atofina BESNO P20 TL is a plasticized grade containing 20 wt.% plasticizer. This means that the mixture contained 15 wt.% plasticizer. Unmodified vermiculite (UVMT) that was also previously exfoliated by thermal shock and/or sonication was also melt compounded into the PA-11 for property comparisons.

The compounding process was carried out using a Nanjing Only Extrusion Machinery Co., Ltd (Model TE-30/600-11-40) co-rotating twin-screw laboratory extruder (diameter = 30 mm, L/D = 40:1) operating at a feed rate of 2 kg/h. The barrel temperature profile ranged from 70 to 230 °C and the screw speed was set at 27 rpm. The extrudate passed through a

cooling water bath system, palletized, and finally dried in a convection oven at 40 °C for 4 days.

3.4. Samples characterization

Elemental composition of clays was determined using X-Ray fluorescence (XRF) spectroscopy. The major elemental analysis was executed on fused beads using an ARL9400XP+X-ray fluorescence spectrometer. The samples were milled in a tungsten-carbide milling pot to achieve particle sizes <75 μm and dried at 100 °C and roasted at 1000 °C to determine the LOI values. Then 1 g sample was mixed with 6 g of lithium tetraborate flux and fused at 1050 °C to make a stable fused glass bead. The Thermo Fisher ARL Perform'X Sequential XRF with OXSAS software was used for analyses.

X-ray diffraction (XRD) was conducted on a PANalytical X'Pert Pro powder diffractometer with a X'Celerator detector and variable divergence and receiving slits with Fe-filtered Co Ka radiation (k = 0.17901 nm) in the 2θ range of 2 - 60° at a scan rate of 1.0°/min.

Fourier transform infrared (FTIR) measurements were done on Perkin-Elmer Spectrum RX I FT-IR spectrometer. Thin polymer test sheets were placed between two KBr crystal windows. The reported spectra represent averages of 32 scans in the wave number range of 4000–550 cm^{-1}, at a resolution of 2 cm^{-1}. The averaged data was background-corrected using a pure KBr pellet.

Thermogravimetric analysis (TGA) was performed on a Perkin Elmer Pyris 4000TGA instrument using the dynamic method. About 15 mg of the sample (clays or polymer composites) were placed in open 150 μL alumina pans. The temperature was scanned from 25 to 950 °C at a rate of 10 °C min^{-1} with air flowing at a rate of 50 mL min^{-1}.

Particle size distribution of the VMT samples, in the range 0.01 μm to 10 mm, was determined using the low angle laser light scattering (LALLS) method on a Malvern Mastersizer 3000 instrument. The refractive indices used were 1.520 (for VMT) and 1.330 (for water). Specific surface area (measured only for VMT samples) was determined using nitrogen and the BET method at liquid nitrogen temperatures with a Micrometrics Tristar II BET instrument. Prior to measurements, samples were degassed under vacuum (10^{-3} mbar) at 100 °C for 24 h. On the other hand, the particle size distribution by wet sieving **(**residue on 44 μm was 0.1%, residue on 10 μm was 2%, and residue on 5 μm was 97.9%) and the surface

area BET (320 m^2/g) of the sepiolite were taken from the technical data sheet provided by the clay manufacturer.

A Zeiss Ultra 55 FESEM Field emission scanning electron microscope (FESEM) was used to study the morphology of the clay samples and the fracture surface morphology of the composites at 1 kV. The composite injection moulded specimens were frozen in liquid nitrogen, cryo-fractured and vacuum dried. The clay samples and the fractured surface of the composite samples were coated with carbon using an EMITECH K950X sputter coater prior to analysis. Surface morphology of the polymers (measured only for DAPA/MMT bionanocomposites) was studied by atomic force microscopy (AFM) using a Nanoscope III AFM instrument and the imaging was done in contact mode at room temperature in air. The membranes were cut into small pieces and placed on a grid. The grid was covered using the commercial tip of Si_3N_4 provided by digital instruments. Cantilever length was kept at 200 μm with a spring constant of 0.12 N/m. The scan heads with a maximum range of 250 nm × 250 nm and Z scale: 250 nm. AFM images given in this work were reproducibly obtained over at least three points on the sample surface. A transmission electron microscope (TEM) (JEM 1200EX, JEOL, Tokyo, Japan) (acceleration voltage100 kV) was used to study the morphological structure of bio-nanocomposites. The samples were cry-sectioned using a diamond knife.

Melt viscosities were determined at 160 ºC in the steady shear, rotational mode. An Anton Paar Physica MCR301 rheometer with a CTD 600a convection hood and fitted with a 50 mm cone-and-plate measuring system was used. The gap was set at 51 μm and the shear rate was varied from 0.1 s^{-1} to 100 s^{-1}.

Dynamic mechanical analysis (DMA) were carried out using a PerkinElmer DMA 8000 instrument in the single cantilever bending mode using a displacement of the amplitude of 0.05 μm at frequencies 1, 10 and 100 Hz. The sample dimensions were as follows: length = 7.35 mm, width = 5.1 mm and thickness = 2.0 mm. The temperature was scanned from −40 to 100 °C for DAPA/bio-nanocomposites and from -150 to 140 °C for PA-11/bio-nanocomposites, at a scan rate of 1 °C/min.

Tensile test specimens were placed in the closed plastic container and maintained for moisture equilibrium at 25 °C and 50%RH for a week before the testing day. Saturated magnesium nitrate solution was used to meet required relative humidity. Mechanical

properties of the specimens were performed on a Lloyds Instruments LRX Plus machine fitted with a 5 kN load cell (ASTM D638). Initial grip separation and crosshead speed were set at 45 mm and 20 mm/min, respectively. Tensile strength, elongation-at-break and Young's modulus were measured and the results reported as averages of at least 7 specimens per sample.

The cone-calorimeter tests (measured only for PA-11/bio-nanocomposites) were performed on a Dual Cone Calorimeter (Fire Testing Technology, U.K.) according to ISO 5660-1. Three specimens of each sample were tested. The dimensions of the samples were 100 x100 x 3 mm. Each specimen was wrapped in aluminium foil and exposed horizontally to a 35 kW m^{-2} external heat flux. A hold-down frame was used to minimize the swelling of the samples. The exhaust gas flow rate was set at 24 L/s. The heat released was calculated from the oxygen consumption. The time to ignition was manually set from the computer's keyboard. The mass loss rate, and the heat release rate and its peak value were obtained from the Fire Testing Technology "ConeCalc" software. FESEM was also used to observe the morphologies of the residue samples (char) obtained from the cone-calorimeter tests. The samples were coated five times with a conductive layer of carbon prior to imaging using an EMITECH K950X sputter coater.

CHAPTER 4

4. RESULTS AND DISCUSSIONS

4.1. Clay characterization

4.1.1. Scanning electron microscopy (SEM)

SEM image with a magnification of 1000 times of the raw bentonite is shown in Figure 4.1. The clay featured some crystalline pseudo-hexagonal edges and semi-rounded micro-sized particles on the surface of the clay mineral particles. However, some irregularly shaped aggregates are also observed. Similar results were observed by Massinga et al. (2010). Most of the particles were much smaller than 10 µm in size and are arranged in face-to-face patterns.

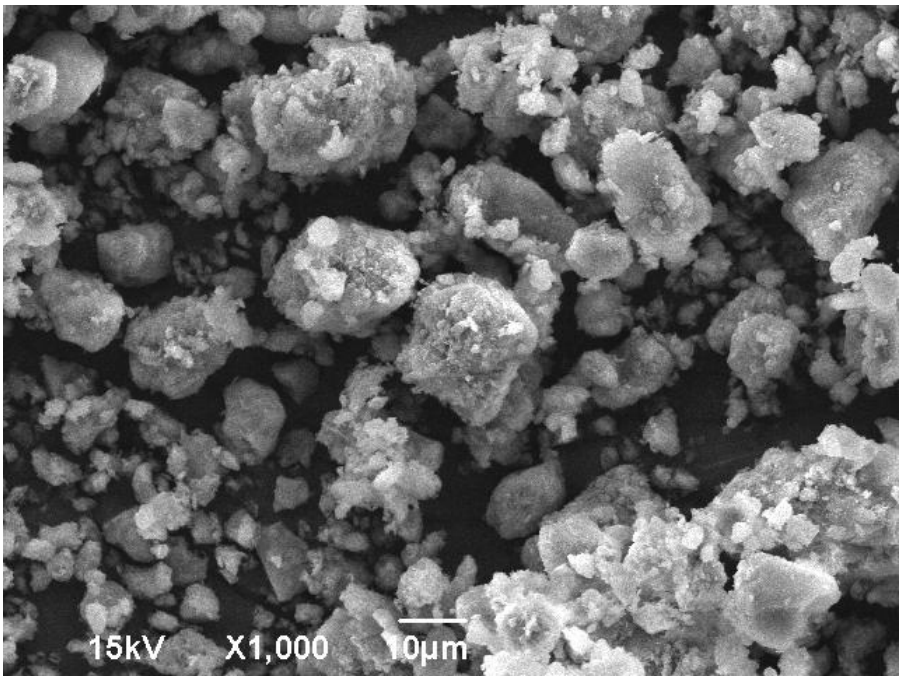

Figure 4.1. SEM image of Boane bentonite sample

SEM micrographs of the neat and ammonium VMT flakes are shown in Figure 4.2. Figure 4.2(a) and (b) and Figure 4.2(c) and (d) show edge-view SEM micrographs of the neat and ammonium-exchanged VMT flakes respectively, with flakes characteristics of a VMT material.

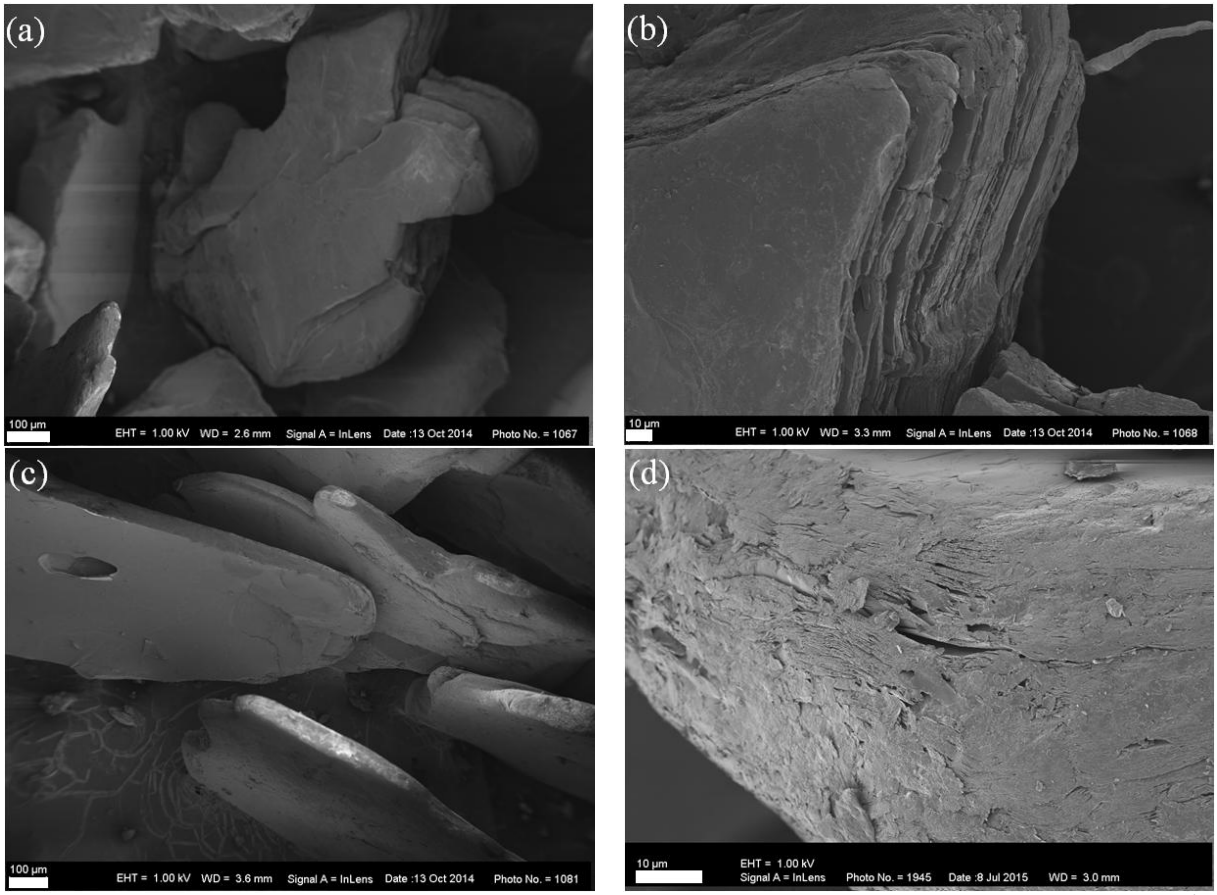

Figure 4.2. SEM micrographs of VMT samples: (a) and (b) Raw; (c) and (d) NH_4^+-exchanged.

SEM micrographs of the expanded VMT flakes are shown in Figure 4.3. Figure 4.3(a), (b), (c) and (d) shows the concertina-like expansion caused by a 700 °C temperature shock and chemical treatment with H_2O_2. From the figure, it is possible to see that after the thermal shock at 700 °C (Figure 4.3 (b)) and chemical treatment with H_2O_2 (Figure 4.3(a)) the expanded VMT particles formed "accordions", however, the individual sheets that make up the original flake remain attached to each other. Clearly the separation of the stacks is imperfect and the thicknesses of the flake lamellae formed are in the micrometre range, i.e. several orders of magnitude thicker than single VMT sheets (Macheca et al., 2016).

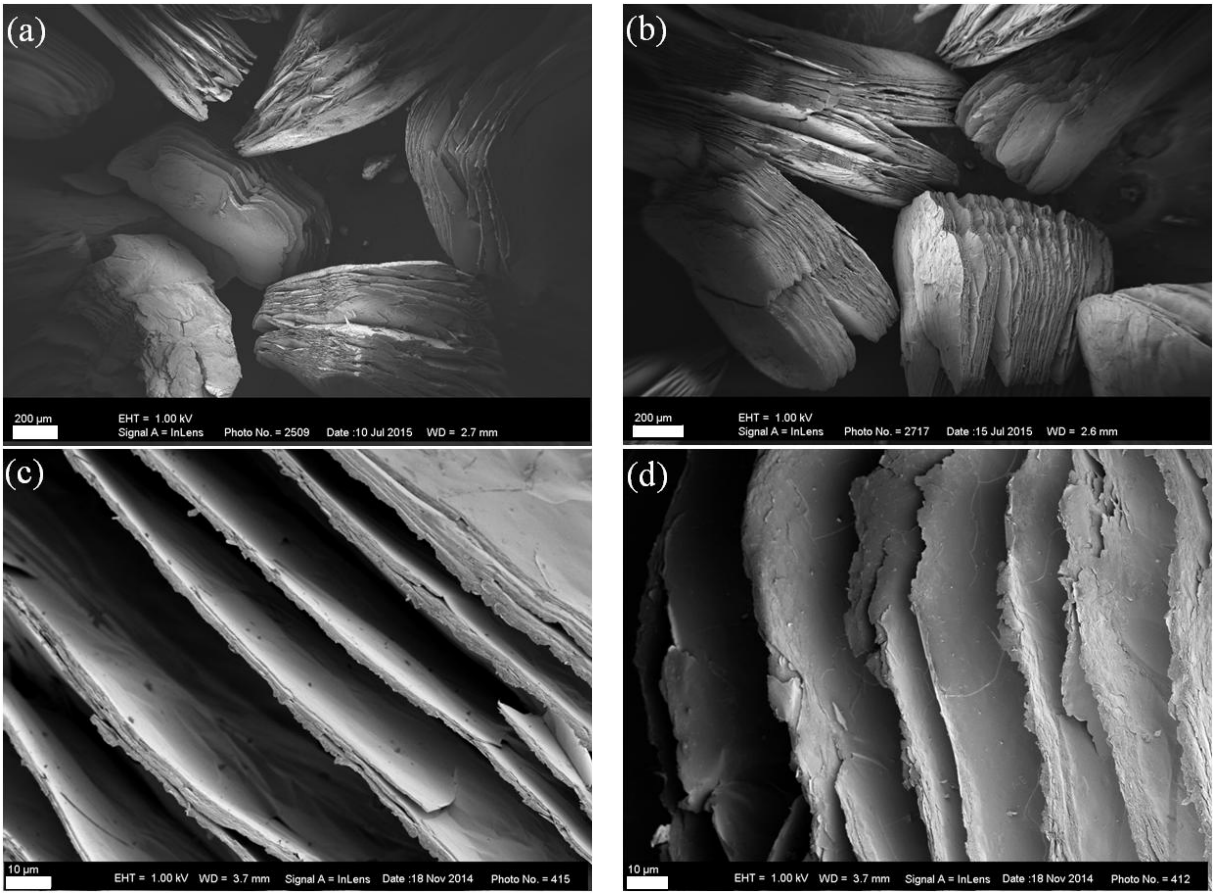

Figure 4.3. SEM micrographs of VMT samples: (a) and (c) H_2O_2-exfoliated; (b) and (d) thermal-exfoliated

SEM micrographs of sonicated VMT flakes are shown in Figure 4.4. The three samples reveal an exfoliated structure with similar morphologies. However when compared to those of sonicated thermally-exfoliated and sonicated H_2O_2-exfoliated clay particles the sonicated organomodified clay particles (OVMT) (Figure 4.4(c)) appear agglomerated. In some cases, a compact layer covering is observed. This can indicate that the protonated amine functional groups at the ends of the polymer chains have definitely compensated the negative charge of clay and thus, the repulsive electrostatic forces were eliminated (Praus et al., 2006).

Figure 4.4 shows also that sonication led to a significant decrease of the particle sizes as observed by others (Ali et al., 2014, Kehal et al., 2010). Although the particle sizes were decreased, the fracture of the VMT layers created irregular shapes for the majority of the particles, but on the whole, they were convex shaped two-dimensional flakes.

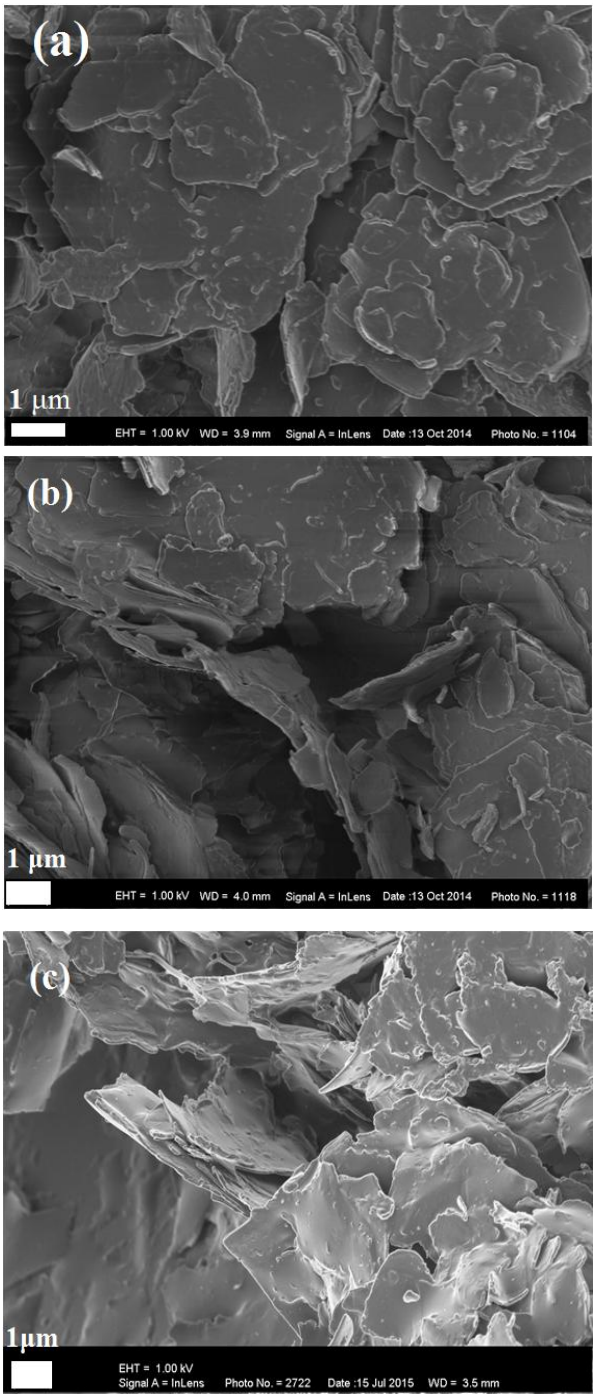

Figure 4.4. SEM micrographs of sonicated VMT flakes: (a) sonicated thermally-exfoliated; (b) sonicated H_2O_2-exfoliated, and (c) sonicated thermally-exfoliated and organomodified.

Figure 4.5 shows the SEM picture of the sepiolite sample. As can be seen, the sepiolite sample has a fibrous and needle-like morphology.

Figure 4.5. SEM micrographs of sepiolite samples (PGS9).

4.1.2. Particle size distribution and BET surface area of VMT samples

The particle size distributions reported in Table 4.1 and in Figure 4.6 confirm that ammonium exchange did not materially affect the particle size distribution. However, sonication caused a significant reduction in size. All particle size distributions showed a bimodal dispersion with a large peak at larger size values and a much smaller peak located at lower particle sizes.

Since the material consists essentially of high aspect ratio flakes, the lower humps are indicative of the variations in the flake thicknesses. In both cases, the peak position is located in the sub-micron range. Table 4.1 indicates that the d_{50} particle size of the NH_4^+-exchanged VMT was 879 µm. This was reduced to 12.4 and 20.9 µm in the sonicated forms of the thermal- and H_2O_2-exfoliated samples, respectively. This corresponds to d_{50} size reductions of by factors of 71 and 42 for the two types. Thus, for the same conditions of sonication (frequency, power, time and temperature), size reduction was more extensive for the thermally expanded VMT sample than the chemically expanded sample. Note that part of the resulting sonicated thermally-exfoliated VMT was used for the organomodification process. However, the organomodification led to an increase of the particle sizes from 12.4 to 139 µm.

Table 4.1 also reports the BET specific surface areas for the VMT samples. Again, there was very little difference in the values for the raw VMT and the ammonium-modified version (1.49 m^2/g versus 1.58 m^2/g). However, sonication produced a significant increase in the

specific surface area to 10.5, 12.4 and 8.78 m^2/g respectively for the sonicated H_2O_2-exfoliated, sonicated thermally-exfoliated and sonicated organomodified VMT. The lower BET specific surface area exhibited by the OVMT sample when compared with UVMT is in agreement with the SEM analysis (Figure 4.4) where it was found that the organomodified clay particles appeared more gathered together with a compact layer covering them.

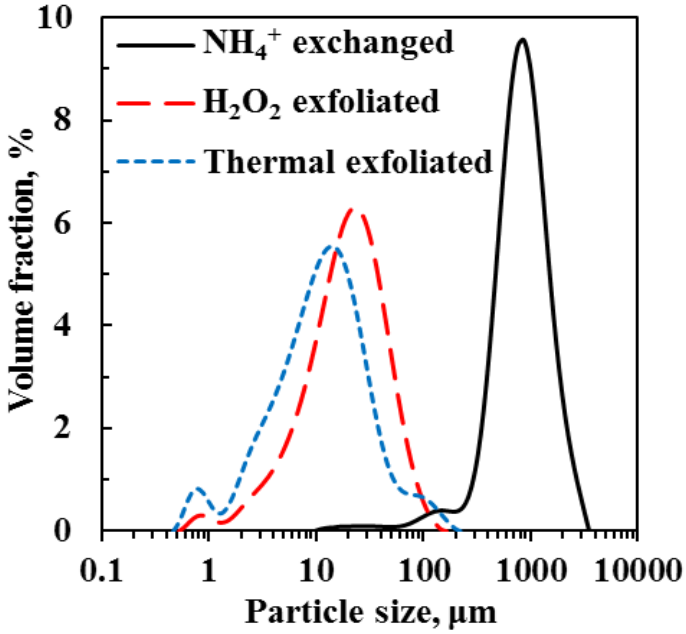

Figure 4.6. Particle size distribution plots of NH_4^+-exchanged vermiculites in neat pre-expanded form together with the sonicated samples that were either thermally or chemically exfoliated.

Since the surface area contributed by the edges of large aspect ratio flakes can be neglected, this implies that the latter flakes were relatively thinner. The BET specific surface area is given by $A_{BET} \approx 2/\rho t$ where ρ is the density and t the thickness of the flakes. The average flake thickness can then be estimated from the BET surface area and the density of the VMT. Assuming ρ = 2.55 g cm^{-3} yields flake thickness estimates of t = 63, t = 74 and t = 89 nm for the sonicated thermal- and H_2O_2-exfoliated forms and for the sonicated organomodified form, respectively. This suggests that the flakes may include nano-scale particles as at least one dimension was less than 100 nm. Furthermore, crude estimates of the flake aspect ratios are obtained by considering the ratio d_{50}/t. These values are also plotted in Table 4.1. However, these analyses did not take into account that the flakes might include lateral splits, i.e. extensive planar cracks. This means that the actual flakes could be thicker and feature lower aspect ratio values than indicated in Table 4.1.

Table 4.1. Particle sizes (μm) and BET surface areas of VMT samples.

Sample	d_{10}	d_{50}	d_{90}	BET, m^2/g	t^a, nm	λ^b(-)
Neat VMT	423	890	1760	1.49	525	1695
NH_4^+-exchanged	421	879	1750	1.58	496	1772
H_2O_2-exfoliated[c]	5.62	20.9	54.0	10.5	74	282
Thermally exfoliated[c]	2.91	12.4	39.2	12.4	63	197
Organomodified VMT[c]	46.8	139	481	8.78	89	1562

[a]Average flake thickness estimated from BET specific surface area.
[b]Apparent aspect ratio estimated from d_{50}/t.
[c]Sonicated samples

4.1.3. X-ray fluorescence (XRF) chemical composition

The XRF chemical composition of the MMT, VMT and PGS9 samples is presented in Table 4.2. Both MMT samples exhibited a high silica content that is attributed to the presence of *ca.* 35.7 wt.% cristobalite as a major impurity (Massinga et al., 2010).

Table 4.2. Chemical composition (dry basis expressed as mass) of the clay samples with the corresponding loss of ignition.

Sample	SiO_2	MgO	Al_2O_3	Fe_2O_3	K_2O	CaO	P_2O_5	TiO_2	LOI
Neat MMT	81.09	2.34	11.09	2.29	0.19	0.47	0.02	0.21	4.75
NH_4^+-exchanged MMT	84.58	1.58	10.79	2.21	0.20	0.06	0.02	0.22	4.82
Neat VMT	42.55	24.39	10.06	9.49	6.21	4.61	1.13	1.16	8.70
NH_4^+-exchanged VMT	43.42	24.18	10.26	9.60	6.23	3.69	1.25	1.16	9.97
H_2O_2-exfoliated VMT[c]	45.67	23.02	8.67	8.62	5.34	3.95	3.48	1.02	16.3
Thermally-exfoliated VMT[c]	43.22	23.96	9.86	9.27	5.97	4.79	1.57	1.13	19.8
Organomodified VMT[c]	43.33	27.63	11.26	8.71	7.33	0.51	0.02	1.22	36.2
Sepiolite (PGS9)	66.04	29.17	2.35	1.06	0.83	0.39	0.03	0.12	12.1

[c]Sonicated samples

The values for the neat vermiculite are consistent with those previously found (Muiambo et al., 2015, Muiambo et al., 2010). Previous analyses established that Palabora ‘‘VMT” is not pure VMT but rather a randomly-interstratified mixed-layer VMT–biotite containing less than 50% VMT (Bassett, 1961, Kehal et al., 2010, Muiambo et al., 2010, Schoeman, 1989, Schwellnus, 1938). The structural formula for this mineral consistent with composition data is given in Scheme 4.I (Muiambo et al., 2010). The differences observed in the XRF analyses evident in Table 4.2 reflect natural variations rather than composition changes caused by the processing of the samples.

$$0.60\,(Mg_{2.60}Fe^{2+}_{0.60})[Si_{3.2}Al_{0.78}Fe^{3+}_{0.02}]O_{10}(OH)_2K^{+}_{0.49}$$
$$+0.40(Mg_{2.60}Fe^{2+}_{0.60})[Si_{3.2}Al_{0.78}Fe^{3+}_{0.02}]O_{10}(OH)_2Mg^{2+}_{0.20}.nH_2O$$

Scheme 4.I. The structural formula for Palabora VMT consistent with XRF data.

4.1.4. X-ray diffraction (XRD)

Figure 4.7 shows the XRD patterns of the pristine MMT and the ammonium exchanged MMT. The pristine clay showed a strong reflection at 2θ = 8.164°, corresponding to a basal spacing of 1.257 nm of the (001) planes. In NH_4^+-MMT, the (001) plane reflection shifted to 7.144°, corresponding to a basal spacing of 1.437 nm. This slight increase in the interlayer spacing of the NH_4^+-MMT sample suggests the ammonium treatment has created a greater disorder of the clay particles when compared to the neat MMT. However, the basal reflection enlargement probably suggests that not all interlayer sites were NH_4^+-exchanged.

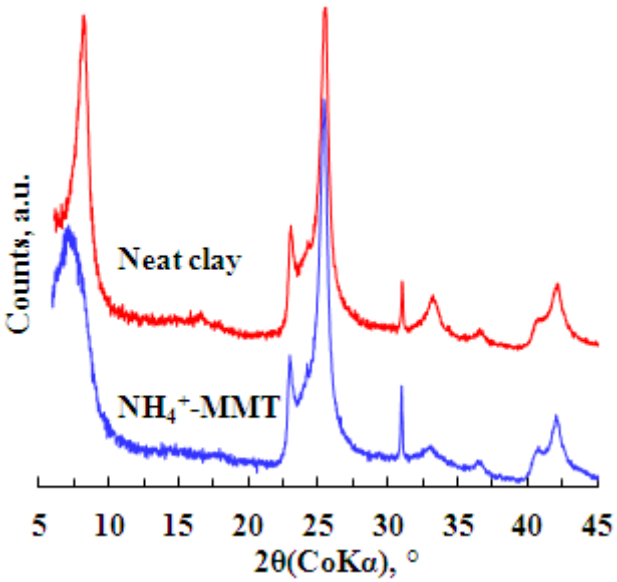

Figure 4.7. XRD patterns for the neat and NH_4^+-MMT.

Figure 4.8 shows the XRD patterns of VMT samples. The neat VMT features multiple reflections, suggesting a mixture of different minerals as reported in the literature (Folorunso et al., 2012, Muiambo et al., 2010). It features a strong broad peak at 2θ = 8.66° (1.19 nm) and weaker reflections at 2θ = 7.20° (1.43 nm) and 2θ = 10.24° (1.00 nm). The 1.43 nm reflection is consistent with a VMT phase with two water layers in the galleries forming hydration shells around the exchangeable cations (Mathieson, 1958). The 1.00 nm reflection is from the mica (biotite/phlogopite). Perfectly alternating 50/50 mixed layered VMT, i.e.

‘‘mica-VMT mixed layers”, features reflections at 2.441 nm (001) and 1.221 nm (002) (Amil et al., 1992, Newman and Brown, 1987). In the present sample, the main peak is located at higher 2θ angles. This and the extensive line broadening are indicative of a random distribution of the VMT and biotite layers.

Two XRD diffractogram sample sets corresponding to the two different exfoliation procedures were obtained. The corresponding pairs were identical indicating that similar products were obtained irrespective of whether the exfoliation was achieved through a thermal shock or hydrogen peroxide treatment. This means that the two procedures delivered similar end products as far as phase composition is concerned.

A broadening of the ‘‘mica-VMT mixed layers” reflections, as well as the disappearance of some of them, were observed in ammonium-exchanged VMT sample as well in the diffractograms of all the sonicated VMT samples. The broadening is attributed to the delamination of VMT sheets together with particle size reductions induced by sonication.

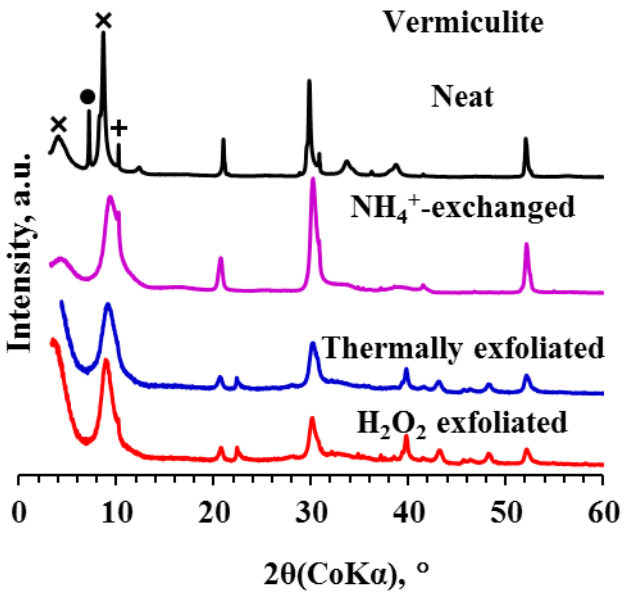

Figure 4.8. X-ray diffraction (XRD) patterns of the various VMT samples. Key: ● = VMT; ✕ = “mica-VMT mixed layers”; and ✚ = mica (biotite/phlogopite).

Figure 4.9 shows the XRD patterns of the clay samples that were used to prepare DAPA-11/bio-nanocomposites namely the sonicated thermally-exfoliated, sonicated organomodified VMT and PGS9. PGS9 shows a strong diffraction peak at $2\theta = 8.468°$. According to Bragg’s equation, the basal spacing is 1.212 nm. As discussed above, a broadening of the ‘‘mica-VMT mixed layers” reflections was observed in the diffractograms of both UVMT and

OVMT, clearly indicating the delamination of vermiculite sheets and a particle size reduction due to sonication.

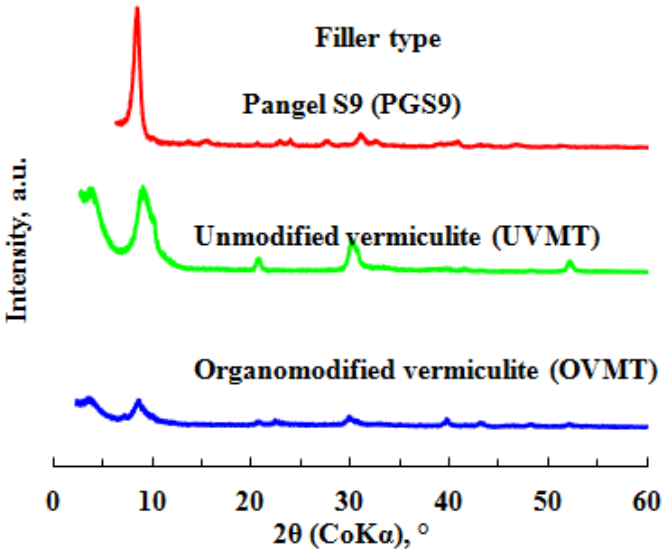

Figure 4.9. XRD patterns for the sonicated thermally-exfoliated, sonicated organomodified VMT and PGS9.

4.1.5. Thermogravimetric analysis (TGA)

Figure 4.10 shows the TGA curves in air environment of neat MMT and NH_4^+-MMT. The TGA results indicate that mass loss proceeded stepwise in all samples. The neat MMT sample showed a higher mass loss compared to the NH_4^+-MMT sample. The DTA signal (not shown) indicated endothermic peaks just below 100 °C for both samples that were attributed to the loss of interlayer water. The endothermic peak was more intense in the neat clay, suggesting that the water content was higher. This was expected as the Ca^{2+} and Na^+ ions have a stronger tendency for hydration than the NH_4^+-MMT ion.

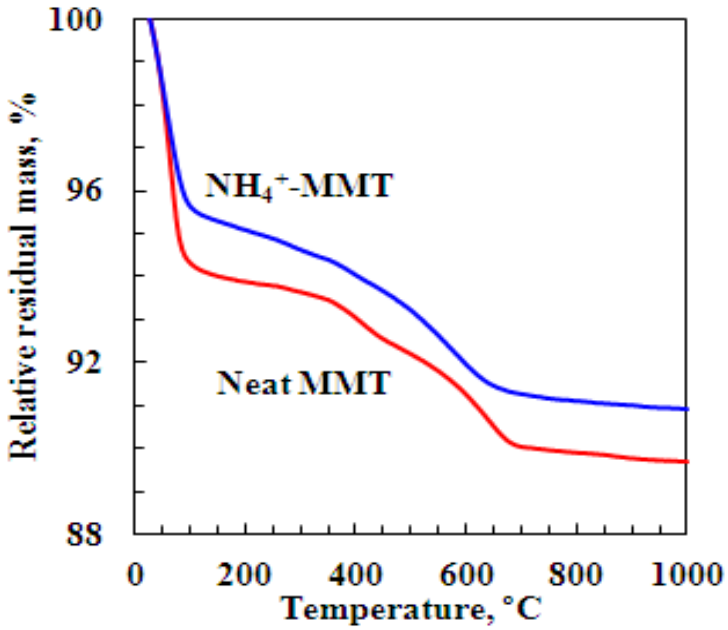

Figure 4.10. TGA curves for the neat clay and NH_4^+-MMT.

Figure 4.11 shows the TGA curves in air environment of pristine VMT and the modified ones (NH_4^+-exchanged, sonicated H_2O_2-exfoliated, sonicated thermal-exfoliated, sonicated organomodified VMT samples) and sepiolite. From this figure, it can be seen that mass loss proceeds stepwise in all samples in the range of temperatures from 50 °C to 900 ºC.

The free water content (water physically absorbed on the surface of the clay and in the interlayer spacing) is present in both samples and these were totally removed at about 150 °C for the neat VMT and for the expanded and sonicated VMT samples. On the other hand, for the NH_4^+-VMT the free water content was only totally released at about 300 °C.

In general, the mass losses from 150 °C to about 300 °C and between 300 and 650 °C in VMT samples are due respectively to the releasing of the interlayer water and to the releasing of some remaining water and to the beginning of dehydroxylation (MacKenzie, 1970). At a temperature higher than 850 °C the mass loss is attributed to the collapse of the crystal structure octahedral sheet. Contrary to that observed for the neat VMT, ammonium VMT exhibited a lower mass loss (regarding the interlayer water and dehydroxylation) in the entire temperature range evaluated, indicating the presence of ammonium ions in the interlayer space of the clay. However, the oganomodified VMT sample showed a higher mass loss in the temperature range between 300 and 950 ºC, as expected. The higher mass loss could be attributed to the thermal decomposition of the dimer fatty acid polyamide used as VMT clay organomodifier.

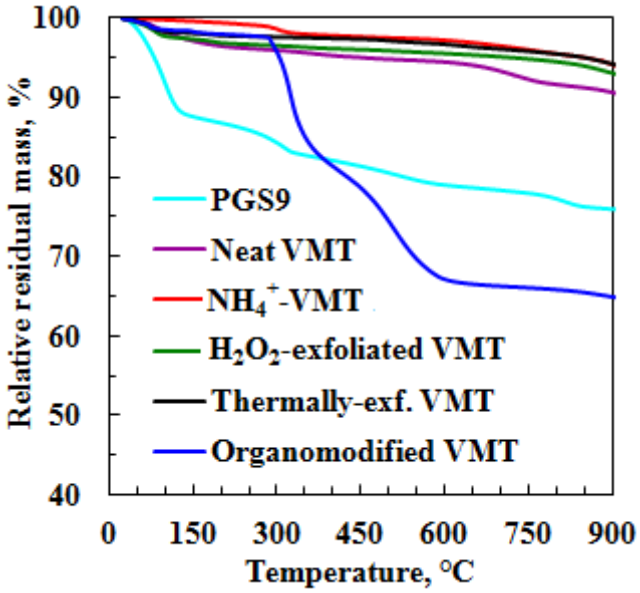

Figure 4.11. TGA curves in air environment of the various clay samples.

On other hand, sepiolite sample also showed a higher mass loss, suggesting the presence of high content of hygroscopic and zeolitic water even though, the clay sample was dried at 60 °C for 24 hours before testing. The main events of mass loss of pristine sepiolite resulting from heating can be basically divided into four regions located at 25 ~150 °C, 150 ~350 °C, 350 ~650 °C and 650-850 °C. Heating sepiolite from room temperature to about 150 °C selectively removes water physically bonded to the clay on the external surface and the zeolitic water from the structural channels. The weight loss observed in the second and third region is respectively related to the dehydration of the first structural water (also called coordinated or bonded water) and of the second structural water. The final region corresponds to the dehydroxylation of internal Mg–OH indicating the structure loss of the sepiolite.

4.2. Composites characterization

The composites characterization section was structured in such a way that the results, discussions and conclusions of each polyamide-clay bio-nanocomposites type (i.e. MMT or VMT bio-nanocomposites based on DAPA and VMT or PGS9 bio-nanocomposites based on PA-11) are presented separately.

4.3. NH_4^+-MMT/bio-nanocomposites based on DAPA

The main focus here was to understand the relationships between the new processing method and structure as well as to understand the relationships between the structure and the properties of the generated nanocomposites.

4.3.1. Electron microscopy (SEM, TEM and AFM)

The SEM micrographs in Figure 4.12 revealed significant changes in the morphologies of the fracture surfaces as the clay content increased (Lee et al., 2007). Distinct clay agglomerates were not visible in the SEM, even at high magnification. However, dispersed clay tactoids were observed in all the clay containing samples. These results indicate that the processing conditions were not effective enough to facilitate complete exfoliation or even intercalation of the clay particles. The fracture surface of the neat DAPA (not shown) was relatively smooth. Those for the bio-nanocomposites had a rough surface appearance. The roughness increased with clay content similar to previous observations (Tjong, 2006). Figure 4.12 also shows the outside surface texture of the sheet prepared using the composite containing 27.5 % clay.

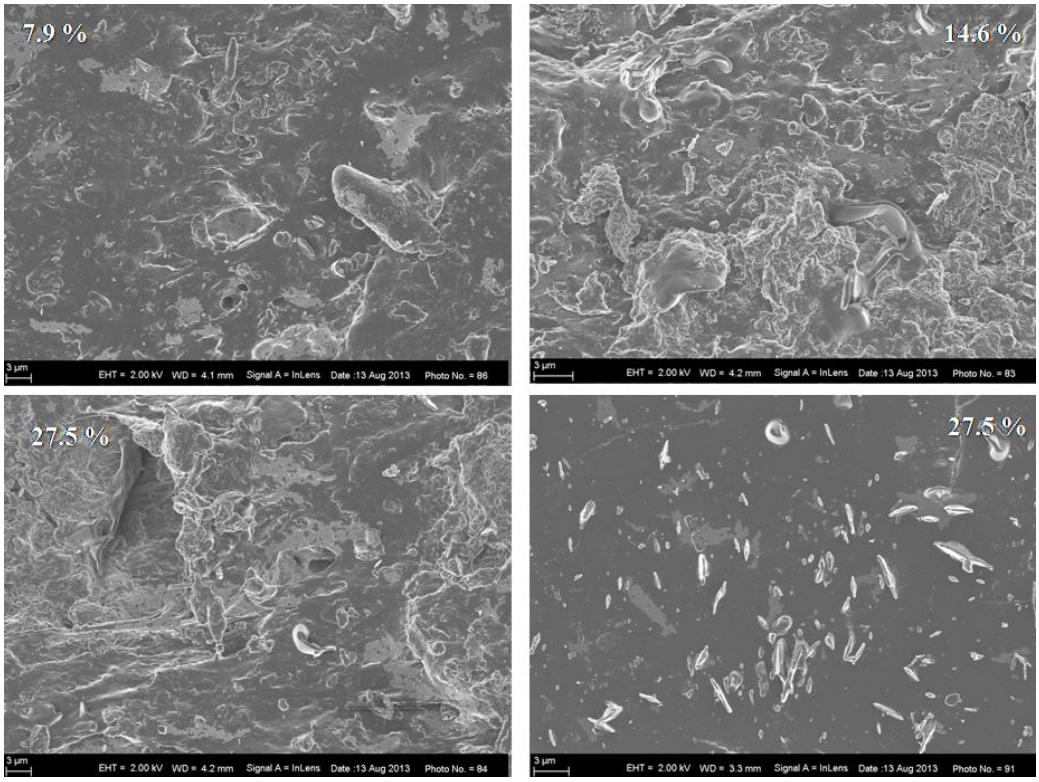

Figure 4.12. SEM images of the fracture surfaces of the DAPA bio-nanocomposites with 7.9, 14.6 and 27.5 wt.% clay. The micrograph at the bottom right shows the surface texture of the pressed sheet for the composite containing 27.5 wt.% clay.

In order to explore the three-dimensional surface morphology of the bio-nanocomposites, the atomic force microscope (AFM) was implemented. The AFM height (topographic) and the phase (elastic) images were simultaneously obtained under tapping conditions on the surface of the bio-nanocomposites as shown in Figure 4.13, indicating high protuberant and clearly visible flakes with a thickness of 50–100 nm in nanoscale.

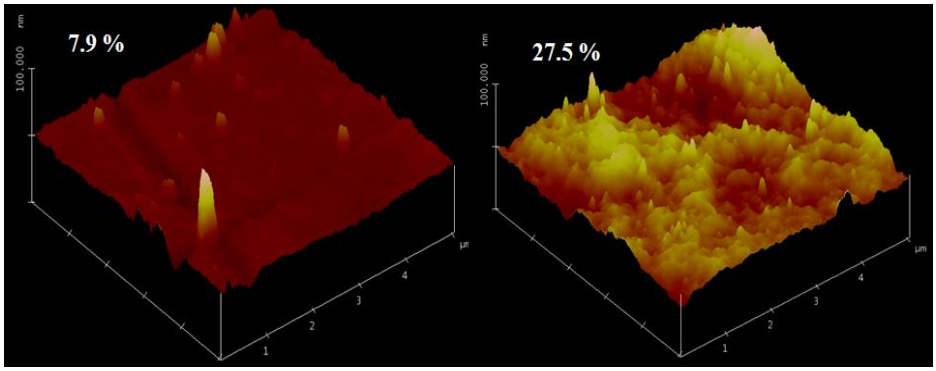

Figure 4.13. AFM images of DAPA bio-composites with different NH_4^+-MMT contents.

Illustrative TEM results for the present bio-nanocomposites are shown in Figure 4.14. The dark lines represent delaminated clay layers dispersed in the polymer matrix. The bio-nanocomposite with 7.9 wt.% clay showed a significant number of individual exfoliated clay sheets dispersed together with thicker tactoids. In the bio-nanocomposite with 27.5 wt.% clay, fewer exfoliated platelets were visible in the bulk and more clay tactoids were observed. Thus, as the clay content increased, the degree of dispersion decreased and the clay was present primarily as tactoids. A similar result was previously reported by Anilkumar et al. (2008). High particle aspect ratios are key for increasing the moduli of filled polymer composites (Mondragón et al., 2009). The TEM micrographs show that even the tactoids featured very high aspect ratios as their thickness corresponded to a few nanometers while their lengths reached 1 μm.

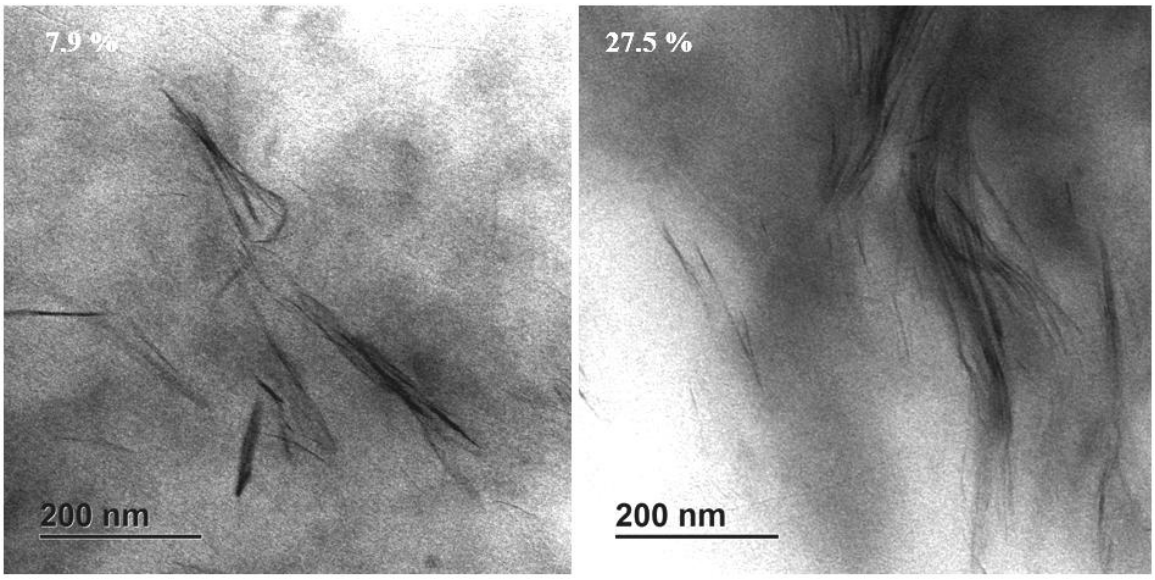

Figure 4.14. TEM images of selected MMT DAPA bio-nanocomposites.

4.3.2. X-ray diffraction (XRD)

The XRD diffractograms of the PA/NH_4^+-MMT bio-nanocomposites, shown in Figure 4.15, featured poorly defined reflections. The (001) plane reflections were broader and less intense but were located at approximately the same angle as for the NH_4^+-MMT clay.

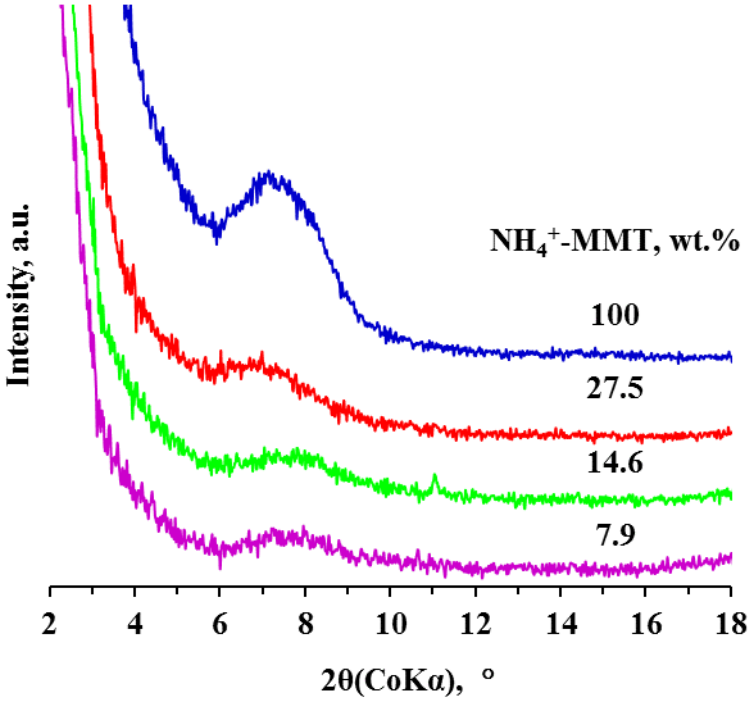

Figure 4.15. XRD patterns of the DAPA bio-nanocomposites compared to the neat NH_4^+-MMT.

The lower intensity is consistent with a certain degree of disorder or even some clay exfoliation. Nevertheless, the presence of (001) reflections is indicative of the retention of neat NH_4^+-MMT clay structure rather than the formation of intercalated microstructures (Pavlidou and Papaspyrides, 2008). Intercalated structures form when the protonated polymer chains enter into the clay galleries causing expansions of up to 3 nm. Thus, intercalated structures form a more or less ordered multilayer structure of alternating polymeric and inorganic layers (Ray and Okamoto, 2003). The present XRD patterns are not consistent with such a situation as the reflections did not shift to lower angles.

4.3.3. Thermogravimetric analysis (TGA)

Mass loss curves vs. temperature of neat DAPA (as received but dried at 60 °C for 24 h) and its clay composites are shown in Figure 4.16. The actual clay content levels of the bio-nanocomposites were determined from the relative mass loss values measured at 1,000 °C for the modified clay and the bio-nanocomposites.

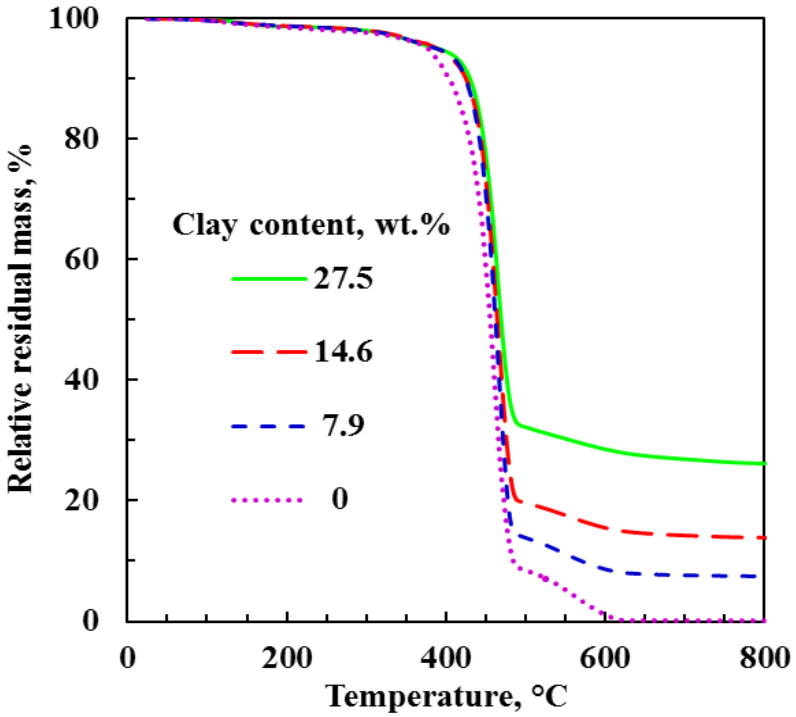

Figure 4.16. TGA curves for the neat DAPA and its bio-nanocomposites.

The mass loss up to 150 °C is often associated with the moisture content of polyamides. This value was 0.15 wt.% for the neat polymer and less than this for the composites. Up to 320 °C, the measured mass loss values for the clay composites were lower than that of the neat DAPA, i.e. 2.7 wt.%. In addition, they followed a similar trend in this temperature range. These observations indicate that the composites were free of residual acetic acid.

Only two major thermal events were observed in the TGA curves of the composites and the neat DAPA. The first stage of degradation involved major mass loss, commencing at 398, 408, 411 and 420 °C for neat polymer and the bio-nanocomposites with a clay content of 7.9, 14.6 and 27.5 wt.%, respectively.

Figure 4.16 also shows that the composite samples were more stable than the neat DAPA under thermo-oxidative degradation conditions. Above 350 °C, the neat polymer showed a rapid mass loss, leaving a 10.5 wt.% residue at 483 °C. This was completely oxidized to volatile products between 520 and 1,000 °C. Above 400 °C, the residues of the polymer composites were higher than that observed for the neat DAPA, indicating that the presence of clay apparently enhanced thermal stability. This can be attributed to barrier effects preventing oxygen diffusion into the matrix and the release to the atmosphere of small molecule fragments generated during the thermal decomposition process (Liu et al., 2004). In addition,

it is clear from Figure 4.16 that the degradation onset temperature was slightly higher for the clay composites. The DTG peaks (Figure 4.17) indicate the temperature corresponding to the maximum degradation. These occurred at about the same temperature for the neat polymer and its composites, i.e. 463 °C.

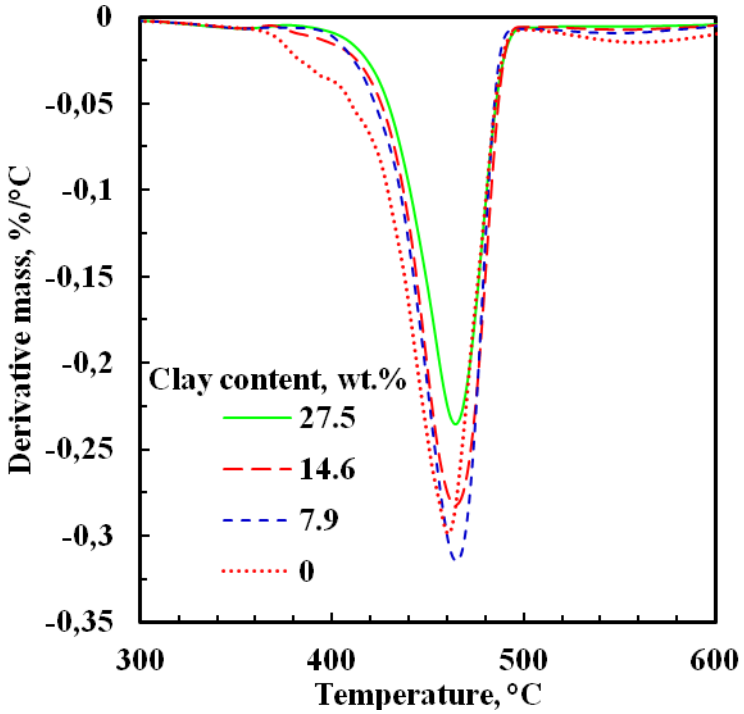

Figure 4.17. The derivative mass loss for the neat DAPA and its bio-nanocomposites.

4.3.4. Viscosity

The rheological behaviour of molten bio-nanocomposites complements XRD and TEM information on the degree of exfoliation of clay platelets in a polymer matrix (Gupta et al., 2005). Figure 4.18 shows the effect of clay content and shear rate on the melt viscosity of DAPA–clay bio-nanocomposites. The high viscosity at low shear rates points to strong interactions between the delaminated clay platelets and the polymer chains or, alternatively, the formation of network structures by clay particle interactions.

Pronounced shear thinning indicates extensive clay exfoliation in a given system (Gupta et al., 2005, Szép et al., 2006, Wagener and Reisinger, 2003). The nanocomposites' internal structure is retained at low shear rates, but at high shear rates, the clay network structures break down and the platelets tend to orient in the flow direction. The resulting platelet alignment decreases the apparent viscosity so that it approaches that of the neat polymer melt (Szép et al., 2006, Wagener and Reisinger, 2003). This ability to reorient the silicate layers or

tactoids in response to externally applied flows also controls the viscoelastic properties of the composites (Wang et al., 2012).

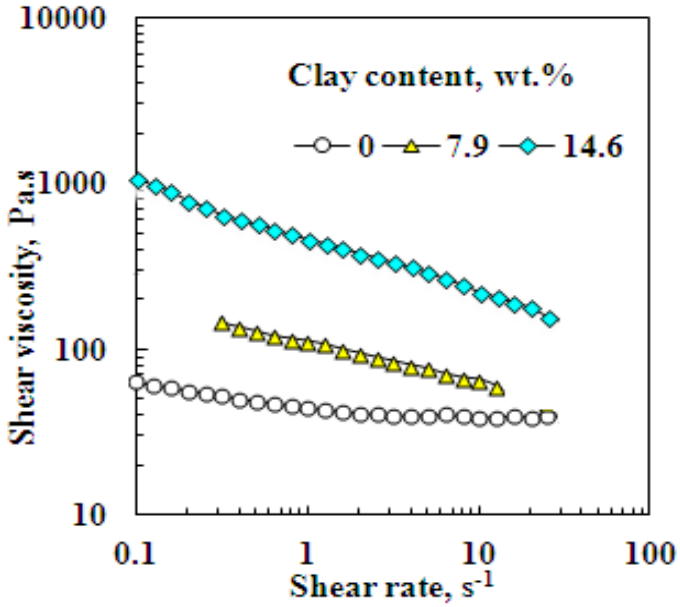

Figure 4.18. Viscosity vs. shear rate for DAPA and its bio-nanocomposite at 160 °C.

4.3.5. Dynamic mechanical analysis (DMA)

Figure 4.19 reveals the effect of the clay on the loss factor (tan δ) for the composites. The glass transition temperature (T_g) values were associated with the peak temperatures of the tan δ–temperature curves. At a frequency of 100 Hz, the T_g shifted from 9.8 °C for the neat polymer to 14.5, 16.0 and 20.2 °C for composites with a clay contents of 7.9, 14.6 and 27.5 wt.%, respectively. In addition, the tan δ peaks became broader and weaker as the clay content increased. These increases in the apparent glass transition temperature T_g indicate that the presence of the clay significantly affected the mobility of the DAPA chain segments.

Figure 4.20 shows the temperature dependence of the storage modulus at 100 Hz for the neat PA and its composites. All the compounds exhibited similar trends with the storage modulus decreasing with increasing temperature. This behaviour can be attributed to the increase in segmental polymer chain motions with temperature as the thermal energy overcomes the interchain hydrogen bonding interactions along the DAPA chains. As expected, the storage modulus values for the composites are higher than that of the neat DAPA in the range of evaluated temperatures. The upward shift indicates that the incorporation of clay remarkably enhanced stiffness, providing a good reinforcing effect.

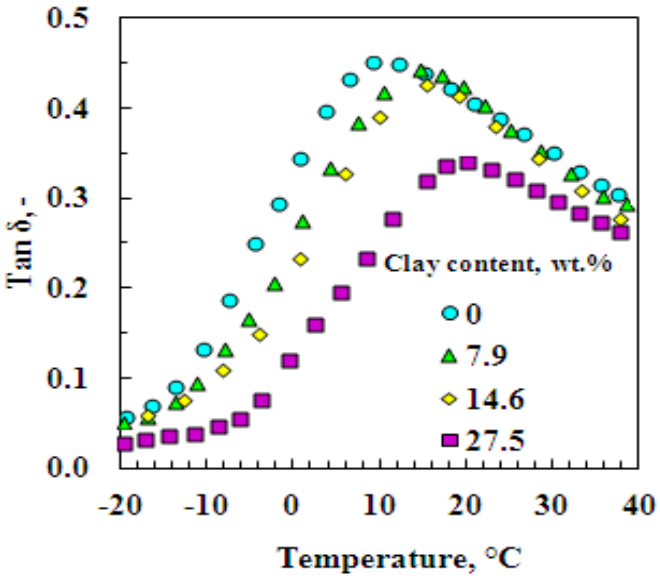

Figure 4.19. Temperature dependence of tan δ at 100 Hz of the DAPA and its bio-nanocomposites.

The storage modulus values for the composites improved as the clay content increased. At -30 °C, i.e. well below the T_g of the neat PA (T_g equals 10 °C, refer to Figure 4.19), the storage modulus values of the composites with clay contents of 7.9, 14.6 and 27.5wt.%were respectively 1.23 (6.27 GPa), 1.74 (8.92 GPa) and 2.5 (12.8 GPa) times higher than that of pure PA (5.12 GPa). At 70 °C, the corresponding ratio and modulus values were 1.99 (69 MPa), 4.97 (172 MPa) and 9.1 (315 MPa), respectively, with the modulus value for the neat PA equal to 35 MPa. These values and Figure 4.19 in general, show that the stiffness enhancement was less pronounced at temperatures below T_g. This behaviour is related to the fact that, below T_g, the polymer is in a glassy state where segmental chain motions are frozen. However, above T_g, when the matrix polymer has a lower stiffness, the reinforcement effect of the clay particles was more prominent. This is attributed to the high surface area of the rigid clay that hampers segmental motions of adjacent polymer chains. This mechanism was previously used to explain the reinforcing action of rigid fillers with high moduli such as layered silicates (Pavlidou and Papaspyrides, 2008). The observed shift in the T_g, as the clay content is increased (Figure 4.19), supports this contention.

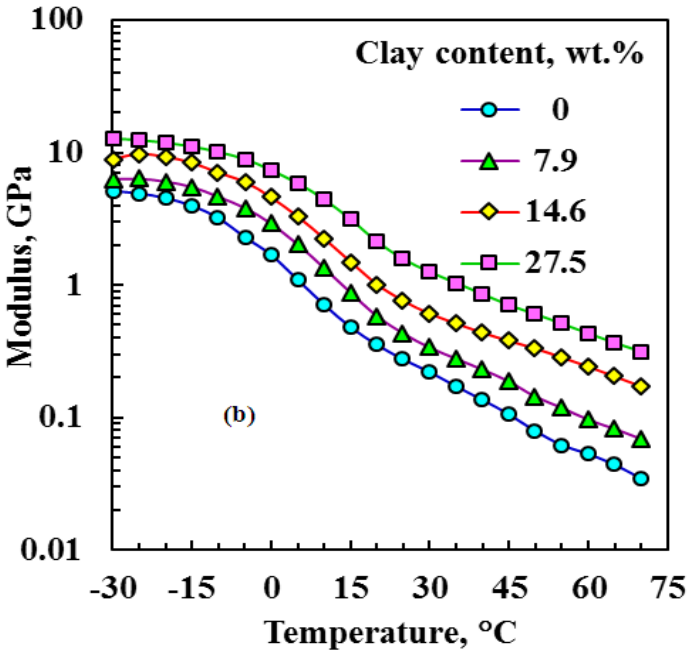

Figure 4.20. Storage modulus at 100 Hz of the DAPA and its bio-nanocomposites.

4.3.6. Discussion

The present data are consistent with a mixed microstructure of exfoliated clay sheets and tactoids with a thickness of less than 50 nm. These thickness dimensions are most likely determined by the conditions the clay experienced in the acetic acid dispersion. According to Yariv (2002), clay tactoids may be regarded as associated colloids. The number of associated sheets present in the clay dispersion is determined by the balance between entropic effects that direct for complete exfoliation and electrostatic forces that direct for larger tactoids. Even in a water medium, NH_4^+-MMT forms tactoids comprising several unit layers (Banin and Lahav, 1968, Edwards et al., 1965). Much larger tactoids are expected in the acetic acid medium as it has a lower dielectric constant than water. Thus, it is likely that the protonated amine end groups on the DAPA chains only displaced the surface charges on the clay tactoids present in the acetic acid dispersion. This is supported by the fact that no evidence of polymer intercalation was found in the present study.

4.3.7. Conclusions

Ammonium ion exchanged MMT bio-nanocomposites, based on a DAPA, were successfully prepared using a surfactant-free approach. This new method did not employ any surfactants. In other words, the matrix MMT compatibilisation did not employ any surfactants. The composites were made by mixing an acetic acid dispersion of partially delaminated clay

particles with a solution of the PA in the same solvent. The composite was recovered via precipitation by adding water.

It is evident from the TEM and XRD results that the composites featured a mixed morphology containing some exfoliated clay sheets together with nano-sized clay tactoids. No evidence of polymer intercalation into the clay galleries was found as indicated in XRD results, suggesting that the clay morphology was fixed at the acetic acid dispersion stage. At best, the protonated amine end groups of the polymer chains only replaced the ammonium ions on the surface of the clay particles originally present in the acetic acid dispersion. This stabilized the clay platelets and compatibilized them with the DAPA matrix.

MMT clay exhibited a reinforcing effect on DAPA as both the modulus and the T_g increased. Addition of 27.5 wt.% clay increased the modulus of the parent polymer by up to a factor of 2.5 in the glassy region and by almost an order of magnitude in the rubbery region. The T_g of the polymer increased by about 5 °C when 27.5 wt.% clay was added. This indicates that the high contact surface area presented by the dispersed clay platelets dispersed in the composites inhibited segmental polymer chain mobility. This implies an effective stiffening of the polymer matrix at temperatures above T_g.

4.4. VMT (exfoliated by thermal shock and H_2O_2 treatment and/or sonication)/bio-nanocomposites based on DAPA

The study compared the effect of the two different exfoliated submicron vermiculite flakes on the mechanical properties of such polyamide/bio-nanocomposites. The primary objective was to gain an understanding of the stiffening mechanisms operating in amorphous polyamide–vermiculite bio-nanocomposites.

4.4.1. Electron microscopy (SEM and TEM)

Representative images of the morphology and orientation of the VMT flakes in the DAPA composites are illustrated in Figures 4.21–4.23. The VMT flakes assumed random orientations within the polymer matrix as clearly indicated in Figure 4.21 (c), (d), (f) and Figure 4.22 (d), (f). However, twisted and folded platelets were also observed.

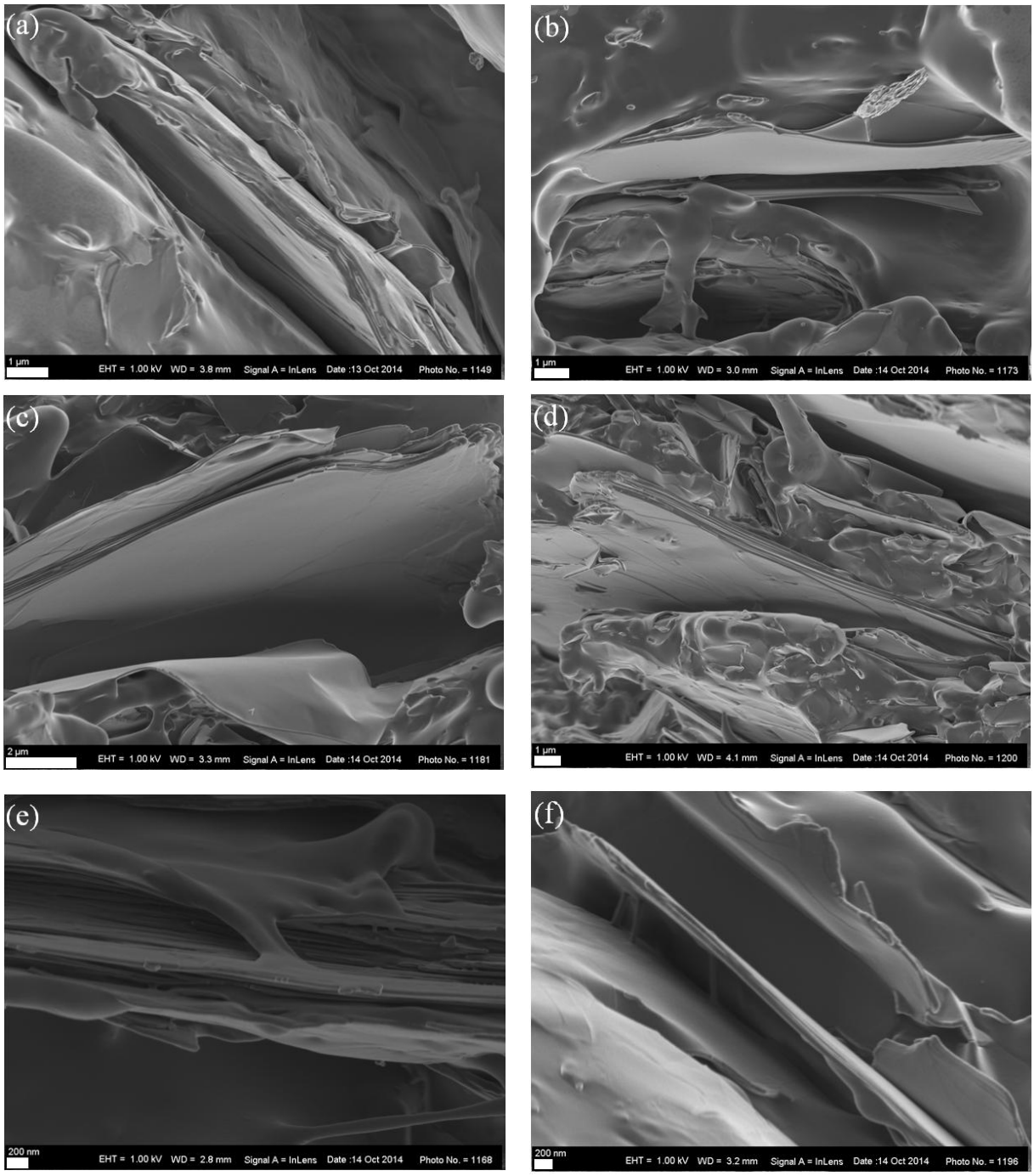

Figure 4.21. Cross sectional SEM images of the DAPA bio-nanocomposites containing (a) 5, (b) 10, (c) 20, (d) 30, (e) 10 and (f) 20 wt.% sonicated H_2O_2 exfoliated VMT.

TEM micrographs taken of microtome of cross-sections (Figure 4.23) show flake thickness in the sub 100 nm range. However, platelets with thickness up to about one micrometre are observed in SEM micrographs (Figures 4.21 and 4.22). The thicker sheets were expected. The VMT used in this work consists of flakes that correspond to randomly interstratified VMT biotite layers (Muiambo et al., 2010). The material basically derives from incomplete

weathering of the biotite part. So the thicker sheets are derived from thick biotite layers. The presence of mica impurities with higher charge densities makes also this VMT harder that would not exfoliate under the conditions we applied. In other words, the shear forces developed during the higher mixing process were not sufficient to break the VMT stacks completely, even though that the exfoliation of the starting VMT was previously helped by thermal shock and H_2O_2 treatment and accomplished with ultrasound.

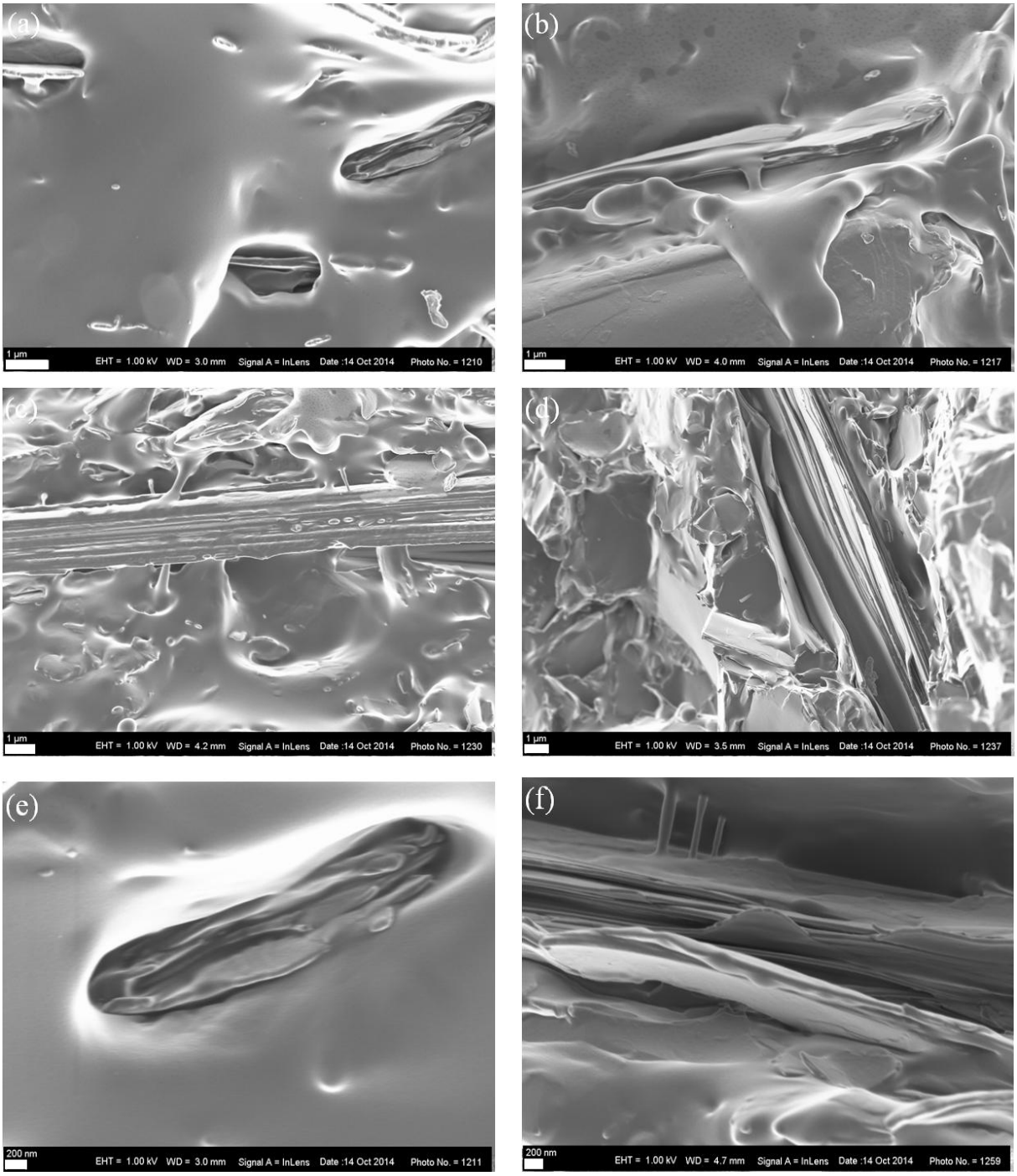

Figure 4.22. Cross sectional SEM images of the DAPA bio-nanocomposites containing (a) 5, (b) 10, (c) 20, (d) 30, (e) 5 and (f) 20 wt.% sonicated thermally exfoliated VMT.

From SEM images (Figures 4.21 (b), (e) and 4.22 (a), (b), (c)) is clearly visible that the DAPA appears to have covered the external surfaces of VMT platelets. This suggests good wetting and a strong interaction between the outer surface of VMT layers and the DAPA matrix. This is supported by the cohesive rather than adhesive failure of the matrix. From Figures 4.21 (f) and 4.22 (f) is clearly visible the presence of ropey polymer structures connecting two flakes.

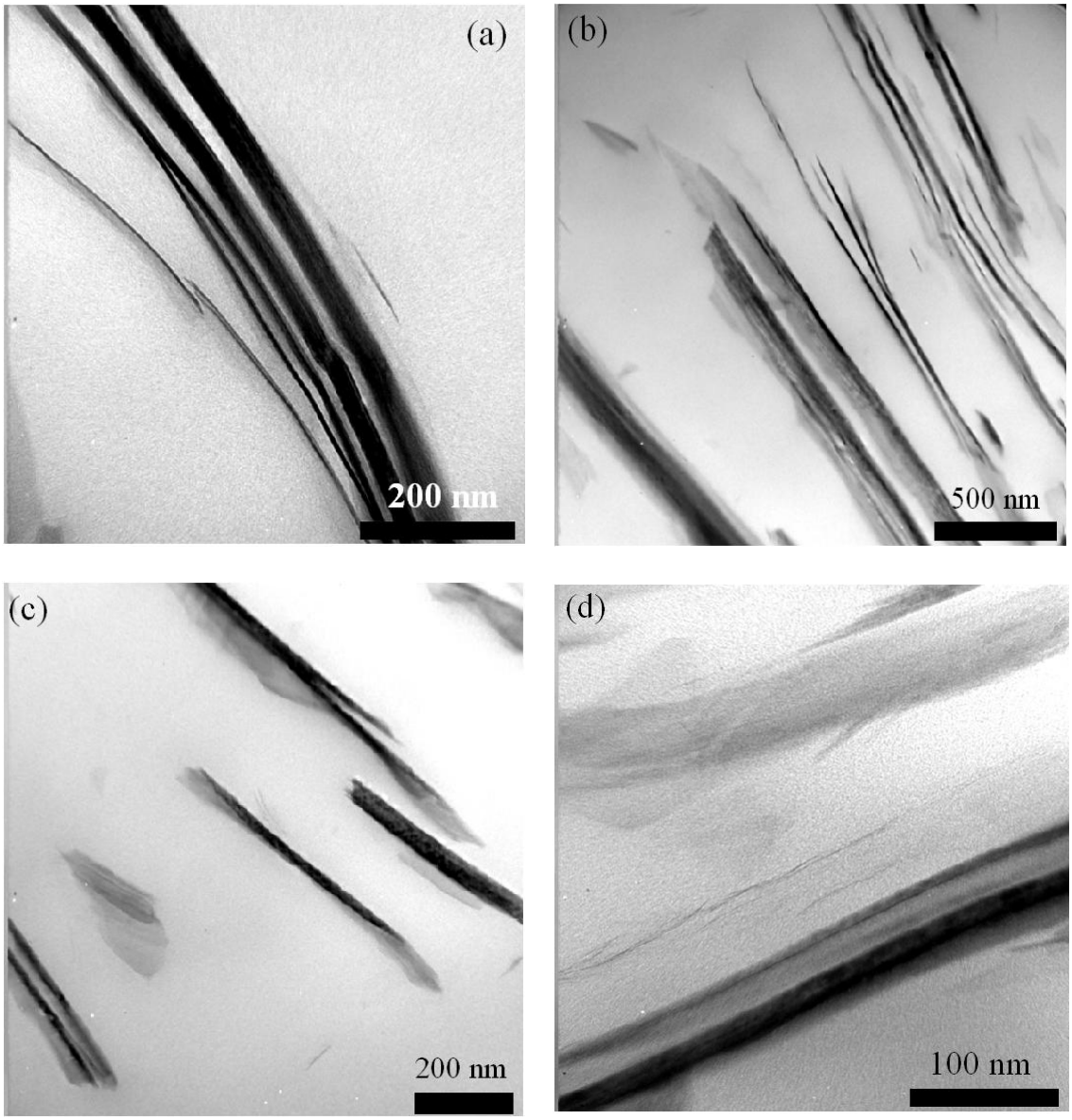

Figure 4.23. TEM images of the DAPA bio-nanocomposites containing (a) 10 and (b) 20 wt.% sonicated H_2O_2-exfoliated VMT and (c) 10 and (d) 20 wt.% sonicated thermally-exfoliated VMT.

From Figures 4.21 and 4.22, it is also possible to see VMT flakes featuring partial delamination, i.e. lateral internal cracks that appear to be devoid of the polymer. It is considered likely that these cavities were not present initially but that they were created during the cryofracturing of the sections containing the rigid VMT sheets. The micrographs evidence for the composites is consistent with a filler morphology comprising a combination of nanoplatelets and micro-flakes. A similar morphology was previously observed for VMT reinforced polyurethane (Qian et al., 2011).

4.4.2. X-ray diffraction

Figure 4.24(a) and (b) show the XRD patterns of PA-sonicated H_2O_2-exfoliated and sonicated thermally-exfoliated VMT composites, respectively. It is clear from the figures that the diffractograms for all composites were quite independent of the concentration of the VMT incorporated and exfoliation method (thermal shock or hydrogen peroxide treatment) used. This was expected as the composite preparation method and the sample preparation procedure did not involve high shear forces that could have caused further delamination of the VMT.

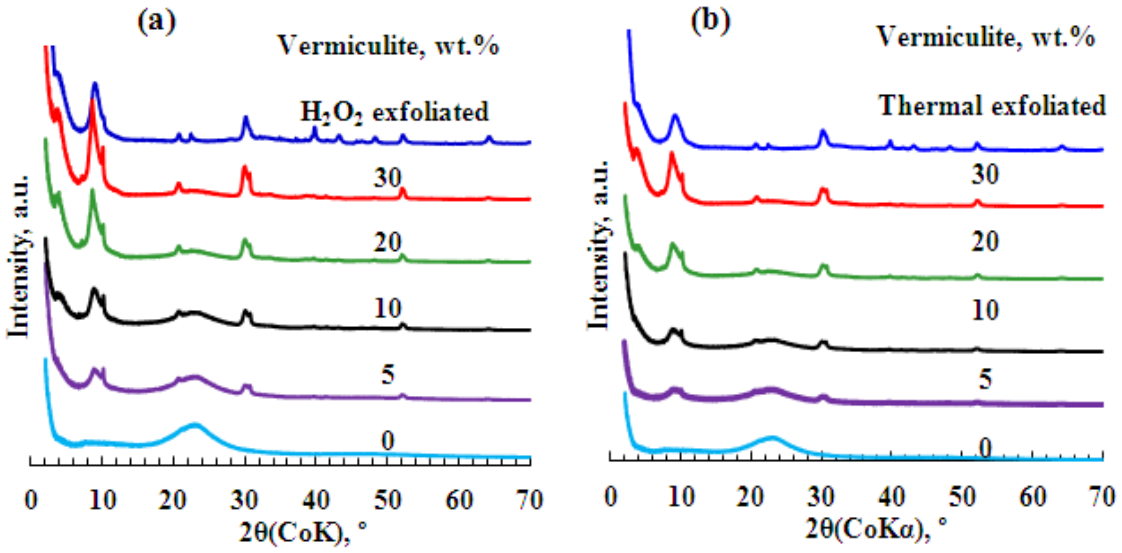

Figure 4.24. XRD patterns of (a) DAPA-sonicated H_2O_2-exfoliated and (b) sonicated thermally-exfoliated VMT bio-nanocomposites as a function of filler content.

As discussed previously for all the sonicated VMT samples, a broadening of the ‘‘mica-VMT mixed layers” reflections as well as the disappearance of some of them were observed in the

PA/VMT composites. This broadening is attributed to the delamination of VMT sheets together with particle size reductions induced by sonication.

4.4.3. Infrared spectroscopy

Figure 4.25 shows the FTIR spectra of the (a) PA-sonicated H_2O_2-exfoliated and (b) sonicated thermally-exfoliated VMT bio-nanocomposites as a function of filler content. The two spectra showed identical behaviour, indicating that similar materials were generated independently of whether the exfoliation was achieved through a thermal shock or hydrogen peroxide treatment. This means that the two procedures delivered similar end products as far as phase composition is concerned. It is evident from the figure that the two spectra were also independent of the concentration of the VMT incorporated. The carbonyl stretching band for the neat polymer appears at around 1645 cm^{-1} and similar bands can be seen in the all composite spectrum. However, the carbonyl stretching band at 1645 cm^{-1} seems to be at lower wave number than the normal carbonyl stretching (1710 cm^{-1}), this may indicate a strong H-bond formation/present in the polymer matrix.

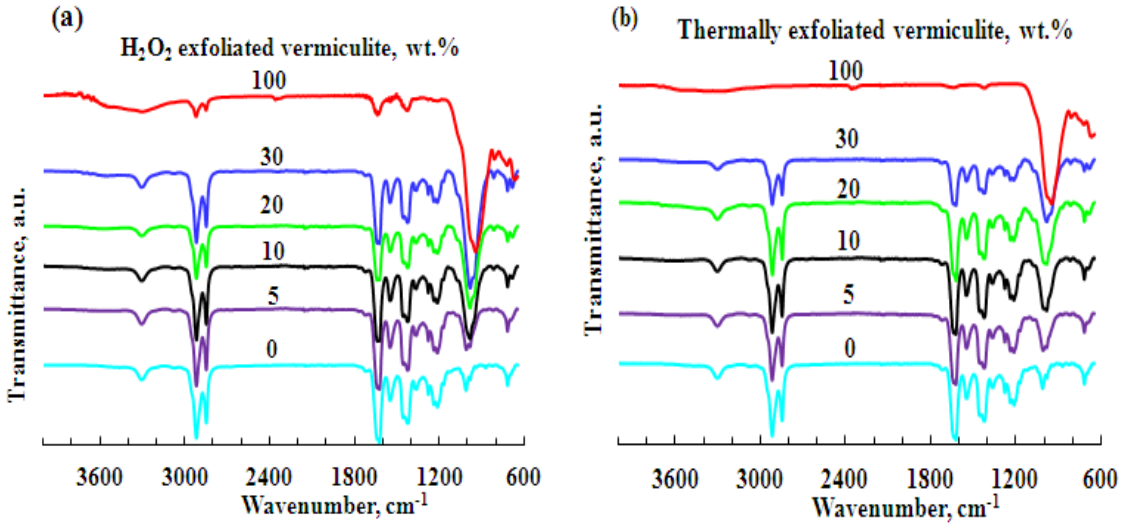

Figure 4.25. FTIR spectra of (a) DAPA-sonicated H_2O_2-exfoliated and (b) sonicated thermally-exfoliated VMT bio-nanocomposites.

4.4.4. Thermogravimetric analysis (TGA)

The variation of weight loss with temperature recorded in an air atmosphere for sonicated H_2O_2- and sonicated thermally-exfoliated DAPA/VMT composites is respectively presented in Figure 4.26 (a) and (b). The corresponding curves exhibited a similar trend irrespective of

whether the exfoliation was achieved through a thermal shock or hydrogen peroxide treatment. The TGA curves for the neat polymer and the composites display two major mass loss steps. Most of the mass loss occurs in the first step in the temperature range 300 °C to 500 °C. The DAPA leaves a char residue of about 10 wt.% at 500 °C and mass loss is complete at ca. 600 °C. Above this temperature, the composites show plateau values corresponding to the inorganic residue derived from the decomposition of the VMT. These were used to confirm filler content of the composites. The first mass loss event commences at higher temperatures in the composites. This reflects the effect of the flake-shaped filler particles that inhibit the mass transfer to the atmosphere of the volatile degradation fragments. However, a radical trapping effect may also play a role (Carvalho et al., 2013). In addition, it is clear from the figure that above 500 °C in both cases (for sonicated H_2O_2- and sonicated thermally-exfoliated DAPA/VMT composites) the residues of the polymer composites were higher than that observed for the neat DAPA in thermo-oxidative degradation conditions used. This indicates that the presence of clay enhanced the thermal stability.

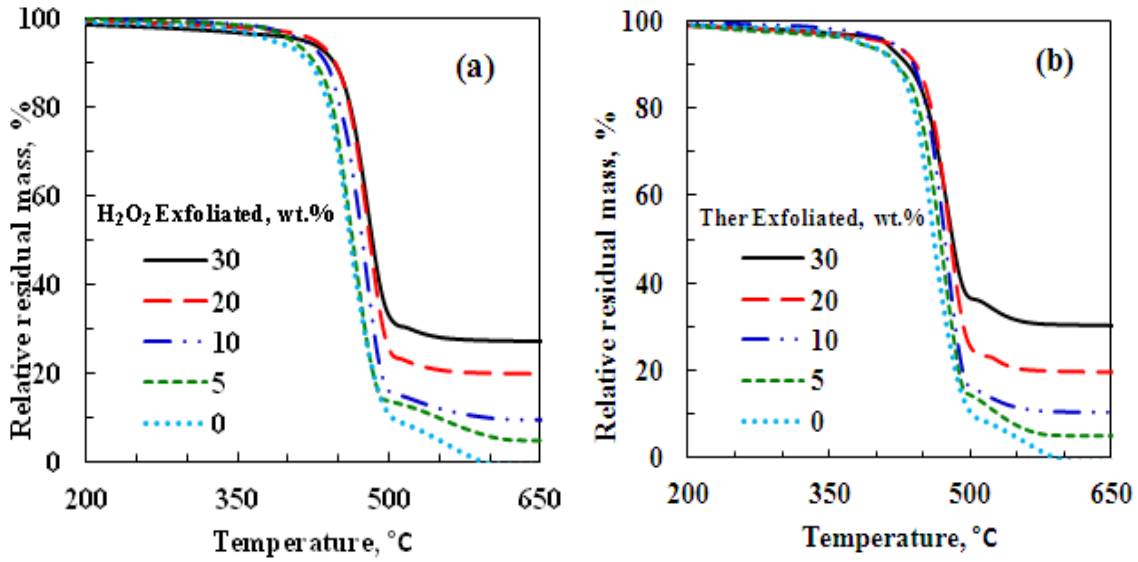

Figure 4.26. TGA curves for sonicated H_2O_2- and sonicated thermally-exfoliated VMT and its DAPA bio-nanocomposites.

4.4.5 Mechanical properties

Figure 4.27(a) shows that the tensile strength increased with filler loading while the elongation at break decreased precipitously. At a loading of 30 wt.% VMT, the tensile

strength was about double of that of the neat DAPA. However, the elongation-at-break was only one tenth of the original value.

a) Modelling the Young's modulus

Figure 4.27(b) shows least square fits of the Halpin-Tsai equations for platelets to Young's modulus data of the present VMT-based composites assuming random platelet alignment. The tensile modulus for the VMT flakes was taken as 175 ± 16 GPa (Suk et al., 2013). The tensile moduli of the PA was taken as the measured value of 33 ± 4 MPa. By considering the random orientation of the platelets and using Equation 2.3 with ξ_T fixed at $\xi_T = 2$, good fits were obtained using $\xi_L = 29.0$ and $\xi_L = 36.4$, for the composites based on H_2O_2-exfoliated and thermal-exfoliated VMT fillers respectively. These values correspond to aspect ratios of the platelets of 43.5 and 54.5. The aspect ratios were calculated using the corrected shape factors equation for platelet reinforcements proposed for the longitudinal (E_{CL}) and transverse (E_{CT}) composite modulus given as $\xi_L = (2w/3t)$ for $\xi_T = 2$ (see heading e)) of the section 2.10.2. In this equation, the ratio w/t represents the aspect ratios, where w and t are the width and thickness of the flakes, respectively.

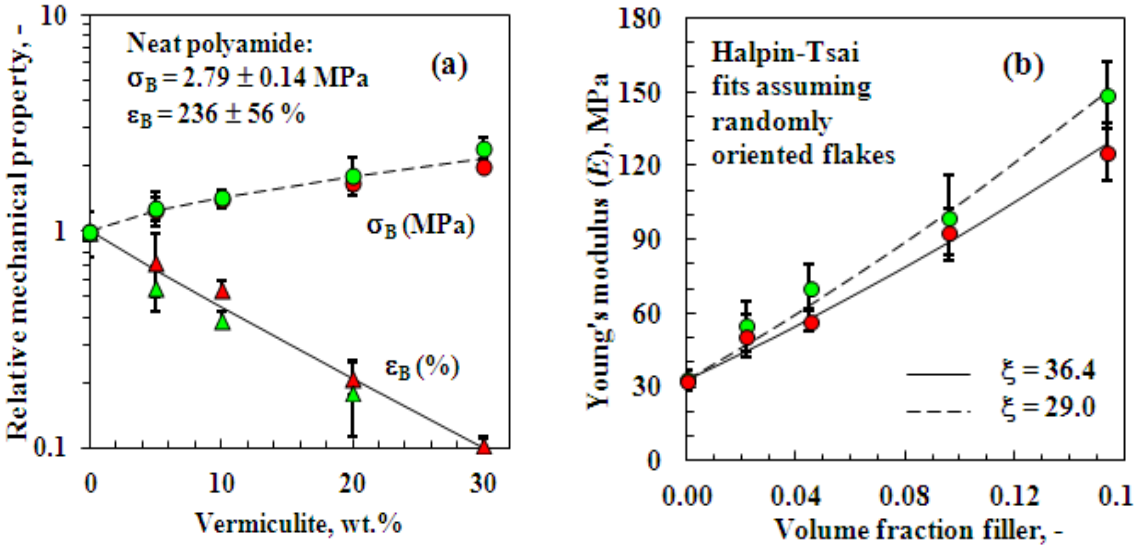

Figure 4.27. Effect of VMT content on (a) the tensile strength and elongation-at-break, and (b) the Young's modulus of DAPA bio-nanocomposites. Green filled symbols: Sonicated thermally-exfoliated VMT. Red filled symbols: Sonicated H_2O_2-exfoliated VMT.

4.4.6 Viscosity

The melt viscosity of filled polymer compounds is important as it relates to the processability by conventional plastic conversion technologies such as extrusion and injection moulding. The melt viscosity is sensitive to the structure, particle size and shape as well as the interface characteristics of the dispersed phase (Ray and Okamoto, 2003). In some suitable instances, rheology can even be used to quantify the shear thinning effect for polymer–clay nanocomposites and thereby to compare the extent of delamination of platelet stacks (Wagener and Reisinger, 2003).

Figure 4.28(a) and (b) show the effect of clay content and shear rate on the melt viscosity of sonicated H_2O_2-exfoliated VMT and sonicated thermally-exfoliated VMT composites, respectively. From the figures, it can be seen that the addition of clay was responsible for a more significant increase of melt viscosity. At low shear rates the composites samples exhibited high viscosity when compared with the neat polymer, and as expected, the viscosity increases with increasing the amount of clay.

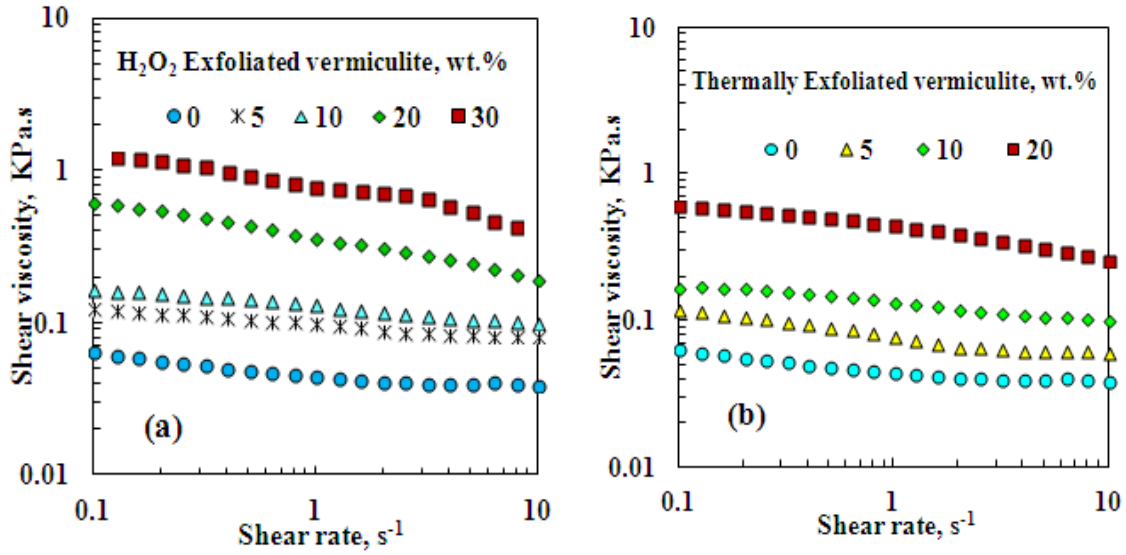

Figure 4.28. Effect of the VMT type, content and shear rate on the viscosity of DAPA bio-nanocomposites at 160 °C. (a) sonicated H_2O_2-exfoliated VMT and (b) sonicated thermally-exfoliated VMT.

For the sonicated H_2O_2-exfoliated VMT, at a loading of 30 wt.%, the viscosity was more than an order of magnitude higher than that of the neat DAPA. This can indicate the strong interactions between the clay particles and the polymer matrix. In fact, the dispersion and

interaction of clay particles in the polymer matrix provide resistance to flow at low shear rates, indicating the presence of yield stress. In other words, at low shear rates, the network structures formed by clay particle interactions remains unaffected by the imposed flow. On the other hand, at high shear rates, the clay loading has only a relatively small influence on the viscosity.

At relatively high shear rates, the neat DAPA and its VMT composites all showed weak shear thinning behaviour. The shear thinning behaviour of the composites is such that their viscosities are comparable with those of neat polymer at high shear rates and can be explained as a result of the reorientation of the silicate layers or tactoids parallel to the flow direction. This ability to re-orient the silicates layers or tactoids in response to externally applied flows also appears to control the viscoelastic properties of the composites (Bhattacharya et al., 2008).

4.4.7 Dynamic mechanical analysis

Typical DMA results of the neat DAPA and its composites are illustrated in Figures 4.29 – 4.34. Figure 4.29(a) and (b) depicts the storage modulus (bending mode) as a function of temperature at a frequency of 100 Hz of the neat DAPA and its VMT composites. From the figure is clearly evident that the addition of VMT to the polymer results in improved storage modulus over the entire temperature range compared to the pure matrix. This indicates that VMT clay was able to affect the chain mobility of polymer matrix.

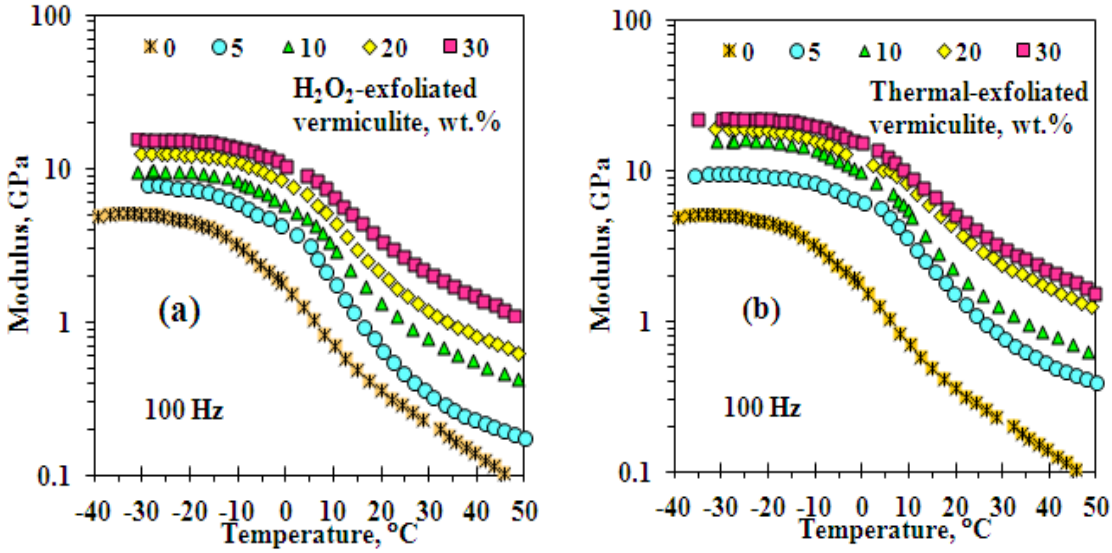

Figure 4.29. Effect of filler loading on storage modulus (bending mode) at a frequency of 100 Hz for (a) sonicate H_2O_2-exfoliated VMT and (b) sonicated thermally-exfoliated VMT DAPA/bio-nanocomposites.

All composite samples showed similar trends with storage modulus decreasing with increasing temperature, indicating the increase in segmental polymer chain motion with temperature. However, the increase of the storage modulus for the composites is in the order of increasing the amount of the clay. At 10 °C, i.e., exactly at the T_g of the neat polymer (refer to Figure 4.30), the sonicated H_2O_2-exfoliated VMT polymer composites with clay contents of 5, 10, 20 and 30 wt.% were respectively 97% (1.40 GPa), 338% (3.11 GPa), 544% (4.57 GPa) and 828% (6.59 GPa) whereas for the sonicated thermally-exfoliated VMT polymer composites with the same clay contents the increase in storage modulus was respectively 295% (2.81 GPa), 623% (5.13 GPa), 1023% (7.97 GPa) and 1185% (9.12 GPa) increase in storage modulus compared to pure polymer (0.71 GPa). At room temperature, i.e., 25 °C, the corresponding increases in storage modulus were respectively, 274% (1.01 GPa), 467% (1.53 GPa), 874% (2.63 GPa) and 893% (1.39 GPa) for sonicated H_2O_2-exfoliated VMT polymer composites and 233% (0.90 GPa), 470% (1.54 GPa), 1030% (3.05 GPa) and 1333% (3.87 GPa) for sonicated thermally-exfoliated VMT polymer composites, respectively with the modulus value for the neat DAPA equal to 0.27 GPa.

As evidenced by Figure 4.29 (a) and (b), although the storage modulus for the composites increases with increasing VMT content, the stiffness enhancement is relatively limited at low temperatures (below T_g). This behaviour can be related to the fact that the polymer is in the glassy state. However, above the T_g, where the polymer matrix softens the reinforcement effect of the two nano-reinforcements increases due to their ability to restrict the motions of the polymer chains.

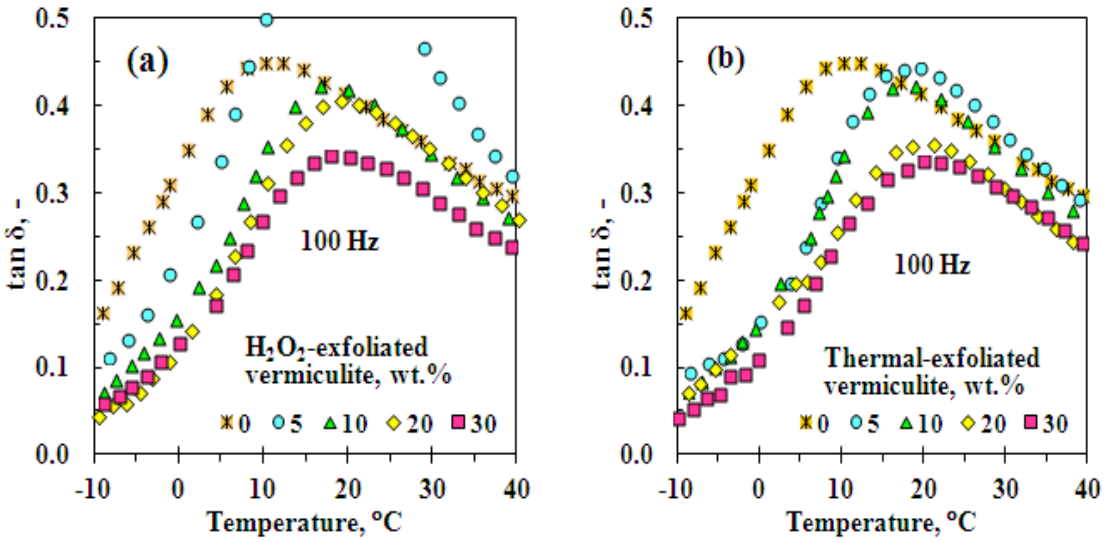

Figure 4.30. Effect of filler loading on tan δ at a frequency of 100 Hz for (a) sonicate H_2O_2-exfoliated VMT and (b) sonicated thermally-exfoliated VMT DAPA/bio-nanocomposites.

The glass transition temperature of each material was estimated from the position of the tan δ peak. The values are reported in Figure 4.30 as a function of filler loading and measurement frequency. For all composites, the presence of the VMT filler caused a large upward shift of up to 10 °C in the T_g. This shift in the glass transition temperature suggests that the presence of the filler constrained polymer chain mobility.

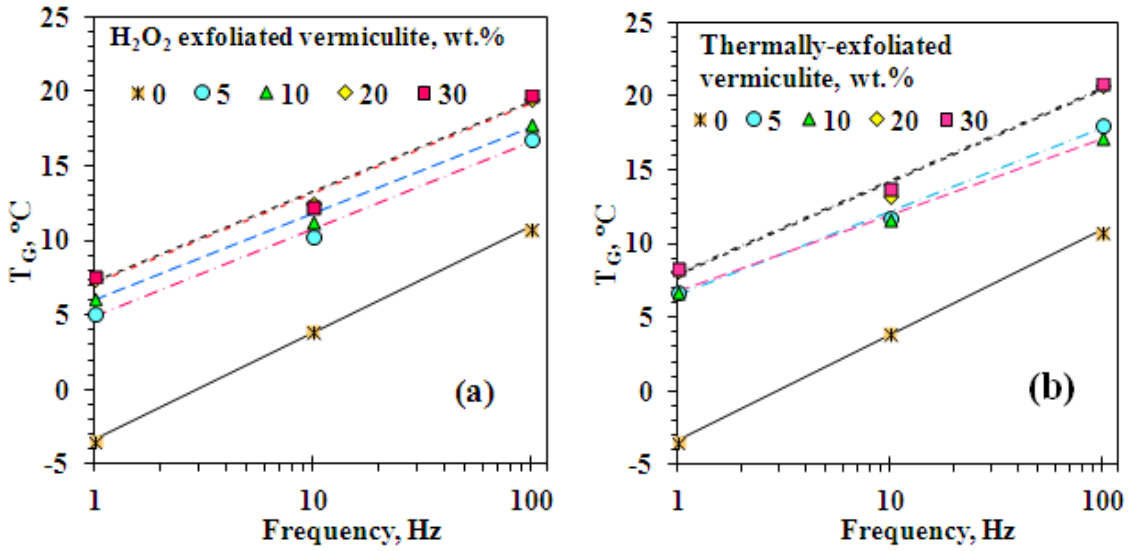

Figure 4.31. Effect of filler loading on the glass transition temperature (from tan δ plots): (a) sonicate H_2O_2-exfoliated VMT and (b) sonicated thermally-exfoliated VMT DAPA/bio-nanocomposites.

As evidenced by Figure 4.30 and Figure 4.31, although T_g increases with increasing VMT content, the composition dependence is weak. The bending modulus for the neat DAPA shows a plateau value at temperatures well below T_g. It decreases rapidly towards much lower values as T_g is approached and passed. The modulus curves for the filled compounds show a similar shape. In essence, they appear shifted upward and towards higher temperatures when compared to the curve for the neat DAPA.

Figure 4.32 shows the effect of filler content and measurement frequency on the modulus plateau values in the glassy region. The modulus does increase slightly with frequency but filler content has a much greater effect. The reinforcing action of the stiff inorganic flakes is the primary reason for the increase in the bending modulus. However, the increased T_g values for the polymer matrix also contributes. These two effects can be removed by scaling the modulus curves and plotting them with respect to the temperature shift with respect to the corresponding glass transition temperatures. Such master curves are plotted in Figure 4.33

and Figure 4.34 for the sonicated H_2O_2- and sonicated thermally-exfoliated VMT composites respectively. They show that this curve shifting approach collapses all the data sets into a single curve for temperatures below T_g. This implies that, in the glassy region, the reinforcing action of the filler is adequately described by a combination of filler micro-mechanics (the primary effect) and a secondary effect associated with the reduction in chain mobility caused by the special confinement effect imposed by the high surface area flakes on the polymer chains. The latter expresses itself by a change in the effective thermal state of the polymer chains that is adequately captured by the apparent shift in the T_g.

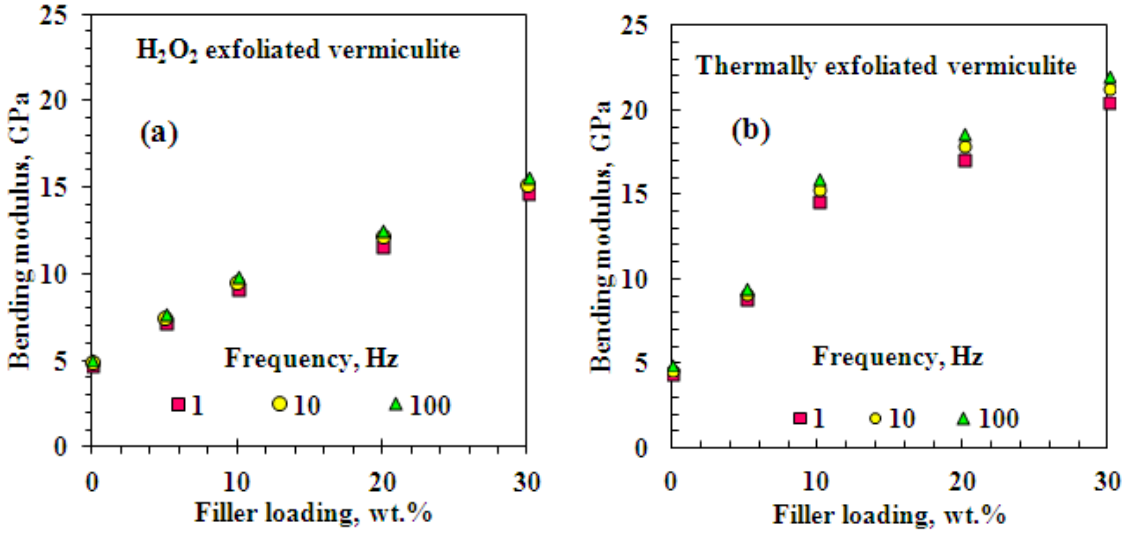

Figure 4.32. Effect of filler loading and measurement frequency on the modulus plateau values in the glassy region for (a) sonicate H_2O_2-exfoliated VMT and (b) sonicated thermally-exfoliated VMT DAPA/bio-nanocomposites.

Significant deviations are apparent at temperatures above T_g with the modulus values failing to form a single band. The scaled modulus curves deviate to higher values as the filler content is increased. Compared to the curve associated with the neat DAPA, the moduli decrease more slowly with increasing temperature. Nevertheless, the curves for compositions containing 20 wt.% and 30 wt.% filler virtually coincide. This means that there must be a tertiary reinforcing effect attributable to the presence of the flakes that reaches a limit beyond which further addition of filler has little effect.

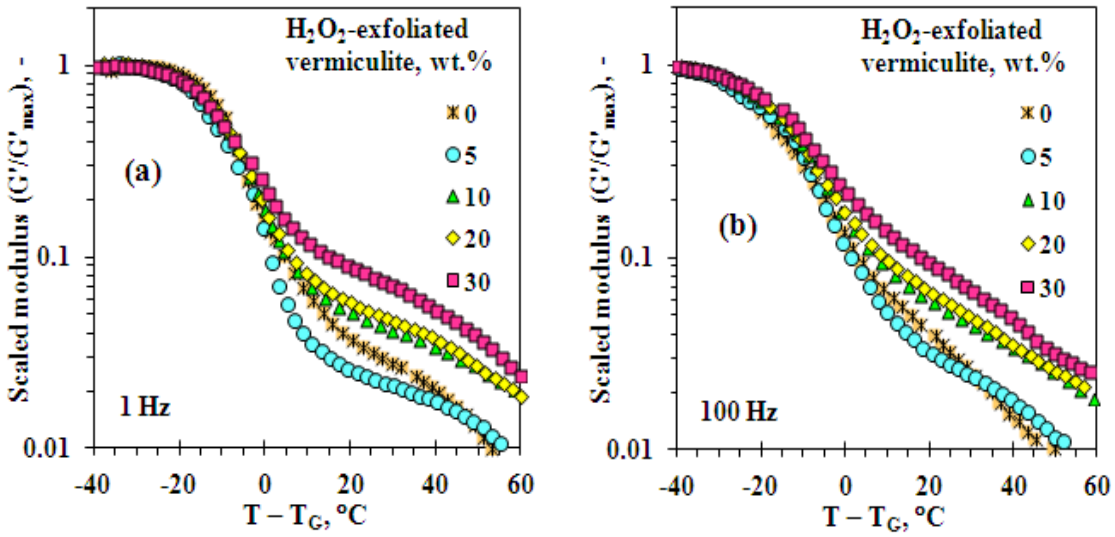

Figure 4.33. Modulus "master curves" generated by scaling with respect to the modulus plateau in the glassy region and a glass transition temperature shift for sonicated H_2O_2-exfoliated VMT DAPA/bio-nanocomposites at a frequency of (a) 1 Hz and (b) 100 Hz.

It is tentatively proposed that virtual crosslinking forms the basis of this tertiary effect. The electron microscopy results have confirmed strong interactions between the DAPA chains and the VMT flake surfaces. That was expected given that, by design, some chain ends are attached to the mineral surface via strong electrostatic forces. Furthermore, the DAPA chains are capable of strong inter-chain hydrogen bonding interactions as well as interactions with the VMT surfaces, whether covered by a polymer or not. Above the glass transition temperature, the chains have considerable mobility. The dynamic nature of hydrogen bonds formation creates a time-varying and spatially fluctuating cross-linked network that connects chains and filler particles. The effective crosslink density of these networks is increased as the filler content increases. Increased crosslink density implies increased the stiffness of the network explaining the higher modulus values at elevated temperature observed in Figure 4.33 and Figure 4.34. Strong interactions between reinforcement and matrix molecules originated from hydrogen bonding were previously observed in DAPA filled with cellulose fibres (Hablot et al., 2010a).

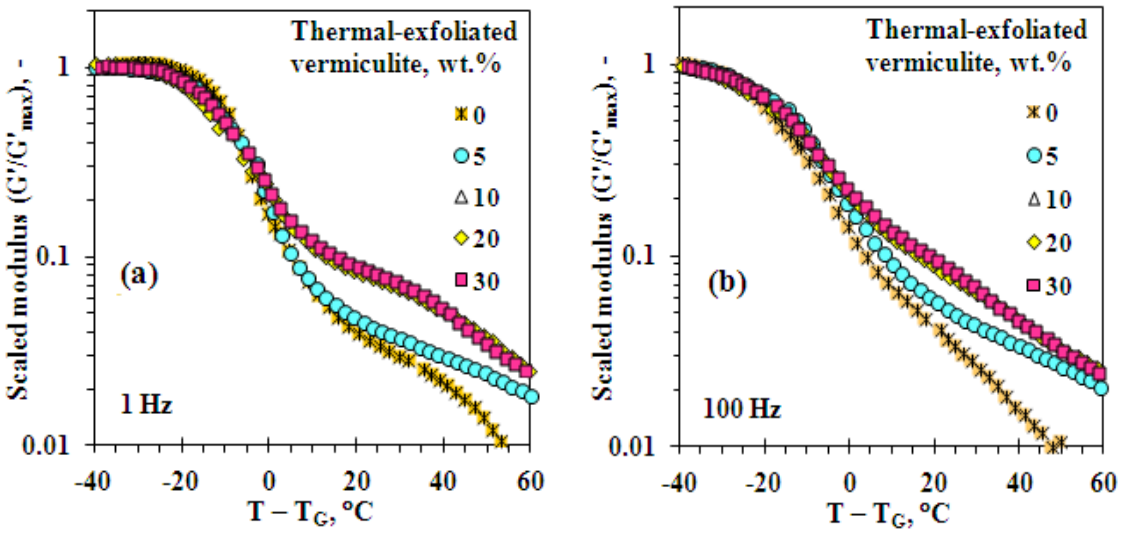

Figure 4.34. Modulus "master curves" generated by scaling with respect to the modulus plateau in the glassy region and a glass transition temperature shift for sonicated thermally-exfoliated VMT DAPA/bio-nanocomposites at a frequency of (a) 1 Hz and (b) 100 Hz.

4.4.8. Conclusions

Submicron VMT flakes bio-nanocomposites, based on a DAPA were successfully prepared using a similar route to the one was applied to prepare the ammonium ion exchanged MMT bio-nanocomposites. The flake-like reinforcement was generated by first exfoliating the mineral via either thermal shock or treatment with hydrogen peroxide followed by sonication. BET surface area measurements and SEM analysis of the VMT exposed to a thermal shock or treatment with hydrogen peroxide followed by sonication showed VMT flakes with a thickness below 100 nm together with thicker flakes. This is an indication that the exfoliation method employed led a reduction in size, which could be explained by the extensive delamination.

XRD results showed that the polymer did not intercalate into the VMT galleries implying that the flake morphology was fixed at the sonication stage. SEM and TEM confirmed the formation of bio-nanocomposites featuring a mixed morphology. The VMT flakes were randomly distributed in the matrix and featured thicknesses ranging from submicron in size down into the nano-range. Good adhesion between the matrix and the flakes was indicted by the fact that cryo-fracturing resulted in cohesive rather than adhesive failure at the flake surface.

Polyamide bio-nanocomposites containing as much as 30 wt.% VMT were obtained. At this filler loading, and depending on the exfoliated clay type (i.e. sonicated H_2O_2- and sonicated thermally-exfoliated VMT), the tensile strength was doubled while the elongation-to-break was decreased by a factor of ten. Halpin-Tsai analysis of the variation in Young's modulus with filler content supported the high aspect ratio nature of the flake reinforcement. The melt viscosity, measured at 160 °C also increased by a factor of about 20 when the filler was added.

The addition of clay also increased the T_g of the polymer by up to 10 °C as indicated by dynamic mechanical analysis. This indicates that the high interfacial surface area, presented by the dispersed nano-platelets in the matrix, significantly impaired the polymer chain mobility. This implies an effective stiffening of the polymer matrix at temperatures above T_g. It also explains, in part, the higher apparent reinforcing effect observed at temperatures above T_g. Analysis of the variation in composite modulus with temperature and composition indicate that, below the glass transition temperature, the composite stiffness is adequately explained by invoking the reinforcing effect of the inorganic filler together with the apparent shift in T_g. It is postulated that dynamic network formation through polymer-filler hydrogen bonding interactions provides a tertiary stiffening mechanism that operates at a temperature above T_g.

By comparing the performance of the two VMT samples (i.e. sonicated H_2O_2- and sonicated thermally-exfoliated VMT), the properties of the sonicated thermally-exfoliated VMT composites were much better than those of the sonicated H_2O_2-exfoliated. Initially, the poor properties exhibited by the sonicated H_2O_2-exfoliated composites were associated with a possible oxidative degradation of polymeric matrix caused by an eventual excess of H_2O_2. However, the FTIR spectroscopy analysis (refer to Figure 4.25) conducted on the neat polymer and its composites did not correlate with the associated hypothesis. No evidence of an oxidative degradation of the polymer caused by H_2O_2 reaction was found. Since the extent of properties enhancement in polymer nanocomposites depends strongly on the high particle aspect ratios, this is an indication that better reinforcement has been obtained with the VMT sample with the higher particle aspect ratios. In the present study, the thermally expanded VMT sample is the one that exhibited the high particle aspect ratios (54.5) than the chemically expanded sample (43.5). This could obviously explain the much better properties

of the sonicated thermally-exfoliated VMT bio-nanocomposites than those of the sonicated H_2O_2-exfoliated ones.

4.5. Melt compounded VMT and PGS9/bio-nanocomposites based on PA-11

Here the main goal was to compare the effect of the organic modification on properties of the generated PA-11/bio-nanocomposites, with emphasis on the mechanical and flame retardant properties. The performance of OVMT and UVMT samples with the commercial sepiolite (PGS9) was also compared. In this particular case, the aspects that were addressed included the effect of the shape of the clay, the aspect ratio of the particles, and the degree of dispersion that was achieved.

4.5.1. Electron microscopy (SEM and TEM)

Representative images of the morphology and orientation of different clays in the 10 wt.% PA-11 bionanocomposites are shown in Figures 4.35 and 4.36. VMT sheets are well dispersed and oriented in the length direction along the dog bone samples as illustrated in Figure 4.35 (a and a') and (b and b'). In addition and as previously observed for DAPA/VMT bio-nanocomposites, the thickness of the relatively large VMT sheets appears to range from micrometers to nanometers. The presence of thicker sheets was expected for the reasons pointed out in the Section 4.4.1.

Fibres alignment in the flow direction along the dog-bone samples was also observed with PGS9 (Figure 4.35(c) and (c')). The images show a good dispersion of the fibres in the polyamide matrix. The images of the fracture surfaces suggest that the sepiolite needles were strongly bonded to the matrix. Consequently, they fractured cleanly in the crack plane of the matrix, i.e. there was negligible fibre pull-out. Small fibre bundles (in white colour) are also visible on the fracture surface of the polyamide bio-nanocomposites. In the case of VMT/bio-nanocomposites, ropey polymer structures connecting adjacent flakes are noticeable in Figure 4.35(b').

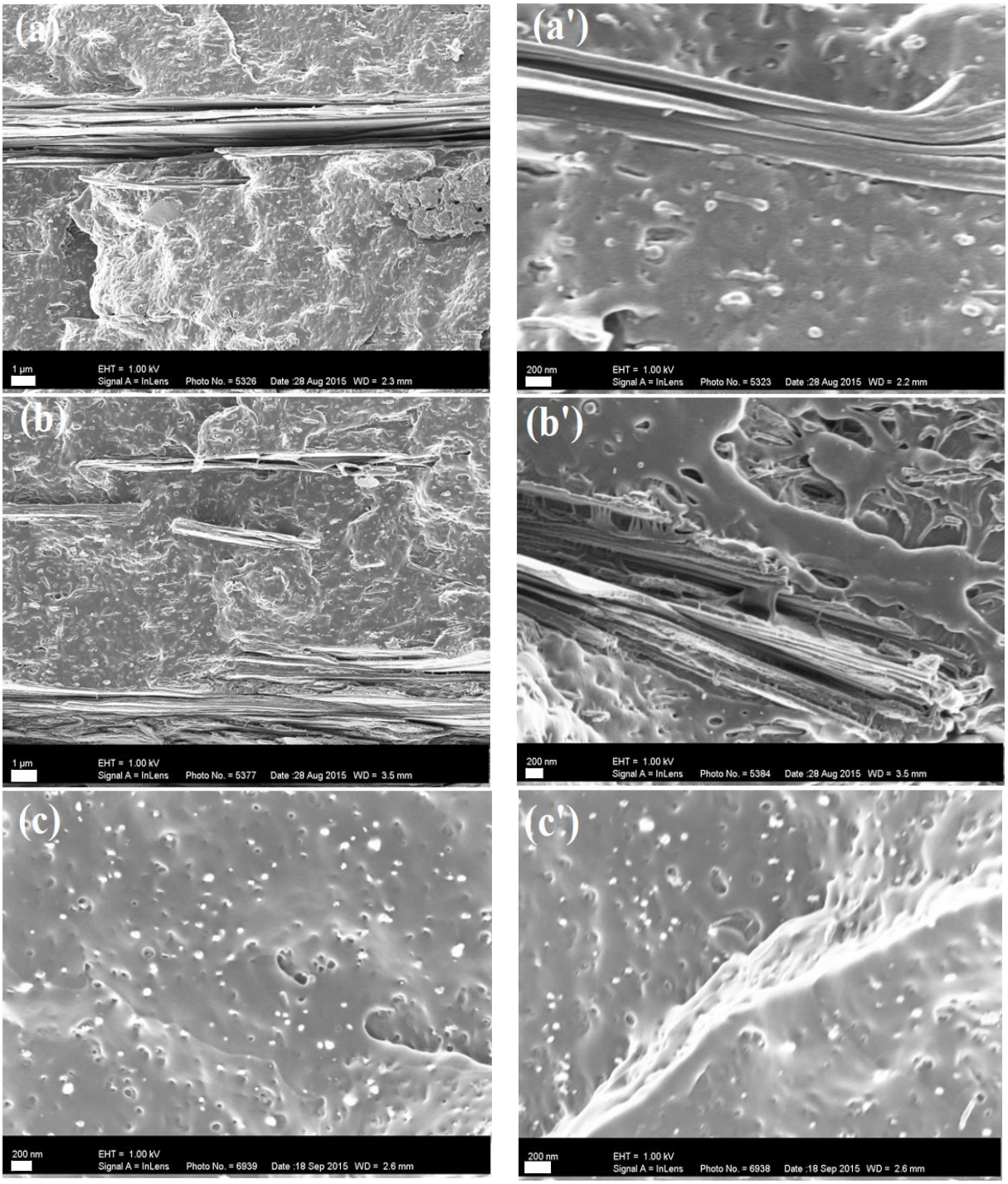

Figure 4.35. Cross-sectional SEM images of 10 wt.% VMT PA-11 bio-nanocomposites: (a, a') UVMT, (b, b') OVMT, and (c, c') PGS9.

Figure 4.36 shows representative TEM micrographs of microtome cross-sections taken from PA-11 clay bio-nanocomposites. They provide information on the local dispersion of the clays in the polyamide matrix.

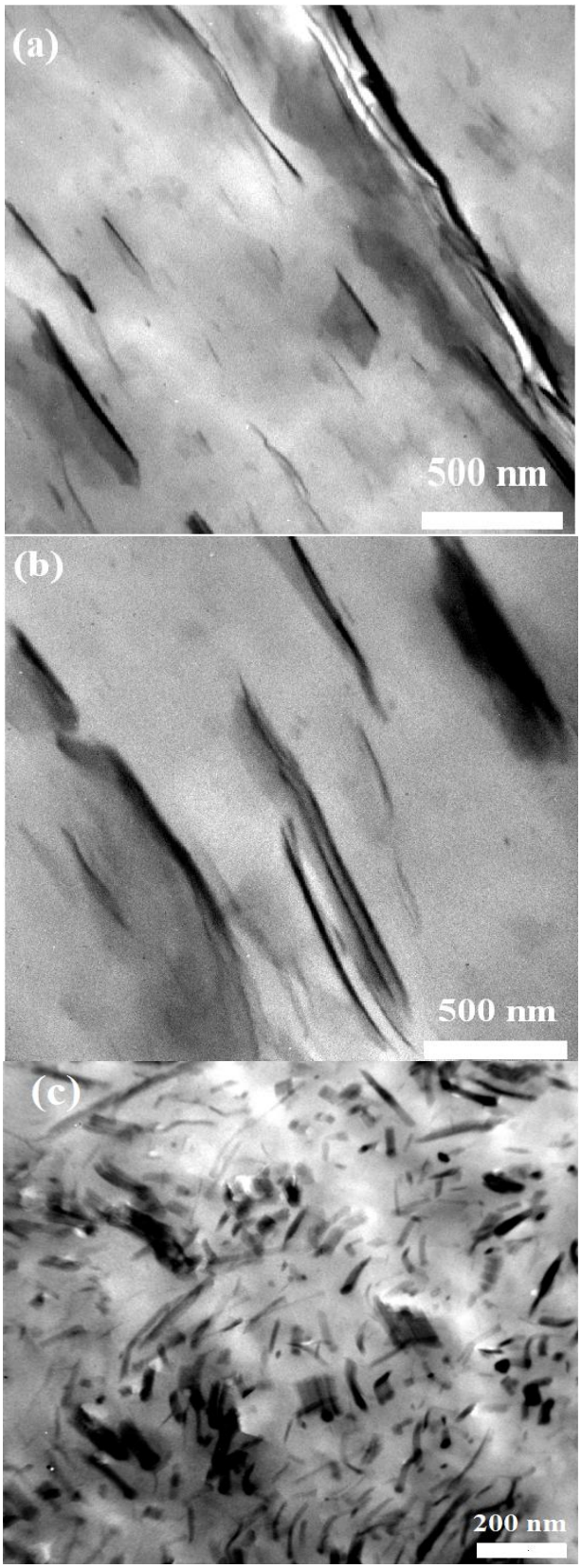

Figure 4.36. TEM images of 10 wt.% clay PA-11 bio-nanocomposites: (a) UVMT, (b) OVMT, and (c) PGS9.

The dark lines represent the individual clay layers, sepiolite needles or their agglomerates, whereas the gray regions correspond to regions of the polyamide matrix. In general, all micrographs reveal that the clays are uniformly dispersed and exfoliated in the PA-11 matrix. The average thickness of clay sheets exceeds several nanometers. Reasonably good nano-dispersion was obtained with sepiolite in PA-11 as shown in Figure 4.36(c). It can be attributed to strong interactions between the polymer and sepiolite through hydrogen bonding interactions between the carbonyl groups of the polymer and the hydroxyl groups situated on the surface of sepiolite. The presence of hydroxyl groups in the sepiolite structure is an attractive feature of this clay. Surface hydroxyl groups make an organic modification of clays unnecessary for polar matrices capable of hydrogen bonding (Fukushima et al., 2012).

4.5.2. X-ray diffraction (XRD)

X-ray diffraction patterns of UVMT, OVMT and PGS9 and their polyamide bio-nanocomposites are shown in Figure 4.37. The neat PA-11 exhibits three main crystalline reflection peaks at about 2θ = 8.3, 23.4 and 26.6° corresponding to (001), (100) and (010/110) planes, respectively. These crystalline peaks correspond to those of the α-polymorph of PA-11 (Hu et al., 2009, Liu et al., 2003, Mago et al., 2011).

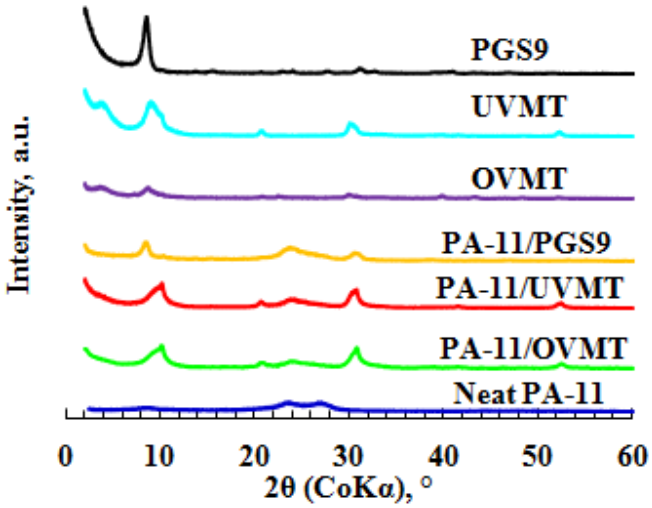

Figure 4.37. XRD patterns of UVMT, OVMT and PGS9/PA-11 bio-nanocomposites with 10 wt.% clay compared to their UVMT, OVMT and PGS9 clay samples.

The reflections from the vermiculite fillers in the bio-nanocomposites are very similar to those of the neat clays, irrespective of clay organomodification. This indicates that the melt compounding step did not result in extensive delamination of the VMT.

With the addition of PGS9 to PA-11, there was also no change in the position of the XRD reflections. Unlike the smectite clays, sepiolite is fibrous in nature and non-swelling. It exhibits a structure where individual tetrahedral-octahedral-tetrahedral layers are strongly held together by covalent bonds. The fibre bundles or aggregates are separated in the nanometer dimension range and dispersed throughout the polymer matrix. However, even completely separation of the fibrous needles will hardly have an effect on the location of the diffraction peaks in the XRD pattern. This explains why no shift of the peaks position of the clay in the XRD pattern of the bionanocomposites was observed (Choudhury et al., 2010, Fukushima et al., 2012, Kumar et al., 2010, Qiu et al., 2011).

4.5.3. Thermogravimetric analysis (TGA)

The variation of weight loss with temperature recorded in an air atmosphere for the various clay bionanocomposites is presented in Figure 4.38. The thermal stability of the bionanocomposites is obviously higher than that of pristine polyamide under thermo-oxidative degradation conditions. This is expected since, the presence of clay enhances thermal stability by acting as a diffusion barrier, thus preventing oxygen diffusion into the matrix and inhibiting the release to the atmosphere of small molecule fragments generated during thermal decomposition (Liu et al., 2004). It is clear from Figure 4.38 that the degradation onset temperature is slightly higher for the bio-nanocomposites compared to the pristine polymer.

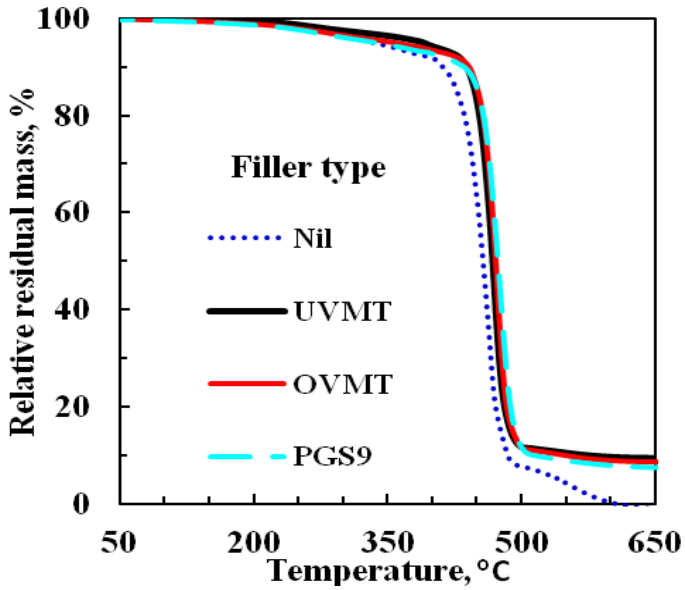

Figure 4.38. TGA curves of neat PA-11 and its 10 wt.% clay bio-nanocomposites.

TGA curves for bio-nanocomposites display two major weight loss steps. The first step, which involves the major degradation, occurs between 250 and 500 °C. In this step, the neat PA-11 records a strong weight loss with about 10.2 wt.% residue at 490 °C. The second step occurs between 480 and 600 °C. At this stage, the remainder is completely decomposed to volatile products. In addition, Figure 4.38 shows that above 500 °C, the amount of residue remaining is higher compared to the pure matrix. In fact, above 500 °C, the clays only loose the physically bonded water, a part of the coordinated water and water evolved from hydroxyl groups. So, the crystal structure hardly changes and the clays remain in the residual chars resulting in the increase of the residue amount (Chen et al., 2012, Frost and Ding, 2003). Above 600 °C, the bionanocomposites show a plateau corresponding to the inorganic part of a residue derived from the decomposition of the clays. Further data are given in Table 4.3, which summarize the residues results obtained at 700 °C for the pure PA-11 and its bionanocomposites. Table 4.3 shows that PA-11/VMT bio-nanocomposites exhibit better thermal stability than the PA-11/PGS9 system.

Table 4.3. % residues at 700 °C for the pure PA-11 and its bio-nanocomposites.

Sample	Remaining residues at 700 °C, wt.%
PA-11	0.00 (at 604 °C)
UVMT	9.25
OVMT	8.60
PGS9	7.26

4.5.4. Tensile properties

Tensile properties of the neat PA-11 and its bionanocomposites are listed in Table 4.4 and shown in Figures 4.39 -4.41. They show histograms of tensile characteristics, i.e. tensile strength, Young's modulus and elongation at break for each bio-nanocomposite formulation. Figures 4.39 and 4.40 show that both tensile strength and Young's modulus are improved by incorporating the clay fillers. However, the change in Young's modulus is more pronounced. For instance, Young's modulus of PA-11 bio-nanocomposites is almost twice of that of neat polymer. However, the bio-nanocomposite filled with PGS9 exhibit the best Young's modulus improvement. The increase is almost a 121% increment compared with neat PA-11.

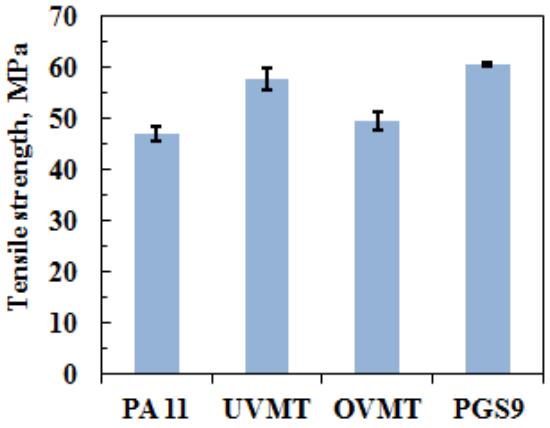

Figure 4.39. Effect of various clay samples on the tensile strength for neat PA-11 and its 10 wt.% clay bio-nanocomposites.

From Table 4.4 it is also observed that tensile properties of the bionanocomposites based on UVMT are better than those filled with OVMT.

Table 4.4. Mechanical properties of PA-11 and 10 wt.% clay PA-11 nanocomposites

Sample	Tensile strength (MPa)	Young's modulus (MPa)	Elongation at break (%)
Neat PA11	46.9±1.4	276±10	190±12
PA11/OVMT	49.6±1.7	527±19	200±12
PA11/UVMT	57.8±2.1	550±25	222±15
PA11/PGS9	60.5±0.4	610±13	90±14

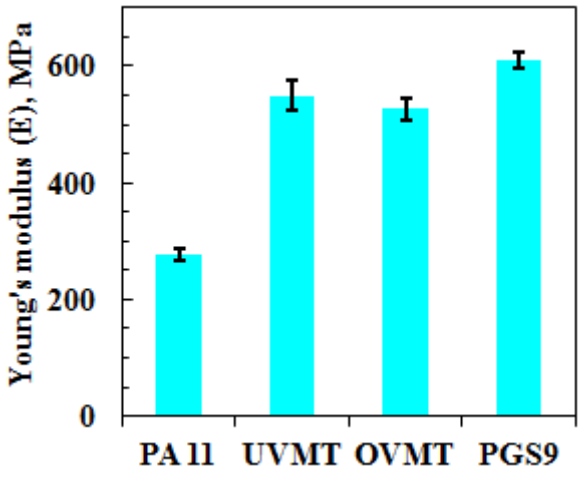

Figure 4.40. Effect of various clay samples on Young's modulus for neat PA-11 and its 10 wt.% clay bio-nanocomposites.

The improvement in tensile properties of PA-11/clay bionanocomposites is due to several factors besides the one related to the stiffness character of the clays. The other factors involve

the aspect ratio and the degree of dispersion clay particles. Additionally, the fine and nanoscale dispersion of the clay plays the major role. The high compatibility with the PA-11 combined with the fibrous nature of sepiolite seems also as favorable factors to improve the tensile properties.

A surprising and most interesting thing is the fact that the addition of vermiculite samples (OVMT and UVMT) led to an increase in elongation at break (Figure 4.41). Similar results were previously reported by Massinga (2013) for EVA- and Tang et al. (2008) for starch-clay nanocomposites. This is because the presence of a plasticizer facilitates the movement of polymer chains, imparting increased polymer flexibility (Tang et al., 2008). On other hand, this could also be due to the plasticizing effect of the galleries, their contribution to the formation of dangling chains and conformational effects at the clay matrix interface (Camargo et al., 2009). Dangling chain is another way to call branches, they are chains suspended laterally to the main backbone. Generally speaking it always related to the hysteresis of a polymeric matrix (repeated cycling under a given stress and so on).

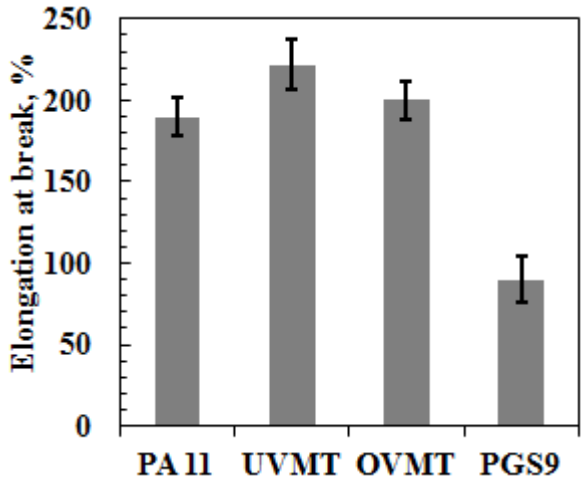

Figure 4.41. Effect of various clay samples on the elongation-at-break for neat PA-11 and its 10 wt.% clay bio-nanocomposites.

4.5.5. Dynamic mechanical analysis

Figure 4.42 summarizes the DMA data in which the dynamic storage modulus is presented as a function of temperature. From the figure, it is observed that at low temperature, where the polymer is in a glassy state, the storage modulus of the bio-nanocomposites (except for that loaded with UVMT) is only slightly higher compared to the neat PA-11. In the rubbery plateau, i.e. above T_g, the storage modulus of all PA-11/clay bionanocomposites is

considerably higher than the pure polymer. At room temperature, i.e., 25°C, the storage modulus values of UVMT, OVMT, and PGS9 bio-nanocomposites are 6.80 (1.10 GPa), 17.5 (1.21 GPa), and 40.8 (1.45 GPa)% higher than that of neat PA-11 (1.03 GPa), respectively.

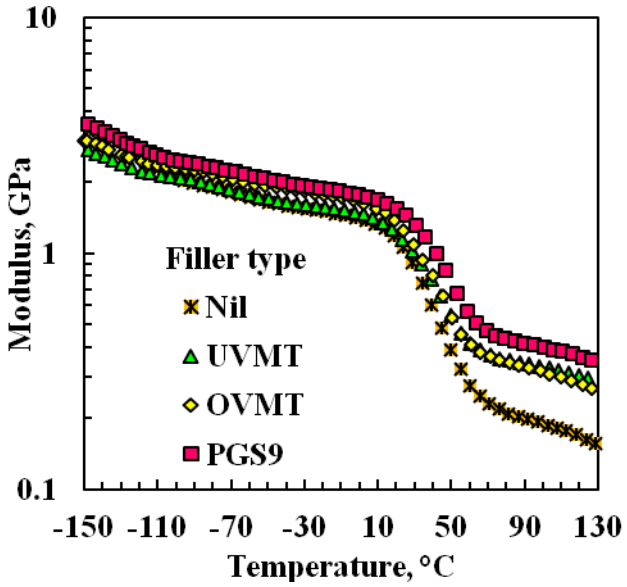

Figure 4.42. Representative plots showing the effect of different nanoparticles on the storage modulus (bending mode) at a frequency of 1 Hz for neat PA-11 and its 10 wt.% clay bio-nanocomposites.

Furthermore, Figure 4.42 also shows that the bio-nanocomposite filled with sepiolite exhibits the highest storage modulus over the entire temperature range compared to the rest of the samples. The results are consistent with the tensile data. The stiffness enhancement is, however, more pronounced at elevated temperatures, making sepiolite the most interesting filler as far as the maintenance of high modulus in temperature is concerned. The high compatibility of sepiolite with PA-11 associated with its fibrous nature could be responsible for the highest storage modulus.

Figure 4.43 shows the plots of tan δ recorded at 1 Hz as a function of temperature for the bio-nanocomposites samples. It is observed that there is no shift of tan δ for the PA-11 bio-nanocomposite filled with UVMT compared to pure PA-11. However, for PA-11/PGS9 bio-nanocomposite, tan δ peaks shifted to higher temperatures by about 8.3 °C compared to pure polyamide (43.7 °C). The increase in the apparent T_g indicates that PGS9 have been able to affect the segmental motions of the pure matrix, i.e., the presence of PGS9 constrained polymer chain mobility. Figure 4.43 shows also a decrease of T_g of PA-11/OVMT bio-

nanocomposite by about 4.4 °C, which is probably due to the amorphous effect from the polymer modifier together with the plasticizing effect from the polymer. Decreased T_g by adding has been reported plasticizer in the literature (Tang et al., 2008, Mali et al., 2006, McHugh & Krochta, 1994). This happens because the polymer matrix becomes less dense and mobility of polymer chains is facilitated with the addition of plasticizer. It is clear from Figure 4.43 that the intensity of the tan δ peaks for all bionanocomposites have decreased compared to pure PA-11, which is an indication of that fewer polymer chains are participating in this transition.

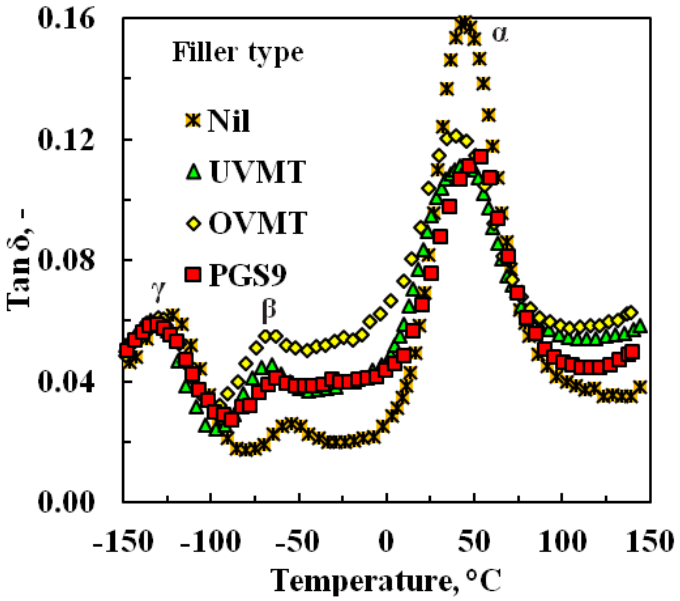

Figure 4.43. Representative plots showing the effect of different nanoparticles on tan δ at a frequency of 1 Hz for neat PA-11 and its 10 wt.% clay bio-nanocomposites.

4.5.6. Flame retardancy of PA-11/clay composites

The heat release rate (*HRR*) and total heat release (*THR*) plots for the neat PA and PA-11/clay bionanocomposites are shown in Figures 4.44 and 4.45 respectively, and some cone-calorimeter test data are listed in Table 4.5.

Table 4.5. Flammability data summary of 10 wt.% clay PA-11 bio-nanocomposites

Property, Units	Clay bio-nanocomposites			
	Pure PA-11	PA-11/UVMT	PA-11/OVMT	PA-11/PGS9
Time to ignition, s	109.5 ± 4.9	101.0 ± 0	103.5 ± 2.1	117.0 ± 2.8
Time to flameout, s	> 800.0	633.0 ± 45.3	684.5 ± 58.7	721.0 ± 52.3
Peak heat release rate, kW/m^2	575.0 ± 52.7	321.3 ± 8.7	298.7 ± 2.3	318.0 ± 15.6
Total heat release, MJ/m^2	88.9 ± 15.3	99.2 ± 5.9	97.6 ± 2.0	93.2 ± 1.6
Peak mass loss rate, g/s	18.1 ± 17.4	13.0 ± 7.0	12.0 ± 13.6	11.8 ± 7.9
MARHE, kW/m^2	176.7 ± 0.3	212.7 ± 0.4	193.9 ± 0.4	179.1 ± 0.1

The data reveal that the bio-nanocomposites show lower peak heat release rates (*pHRR*) compared to pure PA-11, indicating that the addition of clays significantly decreases the flammability of the matrix. For instance, the *pHRR* values (Table 4.5) of PA-11/UVMT, PA-11/OVMT, and PA-11/PGS9 bio-nanocomposites are respectively 321, 299 and 318 kW/m^2, corresponding to a reduction of 44, 48 and 45%, respectively compared to that of neat PA (575 kW/m^2). This suggests that the clays in the matrix exhibit a strong flame retardant effect. Indeed, the dispersed clay enhances the formation of char, which acts as an excellent insulator and mass transport barrier and subsequently, the rate of heat release decreases.

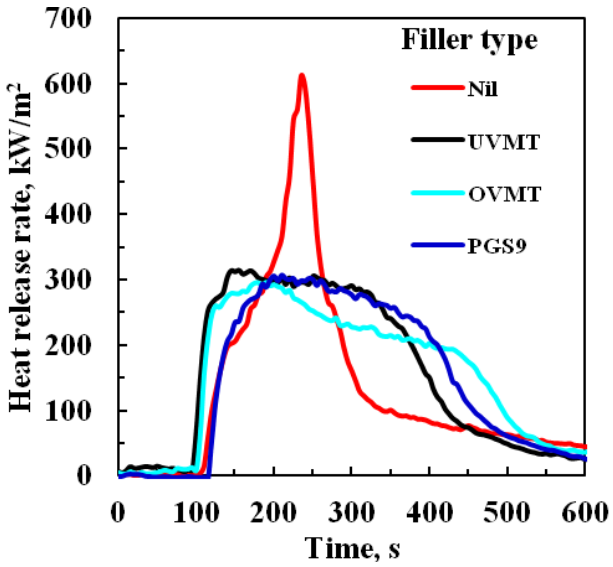

Figure 4.44. Heat release rate (*HRR*) curves of neat PA-11 and its 10 wt.% clay bio-nanocomposites during the cone calorimeter test.

From Table 4.5 it is clear that OVMT showed a better reduction in the *HRR* than the other systems. At least two factors might have contributed to this fact: (1) the surfactant-free organo-modification approach used allows organo-modification of the external surfaces of nano-sized clay sheets suspended in an acidic solution. This may facilitate more effective clay dispersion and to prevent restacking when they are ultimately compounded into the polymer matrix (Macheca et al., 2016). In addition, the organo-modified external surfaces of nano-sized clay sheets may eventually contribute to the formation of the more compact protective layer. Expanded vermiculites are known to have some tendency for adsorbing gases (Muiambo et al., 2010, Schoeman, 1989) and this may contribute to the reduction of the *HRR*.

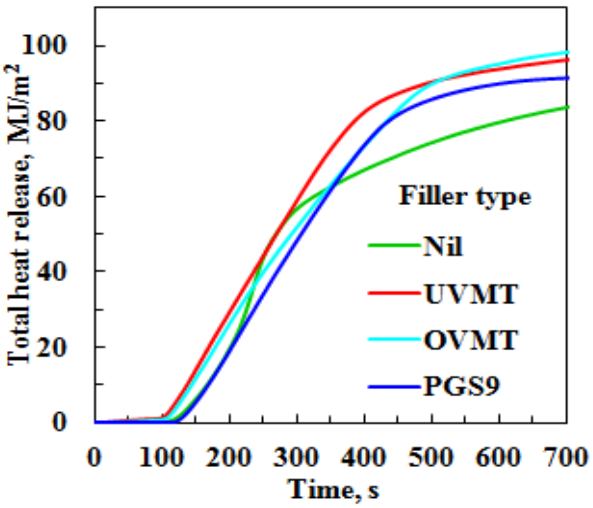

Figure 4.45. Total heat release (*THR*) curves of neat PA-11 and its 10 wt.% clay bio-nanocomposites during the cone calorimeter test.

From Table 4.5, it can be seen that the time to ignition (*TTI*) was slightly shortened for the bio-nanocomposites filled with vermiculite samples (OVMT and UVMT). This is probably due to a catalytic effect of the filler that accelerates the pyrolysis rates and possibly also to the char layer formation on the surface of the materials. A char layer prevents the heat and oxygen from transferring into the matrix interior (Huang et al., 2010). At the initial heating stage, the surface temperature of the vermiculite clay bionanocomposites rises quickly due to the formation of the char layer. This results in faster decomposition of PA-11 on the surface of the bio-nanocomposites. However, the PA-11/PGS9 bionanocomposite, although it has a lower *PHRR* compared to that of PA-11/UVMT, its *TTI* is slightly higher.

Also from the *HRR* plots (Figure 4.44) it can be observed that for the initial 150 s of the combustion the *HRR* for the bio-nanocomposites is higher than that of pure PA-11. This suggests that the addition of VMT and sepiolite accelerate the pyrolysis rate of the neat polymer. This is probably due a catalytic effect of the clays on the matrix.

The data reported in Table 4.5 indicate that the peak mass loss rate (*pMLR*) values of PA-11/UVMT, PA-11/OVMT and PA-11/PGS9 are 13.0, 12.0 and 11.8 g/s, respectively. This corresponds to a reduction of 28.3, 33.9 and 34.8% compared to the neat polyamide (18.1 g/s). Figure 4.46 shows the mass loss rate (*MLR*) recorded during the cone calorimeter experiment for each bio-nanocomposite formulation.

The *MLR* curves are similar to the *HRR* curves, so the reduction of the *MLR* is evidently the primary factor responsible for the lower *HRR* of the bionanocomposites. The reduction on *MRL* suggests that the clays effectively promote the formation of the residues of the flame retardant PA-11 bionanocompites.

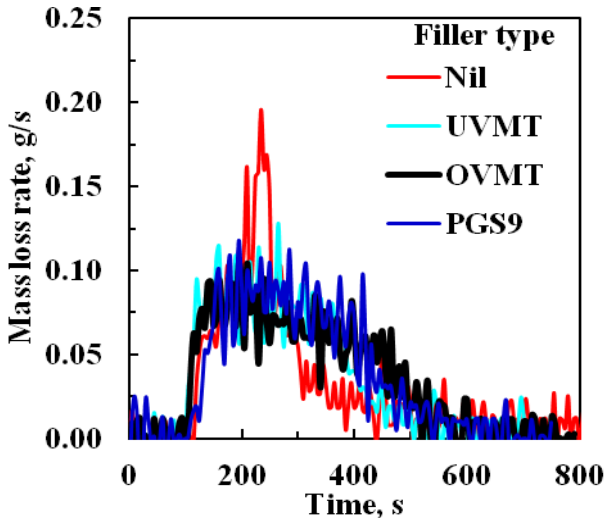

Figure 4.46. Mass loss rate (*MLR*) curves of neat PA-11 and its 10 wt.% clay bio-nanocomposites during the cone calorimeter test.

The smoke production rate (*SPR*) is considered as another important parameter for flame retarded materials, since the release of toxic smoke during a fire is the largest detriment to personal safety at a fire scene (Li et al., 2008).

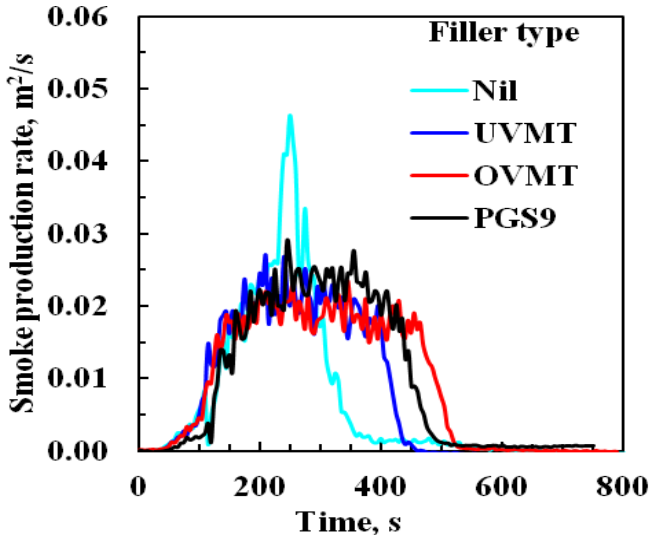

Figure 4.47. Smoke production rate (*SPR*) curves of neat PA-11 and its 10 wt.% clay bio-nanocomposites during the cone calorimeter test.

The *SPR* curves of PA-11 and its clay bio-nanocomposites vs. time are shown in Figure 4.47. Similar to the *HRR*, the *SPR* of the clay bionanocomposites are significantly lower than that of neat polymer. This clearly indicates the efficient role of clays to suppress the smoke production of PA-11 bio-nanocomposites.

4.5.7. Morphologies of char residues and flame retardancy mechanism

To further investigate the influence of the different clays on the flame retardancy mechanism, the morphologies of the residues of their bio-nanocomposites were observed. Figure 4.48 shows the digital photos and inner microstructure SEM images of the residues for the PA-11 bio-nanocomposites after the cone calorimeter test. The residues (Figure 4.48(a), (b) and (c)) exhibit a fibrous char layer structure. Further, a very compact and uniform surface morphology is observed for the char residues of all bio-nanocomposites. This indicates that the presence of clays act positively on the morphology of the formed residues and obviously affect the flame retardancy mechanism of the bio-nanocomposites.

The inner microstructure of the residues of the polymer clay bio-nanocomposites was further compared by SEM analysis. Figure 4.48(a'), (b') and (c') shows respectively, the inner morphologies of residual charred layers for the PA-11/UVMT, PA-11/OVMT, and PA-11/PGS9 bio-nanocomposites, at 1 µm after the cone calorimeter test.

For PA-11/UVMT and PA-11/OVMT bio-nanocomposites, the residues show similar features with thicker and very compact char layers. However, some loose and porous material was noticed on top of the compact layers. The addition of sepiolite (Figure 4.48(c')) also seems to reinforce the char barrier, keeping it more resistant to the disintegrating effect of the bubbles evolved. The char of the PA-11/PGS9 bio-nanocomposite seems to be more homogenous and well packed than those of PA-11/VMT.

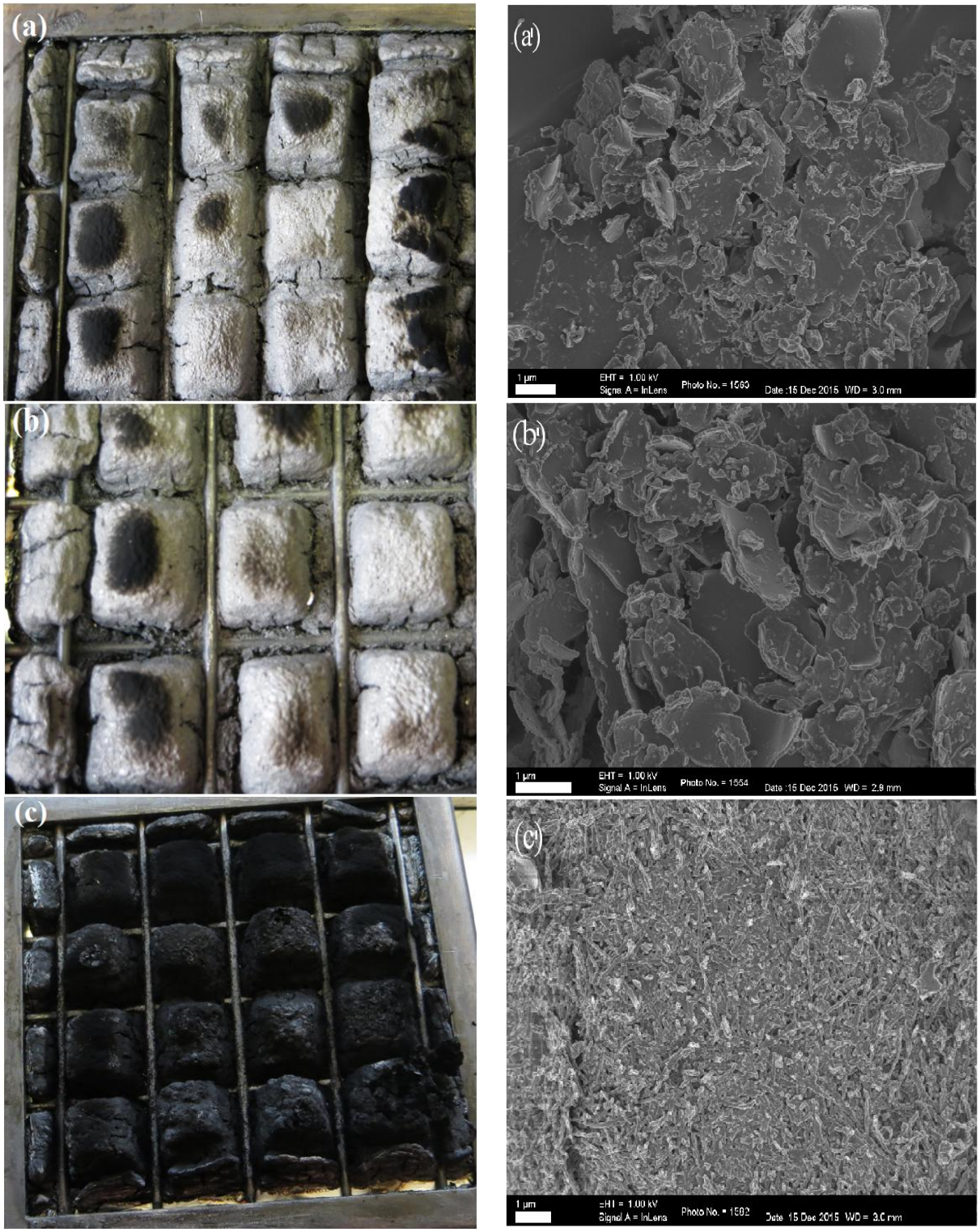

Figure 4.48. Digital photographs and inner microstructure SEM images of the char residues of 10 wt.% clay PA-11 flame retardant bio-nanocomposites after cone calorimeter test: (a) and (a') UVMT, (b) and (b') OVMT and (c) and (c') PGS9.

4.5.8. Conclusions

PA-11 based bio-nanocomposites prepared by adding 10 wt.% filler content of VMT modified by thermal shock and/or sonication and commercial sepiolite (Pangel S9) were successfully obtained by melt blending. Surfactant-free organo-modification approach was employed to modify the VMT clay surface. All clay samples showed a good dispersion and strong interaction between them and polymer matrix, as observed by electron microscopy (SEM and TEM) analysis and X-Ray diffraction (XRD). However, VMT sheets showed a limited dispersion on polymer matrix as compared to PGS9. This led the formation of polymer bio-nanocomposites with a mixed morphology. This behaviour was expected since the VMT used here is a natural mineral, consisting of flakes that correspond to randomly interstratified VMT biotite layers. Thus, even though that the exfoliation of the starting VMT was previously helped by thermal shock and accomplished with ultrasound, the shear forces developed by melt compounding were not sufficient to delaminate the vermiculite stacks completely.

Tensile properties results showed improvements in tensile strength and Young's modulus increased with the presence of the nano-fillers. However, the effect of clays in polymer matrix was more pronounced for the Young's modulus. Young's modulus of the bio-nanocomposites was almost double that of the neat polymer. Thermo-mechanical results also showed improvements in storage modulus with the addition of all particles, especially in the temperature range corresponding to the rubbery plateau (above the T_g). The observed improvements in tensile and thermo-mechanical properties for the lamellar silicate and/or fibre-based bio-nanocomposites seem to be more influenced by the stiff nature of clay fillers rather than the degree of exfoliation of the clay particles in the polymer matrix. The observed improvements in tensile and thermo-mechanical properties may also involve a combined effect of the possible strong interactions between the clay particles and PA-11 molecules originated from hydrogen bonding between the carbonyl group of polyamide and the hydroxyl groups belong to the structure of UVMT, OVMT, and PGS9.

Cone calorimeter test results showed that the peak heat release rate (*pHRR*) and smoke production rate (*SPR*) values of the PA-11/clays were significantly decreased compared to those of the neat polymer. This indicates that the addition of clays not only decreased the flammability of polyamide but also effectively suppressed the smoke production of the bio-nanocomposites. The digital photographs and SEM images of the residues of flame retardant

polymer bio-nanocomposites after the cone calorimeter test confirmed the formation of charred layer/fibre structures. A very compact and uniform surface morphology was observed for the char residues of the composites. This indicates that the presence of these clays contributes positively on the morphology of the formed residues and obviously affects the flame retardancy mechanism of the generated materials.

CHAPTER 5

5. GENERAL CONCLUSIONS

A novel method for clay surface modification, the so-called "surfactant-free organo-modification approach" was developed for the fabrication of DAPA/clay bio-nanocomposites. The method did not employ any surfactants for the matrix-clay compatibilisation. The method is essentially based on the use of DAPA with protonated amine end groups as clay modifiers via solution intercalation route. The clay modification route outlined above was successfully applied to the standard smectite and VMT clays. They were ultimately chosen on the basis of their great ability to exfoliate into nano-thick sheets.

DAPA/clay bio-nanocomposites containing either MMT or VMT were successfully prepared using the "surfactant-free organo-modification approach". In both cases, the bio-nanocomposites featured a mixed morphology containing some exfoliated clay sheets together with nano-sized clay tactoids. Filler content (MMT or VTM) was varied up to 30 wt.%. At this filler loading, the melt viscosity, tensile strength and Young's modulus increased. DMA showed that the T_g of the polymer increased when the fillers were added. This indicates that the high interfacial surface area, presented by the clay platelets dispersed in the matrix, significantly impaired the polymer chain mobility.

In the particular case of amorphous DAPA/VMT bio-nanocomposites, the DMA suggests that three stiffening mechanisms were operating. The reinforcing effect of the high stiffness inorganic flakes is the primary contributor. Together with the chain confinement effect, that expresses itself in an apparent increase in the glass transition temperature; this provided an adequate rationalisation of the stiffness variation below T_g. However, an additional stiffening effect is indicated at temperatures above T_g. The mechanism may involve dynamic network formation based on fluctuating hydrogen bonding interactions between the matrix polymer chains and the filler particles.

Based on these results, it can be concluded that a "surfactant-free organo-modification approach" can provide enhanced control of the polymer/clay nanocomposites morphology. By using this technique DAPA/clay bio-nanocomposites with excellent properties can be

successfully prepared. The "surfactant-free organo-modification approach" offers an alternative to the conventional polymer nanocomposites preparation route. The latter are in effect surfactant modified clays. The technique is of interest because it also allows organo-modification of the external surfaces of nano-sized clay sheets suspended in an acidic solution. This may facilitate clay dispersion and to prevent restacking when they are ultimately compounded into the polymer matrix. Moreover, using the solution route it was possible to prepare compounds with a very high overall clay content. These values are usually impossible to achieve with conventional techniques such as extrusion compounding. To the best of our knowledge, this is the first work for nanocomposites made with DAPA.

A further goal of the research was to extend the application of the organo-modified VMT (OVMT) to the semi-crystalline polyamide (PA-11). In this particular case, organomodified- and unmodified VMT (UVMT) and commercial sepiolite (PGS9) were considered. The clays (UVMT, OVMT and PGS9) were melt-compounded into the PA-11 to form products that contained either no filler, i.e. neat PA-11 or 10 wt.% clay. The aspects that were addressed included the effect of VMT organomodification, the effect of the shape of the clays, the aspect ratio of the particles, and the degree of dispersion that was achieved on properties of the generated PA-11/bio-nanocomposites. The emphasis was given to the mechanical and flame retardant properties. PA-11/clay bio-nanocomposites were successfully prepared. Tensile properties results showed improvements in tensile strength and Young's modulus increased with the presence of the nano-fillers. Young's modulus of the bio-nanocomposites was almost the double of that of the neat polymer. Thermo-mechanical results also showed improvements in storage modulus with the addition of all particles, especially in the temperature range corresponding to the rubbery plateau (above the T_g). Cone calorimeter test results showed that the *pHRR* and *SPR* values of the PA-11/clays significantly decreased compared with those of neat polymer. This indicates that the addition of clays not only decreased the flammability of polyamide but also effectively reduced smoke production.

Based on this results, it seems reasonable to conclude that in fact it is not necessary to organomodify the clays with cationic surfactants in order to obtain PA11-clay bio-nanocomposites with acceptable mechanical and flame retardant properties.

REFERENCES

ADAME, D. & BEALL, G. W. 2009. Direct measurement of the constrained polymer region in polyamide/clay nanocomposites and the implications for gas diffusion. *Applied Clay Science,* 42**,** 545-552.

AESCHELMANN, F. & CARUS, M. 2015. Biobased Building Blocks and Polymers in the World: Capacities, Production, and Applications–Status Quo and Trends Towards 2020. *Industrial Biotechnology,* 11**,** 154-159.

AFFDL, J. & KARDOS, J. 1976. The Halpin-Tsai equations: a review. *Polymer Engineering & Science,* 16**,** 344-352.

AHLRICHS, J., SERNA, C. & SERRATOSA, J. 1975. Structural hydroxyls in sepiolites. *Clays and clay minerals,* 23**,** 119-124.

AHMADI, S. J., HUANG, Y. & LI, W. 2005. Fabrication and physical properties of EPDM–organoclay nanocomposites. *Composites Science and Technology,* 65**,** 1069-1076.

AL-SALEH, M. H. & SUNDARARAJ, U. 2011. Review of the mechanical properties of carbon nanofiber/polymer composites. *Composites Part A: Applied Science and Manufacturing,* 42**,** 2126-2142.

ALDOUSIRI, B., DHAKAL, H., ONUH, S., ZHANG, Z., BENNETT, N. & RICHARDSON, M. 2012. Effect of layered silicate reinforcement on the structure and mechanical properties of spent polyamide-12 nanocomposites. *Composites Part B: Engineering,* 43**,** 1363-1367.

ALEXANDRE, B., LANGEVIN, D., MÉDÉRIC, P., AUBRY, T., COUDERC, H., NGUYEN, Q., SAITER, A. & MARAIS, S. 2009. Water barrier properties of polyamide 12/montmorillonite nanocomposite membranes: structure and volume fraction effects. *Journal of membrane science,* 328**,** 186-204.

ALEXANDRE, B., MARAIS, S., LANGEVIN, D., MÉDÉRIC, P. & AUBRY, T. 2006. Nanocomposite-based polyamide 12/montmorillonite: relationships between structures and transport properties. *Desalination,* 199**,** 164-166.

ALEXANDRE, M. & DUBOIS, P. 2000. Polymer-layered silicate nanocomposites: preparation, properties and uses of a new class of materials. *Materials Science and Engineering: R: Reports,* 28**,** 1-63.

ALI, F., REINERT, L., LÉVÊQUE, J.-M., DUCLAUX, L., MULLER, F., SAEED, S. & SHAH, S. S. 2014. Effect of sonication conditions: solvent, time, temperature and reactor type on the preparation of micron sized vermiculite particles. *Ultrasonics sonochemistry,* 21**,** 1002-1009.

AMIL, A. R., DE LA CRUZ, F. A., VILA, E. & CONDE, A. R. 1992. Study of a material from Libby, Montana containing vermiculite and hydrobiotite; intercalation with aliphatic amines. *Clay minerals,* 27**,** 257-263.

ANILKUMAR, S., KUMARAN, M. & THOMAS, S. 2008. Characterization of EVA/clay nanocomposite membranes and its pervaporation performance. *The Journal of Physical Chemistry B,* 112**,** 4009-4015.

ANNABI-BERGAYA, F. 2008. Layered clay minerals. Basic research and innovative composite applications. *Microporous and Mesoporous Materials,* 107**,** 141-148.

ANSARI, S. & GIANNELIS, E. P. 2009. Functionalized graphene sheet—Poly (vinylidene fluoride) conductive nanocomposites. *Journal of Polymer Science Part B: Polymer Physics*, 47**,** 888-897.

ARANDA, P., KUN, R., MARTÍN-LUENGO, M. A., LETAÏEF, S., DÉKÁNY, I. & RUIZ-HITZKY, E. 2007. Titania− sepiolite nanocomposites prepared by a surfactant templating colloidal route. *Chemistry of Materials,* 20**,** 84-91.

ARANDA, P. & RUIZ-HITZKY, E. 1992. Poly (ethylene oxide)-silicate intercalation materials. *Chemistry of Materials,* 4**,** 1395-1403.

ARASH, B., WANG, Q. & VARADAN, V. 2014. Mechanical properties of carbon nanotube/polymer composites. *Scientific reports,* 4.

ARORA, A. & PADUA, G. 2010. Review: nanocomposites in food packaging. *Journal of Food Science,* 75**,** R43-R49.

BABU, R. P., O'CONNOR, K. & SEERAM, R. 2013. Current progress on bio-based polymers and their future trends. *Progress in Biomaterials,* 2**,** 1-16.

BAILEY, S. 1980. Summary of recommendations of AIPEA nomenclature committee on clay minerals. *American Mineralogist,* 65**,** 1-7.

BALLARD, D. & RIDEAL, G. 1983. Flexible inorganic films and coatings. *Journal of Materials Science,* 18**,** 545-561.

BANIASADI, H., SA, A. R. & NIKKHAH, S. J. 2010. Investigation of in situ prepared polypropylene/clay nanocomposites properties and comparing to melt blending method. *Materials & Design,* 31**,** 76-84.

BANIN, A. & LAHAV, N. 1968. Optical study of particle size of montmorillonite with various adsorbed cations. *Nature,* 217**,** 1146-1147.

BARABASZOVÁ, K. Č. & VALÁŠKOVÁ, M. 2013. Characterization of vermiculite particles after different milling techniques. *Powder Technology,* 239**,** 277-283.

BARRY, C. M., BAKER, A. & MEAD, J. L. 2006. Introduction to Polymers and Plastics. *Handbook of Plastics Technology***,** 1.1-1.49.

BARSHAD, I. 1948. Vermiculite and its relation to biotite as revealed by base exchange reactions, X-ray analyses, differential thermal curves, and water content. *American Mineralogist,* 33**,** 655-678.

BARSHAD, I. 1949. The nature of lattice expansion and its relation to hydration in montmorillonite and vermiculite. *The American mineralogist: journal of the Mineralogical Society of America,* 34**,** 675-684.

BARSHAD, I. 1952. Factors affecting the interlayer expansion of vermiculite and montmorillonite with organic substances. *Soil Science Society of America Journal,* 16**,** 176-182.

BASSETT, W. A. 1961. The geology of vermiculite occurrences. *Clays and clay minerals,* 10**,** 61-69.

BASURTO, F., GARCÍA-LÓPEZ, D., VILLARREAL-BASTARDO, N., MERINO, J. & PASTOR, J. 2013. Composites and nanocomposites of ABS: Synergy between glass fiber and nano-sepiolite. *Composites Part B: Engineering,* 47**,** 42-47.

BASURTO, F. C., GARCÍA-LÓPEZ, D., VILLARREAL-BASTARDO, N., MERINO, J. C. & PASTOR, J. M. 2012. Nanocomposites of ABS and sepiolite: Study of different clay modification processes. *Composites Part B: Engineering,* 43**,** 2222-2229.

BAUMEISTER, W. & HAHN, M. 1976. An improved method for preparing single crystal specimen supports: H 2 O 2 exfoliation of vermiculite. *Micron (1969),* 7**,** 247-251.

BCCRESEARCH. Available at: http://www.bccresearch.com [Accessed 10 November 2015]

BERGAYA, F. & LAGALY, G. 2001. Surface modification of clay minerals. *Applied Clay Science,* 19**,** 1-3.

BERGAYA, F. & LAGALY, G. 2011. Intercalation processes of layered minerals. *Layered Mineral Structures and Their Application in Advanced Technologies.*

BERGAYA, F. & LAGALY, G. 2013. *Handbook of clay science* (Vol. 5), Newnes.

BERGAYA, F., JABER, M. & LAMBERT, J.F. 2012. Clays and clay minerals as layered nanofiller for (bio) polymers. *In Environmental Silicate Nano-Biocomposites* (pp. 41-75). Springer London

BERGAYA, F., LAGALY, G. & VAYER, M. 2006. .10 Cation and Anion Exchange. *Developments in clay science,* 1**,** 979-1001.

BEYER, G. 2002. Nanocomposites: a new class of flame retardants for polymers. *Plastics, Additives and Compounding,* 4**,** 22-28.

BHARADWAJ, R., MEHRABI, A., HAMILTON, C., TRUJILLO, C., MURGA, M., FAN, R., CHAVIRA, A. & THOMPSON, A. 2002. Structure–property relationships in cross-linked polyester–clay nanocomposites. *Polymer,* 43**,** 3699-3705.

BHATTACHARYA, S., GUPTA, R. & KAMAL, M. 2008. *Polymeric nanocomposites theory and practice,* Carl Hanser Publishers.

BILOTTI, E., FISCHER, H. & PEIJS, T. 2008. Polymer nanocomposites based on needle-like sepiolite clays: Effect of functionalized polymers on the dispersion of nanofiller, crystallinity, and mechanical properties. *Journal of Applied Polymer Science,* 107**,** 1116-1123.

BILOTTI, E., ZHANG, R., DENG, H., QUERO, F., FISCHER, H. & PEIJS, T. 2009. Sepiolite needle-like clay for PA6 nanocomposites: An alternative to layered silicates? *Composites Science and Technology,* 69**,** 2587-2595.

BRAUNER, K. & PREISINGER, A. 1956. Structure and origin of sepiolite. *Miner. Petr. Mitt,* 6**,** 120-140.

BREAKWELL, I. K., HOMER, J., LAWRENCE, M. A. & MCWHINNIE, W. R. 1995. Studies of organophilic clays: the distribution of quaternary ammonium compounds on clay surfaces and the role of impurities. *Polyhedron,* 14**,** 2511-2518.

BRINDLEY, G. & PEDRO, G. 1975. Meeting of the Nomenclature Committee of AIPEA. *Clays and clay minerals,* 23**,** 413-414.

BROWN, G. 1972. The X-ray identification and crystal structures of clay minerals.

BROWN, G. T. & BRINDLEY, G. 1980. X-ray diffraction procedures for clay mineral identification. *Crystal structures of clay minerals and their X-ray identification,* 5**,** 305-359.

CABEDO, L. S., GIMÉNEZ, E., LAGARON, J. M., GAVARA, R. & SAURA, J. J. 2004. Development of EVOH-kaolinite nanocomposites. *Polymer,* 45**,** 5233-5238.

CAMARGO, P. H. C., SATYANARAYANA, K. G. & WYPYCH, F. 2009. Nanocomposites: synthesis, structure, properties and new application opportunities. *Materials Research,* 12**,** 1-39.

CARRADO, K. A. 2000. Synthetic organo-and polymer–clays: preparation, characterization, and materials applications. *Applied Clay Science,* 17**,** 1-23.

CARVALHO, H. W. P., SANTILLI, C. V., BRIOIS, V. & PULCINELLI, S. H. 2013. Polymer-clay nanocomposites thermal stability: experimental evidence of the radical trapping effect. *RSC Advances,* 3**,** 22830-22833.

CASAL, B., MERINO, J., SERRATOSA, J.-M. A. & RUIZ-HITZKY, E. 2001. Sepiolite-based materials for the photo-and thermal-stabilization of pesticides. *Applied Clay Science,* 18**,** 245-254.

CASSAGNAU, P. 2008. Melt rheology of organoclay and fumed silica nanocomposites. *Polymer,* 49**,** 2183-2196.

CHAIKO, D. J. & LEYVA, A. A. 2005. Thermal transitions and barrier properties of olefinic nanocomposites. *Chemistry of Materials,* 17**,** 13-19.

CHAVARRIA, F. & PAUL, D. 2004. Comparison of nanocomposites based on nylon 6 and nylon 66. *Polymer,* 45**,** 8501-8515.

CHEN, H., LU, H., ZHOU, Y., ZHENG, M., KE, C. & ZENG, D. 2012. Study on thermal properties of polyurethane nanocomposites based on organo-sepiolite. *Polymer Degradation and Stability,* 97**,** 242-247.

CHEN, J., CHEN, J., ZHU, S., CAO, Y. & LI, H. 2011. Mechanical properties, morphology, and crystal structure of polypropylene/chemically modified attapulgite nanocomposites. *Journal of Applied Polymer Science,* 121**,** 899-908.

CHEN, S., WANG, B., KANG, J., CHEN, J., GAI, J., YANG, L. & CAO, Y. 2013. Synergistic effect of organic vermiculite on the flame retardancy and thermal stability of intumescent polypropylene composites. *Journal of Macromolecular Science, Part B,* 52**,** 1212-1225.

CHEONG, J. Y., AHN, J., SEO, M. & NAM, Y. S. 2015. Flame-retardant, flexible vermiculite–polymer hybrid film. *RSC Advances,* 5**,** 61768-61774.

CHIVRAC, F., POLLET, E. & AVÉROUS, L. 2009. Progress in nano-biocomposites based on polysaccharides and nanoclays. *Materials Science and Engineering: R: Reports,* 67**,** 1-17.

CHO, J. & PAUL, D. 2001. Nylon 6 nanocomposites by melt compounding. *Polymer,* 42**,** 1083-1094.

CHOUDALAKIS, G. & GOTSIS, A. 2009. Permeability of polymer/clay nanocomposites: a review. *European Polymer Journal,* 45**,** 967-984.

CHOUDHURY, A., BHOWMICK, A. K. & ONG, C. 2010. Effect of different nanoparticles on thermal, mechanical and dynamic mechanical properties of hydrogenated nitrile butadiene rubber nanocomposites. *Journal of Applied Polymer Science,* 116**,** 1428-1441.

CHUNG, H. & DAS, S. 2008. Functionally graded Nylon-11/silica nanocomposites produced by selective laser sintering. *Materials Science and Engineering: A,* 487**,** 251-257.

CÍLEK, V. G. & DUDA, J. 1989. *Industrial minerals of Mozambique,* Geological Survey.

COLEMAN, J. N., KHAN, U. & GUN'KO, Y. K. 2006. Mechanical reinforcement of polymers using carbon nanotubes. *Advanced materials,* 18**,** 689-706.

COMPREHENSIVE CASTOR OIL REPORT 2013. Castor Oil India. Available at: http://www.castoroil.in/downloads/download.php?name=Preview_of_Comprehensive_Castor_Oil_Report.pdf [Accessed 17 November 2015].

COUDERC, P. & DOUILLET, P. 1973. Industrial vermiculites-exfoliation and mineralogical and chemical properties. *Bulletin de la societe francaise de ceramique***,** 51-59.

DAKOVIĆ, A., MATIJAŠEVIĆ, S., ROTTINGHAUS, G. E., LEDOUX, D. R., BUTKERAITIS, P. & SEKULIĆ, Ž. 2008. Aflatoxin B 1 adsorption by natural and copper modified montmorillonite. *Colloids and Surfaces B: Biointerfaces,* 66**,** 20-25.

DE AZEREDO, H. M. 2009. Nanocomposites for food packaging applications. *Food Research International,* 42**,** 1240-1253.

DE ESPINOSA, L. M. & MEIER, M. A. 2011. Plant oils: the perfect renewable resource for polymer science?! *European Polymer Journal,* 47**,** 837-852.

DE HARO, M. J., BLANES, J. M. N., POYATO, J., PÉREZ-MAQUEDA, L., LERF, A. & PÉREZ-RODRíGUEZ, J. 2004. Effects of mechanical treatment and exchanged cation on the microporosity of vermiculite. *Journal of Physics and Chemistry of Solids,* 65**,** 435-439.

DE HARO, M. J., PÉREZ-RODRÍGUEZ, J., POYATO, J., PÉREZ-MAQUEDA, L., RAMÍREZ-VALLE, V., JUSTO, A., LERF, A. & WAGNER, F. 2005. Effect of ultrasound on preparation of porous materials from vermiculite. *Applied Clay Science,* 30**,** 11-20.

DE PAIVA, L. B., MORALES, A. R. & DÍAZ, F. R. V. 2008. Organoclays: properties, preparation and applications. *Applied Clay Science,* 42**,** 8-24.

DE SOUSA RODRIGUES, L. A., FIGUEIRAS, A., VEIGA, F., DE FREITAS, R. M., NUNES, L. C. C., DA SILVA FILHO, E. C. & DA SILVA LEITE, C. M. 2013. The systems containing clays and clay minerals from modified drug release: A review. *Colloids and Surfaces B: Biointerfaces,* 103**,** 642-651.

DEL HOYO, C. 2007. Layered double hydroxides and human health: an overview. *Applied Clay Science,* 36**,** 103-121.

DUBOIS, J.-L. 2012. Refinery of the Future: Feedstock, Processes, Products. *Biorefinery: From Biomass to Chemicals and Fuels*.

EDA, G. & CHHOWALLA, M. 2009. Graphene-based composite thin films for electronics. *Nano Letters,* 9**,** 814-818.

EDWARDS, D., POSNER, A. & QUIRK, J. 1965. Repulsion of chloride ions by negatively charged clay surfaces. Part 2.—monovalent cation montmorillonites. *Transactions of the Faraday Society,* 61**,** 2816-2819.

EVANS, A. M. 1993. Oxford: *Blackwell Scientific Publications*.

FAN, X., DENG, Y., WATERHOUSE, J. & PFROMM, P. 1997. Institute of Paper Science and Technology Atlanta, Georgia.

FISCHER, H. 2003. Polymer nanocomposites: from fundamental research to specific applications. *Materials Science and Engineering: C,* 23**,** 763-772.

FISCHER, H., GIELGENS, L. & KOSTER, T. 1999. Nanocomposites from polymers and layered minerals. *Acta polymerica,* 50**,** 122-126.

FOLORUNSO, O., DODDS, C., DIMITRAKIS, G. & KINGMAN, S. 2012. Continuous energy efficient exfoliation of vermiculite through microwave heating. *International Journal of Mineral Processing,* 114**,** 69-79.

FORNES, T., HUNTER, D. & PAUL, D. 2004. Effect of sodium montmorillonite source on nylon 6/clay nanocomposites. *Polymer,* 45**,** 2321-2331.

FORNES, T. & PAUL, D. 2003a. Crystallization behavior of nylon 6 nanocomposites. *Polymer,* 44**,** 3945-3961.

FORNES, T. & PAUL, D. 2003b. Formation and properties of nylon 6 nanocomposites. *Polímeros,* 13**,** 212-217.

FORNES, T. & PAUL, D. 2004. Structure and properties of nanocomposites based on nylon-11 and-12 compared with those based on nylon-6. *Macromolecules,* 37**,** 7698-7709.

FORNES, T., YOON, P., HUNTER, D., KESKKULA, H. & PAUL, D. 2002. Effect of organoclay structure on nylon 6 nanocomposite morphology and properties. *Polymer,* 43**,** 5915-5933.

FORNES, T., YOON, P., KESKKULA, H. & PAUL, D. 2001. Nylon 6 nanocomposites: the effect of matrix molecular weight. *Polymer,* 42**,** 09929-09940.

FRANCHINI, E., GALY, J. & GÉRARD, J.-F. 2009. Sepiolite-based epoxy nanocomposites: Relation between processing, rheology, and morphology. *Journal of colloid and interface science,* 329**,** 38-47.

FROST, R. L. & DING, Z. 2003. Controlled rate thermal analysis and differential scanning calorimetry of sepiolites and palygorskites. *Thermochimica Acta,* 397**,** 119-128.

FU, S.-Y., FENG, X.-Q., LAUKE, B. & MAI, Y.-W. 2008. Effects of particle size, particle/matrix interface adhesion and particle loading on mechanical properties of particulate–polymer composites. *Composites Part B: Engineering,* 39**,** 933-961.

FUKUSHIMA, K., TABUANI, D. & CAMINO, G. 2012. Poly (lactic acid)/clay nanocomposites: effect of nature and content of clay on morphology, thermal and thermo-mechanical properties. *Materials Science and Engineering: C,* 32**,** 1790-1795.

FUKUSHIMA, K., TABUANI, D., ABBATE, C., ARENA, M. & FERRERI, L. 2010. Effect of sepiolite on the biodegradation of poly(lactic acid) and polycaprolactone. *Polymer Degradation Stability,* 95(10), 2049–2056.

GAHLEITNER, M. 2001. Melt rheology of polyolefins. *Progress in Polymer Science,* 26**,** 895-944.

GALAN, E. 1996. Properties and applications of palygorskite-sepiolite clays. *Clay minerals,* 31**,** 443-454.

GALIMBERTI, M., CIPOLLETTI, V. & COOMBS, M. 2013. Application of clay polymer nanocomposites. *Handbook of Clay Science.* Elsevier Amsterdam.

GAO, J., ZHANG, Q., WANG, K., FU, Q., CHEN, Y., CHEN, H., HUANG, H. & REGO, J. M. 2012. Effect of shearing on the orientation, crystallization and mechanical properties of HDPE/attapulgite nanocomposites. *Composites Part A: Applied Science and Manufacturing,* 43**,** 562-569.

GARCÍA-LÓPEZ, D., FERNÁNDEZ, J. F., MERINO, J. C., SANTARÉN, J. & PASTOR, J. M. 2010. Effect of organic modification of sepiolite for PA 6 polymer/organoclay nanocomposites. *Composites Science and Technology,* 70**,** 1429-1436.

GARCÍA, N., GUZMÁN, J., BENITO, E., ESTEBAN-CUBILLO, A., AGUILAR, E., SANTARÉN, J. & TIEMBLO, P. 2011. Surface modification of sepiolite in aqueous gels by using methoxysilanes and its impact on the nanofiber dispersion ability. *Langmuir,* 27**,** 3952-3959.

GIANNELIS, E. P. 1996. Polymer layered silicate nanocomposites. *Advanced materials,* 8**,** 29-35.

GNANASEKARAN, D., SHANAVAS, A., FOCKE, W.W. & SADIKU, R. 2015. Polyhedral oligomeric silsesquioxane/polyamide bio-nanocomposite membranes: structure-gas transport properties. *RSC Advances,* 5(15), 11272-11283.

GONZÁLEZ, A., DASARI, A., HERRERO, B., PLANCHER, E., SANTARÉN, J., ESTEBAN, A. & LIM, S.-H. 2012. Fire retardancy behavior of PLA based nanocomposites. *Polymer Degradation and Stability,* 97**,** 248-256.

GOPAKUMAR, T., LEE, J., KONTOPOULOU, M. & PARENT, J. 2002. Influence of clay exfoliation on the physical properties of montmorillonite/polyethylene composites. *Polymer,* 43**,** 5483-5491.

GREENLAND, D. 1963. Adsorption of polyvinyl alcohols by montmorillonite. *Journal of Colloid Science,* 18**,** 647-664.

GRIM, R.E. 1962. Clay mineralogy. *Scince,* 135(3507), pp. 890-898.

GRIM, R. & GUVEN, N. 1978. Developments in sedimentology. *Bentonites—Geology, Mineralogy, Properties and UsesElsevier, New York.*

GRIM, R. E. 1968. Clay MineralogyMcGraw-Hill. *New York***,** 214.

GROVES, R. 1939. Exfoliation of vermiculite by chemical means. *Nature,* 144**,** 554.

GUGGENHEIM, S., ADAMS, J., BAIN, D., BERGAYA, F., BRIGATTI, M. F., DRITS, V., FORMOSO, M. L., GALÁN, E., KOGURE, T. & STANJEK, H. 2006. Summary of recommendations of nomenclature committees relevant to clay mineralogy: report of the Association Internationale pour l'Etude des Argiles (AIPEA) Nomenclature Committee for 2006. *Clay minerals,* 41**,** 863-877.

GUGGENHEIM, S., ALIETTI, A., DRITS, V. A., FORMOSO, M. L., GALAN, E., KOESTER, H. M., PAQUET, H., WATANABE, T., BAIN, D. C. & HUDNALL, W. H. 1997. Report of the Association Internationale pour l'Etude des Argiles (AIPEA) Nomenclature Committee for 1996. *Clays and clay minerals,* 45**,** 298-300.

GUGGENHEIM, S. & MARTIN, R. 1995. Definition of clay and clay mineral: joint report of the AIPEA nomenclature and CMS nomenclature committees. *Clays and clay minerals,* 43**,** 255-256.

GUPTA, R. K., PASANOVIC-ZUJO, V. & BHATTACHARYA, S. 2005. Shear and extensional rheology of EVA/layered silicate-nanocomposites. *Journal of Non-Newtonian Fluid Mechanics,* 128**,** 116-125.

HABLOT, E., DONNIO, B., BOUQUEY, M. & AVÉROUS, L. 2010a. Dimer acid-based thermoplastic bio-polyamides: reaction kinetics, properties and structure. *Polymer,* 51**,** 5895-5902.

HABLOT, E., MATADI, R., AHZI, S. & AVÉROUS, L. 2010b. Renewable biocomposites of dimer fatty acid-based polyamides with cellulose fibres: thermal, physical and mechanical properties. *Composites Science and Technology,* 70**,** 504-509.

HABLOT, E., MATADI, R., AHZI, S., VAUDEMOND, R., RUCH, D. & AVÉROUS, L. 2010c. Yield behaviour of renewable biocomposites of dimer fatty acid-based polyamides with cellulose fibres. *Composites Science and Technology,* 70**,** 525-529.

HALL, M. R. 2010. *Materials for energy efficiency and thermal comfort in buildings*, Elsevier.

HE, X., YANG, J., ZHU, L., WANG, B., SUN, G., LV, P., PHANG, I. Y. & LIU, T. 2006. Morphology and melt rheology of nylon 11/clay nanocomposites. *Journal of Applied Polymer Science,* 102**,** 542-549.

HILLIER, S., MARWA, E. & RICE, C. 2013. On the mechanism of exfoliation of 'Vermiculite'. *Clay minerals,* 48**,** 563-582.

HO, D. L. & GLINKA, C. J. 2003. Effects of solvent solubility parameters on organoclay dispersions. *Chemistry of Materials,* 15**,** 1309-1312.

HORROCKS, A. R. & PRICE, D. 2001. *Fire retardant materials*, Woodhead Publishing.

HU, G.-S., DING, Z.-Y., LI, Y.-C. & WANG, B.-B. 2009. Crystalline morphology and melting behavior of nylon11/ethylene-vinyl alcohol/dicumyl peroxide blends. *Journal of polymer research,* 16**,** 263-269.

HU, Y., SHEN, L., YANG, H., WANG, M., LIU, T., LIANG, T. & ZHANG, J. 2006. Nanoindentation studies on Nylon 11/clay nanocomposites. *Polymer testing,* 25**,** 492-497.

HUANG, D., MU, B. & WANG, A. 2012. Preparation and properties of chitosan/poly (vinyl alcohol) nanocomposite films reinforced with rod-like sepiolite. *Materials Letters,* 86**,** 69-72.

HUANG, G., GAO, J., LI, Y., HAN, L. & WANG, X. 2010. Functionalizing nano-montmorillonites by modified with intumescent flame retardant: preparation and application in polyurethane. *Polymer Degradation and Stability,* 95**,** 245-253.

HUO, X., WU, L., LIAO, L., XIA, Z. & WANG, L. 2012. The effect of interlayer cations on the expansion of vermiculite. *Powder Technology,* 224**,** 241-246.

IIJIMA, S. 1991. Helical microtubules of graphitic carbon. *Nature,* 354**,** 56-58.

INGLETHORPE, S., MORGAN, D. & HIGHLEY, D. E. 1993. *Industrial Minerals laboratory manual: bentonite*, British Geological Survey, Mineralogy and Petrology Group.

JARIYAVIDYANONT, K., FOCKE, W. & ANDROSCH, R. 2006. Crystallization kinetics of polyamide 11 in the presence of sepiolite and montmorillonite nanofillers. *Colloid and Polymer Science*, 1-9.

JUNIOR, C. 2002. WD Ciência e engenharia de materiais: uma introdução. *Rio de Janeiro: LTC*.

MASSINGA, P. H. 2013. *Surfactant intercalated koppies and Boane bentonites for polymer nanotechnology*. University of Pretoria.

JUSTO, A., MAQUEDA, C., PEREZ-RODRÍGUEZ, J. L. & MORILLO, E. 1989. Expansibility of some vermiculites. *Applied Clay Science,* 4**,** 509-519.

JUSTO, A., PÉREZ-RODRÍGUEZ, J. & SÁNCHEZ-SOTO, P. 1993. Thermal study of vermiculites and mica-vermiculite interstratifications. *Journal of Thermal Analysis and Calorimetry,* 40**,** 59-65.

KALKAN, Z. S. & GOETTLER, L. A. 2009. In situ polymerization of polyamide 66 nanocomposites utilizing interfacial polycondensation. II. Sodium montmorillonite nanocomposites. *Polymer Engineering and Science,* 49(9), 1825–1831.

KAWASUMI, M. 2004. The discovery of polymer-clay hybrids. *Journal of Polymer Science Part A: Polymer Chemistry,* 42**,** 819-824.

KAYA, E. D. 2006. *Development of layered silicate/epoxy nanocomposites.* Citeseer.

KEHAL, M., REINERT, L. & DUCLAUX, L. 2010. Characterization and boron adsorption capacity of vermiculite modified by thermal shock or H_2O_2 reaction and/or sonication. *Applied Clay Science,* 48**,** 561-568.

KHAN, A., SHAMSI, M. H. & CHOI, T.-S. 2009. Correlating dynamical mechanical properties with temperature and clay composition of polymer-clay nanocomposites. *Computational Materials Science,* 45**,** 257-265.

KILIARIS, P. & PAPASPYRIDES, C. 2010. Polymer/layered silicate (clay) nanocomposites: an overview of flame retardancy. *Progress in Polymer Science,* 35**,** 902-958.

KIM, H. & MACOSKO, C. W. 2009. Processing-property relationships of polycarbonate/graphene composites. *Polymer,* 50**,** 3797-3809.

KOGEL, J. E. 2006. *Industrial minerals & rocks: commodities, markets, and uses,* SME.

KOH, H. C., PARK, J. S., JEONG, M. A., HWANG, H. Y., HONG, Y. T., HA, S. Y. & NAM, S. Y. 2008. Preparation and gas permeation properties of biodegradable polymer/layered silicate nanocomposite membranes. *Desalination,* 233**,** 201-209.

KORNMANN, X., LINDBERG, H. & BERGLUND, L. A. 2001. Synthesis of epoxy–clay nanocomposites. Influence of the nature of the curing agent on structure. *Polymer,* 42**,** 4493-4499.

KOZLOWSKI, R., MIELENIAK, B., HELWIG, M. & PRZEPIERA, A. 1999. Flame resistant lignocellulosic-mineral composite particleboards. *Polymer Degradation and Stability,* 64**,** 523-528.

KUILLA, T., BHADRA, S., YAO, D., KIM, N. H., BOSE, S. & LEE, J. H. 2010. Recent advances in graphene based polymer composites. *Progress in Polymer Science,* 35**,** 1350-1375.

KUMAR, A. P., DEPAN, D., TOMER, N. S. & SINGH, R. P. 2009. Nanoscale particles for polymer degradation and stabilization—trends and future perspectives. *Progress in Polymer Science,* 34**,** 479-515.

KUMAR, K. D., TSOU, A. H. & BHOWMICK, A. K. 2010. Unique tackification behavior of needle-like sepiolite nanoclay in brominated isobutylene-co-p-methylstyrene (BIMS) rubber. *Macromolecules,* 43**,** 4184-4193.

LA SCALA, J. J., SANDS, J. M., ORLICKI, J. A., ROBINETTE, E. J. & PALMESE, G. R. 2004. Fatty acid-based monomers as styrene replacements for liquid molding resins. *Polymer,* 45**,** 7729-7737.

LAGALY, G. 1981. Characterization of clays by organic compounds. *CLAY MINER. Clay Miner.,* 16**,** 1.

LAGALY, G. 1982. Layer Charge Heterogeneity in Vermiculites. *Clays clay miner*. 30: 215-222.

LAGALY, G. 1986. Interaction of alkylamines with different types of layered compounds. *Solid State Ionics,* 22**,** 43-51.

LAGARON, J., CABEDO, L., CAVA, D., FEIJOO, J., GAVARA, R. & GIMENEZ, E. 2005. Improving packaged food quality and safety. Part 2: Nanocomposites. *Food Additives and Contaminants,* 22**,** 994-998.

LAMBERT, J. & BERGAYA, F. 2013. Smectites-polymer nanocomposites. *Handbook of Clay Science,*, 5.

LAO, S., KOO, J., MOON, T., LONDA, M., IBEH, C., WISSLER, G. & PILATO, L. 2011. Flame-retardant polyamide 11 nanocomposites: further thermal and flammability studies. *Journal of Fire Sciences***,** 0734904111404658.

LAO, S., YONG, W., NGUYEN, K., MOON, T., KOO, J., PILATO, L. & WISSLER, G. 2010. Flame-retardant polyamide 11 and 12 nanocomposites: processing, morphology, and mechanical properties. *Journal of composite materials,* 44**,** 2933-2951.

LAO, S. C., WU, C., MOON, T. J., KOO, J. H., MORGAN, A., PILATO, L. & WISSLER, G. 2009. Flame-retardant polyamide 11 and 12 nanocomposites: thermal and flammability properties. *Journal of composite materials,* 43**,** 1803-1818.

LAOUTID, F., BONNAUD, L., ALEXANDRE, M., LOPEZ-CUESTA, J.-M. & DUBOIS, P. 2009. New prospects in flame retardant polymer materials: from fundamentals to nanocomposites. *Materials Science and Engineering: R: Reports,* 63**,** 100-125.

LE DRED, R. 1968. *Contribution à l'étude d'un interstratifié mica-vermiculite: formation de complexes salins interfoliaires, réaction d'oxydo-réduction au sein du feuillet silicaté.*

LEBARON, P. C., WANG, Z. & PINNAVAIA, T. J. 1999. Polymer-layered silicate nanocomposites: an overview. *Applied Clay Science,* 15**,** 11-29.

LECOUVET, B., GUTIERREZ, J., SCLAVONS, M. & BAILLY, C. 2011. Structure–property relationships in polyamide 12/halloysite nanotube nanocomposites. *Polymer Degradation and Stability,* 96**,** 226-235.

LEE, H. M., PARK, B. J., CHOI, H. J., GUPTA, R. K. & BHATTACHARY, S. N. 2007. Preparation and rheological characteristics of ethylene-vinyl acetate copolymer/organoclay nanocomposites. *Journal of Macromolecular Science, Part B: Physics,* 46**,** 261-273.

LEE, J. & LEE, H. 2004. Characterization of organobentonite used for polymer nanocomposites. *Materials chemistry and physics,* 85**,** 410-415.

LEE, S.-R., PARK, H.-M., LIM, H., KANG, T., LI, X., CHO, W.-J. & HA, C.-S. 2002. Microstructure, tensile properties, and biodegradability of aliphatic polyester/clay nanocomposites. *Polymer,* 43**,** 2495-2500.

LEE, Y. R., RAGHU, A. V., JEONG, H. M. & KIM, B. K. 2009. Properties of waterborne polyurethane/functionalized graphene sheet nanocomposites prepared by an in situ method. *Macromolecular Chemistry and Physics,* 210**,** 1247-1254.

LEHTO, T. & GONCALVES, R. 2008. Mineral resources potential in Mozambique. *Geological Survey of Finland*.

LESZCZYŃSKA, A., NJUGUNA, J., PIELICHOWSKI, K. & BANERJEE, J. 2007a. Polymer/montmorillonite nanocomposites with improved thermal properties: Part I. Factors influencing thermal stability and mechanisms of thermal stability improvement. *Thermochimica Acta,* 453**,** 75-96.

LESZCZYŃSKA, A., NJUGUNA, J., PIELICHOWSKI, K. & BANERJEE, J. 2007b. Polymer/montmorillonite nanocomposites with improved thermal properties: Part II. Thermal stability of montmorillonite nanocomposites based on different polymeric matrixes. *Thermochimica Acta,* 454**,** 1-22.

LI, Y., HU, G. & WANG, B. 2010. Morphology development and non-isothermal crystallization behavior of polyamide 11/ethylene-vinyl alcohol blends. *Journal of Applied Polymer Science,* 118**,** 2126-2133.

LI, Y., LI, B., DAI, J., JIA, H. & GAO, S. 2008. Synergistic effects of lanthanum oxide on a novel intumescent flame retardant polypropylene system. *Polymer Degradation and Stability,* 93**,** 9-16.

LIANG, J., WANG, Y., HUANG, Y., MA, Y., LIU, Z., CAI, J., ZHANG, C., GAO, H. & CHEN, Y. 2009. Electromagnetic interference shielding of graphene/epoxy composites. *Carbon,* 47**,** 922-925.

LIMA, A. B. T. 2007. *Aplicações de cargas minerais em polímeros.* Universidade de São Paulo.

LIU, M., PU, M. & MA, H. 2012. Preparation, structure and thermal properties of polylactide/sepiolite nanocomposites with and without organic modifiers. *Composites Science and Technology,* 72**,** 1508-1514.

LIU, R., FROST, R. L., MARTENS, W.N. & YUAN, Y. 2008. Synthesis, characterization of mono, di and tri alkyl surfactant intercalated Wyoming montmorillonite for the removal of phenol from aqueous systems. *Journal of Colloid and Interface Science,* 327, 287–294.

LIU, T., LIM, K. P., TJIU, W. C., PRAMODA, K. & CHEN, Z.-K. 2003. Preparation and characterization of nylon 11/organoclay nanocomposites. *Polymer,* 44**,** 3529-3535.

LIU, X. & WU, Q. 2002. Polyamide 66/clay nanocomposites via melt intercalation. *Macromolecular Materials and Engineering,* 287**,** 180-186.

LIU, X., WU, Q. & BERGLUND, L. A., 2002. Polymorphism in polyamide 66/clay nanocomposites. *Polymer,* 43(18), 4967–4972.

LIU, Y. & KUMAR, S. 2014. Polymer/carbon nanotube nanocomposite fibers–a review. *ACS applied materials & interfaces,* 6**,** 6069-6087.

LIU, Z., CHEN, K. & YAN, D. 2004. Nanocomposites of poly (trimethylene terephthalate) with various organoclays: morphology, mechanical and thermal properties. *Polymer testing,* 23**,** 323-331.

LÓPEZ-GALINDO, A., VISERAS, C. & CEREZO, P. 2007. Compositional, technical and safety specifications of clays to be used as pharmaceutical and cosmetic products. *Applied Clay Science,* 36**,** 51-63.

LOTTI, C., ISAAC, C. S., BRANCIFORTI, M. C., ALVES, R. M., LIBERMAN, S. & BRETAS, R. E. 2008. Rheological, mechanical and transport properties of blown

films of high density polyethylene nanocomposites. *European Polymer Journal,* 44**,** 1346-1357.

LU, H., SHEN, H., SONG, Z., SHING, K. S., TAO, W. & NUTT, S. 2005. Rod-like silicate-epoxy nanocomposites. *Macromolecular rapid communications,* 26**,** 1445-1450.

LUNT, J. 1998. Large-scale production, properties and commercial applications of polylactic acid polymers. *Polymer Degradation and Stability,* 59**,** 145-152.

MACHECA, A., GNANASEKARAN, D. & FOCKE, W. W. 2014. Surfactant-free dimer fatty acid polyamide/montmorillonite bio-nanocomposites. *Colloid and Polymer Science,* 292**,** 669-676.

MACHECA, A. D., FOCKE, W. W., MUIAMBO, H. F. & KACI, M. 2016. Stiffening mechanisms in vermiculite–amorphous polyamide bio-nanocomposites. *European Polymer Journal,* 74**,** 51-63.

McHUGH, T. H., & KROCHTA, J. M. 1994. Sorbitol- vs glycerol plasticized whey protein edible films: Integrated oxygen permeability and tensile property evaluation. Journal of Agricultural and Food Chemistry, 42, 841–845.

MACKENZIE, R. C. 1970. *Differential thermal analysis*, Academic Press.

MAGO, G., KALYON, D. M. & FISHER, F. T. 2011. Nanocomposites of polyamide-11 and carbon nanostructures: Development of microstructure and ultimate properties following solution processing. *Journal of Polymer Science Part B: Polymer Physics,* 49**,** 1311-1321.

MAISONNEUVE, L., LEBARBÉ, T., GRAU, E. & CRAMAIL, H. 2013. Structure–properties relationship of fatty acid-based thermoplastics as synthetic polymer mimics. *Polymer Chemistry,* 4**,** 5472-5517.

MALI, S., GROSSMANN, M. V. E., GARCIA, M. A., MARTINO, M. N., & ZARITZKY, N. E. 2006. Effects of controlled storage on thermal, mechanical and barrier properties of plasticized films from different starch sources. Journal of Food Engineering, 75, 453–460.

MANIAS, E., TOUNY, A., WU, L., STRAWHECKER, K., LU, B. & CHUNG, T. 2001. Polypropylene/montmorillonite nanocomposites. Review of the synthetic routes and materials properties. *Chemistry of Materials,* 13**,** 3516-3523.

MAQUEDA, C., PEREZ-RODRIGUEZ, J. L., ŠUBRT, J. & MURAFA, N. 2009. Study of ground and unground leached vermiculite. *Applied Clay Science,* 44**,** 178-184.

MARCOS, C. & RODRÍGUEZ, I. 2010. Expansion behaviour of commercial vermiculites at 1000 C. *Applied Clay Science,* 48**,** 492-498.

MARCOS, C. & RODRÍGUEZ, I. 2011. Expansibility of vermiculites irradiated with microwaves. *Applied Clay Science,* 51**,** 33-37.

MARCOS, C. & RODRÍGUEZ, I. 2014. Exfoliation of vermiculites with chemical treatment using hydrogen peroxide and thermal treatment using microwaves. *Applied Clay Science,* 87**,** 219-227.

MARTIN, R., BAILEY, S., EBERL, D., FANNING, D., GUGGENHEIM, S., KODAMA, H., PEVEAR, D., SRODON, J. & WICKS, F. 1991. Report of the clay minerals

society nomenclature committee; revised classification of clay materials. *Clays and clay minerals,* 39**,** 333-335.

MARWA, E. M., MEHARG, A. A. & RICE, C. M. 2009. The effect of heating temperature on the properties of vermiculites from Tanzania with respect to potential agronomic applications. *Applied Clay Science,* 43**,** 376-382.

MASSINGA, P. H., FOCKE, W. W., DE VAAL, P. L. & ATANASOVA, M. 2010. Alkyl ammonium intercalation of Mozambican bentonite. *Applied Clay Science,* 49**,** 142-148.

MATADI, R., HABLOT, E., WANG, K., BAHLOULI, N., AHZI, S. & AVÉROUS, L. 2011. High strain rate behaviour of renewable biocomposites based on dimer fatty acid polyamides and cellulose fibres. *Composites Science and Technology,* 71**,** 674-682.

MATHIESON, A. M. 1958. Mg-vermiculite: a refinement and re-examination of the crystal structure of the 14.36 Å phase. *Amer. Min.,* 43**,** 216-227.

MATHIESON, A. M. & WALKER, G. 1954. Crystal structure of magnesium-vermiculite. *American Mineralogist,* 39**,** 231-255.

MEREDITH, R. 1998. Engineers handbook of industrial microwave heating. lEE. *London, UK*.

MEZGER, T. G. 2006. *The rheology handbook: for users of rotational and oscillatory rheometers,* Vincentz Network GmbH & Co KG.

MIDGLEY, H. & MIDGLEY, C. 1960. The mineralogy of some commercial vermiculites. *Clay minerals,* 4**,** 142-150.

MITTAL, V. 2009. Polymer layered silicate nanocomposites: a review. *Materials,* 2**,** 992-1057.

MITTAL, V. 2013. Epoxy–Vermiculite Nanocomposites. *Thermoset Nanocomposites***,** 1-16.

MOHANTY, A., MISRA, M. & DRZAL, L. 2002. Sustainable bio-composites from renewable resources: opportunities and challenges in the green materials world. *Journal of Polymers and the Environment,* 10**,** 19-26.

MONDRAGÓN, M., HERNÁNDEZ, E., RIVERA-ARMENTA, J. & RODRÍGUEZ-GONZÁLEZ, F. 2009. Injection molded thermoplastic starch/natural rubber/clay nanocomposites: morphology and mechanical properties. *Carbohydrate Polymers,* 77**,** 80-86.

MOURITZ, A. & GIBSON, A. 2006. Fire reaction properties of composites. *Fire properties of polymer composite materials***,** 59-101.

MUCHANGOS, A. C. D. 2000. *Mineralogy and geochemistry of bauxite and bentonite deposits from Mozambique=, Mineralogie en geochemie van bauxite en bentonite deposities van Mozambique.* Universiteit Utrecht.

MUIAMBO, H. F. & FOCKE, W. W. 2012. Ion exchanged vermiculites with lower expansion onset temperatures. *Molecular Crystals and Liquid Crystals,* 555**,** 65-75.

MUIAMBO, H. F., FOCKE, W. W., ATANASOVA, M. & BENHAMIDA, A. 2015. Characterization of urea-modified Palabora vermiculite. *Applied Clay Science,* 105**,** 14-20.

MUIAMBO, H. F., FOCKE, W. W., ATANASOVA, M., VAN DER WESTHUIZEN, I. & TIEDT, L. R. 2010. Thermal properties of sodium-exchanged Palabora vermiculite. *Applied Clay Science,* 50**,** 51-57.

MUROMTSEV, V., ZOLOTUKHINA, N. & MAMINA, A. K. 1990. X-RAY, IR Spectroscopic, and chemical-analysis of products of reaction between vermiculite and hydrogen-peroxide solution. *Inorganic Materials,* 26**,** 868-871.

MURRAY, H. 2002. Industrial clays case study. *Mining, Minerals and Sustainable Development,* 64**,** 1-9.

MURRAY, H. H. 1999. Applied clay mineralogy today and tomorrow. *Clay minerals,* 34**,** 39-39.

MURRAY, H. H. 2000. Traditional and new applications for kaolin, smectite, and palygorskite: a general overview. *Applied Clay Science,* 17**,** 207-221.

NAGATA, H., SHIMODA, S. and SUDO, T. 1974. On dehydration of bound water of sepiolite, *Clays Clay Miner*. **22**: 285-293.

NEWMAN, A. & BROWN, G. 1987. The chemical constitution of clays. *Monograph, Mineralogical Society***,** 1-128.

NGUYEN, A., REINERT, L., LÉVÊQUE, J.-M., BEZIAT, A., DEHAUDT, P., JULIAA, J.-F. & DUCLAUX, L. 2013. Preparation and characterization of micron and submicron-sized vermiculite powders by ultrasonic irradiation. *Applied Clay Science,* 72**,** 9-17.

NICOLOSI, V., CHHOWALLA, M., KANATZIDIS, M. G., STRANO, M. S. & COLEMAN, J. N. 2013. Liquid exfoliation of layered materials. *Science,* 340**,** 1226419.

NIELSEN, L. E. 1967. Models for the permeability of filled polymer systems. *Journal of Macromolecular Science—Chemistry,* 1**,** 929-942.

NIGAM, V., SONI, H., SAROOP, M., VERMA, G., BHATTACHARYA, A. & SETUA, D. 2012. Thermal, morphological, and X-ray study of polymer-clay nanocomposites. *Journal of Applied Polymer Science,* 124**,** 3236-3244.

NORRISH, K. 1954. The swelling of montmorillonite. *Discussions of the Faraday society,* 18**,** 120-134.

NORRISH, K. Factors in the weathering of mica to vermiculite. Proc. Int. Clay Conf., Madrid, 1972. Div. Ciencias CSIC, Madrid.

OBUT, A. & GIRGIN, İ. 2002. Hydrogen peroxide exfoliation of vermiculite and phlogopite. *Minerals Engineering,* 15**,** 683-687.

OGUNNIYI, D. 2006. Castor oil: a vital industrial raw material. *Bioresource technology,* 97**,** 1086-1091.

OKADA, A., KAWASUMI, M., USUKI, A., KOJIMA, Y., KURAUCHI, T. & KAMIGAITO, O. Nylon 6–clay hybrid. MRS Proceedings, 1989. Cambridge Univ Press, 45.

ORIAKHI, C. 1998. Nano sandwiches. *Chemistry in Britain,* 34**,** 59-62.

ÖZCAN, A. & ÖZCAN, A. S. 2005. Adsorption of Acid Red 57 from aqueous solutions onto surfactant-modified sepiolite. *Journal of Hazardous Materials,* 125**,** 252-259.

PADILHA, A. F. 1997. Microestrutura e Propriedades. *São Paulo: Hemus*.

PALANIANDY, S. & AZIZLI, K. A. M. 2009. Mechanochemical effects on talc during fine grinding process in a jet mill. *International Journal of Mineral Processing,* 92**,** 22-33.

PALANIANDY, S., AZIZLI, K. A. M., HUSSIN, H. & HASHIM, S. F. S. 2008. Mechanochemistry of silica on jet milling. *Journal of Materials Processing Technology,* 205**,** 119-127.

PATEL, M., BASTIOLI, C., MARINI, L. & WÜRDINGER, E. 2005. Life-cycle Assessment of Bio-based Polymers and Natural Fiber Composites. *Biopolymers online*.

PAUL, D. & ROBESON, L. 2008. Polymer nanotechnology: nanocomposites. *Polymer,* 49**,** 3187-3204.

PAVLIDOU, S. & PAPASPYRIDES, C. 2008. A review on polymer–layered silicate nanocomposites. *Progress in Polymer Science,* 33**,** 1119-1198.

PÉREZ-MAQUEDA, L., CANEO, O., POYATO, J. & PÉREZ-RODRÍGUEZ, J. 2001. Preparation and characterization of micron and submicron-sized vermiculite. *Physics and Chemistry of Minerals,* 28**,** 61-66.

PÉREZ-MAQUEDA, L., DURAN, A. & PÉREZ-RODRÍGUEZ, J. 2005. Preparation of submicron talc particles by sonication. *Applied Clay Science,* 28**,** 245-255.

PÉREZ-MAQUEDA, L., POYATO, J. & PEREZ-RODRIGUEZ, J. 2004. Effect of sonication on the thermal decomposition of ammonium vermiculite as studied by TG-MS hyphenated technique. *Journal of Thermal Analysis and Calorimetry,* 78**,** 375-383.

PÉREZ-RODRÍGUEZ, J., CARRERA, F., POYATO, J. & PÉREZ-MAQUEDA, L. 2002. Sonication as a tool for preparing nanometric vermiculite particles. *Nanotechnology,* 13**,** 382.

PEREZ-RODRLGUEZ, J. 2003. TRASFORMATION OF CLAY MINERALS ON GRINDING: A REVIEW. *Applied Study of Cultural Heritage and Clays,* 13**,** 425.

PERRAKI, T. and ORFANOUDAKI, A. 2008. Study of raw and ther-mally treated sepiolite from the Mantoudi area, Euboea, Greece, *J. Therm. Anal. Calor*. 91: 589-593.

PETERS, D. 1996. Ultrasound in materials chemistry. *Journal of Materials Chemistry,* 6**,** 1605-1618.

PETERSSON, L. & OKSMAN, K. 2006. Biopolymer based nanocomposites: comparing layered silicates and microcrystalline cellulose as nanoreinforcement. *Composites Science and Technology,* 66**,** 2187-2196.

PIRINGER, O. G. & BANER, A. L. 2008. *Plastic packaging: interactions with food and pharmaceuticals*, John Wiley & Sons.

POLYMER INNOVATION BLOG. Available at: http://polymerinnovationblog.com/bio-polyamides-where-do-they-come-from [Accessed 10 June 2015].

POWELL, C. E. & BEALL, G. W. 2007. Physical properties of polymer/clay nanocomposites. *Physical properties of polymers handbook.* Springer.

POYATO, J., PÉREZ-RODRÍGUEZ, J. L., LERF, A. & WAGNER, F. E. 2012. Sonication induced reduction of the Ojen (Andalucia, Spain) vermiculite under air and under nitrogen. *Ultrasonics sonochemistry,* 19**,** 373-375.

POYATO, J., PÉREZ-RODRÍGUEZ, J. L., RAMÍREZ-VALLE, V., LERF, A. & WAGNER, F. E. 2009. Sonication induced redox reactions of the Ojén (Andalucía, Spain) vermiculite. *Ultrasonics sonochemistry,* 16**,** 570-576.

PRAMODA, K., LIU, T., LIU, Z., HE, C. & SUE, H.-J. 2003. Thermal degradation behavior of polyamide 6/clay nanocomposites. *Polymer Degradation and Stability,* 81**,** 47-56.

PRAUS, P., TURICOVÁ, M., ŠTUDENTOVÁ, S. & RITZ, M. 2006. Study of cetyltrimethylammonium and cetylpyridinium adsorption on montmorillonite. *Journal of colloid and interface science,* 304**,** 29-36.

PREISINGER, A. 1963. Clays and clay minerals. *Earth Science Series***,** 365.

PRIOLO, M. A., HOLDER, K. M., GREENLEE, S. M. & GRUNLAN, J. C. 2012. Transparency, Gas barrier, and moisture resistance of large-aspect-ratio vermiculite nanobrick wall thin films. *ACS applied materials & interfaces,* 4**,** 5529-5533.

QIAN, Y., LINDSAY, C. I., MACOSKO, C. & STEIN, A. 2011. Synthesis and properties of vermiculite-reinforced polyurethane nanocomposites. *ACS applied materials & interfaces,* 3**,** 3709-3717.

QIU, Z.-C., ZHANG, J.-J., NIU, Y., HUANG, C.-L., YANG, K.-K. & WANG, Y.-Z. 2011. Preparation of poly (p-dioxanone)/sepiolite nanocomposites with excellent strength/toughness balance via surface-initiated polymerization. *Industrial & Engineering Chemistry Research,* 50**,** 10006-10016.

QUAN, H., ZHANG, B.-Q., ZHAO, Q., YUEN, R. K. & LI, R. K. 2009. Facile preparation and thermal degradation studies of graphite nanoplatelets (GNPs) filled thermoplastic polyurethane (TPU) nanocomposites. *Composites Part A: Applied Science and Manufacturing,* 40**,** 1506-1513.

RAMANATHAN, T., ABDALA, A., STANKOVICH, S., DIKIN, D., HERRERA-ALONSO, M., PINER, R., ADAMSON, D., SCHNIEPP, H., CHEN, X. & RUOFF, R. 2008. Functionalized graphene sheets for polymer nanocomposites. *Nature nanotechnology,* 3**,** 327-331.

RAMÍREZ-VALLE, V., JIMÉNEZ DE HARO, M., AVILÉS, M., PÉREZ-MAQUEDA, L., DURÁN, A., PASCUAL, J. & PÉREZ-RODRÍGUEZ, J. 2006. Effect of interlayer cations on high-temperature phases of vermiculite. *Journal of Thermal Analysis and Calorimetry,* 84**,** 147-155.

RAMKUMAR, D. & BHATTACHARYA, M. 1998. Steady shear and dynamic properties of biodegradable polyesters. *Polymer Engineering & Science,* 38**,** 1426-1435.

RAY, S. S. & BOUSMINA, M. 2005. Biodegradable polymers and their layered silicate nanocomposites: in greening the 21st-century materials world. *Progress in materials science,* 50**,** 962-1079.

RAY, S. S. & OKAMOTO, M. 2003. Polymer/layered silicate nanocomposites: a review from preparation to processing. *Progress in Polymer Science,* 28**,** 1539-1641.

REINHOLDT, M. X., HUBERT, F., FAUREL, M., TERTRE, E., RAZAFITIANAMAHARAVO, A., FRANCIUS, G., PRÊT, D., PETIT, S., BÉRÉ, E. & PELLETIER, M. 2013. Morphological properties of vermiculite particles in size-selected fractions obtained by sonication. *Applied Clay Science,* 77**,** 18-32.

ROY, N. & BHOWMICK, A. K. 2010. Novel in situ polydimethylsiloxane-sepiolite nanocomposites: Structure-property relationship. *Polymer,* 51**,** 5172-5185.

RUIZ-HITZKY, E. & ARANDA, P. 1990. Polymer-salt intercalation complexes in layer silicates. *Advanced materials,* 2**,** 545-547.

RYTWO, G., TROPP, D. & SERBAN, C. 2002. Adsorption of diquat, paraquat and methyl green on sepiolite: experimental results and model calculations. *Applied Clay Science,* 20**,** 273-282.

SAHOO, N. G., RANA, S., CHO, J. W., LI, L. & CHAN, S. H. 2010. Polymer nanocomposites based on functionalized carbon nanotubes. *Progress in Polymer Science,* 35**,** 837-867.

SAMYN, F., BOURBIGOT, S., JAMA, C., BELLAYER, S., NAZARE, S., HULL, R., CASTROVINCI, A., FINA, A. & CAMINO, G. 2008. Crossed characterisation of polymer-layered silicate (PLS) nanocomposite morphology: TEM, X-ray diffraction, rheology and solid-state nuclear magnetic resonance measurements. *European Polymer Journal,* 44**,** 1642-1653.

SATYANARAYANA, K. G., ARIZAGA, G. G. & WYPYCH, F. 2009. Biodegradable composites based on lignocellulosic fibers—An overview. *Progress in Polymer Science,* 34**,** 982-1021.

SCHOEMAN, J. 1989. Mica and vermiculite in South Africa. *Journal of the South African Institute of Mining and Metallurgy***,** 1-12.

SCHWELLNUS, C. M. 1938. *Vermiculite deposits in the Palaboroa area, NE Transvaal*.

SEPEHR, M., UTRACKI, L. A., ZHENG, X. & WILKIE, C. A. 2005. Polystyrenes with macro-intercalated organoclay. Part II. Rheology and mechanical performance. *Polymer,* 46**,** 11569-11581.

SHAH, R. K. & PAUL, D. 2004. Nylon 6 nanocomposites prepared by a melt mixing masterbatch process. *Polymer,* 45**,** 2991-3000.

SHEN, L., LIN, Y. J., DU, Q. G., ZHONG, W. & YANG, Y. L. 2005. Preparation and rheology of polyamide-6/attapulgite nanocomposites and studies on their percolated structure. Polymer, 46(15), 5758–5766.

SOHEILMOGHADDAM, M., WAHIT, M. U., YUSSUF, A. A., AL-SALEH, M. A. & WHYE, W. T. 2014. Characterization of bio regenerated cellulose/sepiolite nanocomposite films prepared via ionic liquid. *Polymer testing,* 33**,** 121-130.

SHIROZU, H., BAILEY, S. W. 1966. Crystal Structure of a Two-Layer Mg–vermiculite. *Am. miner*. 51: 1124–1143.

SOLOMON, M. J., ALMUSALLAM, A. S., SEEFELDT, K. F., SOMWANGTHANAROJ, A. & VARADAN, P. 2001. Rheology of polypropylene/clay hybrid materials. *Macromolecules,* 34**,** 1864-1872.

SONG, P. A., LIU, L., FU, S., YU, Y., JIN, C., WU, Q., ZHANG, Y. & LI, Q. 2013. Striking multiple synergies created by combining reduced graphene oxides and carbon nanotubes for polymer nanocomposites. *Nanotechnology*, 24**,** 125704.

SONG, L., HU, Y., HE, Q. & YOU, F. 2008. Study on crystallization, thermal and flame retardant properties of nylon 66/organoclay nanocomposites by in situ polymerization. *Journal of Fire Sciences,* 26 (6), 475–492.

SOUZA, M. A., PESSAN, L. A. & RODOLFO JR, A. 2006. Poly (vinyl chloride)(PVC)/organoclay nanocomposites. *Polímeros,* 16**,** 257-262.

SPICCIA, N. D., BORDER, E., ILLESINGHE, J., JACKSON, W. R. & ROBINSON, A. J. 2013. Preparation of a nylon-11 precursor from renewable canola oil. *Synthesis,* 45**,** 1683-1688.

SPITALSKY, Z., TASIS, D., PAPAGELIS, K. & GALIOTIS, C. 2010. Carbon nanotube–polymer composites: chemistry, processing, mechanical and electrical properties. *Progress in Polymer Science,* 35**,** 357-401.

STANKOVICH, S., DIKIN, D. A., DOMMETT, G. H., KOHLHAAS, K. M., ZIMNEY, E. J., STACH, E. A., PINER, R. D., NGUYEN, S. T. & RUOFF, R. S. 2006. Graphene-based composite materials. *Nature,* 442**,** 282-286.

STORZ, H. & VORLOP, K.-D. 2013. Bio-based plastics: status, challenges and trends. *Appl. Agric. Forestry Res,* 63**,** 321-332.

SUK, J. W., PINER, R. D., AN, J. & RUOFF, R. S. 2013. Evaluation of elastic modulus of ultra-thin vermiculite membranes by contact mode atomic force microscopy imaging. *Thin Solid Films,* 527**,** 205-209.

SZÁZDI, L., POZSGAY, A. & PUKÁNSZKY, B. 2007. Factors and processes influencing the reinforcing effect of layered silicates in polymer nanocomposites. *European Polymer Journal,* 43**,** 345-359.

SZÉP, A., SZABÓ, A., TÓTH, N., ANNA, P. & MAROSI, G. 2006. Role of montmorillonite in flame retardancy of ethylene–vinyl acetate copolymer. *Polymer Degradation and Stability,* 91**,** 593-599.

TAKAHASHI, S., GOLDBERG, H., FEENEY, C., KARIM, D., FARRELL, M., O'LEARY, K. & PAUL, D. 2006. Gas barrier properties of butyl rubber/vermiculite nanocomposite coatings. *Polymer,* 47**,** 3083-3093.

TAKASE, Y., LEE, J., SCHEINBEIM, J. & NEWMAN, B. 1991. High-temperature characteristics of nylon-11 and nylon-7 piezoelectrics. *Macromolecules,* 24**,** 6644-6652.

TANG, X., ALAVI, S. AND HERALD, T.J. 2008. Effects of plasticizers on the structure and properties of starch–clay nanocomposite films. *Carbohydrate Polymers,* 74, 552-558.

TARAMESHLOU, M., JAFARI, S. H., KHONAKDAR, H. A., FARMAHINI-FARAHANI, M. & AHMADIAN, S. 2007. Synthesis of exfoliated polyamide 66/organically modified montmorillonite nanocomposites by in situ interfacial polymerization. *Polymer Composites,* 28(6), 733–738.

TARTAGLIONE, G., TABUANI, D., CAMINO, G. & MOISIO, M. 2008. PP and PBT composites filled with sepiolite: morphology and thermal behaviour. *Composites Science and Technology,* 68**,** 451-460.

THELLEN, C., ORROTH, C., FROIO, D., ZIEGLER, D., LUCCIARINI, J., FARRELL, R., D'SOUZA, N. A. & RATTO, J. A. 2005. Influence of montmorillonite layered silicate on plasticized poly (L-lactide) blown films. *Polymer,* 46**,** 11716-11727.

THENG, B. K. G. 2012. *Formation and properties of clay-polymer complexes,* Elsevier.

TJONG, S. 2006. Structural and mechanical properties of polymer nanocomposites. *Materials Science and Engineering: R: Reports,* 53**,** 73-197.

TJONG, S. & MENG, Y. 2003a. Impact-modified polypropylene/vermiculite nanocomposites. *Journal of Polymer Science Part B: Polymer Physics,* 41**,** 2332-2341.

TJONG, S. & MENG, Y. 2003b. Preparation and characterization of melt-compounded polyethylene/vermiculite nanocomposites. *Journal of Polymer Science Part B: Polymer Physics,* 41**,** 1476-1484.

TJONG, S., MENG, Y. & HAY, A. 2002. Novel preparation and properties of polypropylene-vermiculite nanocomposites. *Chemistry of Materials,* 14**,** 44-51.

TORRÓ-PALAU, A., FERNÁNDEZ-GARCÍA, J. C., ORGILÉS-BARCELÓ, A. C., PASTOR-BLAS, M. M. & MARTÍN-MARTÍNEZ, J. 1997. Structural modification of sepiolite (natural magnesium silicate) by thermal treatment: effect on the properties of polyurethane adhesives. *International journal of adhesion and adhesives,* 17**,** 111-119.

TOUCHALEAUME, F., SOULESTIN, J., SCLAVONS, M., DEVAUX, J., LACRAMPE, M. & KRAWCZAK, P. 2011. One-step water-assisted melt-compounding of polyamide 6/pristine clay nanocomposites: An efficient way to prevent matrix degradation. *Polymer Degradation and Stability,* 96**,** 1890-1900.

TUCKER III, C. L. & LIANG, E. 1999. Stiffness predictions for unidirectional short-fiber composites: review and evaluation. *Composites Science and Technology,* 59**,** 655-671.

TUNNEY, J. J. & DETELLIER, C. 1996. Aluminosilicate nanocomposite materials. Poly (ethylene glycol)-kaolinite intercalates. *Chemistry of Materials,* 8**,** 927-935.

TÜRÜNÇ, O., FIRDAUS, M., KLEIN, G. & MEIER, M. A. 2012. Fatty acid derived renewable polyamides via thiol–ene additions. *Green chemistry,* 14**,** 2577-2583.

TYLER, D. R. 2004. Mechanistic aspects of the effects of stress on the rates of photochemical degradation reactions in polymers. *Journal of Macromolecular Science, Part C: Polymer Reviews,* 44**,** 351-388.

USUKI, A., KOJIMA, Y., KAWASUMI, M., OKADA, A., FUKUSHIMA, Y., KURAUCHI, T. & KAMIGAITO, O. 1993. Synthesis of nylon 6-clay hybrid. *Journal of Materials Research,* 8**,** 1179-1184.

UTRACKI, L. 2008. Polymeric nanocomposites: compounding and performance.

UTRACKI, L. A. 2004. *Clay-containing polymeric nanocomposites*, iSmithers Rapra Publishing.

VAIA, R. A. & GIANNELIS, E. P. 1997. Lattice model of polymer melt intercalation in organically-modified layered silicates. *Macromolecules,* 30**,** 7990-7999.

VAIA, R. A., TEUKOLSKY, R. K. & GIANNELIS, E. P. 1994. Interlayer structure and molecular environment of alkylammonium layered silicates. *Chemistry of Materials,* 6**,** 1017-1022.

VAIA, R. A. & WAGNER, H. D. 2004. Framework for nanocomposites. *Materials today,* 7**,** 32-37.

VALÁŠKOVÁ, M. & MARTYNKOVA, G. S. 2012. Vermiculite: structural properties and examples of the use. *Clay minerals in nature-their characterization, modification and application, InTech***,** 209-238.

VAN ES, M. A. 2001. *Polymer-clay nanocomposites: the importance of particle dimensions*, TU Delft, Delft University of Technology.

VAN OSS, C. & GIESE, R. 2003. Surface modification of clays and related materials. *Journal of dispersion science and technology,* 24**,** 363-376.

VLASVELD, D., DE JONG, M., BERSEE, H., GOTSIS, A. & PICKEN, S. 2005a. The relation between rheological and mechanical properties of PA6 nano-and micro-composites. *Polymer,* 46**,** 10279-10289.

VLASVELD, D., GROENEWOLD, J., BERSEE, H., MENDES, E. & PICKEN, S. 2005b. Analysis of the modulus of polyamide-6 silicate nanocomposites using moisture controlled variation of the matrix properties. *Polymer,* 46**,** 6102-6113.

VLASVELD, D., GROENEWOLD, J., BERSEE, H. & PICKEN, S. 2005c. Moisture absorption in polyamide-6 silicate nanocomposites and its influence on the mechanical properties. *Polymer,* 46**,** 12567-12576.

VLASVELD, D., VAIDYA, S., BERSEE, H. & PICKEN, S. 2005d. A comparison of the temperature dependence of the modulus, yield stress and ductility of nanocomposites based on high and low MW PA6 and PA66. *Polymer,* 46**,** 3452-3461.

VOLLE, N., CHALLIER, L., BURR, A., GIULIERI, F., PAGNOTTA, S. & CHAZE, A.-M. 2011. Maya Blue as natural coloring fillers in a multi-scale polymer-clay nanocomposite. *Composites Science and Technology,* 71**,** 1685-1691.

WAGENER, R. & REISINGER, T. J. 2003. A rheological method to compare the degree of exfoliation of nanocomposites. *Polymer,* 44**,** 7513-7518.

WALKER, G. 1947. The mineralogy of some Aberdeenshire soil clays. *Clay Min. Bull,* 1.

WALKER, G. 1949. Water layers in vermiculite. *Nature,* 163**,** 726.

WALKER, G. 1950. Vermiculite-organic complexes.

WALKER, G. 1951. Vermiculites and some related mixed-layer minerals. *Pp. 199À223 in: X-ray Identification and Crystal Structures of Clay Minerals (GW Brindley, editor). Mineralogical Society, London*.

WALKER, G. 1960. Macroscopic swelling of vermiculite crystals in water. *Nature,* 187**,** 312-313.

WALKER, G. & GARRETT, W. 1967. Chemical exfoliation of vermiculite and the production of colloidal dispersions. *Science,* 156**,** 385-387.

WALKER, G. & MILNE, A. 1950. Hydration of vermiculite saturated with various cations. *Transactions 4th Int. Cong. Soil Sci.,* 2**,** 62-67.

WANG, B., WAN, T. & ZENG, W. 2012. Rheological and thermal properties of polylactide/organic montmorillonite nanocomposites. *Journal of Applied Polymer Science,* 125.

WANG, C. H., AUAD, M. L., MARCOVICH, N. E. & NUTT, S. 2008. Synthesis and characterization of organically modified attapulgite/polyurethane nanocomposites. *Journal of Applied Polymer Science,* 109**,** 2562-2570.

WANG, L., CHEN, Z., WANG, X., YAN, S., WANG, J. & FAN, Y. 2011. Preparations of organo-vermiculite with large interlayer space by hot solution and ball milling methods: A comparative study. *Applied Clay Science,* 51**,** 151-157.

WANG, S., HU, Y., ZONG, R., TANG, Y., CHEN, Z. & FAN, W. 2004. Preparation and characterization of flame retardant ABS/montmorillonite nanocomposite. *Applied Clay Science,* 25**,** 49-55.

WANG, W., ZHANG, J. & WANG, A. 2009. Preparation and swelling properties of superabsorbent nanocomposites based on natural guar gum and organo-vermiculite. *Applied Clay Science,* 46**,** 21-26.

WARD, W., GAINES, G., ALGER, M. & STANLEY, T. 1991. Gas barrier improvement using vermiculite and mica in polymer films. *Journal of membrane science,* 55**,** 173-180.

WEISS, A. 1963. Organic Derivatives of Mica-type Layer-Silicates. *Angewandte Chemie International Edition in English,* 2**,** 134-144.

WEISS, J., TAKHISTOV, P., & MCCLEMENTS, D. J. 2006. Functional materials in food nanotechnology. *Journal of Food Science,* 71(9), R107–R116.

WIEWIORA, A., PÉREZ-RODRí, J., PEREZ-MAQUEDA, L. & DRAPAŁA, J. 2003. Particle size distribution in sonicated high-and low-charge vermiculites. *Applied Clay Science,* 24**,** 51-58.

WU, B., QI, S. & WANG, X. 2010. Thermal behaviour of poly (vinyl chloride) treated with montmorillonite-silica-3-triethoxysilyl-1-propanamine (K-Si-MMT) nanocomposites. *Polymer Testing,* 29**,** 717-722.

WU, S.-L., SCHEINBEIM, J. & NEWMAN, B. 1999. Ferroelectricity and piezoelectricity of nylon 11 films with different draw ratios. *Journal of Polymer Science Part B: Polymer Physics,* 37**,** 2737-2746.

XIE, S., ZHANG, S., WANG, F., YANG, M., SÉGUÉLA, R. & LEFEBVRE, J.-M. 2007. Preparation, structure and thermomechanical properties of nylon-6 nanocomposites with lamella-type and fiber-type sepiolite. *Composites Science and Technology,* 67**,** 2334-2341.

XIE, W., GAO, Z., PAN, W.-P., HUNTER, D., SINGH, A. & VAIA, R. 2001. Thermal degradation chemistry of alkyl quaternary ammonium montmorillonite. *Chemistry of Materials,* 13**,** 2979-2990.

XU, B., HUANG, W. M., PEI, Y. T., CHEN, Z. G., KRAFT, A., REUBEN, R., DE HOSSON, J. T. M. & FU, Y. Q. 2009. Mechanical properties of attapulgite clay reinforced polyurethane shape-memory nanocomposites. *European Polymer Journal,* 45**,** 1904-1911.

XU, J., LI, R., XU, Y., LI, L. & MENG, Y. 2005. Preparation of poly (propylene carbonate)/organo-vermiculite nanocomposites via direct melt intercalation. *European Polymer Journal,* 41**,** 881-888.

XU, J., MENG, Y., LI, R., XU, Y. & RAJULU, A. 2003. Preparation and properties of poly (vinyl alcohol)–vermiculite nanocomposites. *Journal of Polymer Science Part B: Polymer Physics,* 41**,** 749-755.

YAN, W., LIN, R. & BHATTACHARYYA, D. 2006. Particulate reinforced rotationally moulded polyethylene composites–Mixing methods and mechanical properties. *Composites Science and Technology,* 66**,** 2080-2088.

YANG, Y., ZHU, Z.-K., YIN, J., WANG, X.-Y. & QI, Z.-E. 1999. Preparation and properties of hybrids of organo-soluble polyimide and montmorillonite with various chemical surface modification methods. *Polymer,* 40**,** 4407-4414.

YANG, Z., HUANG, S. & LIU, T. 2011. Crystallization behavior of polyamide 11/multiwalled carbon nanotube composites. *Journal of Applied Polymer Science,* 122**,** 551-560.

YAO, Y., LU, G.-Q., BOROYEVICH, D. & NGO, K. D. 2015. Survey of high-temperature polymeric encapsulants for power electronics packaging. *Components, Packaging and Manufacturing Technology, IEEE Transactions on,* 5**,** 168-181.

YARIV, S. 2002. IR spectroscopy and thermo-IR spectroscopy in the study of the fine structure of organo-clay complexes. *Organo-clay complexes and interactions,* 345**,** 462.

YEH, J. T., WANG, C. K., HU, P., LAI, Y. C., HUANG, L. K. & TSAI, F. C. 2012. Ultradrawing properties of ultrahigh-molecular-weight polyethylene/attapulgite fibers. *Polymer International,* 61**,** 982-989.

YOUNG, R. J. & LOVELL, P. A. 2011. *Introduction to polymers*, CRC press.

YU, M., ZHANG, Q. & FU, Q. 2004. Preparation and characterization of polyamide 11/clay nanocomposites*. *高分子科学,* 22**,** 43-47.

YU, Y., QI, S., ZHAN, J., WU, Z., YANG, X. & WU, D. 2011. Polyimide/sepiolite nanocomposite films: Preparation, morphology and properties. *Materials Research Bulletin,* 46**,** 1593-1599.

ZANETTI, M., LOMAKIN, S. & CAMINO, G. 2000. Polymer layered silicate nanocomposites. *Macromolecular Materials and Engineering,* 279**,** 1-9.

ZHANG, G., LI, Y. & YAN, D. 2004a. Polymorphism in nylon-11/montmorillonite nanocomposite. *Journal of Polymer Science Part B: Polymer Physics,* 42**,** 253-259.

ZHANG, K., XU, J., WANG, K., CHENG, L., WANG, J. & LIU, B. 2009. Preparation and characterization of chitosan nanocomposites with vermiculite of different modification. *Polymer Degradation and Stability,* 94**,** 2121-2127.

ZHANG, Q., MO, Z., ZHANG, H., LIU, S. & CHENG, S. Z. 2001. Crystal transitions of Nylon 11 under drawing and annealing. *Polymer,* 42**,** 5543-5547.

ZHANG, Q., YU, M. & FU, Q. 2004b. Crystal morphology and crystallization kinetics of polyamide-11/clay nanocomposites. *Polymer International,* 53**,** 1941-1949.

ZHANG, X., YANG, G. & LIN, J. 2006a. Crystallization behavior of nylon 11/montmorillonite nanocomposites under annealing. *Journal of Applied Polymer Science,* 102**,** 5483-5489.

ZHANG, X., YANG, G. & LIN, J. 2006b. Synthesis, rheology, and morphology of nylon-11/layered silicate nanocomposite. *Journal of Polymer Science Part B: Polymer Physics,* 44**,** 2161-2172.

ZHANG, Y., WANG, B. & HU, G. 2012. Isothermal crystallization kinetics and melting behavior of polyamide 11/silica nanocomposites prepared by in situ melt polymerization. *Journal of Applied Polymer Science,* 123**,** 273-279.

ZHAO, C., QIN, H., GONG, F., FENG, M., ZHANG, S. & YANG, M. 2005. Mechanical, thermal and flammability properties of polyethylene/clay nanocomposites. *Polymer Degradation and Stability,* 87**,** 183-189.

APPENDICES

Appendix A: Publications and conference proceedings

Publications

- Macheca, A. D., Focke, W. W., Muiambo, H. F., Kaci, M. (2016). Stiffening mechanisms in vermiculite–amorphous polyamide bio-nanocomposites, *European Polymer Journal* (74) 51–63.
- Macheca, A. D., Gnanasekaran, D., Focke, W. W. (2014). Surfactant-free dimer fatty acid polyamide/montmorillonite bio-nanocomposites, *Colloid Polym. Sci*. 292 (3) (2014) 669–676.

Pending publication:

- Macheca, A. D., Focke, W. W., Kaci, M. Morphological, Thermal, Mechanical and Flame Retardant Properties Characterization of Polyamide 11 Bionanocomposites Based on Various Clays: Vermiculite, Sepiolite and Montmorillonite (2016).

Conference contributions:

- Macheca, A. D., Gnanasekaran, D., Focke, W. W. (2015). Surfactant-free dimer fatty acid polyamide/montmorillonite bio-nanocomposites. Poster presentation at the 13th UNESCO/IUPAC Workshop & Conference on Macromolecules & Materials, Port Elizabeth, South Africa, September, 2015.
- Macheca, A. D., Gnanasekaran, D., Focke, W. W. (2015). Surfactant-free dimer fatty acid polyamide/montmorillonite bio-nanocomposites. Poster presentation at the 4th Nano Today Conference, Dubai, United Arab Emirates, December 2015.

Appendix B: Preparation of NH_4^+-MMT/bio-nanocomposites based on DAPA via solution route

SEM images of neat Boane Bentonite

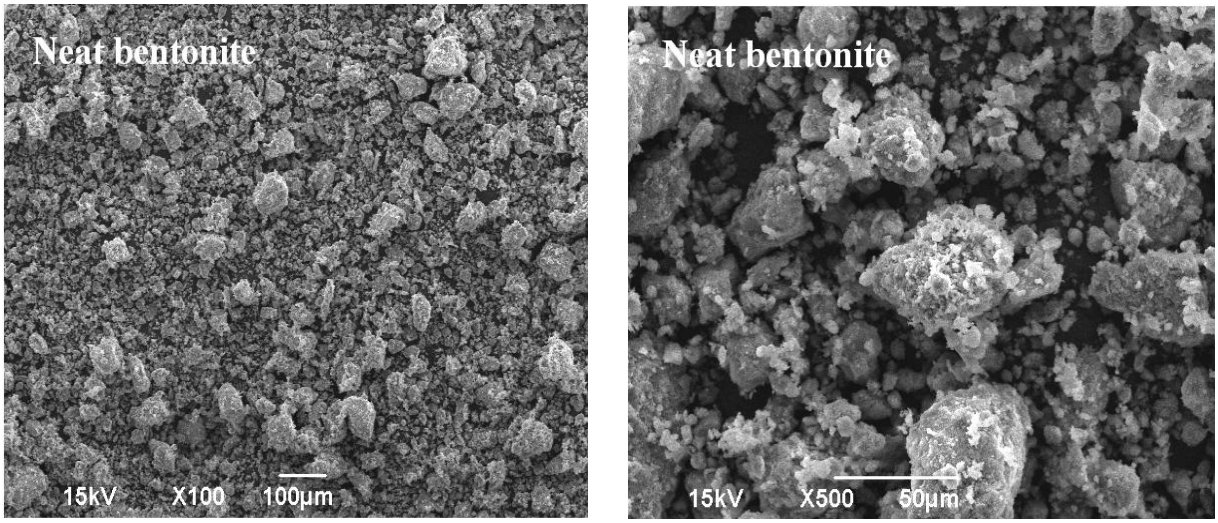

Figure B-1. SEM images of neat Boane bentonite at 100 and 500 magnification.

AFM images of PA bio-nanocomposites with different NH_4^+-MMT

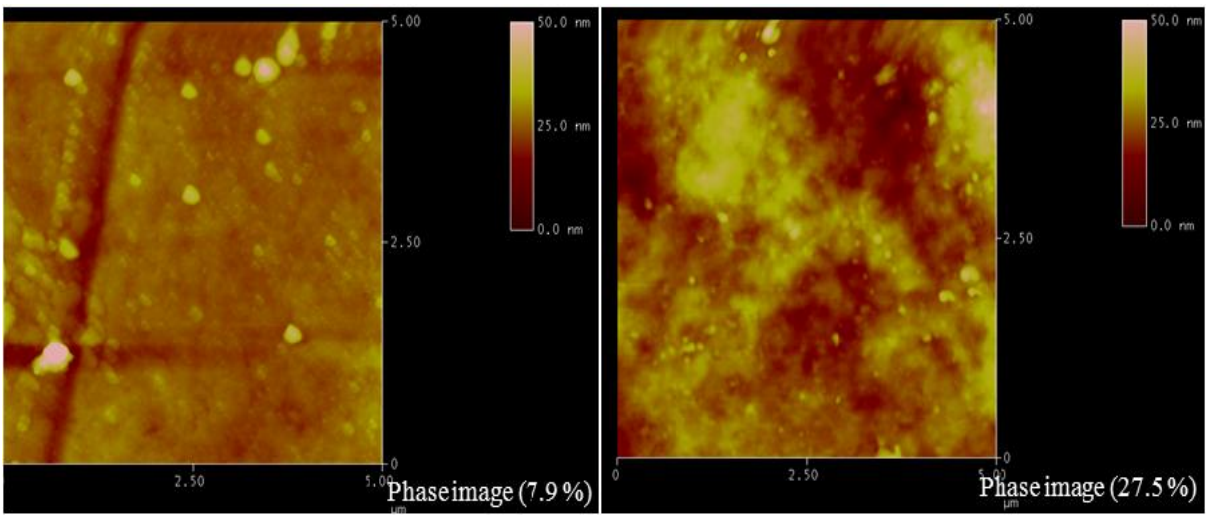

Figure B-2. AFM images of bio-nanocomposites with 7.9 and 27.5 wt.% NH_4^+-MMT

Dynamic Mechanical Analysis of bio-nanocomposites with different clay contents

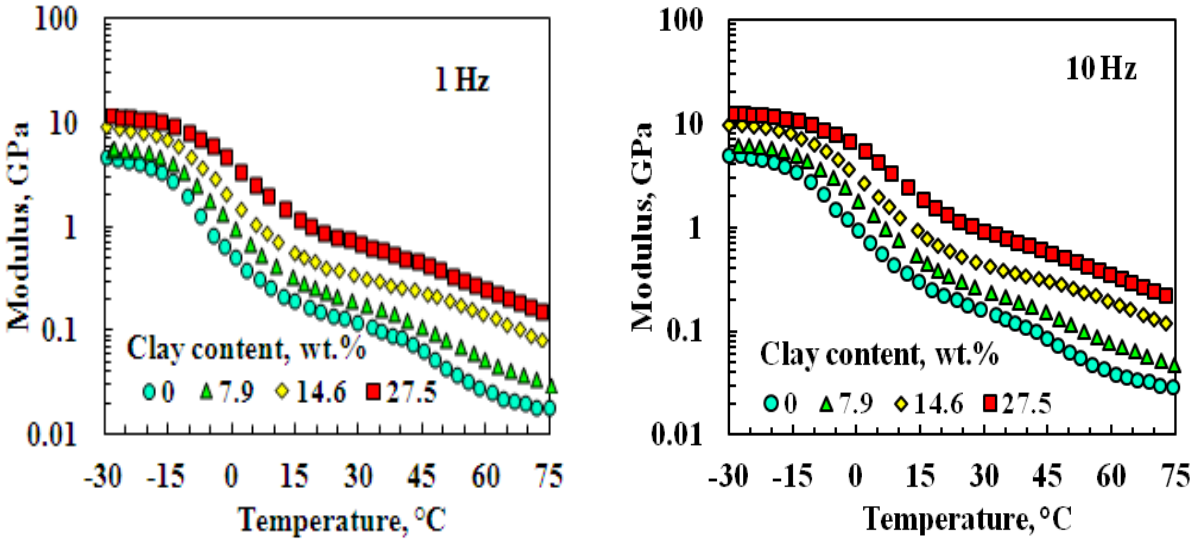

Figure B-3. Storage modulus at 1 and 10 Hz of the neat PA and its bio-nanocomposites.

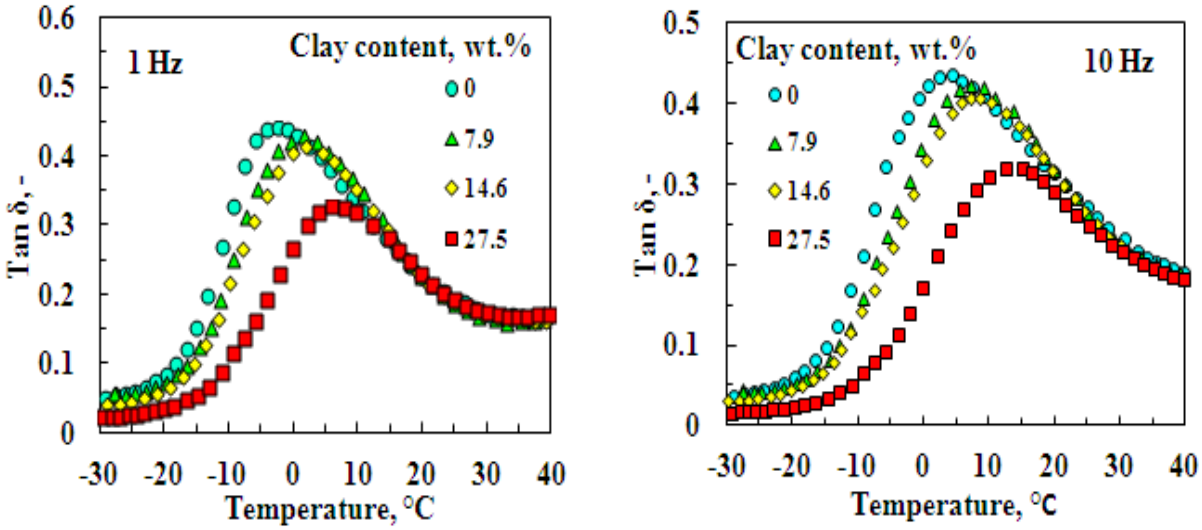

Figure B-4. Temperature dependence of tan δ at 1 and 10 Hz of the neat PA and its bio-nanocomposites.

Appendix C: Preparation of VMT (exfoliated by thermal shock and H_2O_2 treatment and/or sonication)/bio-nanocomposites based on DAPA via solution route

SEM images of neat Palabora vermiculite

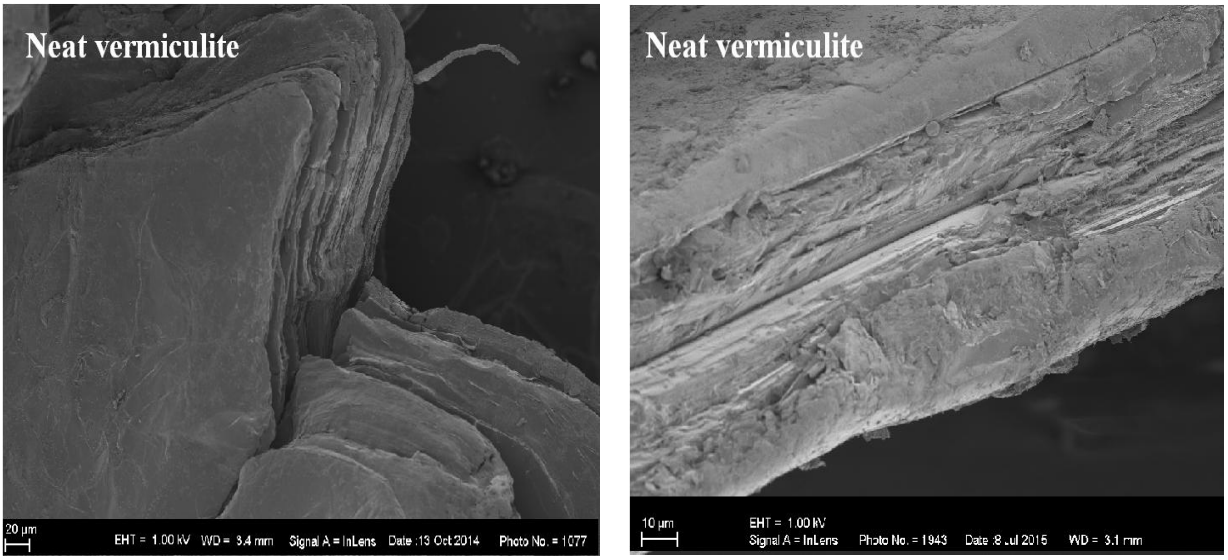

Figure C-1. SEM images of neat VMT at 20 µm (left) and 10 µm (right).

SEM images of thermally-expanded vermiculite

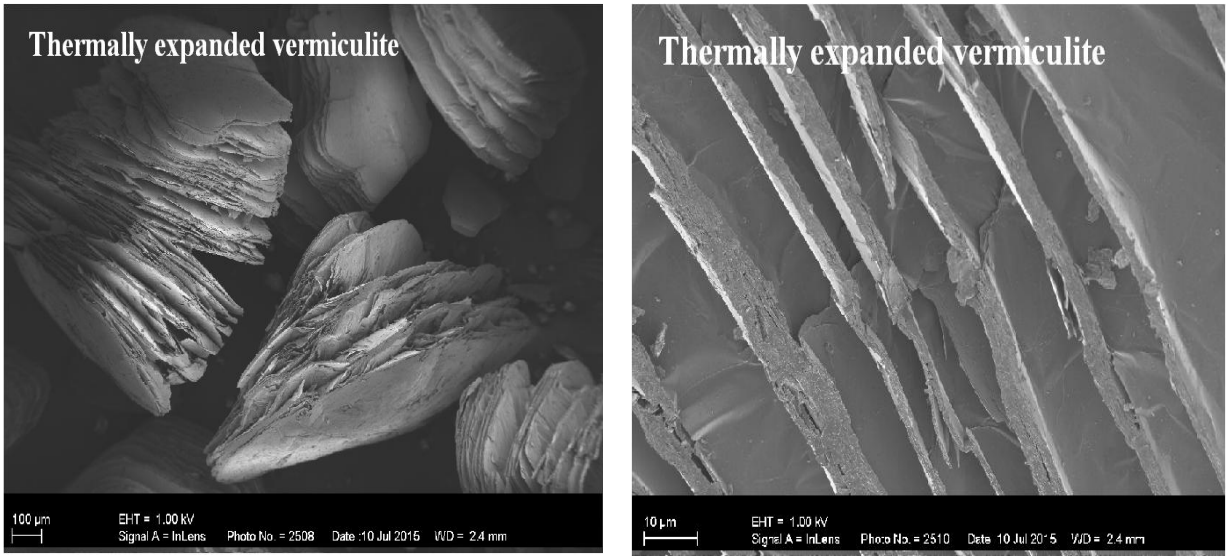

Figure C-2. SEM images of thermally-expanded VMT at 100 µm (left) and 10 µm (right).

SEM images of H_2O_2-expanded vermiculite

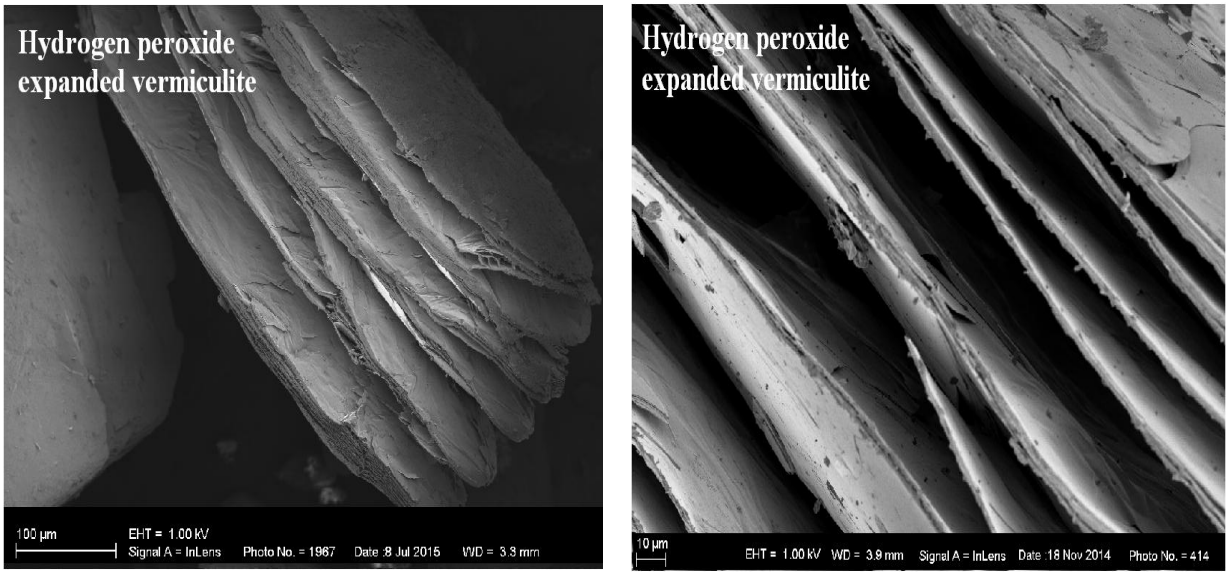

Figure C-3. SEM images of H_2O_2-expanded VMT at 100 µm (left) and 10 µm (right).

SEM images of thermally and H_2O_2-expanded and sonicated vermiculite

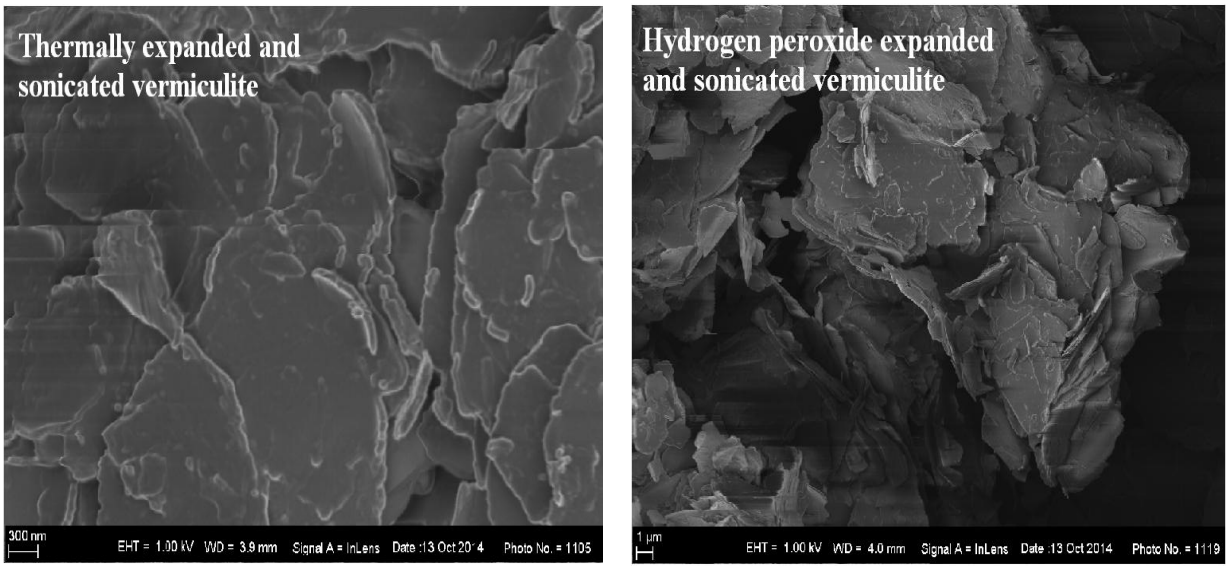

Figure C-4. SEM images of thermally and H_2O_2-expanded and sonicated VMT.

SEM images of thermally-expanded and sonicated vermiculite bio-nanocomposites

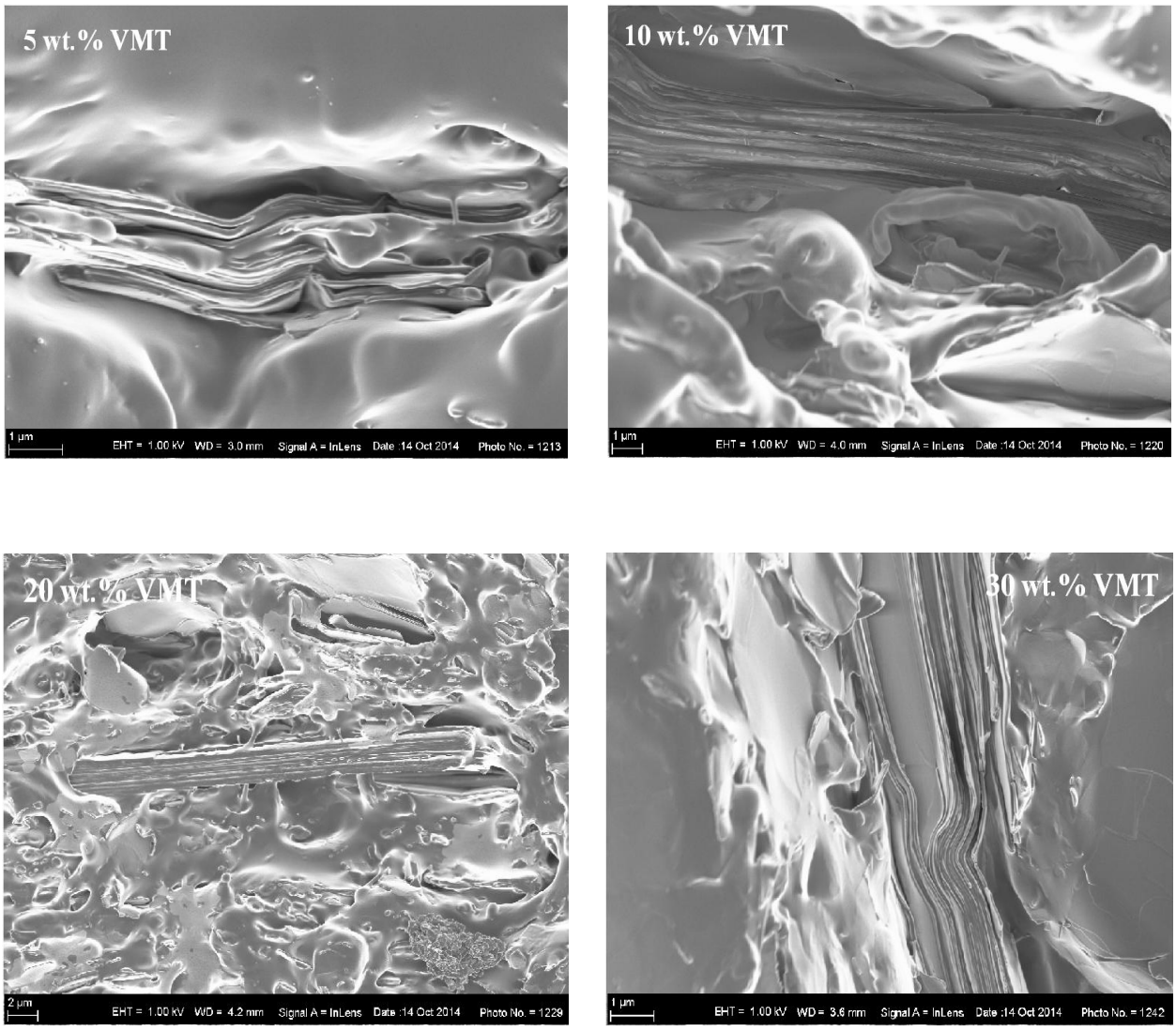

Figure C-5. Cross sectional SEM images of the PA bio-nanocomposites containing 5, 10, 20, and 30 wt.% sonicated thermally-exfoliated VMT.

SEM images of H_2O_2-expanded and sonicated vermiculite bio-nanocomposites

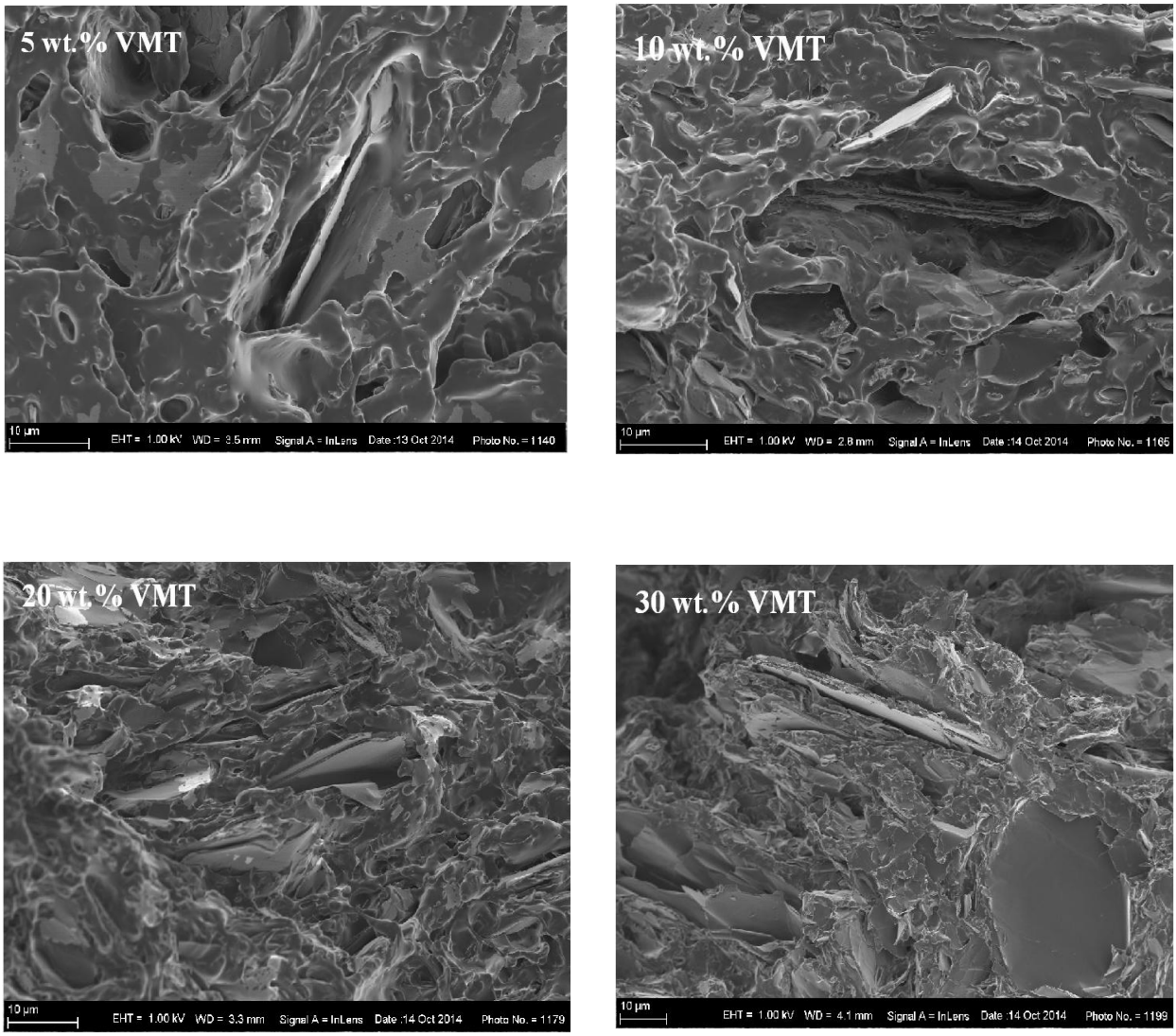

Figure C-6. Cross-sectional SEM images of the PA bio-nanocomposites containing 5, 10, 20, and 30 wt.% sonicated H_2O_2-exfoliated VMT.

TEM images of thermally-expanded and sonicated vermiculite bio-nanocomposites

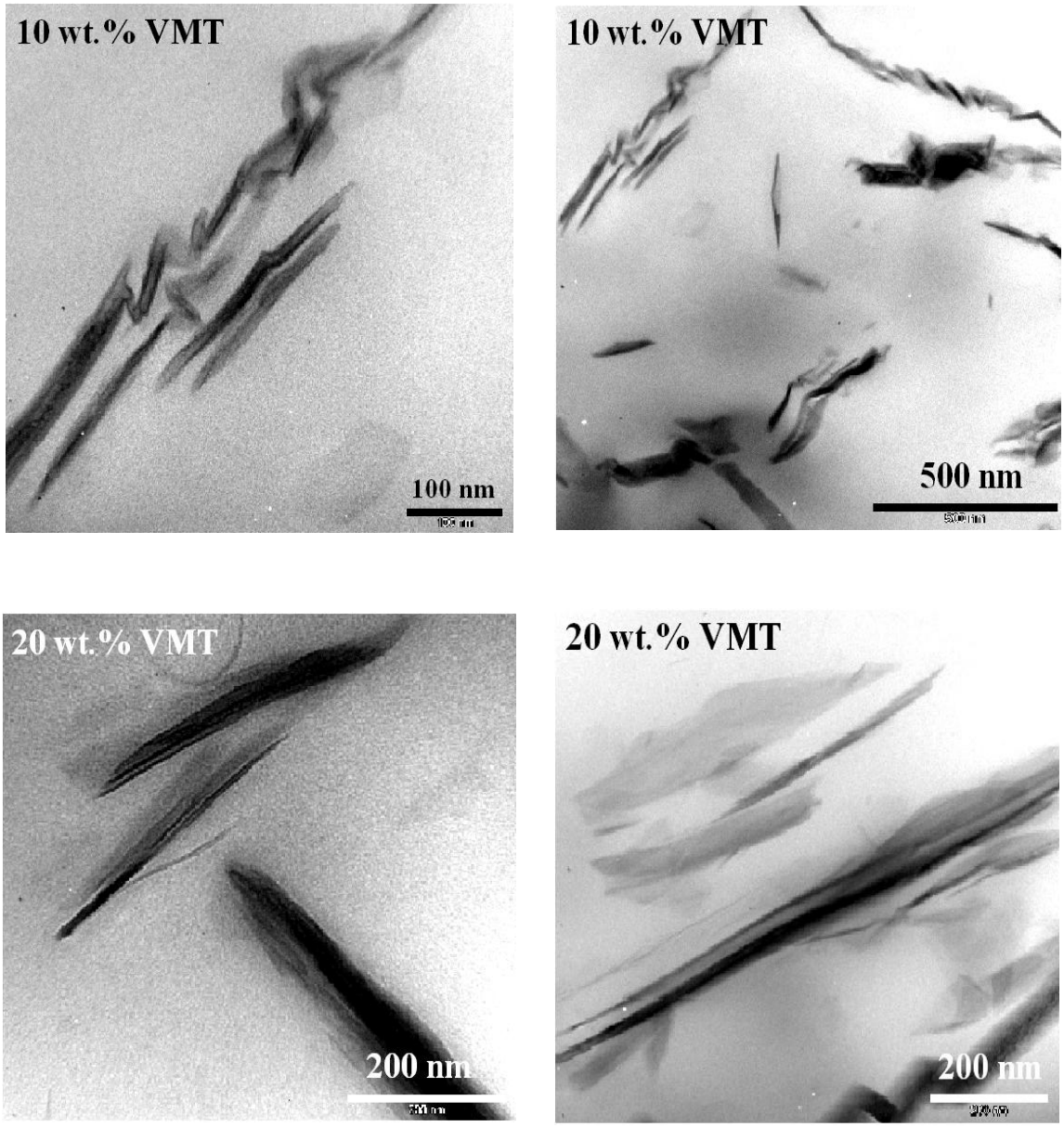

Figure C-7. TEM images of the PA bio-nanocomposites containing 10 and 20 wt.% sonicated thermally-exfoliated VMT.

TEM images of H_2O_2-expanded and sonicated vermiculite bio-nanocomposites

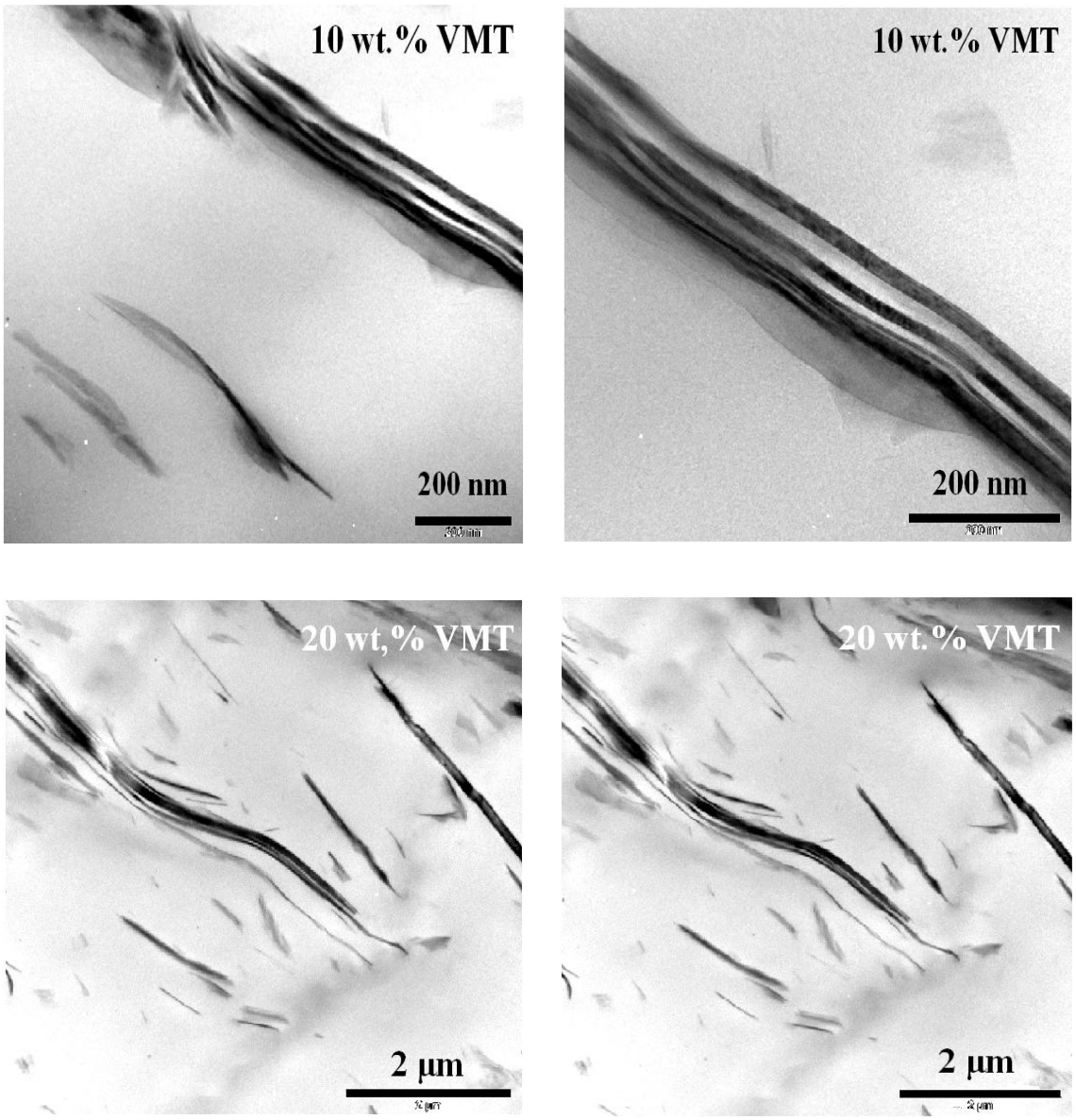

Figure C-8. TEM images of the PA bio-nanocomposites containing 10 and 20 wt.% sonicated H_2O_2-exfoliated VMT.

Dynamic Mechanical Analysis of bio-nanocomposites with different clay contents

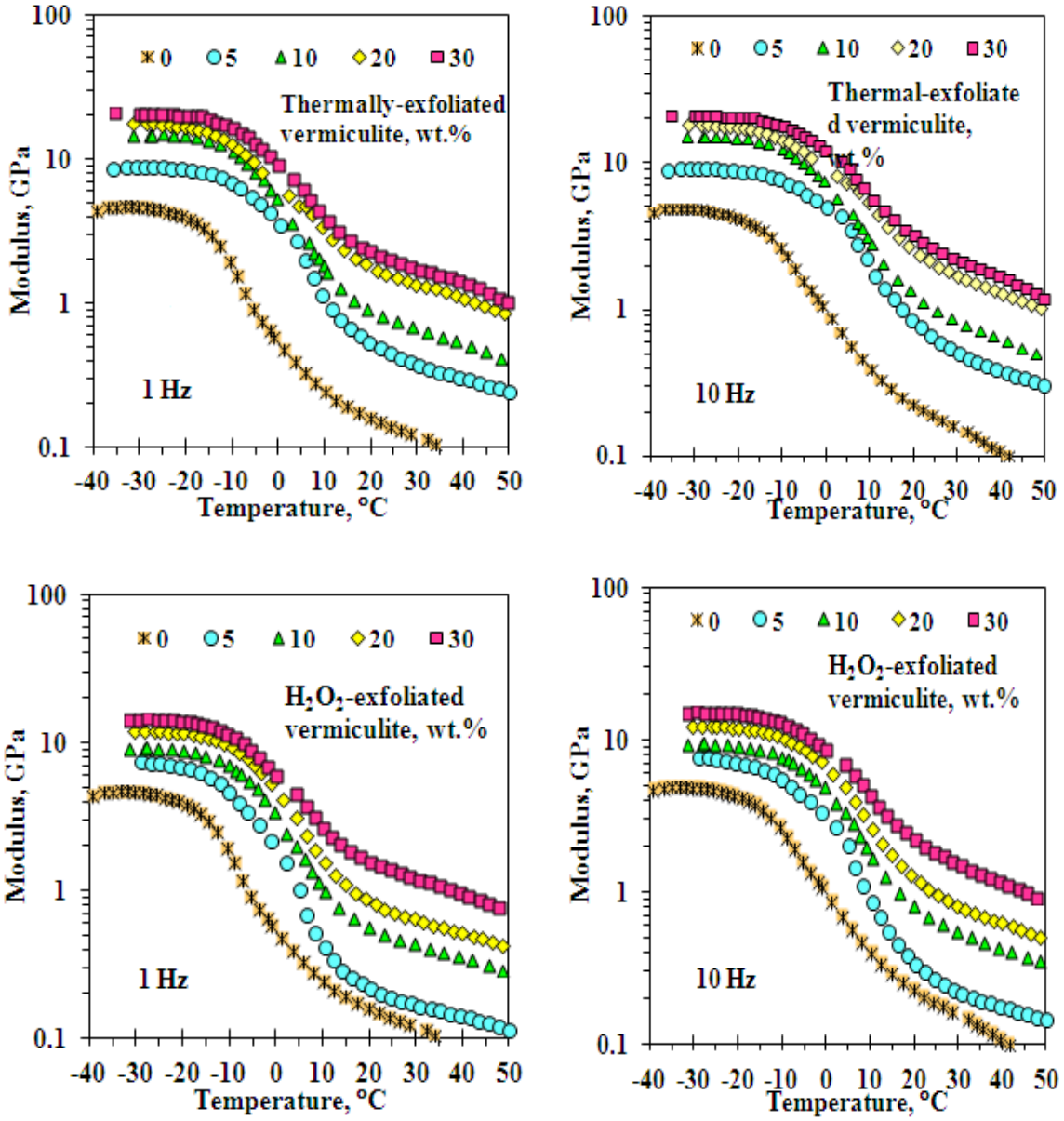

Figure C-9. Effect of filler loading on storage modulus (bending mode) at a frequency of 1 and 10 Hz for sonicated thermally- and H_2O_2-exfoliated VMT bio-nanocomposites.

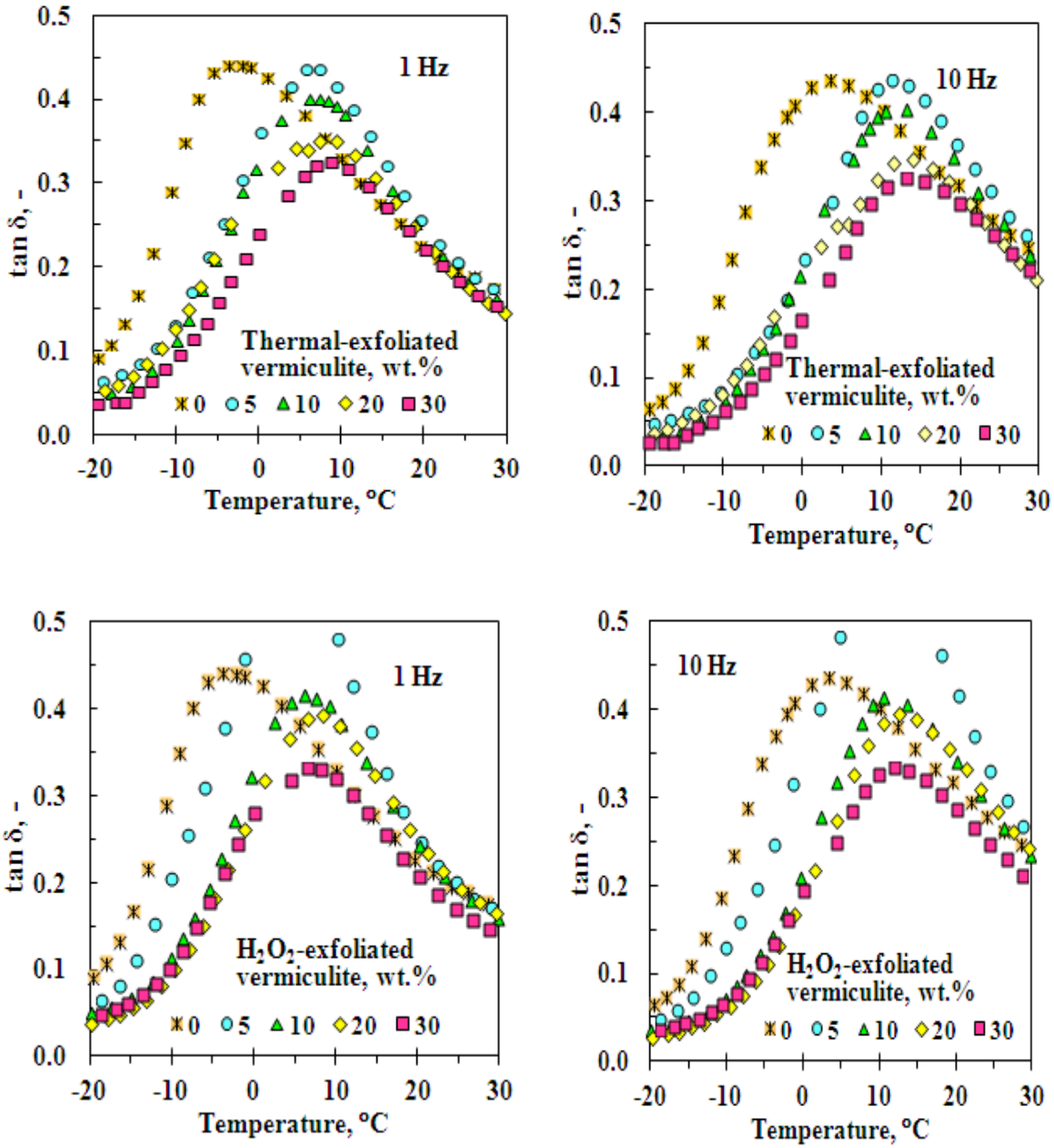

Figure C-10. Effect of filler loading on tan δ at a frequency of 1 and 10 Hz for sonicated thermally- and H_2O_2-exfoliated VMT bio-nanocomposites.

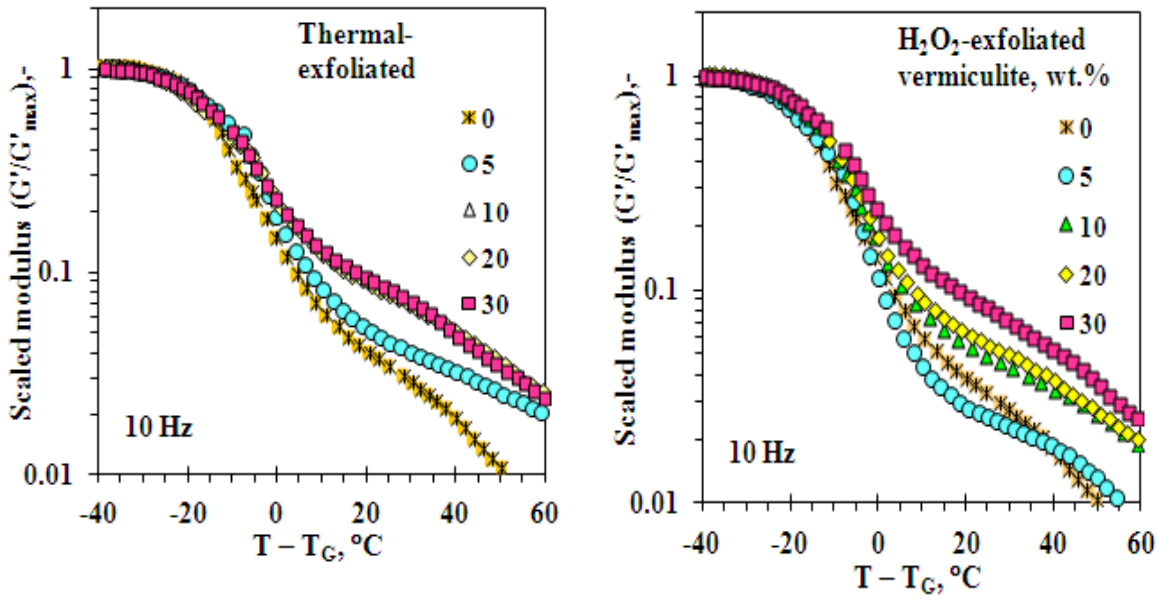

Figure C-11. Modulus "master curves" generated by scaling with respect to the modulus plateau in the glassy region and a glass transition temperature shift for sonicated thermally- and H_2O_2-exfoliated VMT bio-nanocomposites at a frequency of 10 Hz.

Appendix D: Preparation of VMT and PGS9/bio-nanocomposites based on PA-11 via melt compounding

SEM images of sepiolite PGS9 and sonicated organo-modified vermiculite

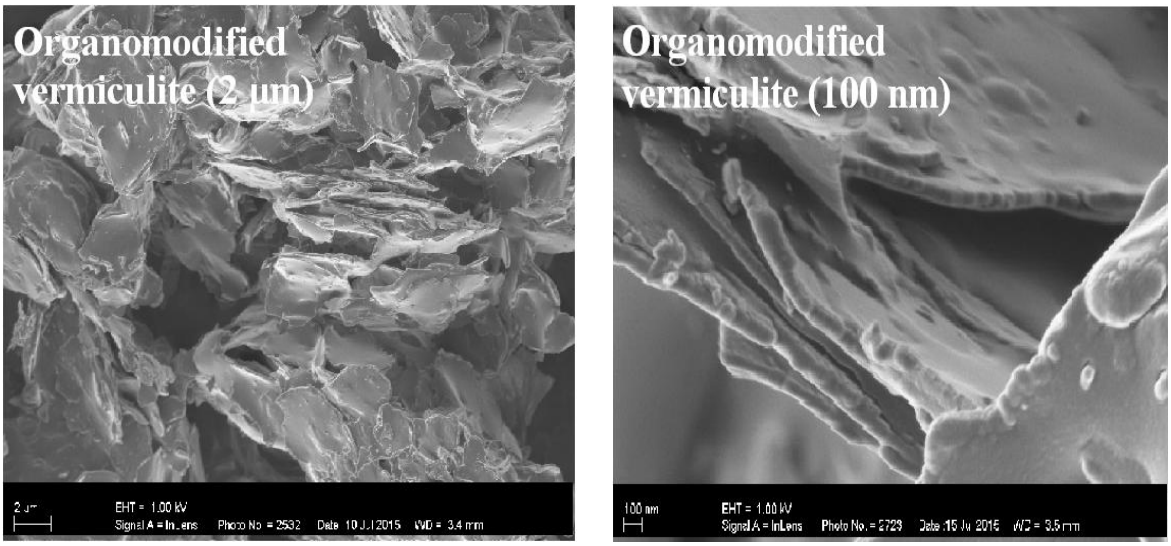

Figure D-1. SEM images of sonicated organo-modified VMT (OVMT) at 2 µm and 100 nm.

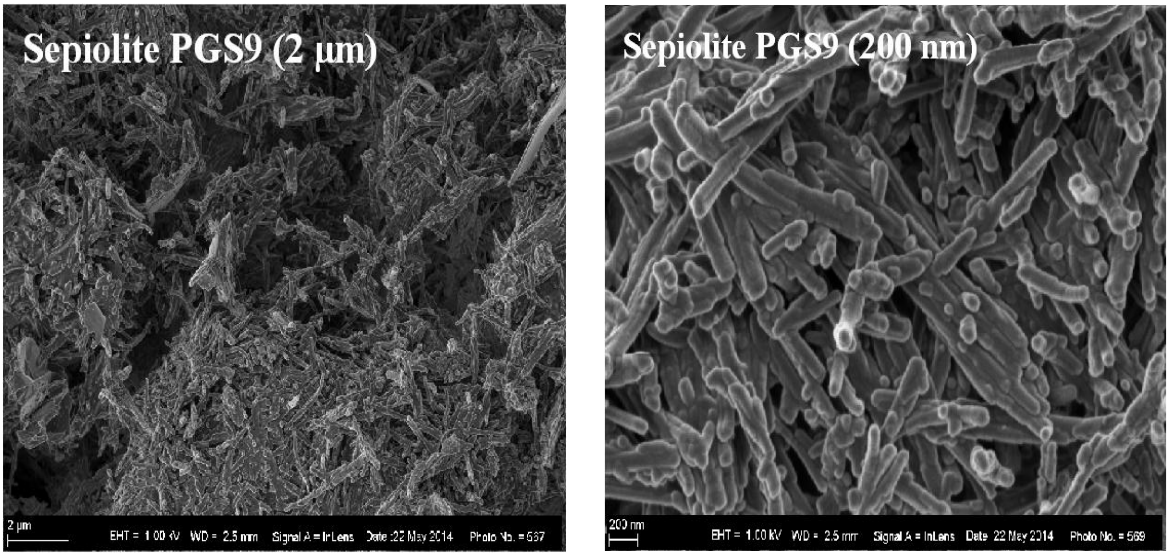

Figure D-2. SEM images of PGS9 at 2 µm and 100 nm.

SEM images of various clays PA **bio-nanocomposites**

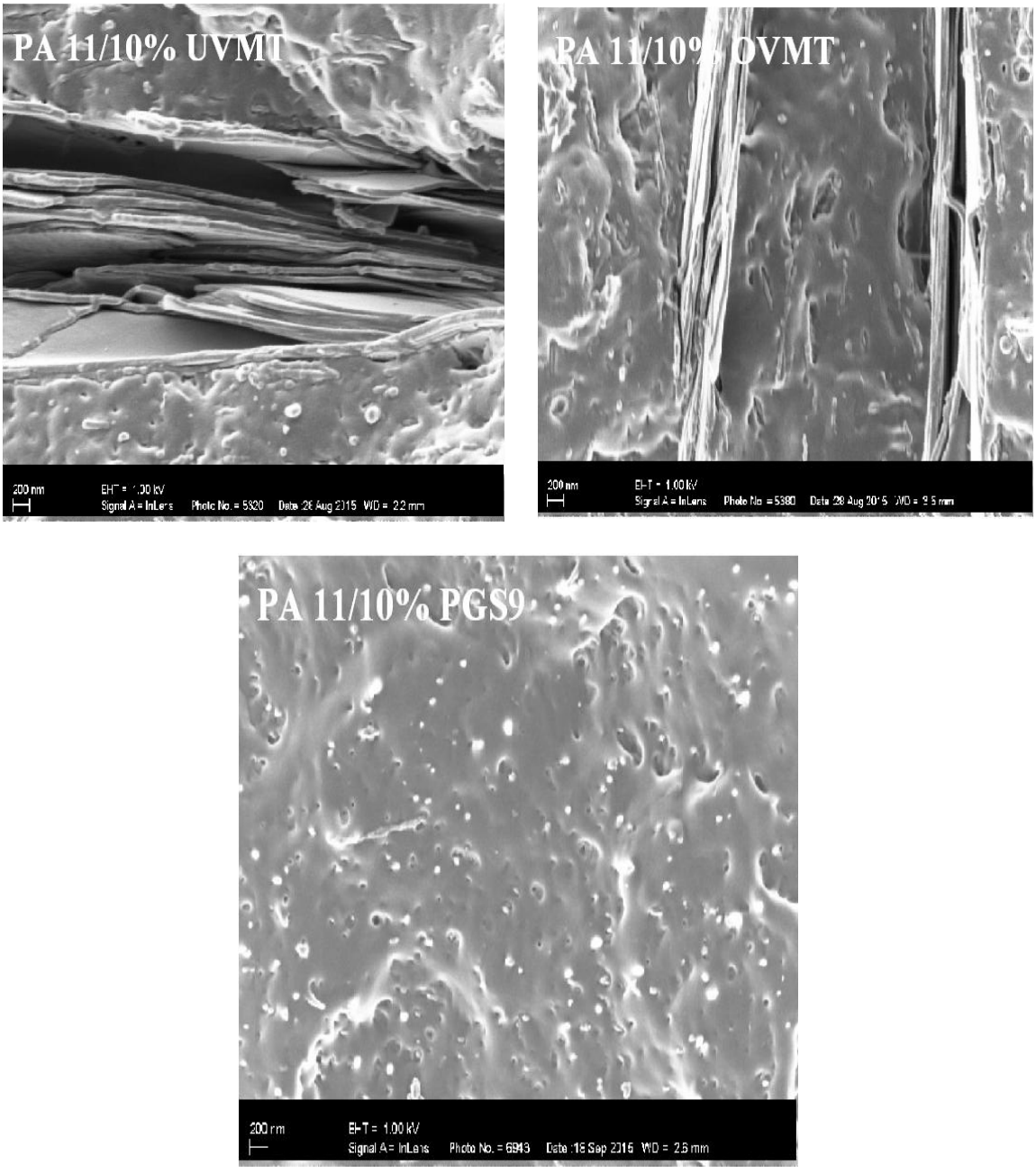

Figure D-3. Cross-sectional SEM VMT (OVMT and UVMT), and PGS9 PA-11/bio-nanocmposites at 200 nm.

TEM images of various clays PA bio-nanocomposites

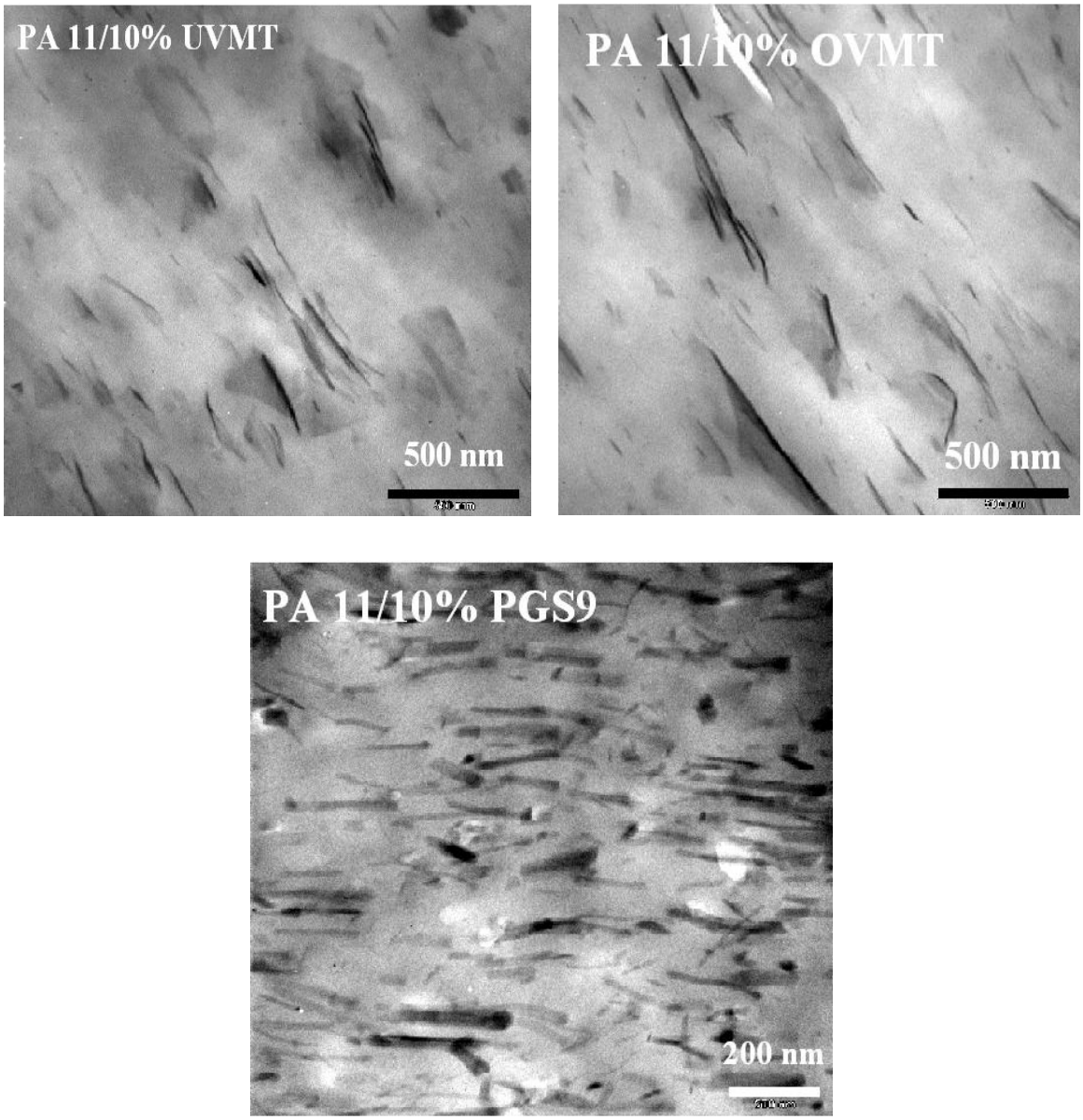

Figure D-4. TEM images of VMT (OVMT and UVMT), and PGS9 PA-11/bio-nanocmposites.

Dynamic Mechanical Analysis of bio-nanocomposites with different clay contents

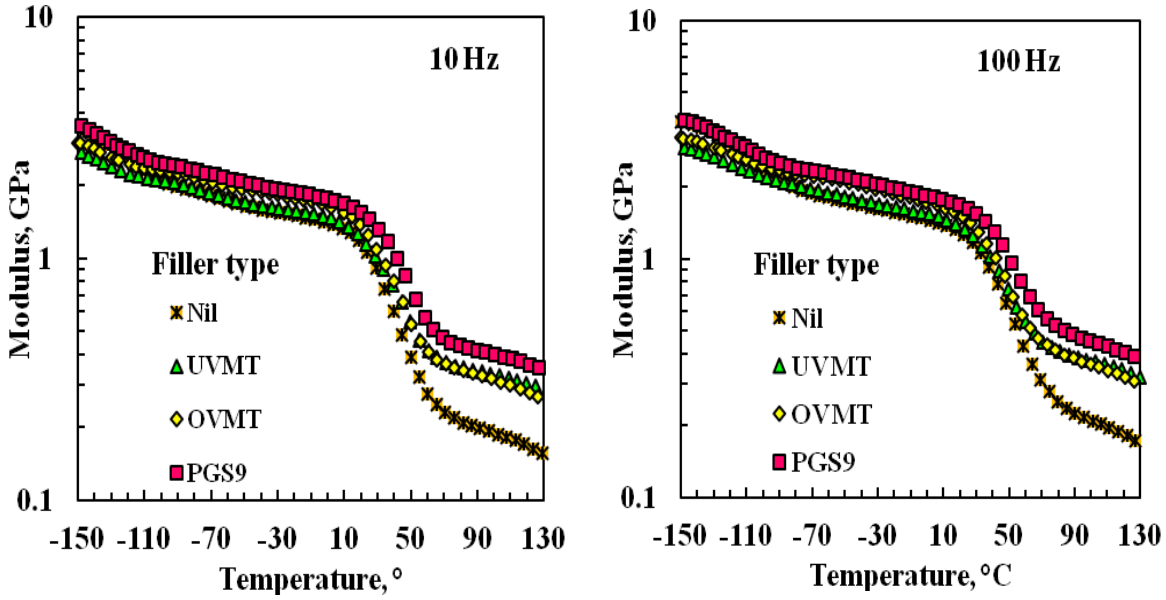

Figure D-5. Effect of filler loading on storage modulus (bending mode) at a frequency of 10 and 100 Hz for VMT (OVMT and UVMT), and PGS9 PA-11/bio-nancomposites.

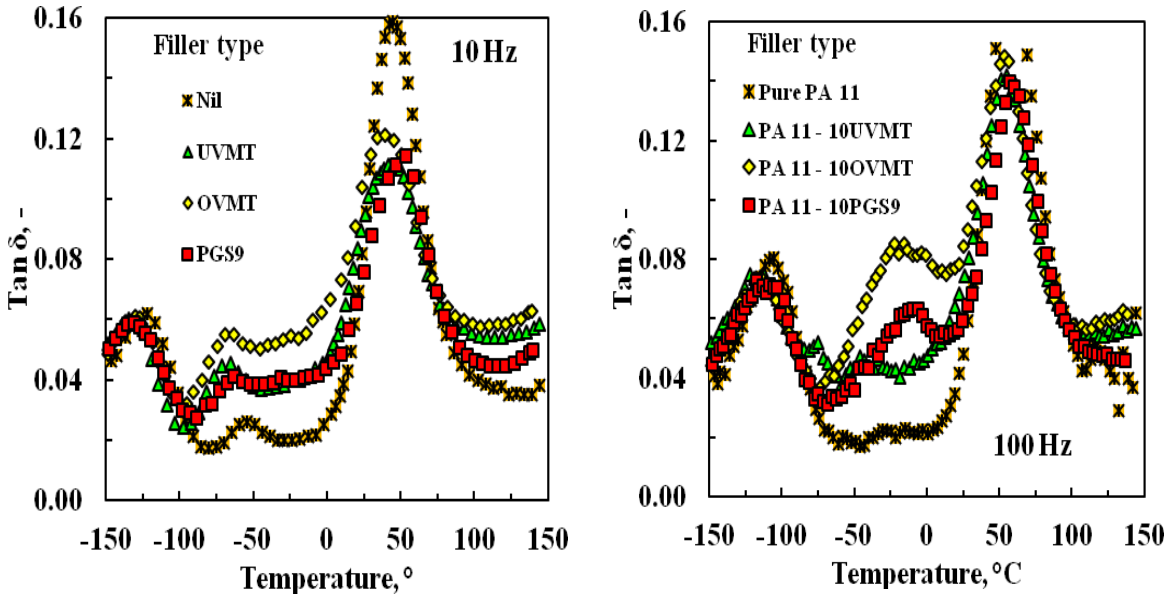

Figure D-6. Effect of filler loading on tan δ at a frequency of 10 and 100 Hz for VMT (OVMT and UVMT), and PGS9 PA-11/bio-nancomposites.

Appendix E: Products Technical data sheets

Mandoval Vermiculite Technical data sheet

MANDOVAL VERMICULITE

TECHNICAL DATA

TO: _____

FAX NO: _____

Raw Vermiculite
Vermiculite is a micaceous mineral. Mandoval's vermiculite consists of golden/brown flakes carefully classified into 5 grade each having a specified range of particle size.

Exfoliation of Vermiculite
Exfoliation occurs at right angles to the cleavage planes, causing the flakes to expand into concertina-shaped granules.

Commercial exfoliation of vermiculite is achieved by passing the crude vermiculite in a controlled manner through a furnace chamber at elevated temperatures. Vermiculite reabsorbs some moisture after exfoliation.

Sintering Temperature
About 1,260°C.

Melting Point
About 1,315°C.

Specific Heat
0.2.

Specific Gravity
2.6.

pH Value
8-8,6 owing to the presence of associated carbonaceous rock, the reaction is normally alkaline as these break down into alkali oxides/hydroxides.

Thermal Conductivity
Vermiculite has low thermal capacity and high thermal insulation properties. Thermal conductivity at normal atmospheric temperatures:
k = 0.062 - 0.065 W/m°C

Incombustibility
Vermiculite is incombustible.

Water Holding Capacity
Exfoliated vermiculite will readily hold water within the interlaminar voids. The water retained as a percentage of the air dry weight is 240%.

Cation Exchange Properties
The exchangeable cation normally present in vermiculite is magnesium. The cation exchange capacity is 90-100 milli-equivalents per 100 grams.

Vermiculite is clean to handle, non-abrasive, reflective, rot-proof, odourless, mouldable, non-irritant.

Typical Chemical Analysis
The chemical analysis of raw and exfoliated vermiculite is identical. The major elements are:

SiO_2	39.37%*
TiO_2	1.25%
Al_2O_3	12.08%
Fe_2O_3	5.45%
FeO	1.17%
MnO	0.30%
MgO	23.37%
CaO	1.46%
Na_2O	0.80%
K_2O	2.46%
$H_2O + 105°C$	5.17%
$H_2O - 105°C$	6.02%
CO_2	0.60%
P_2O_5	0.15%
Li_2O	0.03%
*Free silica content	<1.0%

Insolubility
Vermiculite is insoluble in water and organic solvents

Sizes and Densities of the standard grades as packed per 100 litre bag.

Grade	Approx Size of Granule	Bag Mass	*kg/m³ *g/litre
Large	8mm & smaller	7kg	Max. 80
Medium	4mm & smaller	8kg	Max. 90
Fine	2mm & smaller	9kg	Max. 112
Superfine	1mm & smaller	10kg	Max. 125
Micron	0.5mm & smaller	10kg	Max. 137.5

Prices on request
Prices quoted are exclusive of VAT

(Prices are subject to change without notice)

MANDOVAL VERMICULITE CC
Reg. No. CK2000/043769/23

2 Johnson Street, Alrode
P.O. Box 124114, Alrode
Tel: (011) 864-5205
Fax: (011 908-3049

E-Mail: mandoval@mandoval.co.za

PRODUCT DATA SHEET

MOZAMBIQUE BENTONITE

CHEMICAL COMPOSITION:

Hydrous Aluminium Silicate

FORMULA:

$H_2O.Al_2O_3.4SiO_2.nH_2O$

Mozambique Bentonite is comprised of the clay mineral montmorillonite and Silica in the form of cristobalite.

TYPICAL CHEMICAL ANALYSIS

SiO_2	77,3%
Al_2O_3	11,9%
Fe_2O_3	1.94%
CaO	0,5%
MgO	2,4%
Na_2O	0,6%
K_2O	0,04%
TiO_2	0,2%
P_2O_5	<0,02%
L.O.I.	5,1%

TYPICAL MINERALOGICAL ANALYSIS

Montmorrillonite	60%
Quartz/Cristobalite	20%
Perlite/Rheolite/Glass Phase	20%

PHYSICAL PROPERTIES

Colour	Off White
Moisture	12% Max.
Reflectance	Minimum 70
pH	8,5 - 9
Bulk Density	0,95 – 1,1g/cm3
Base exchange	70 meq/100gm
Grading	1% max retained on 75 micron

Aug-10

G&W Base and Industrial Minerals (Pty) Ltd,
t/a G&W Mineral Resources
Co. Reg: 1951/00928/07

Tel + 27(0)11 878 0300 **Fax** + 27(0)11 878 2720
155 Immelman Road, Wadeville, P.O. Box 14052,Wadeville 1422, Gauteng,South Africa
Email laboratory@gwminerals.co.za www.gwminerals.co.za

Sepiolite Pangel S9 Technical data sheet

TOLSA

FT-026-96-09
HT-01-01/ESP-ENG

HOJA TÉCNICA

TECHNICAL DATA SHEET

PANGEL S9

MINERALOGÍA[1]

Sepiolita
(Libre de asbestos)

SEPIOLITA	> 85 %
OTRAS ARCILLAS	< 15 %

MINERALOGY[1]

Sepiolite
(Asbestos free)

SEPIOLITE	> 85 %
OTHER CLAYS	< 15 %

COMPOSICIÓN QUÍMICA[1]

Silicato magnésico hidratado

CHEMICAL COMPOSITION[1]

Hydrous magnesium silicate

Fecha de revisión 14/12/2004 Issue Date

C/CAMPEZO, 2, EDIFICIO 4, 2°
28022 – MADRID (SPAIN)

TELF. (+34) 913.220.100
FAX (+34) 913.220.101
pangel@tolsa.com

TOLSA

FT-026-96-09
HT-01-01/ESP-ENG

PROPIEDADES FÍSICO-QUÍMICAS — PHYSICO-CHEMICAL PROPERTIES

Color	Crema claro/Light cream		..... Colour
Apariencia	Polvo fluido/Free-flowing powder		.....Appearance

	Método[3] Method	Valor típico[1] Typical Value[1]	Especificacion[2] Specification[2]	
Humedad (%)	NET-079	6	< 10	..... Moisture
Densidad Aparente (g/l)	NET-005	60	60 ± 30	..... Bulk density
pH	NET-077	8'8		..... pH
Viscosidad Brookfield (cP)*	NET-129	39.000	30.000-60.000	..... Brookfield viscosity*
Sinéresis (%)**	NET-066	0		..... Synerisis
Absorción D.O.P. (%)	NET-068	290		..... D.O.P Absorption
Superficie específica BET, N_2 (m^2/g) .	NET-069	320		..... Surface area BET, N_2

* Suspensión al 6 % en agua, agitando a alta cizalla (18 m/s) durante 5 minutos

** Suspensión al 3 % en agua, agitando durante un minuto Sinéresis medida a las 72 horas.

* Suspension at 6% in water, stirred at high shear for 5 minutes.

** Suspension at 3% in water, stirred for 1 min. . Syneresis measured after 72 hours.

DISTRIBUCIÓN GRANULOMÉTRICA POR TAMIZADO EN HÚMEDO (NET-036) — PARTICLE SIZE DISTRIBUTION BY WET SIEVING

VALORES TÍPICOS[1] TYPICAL VALUES	%	ESPECIFICACIONES[2] SPECIFICATIONS	%
Residuo en/Residue on 44 µm	0'1	Residuo en/Residue on 44 µm	< 0'5
Residuo en/Residue on 10 µm	2'0	Residuo en/Residue on 10 µm	< 5
Inferior a /Finer than 5 µm	97'9	Inferior a/Finer than 5 µm	> 90

[1] *Estos datos corresponden a análisis medios de nuestros productos.*

[2] *Aplicable al conjunto del lote.*

[3] *NET = Tolsa method*

[1] *These data are an average analysis of our products.*

[2] *Applicable to the whole batch.*

Montmorillinite Cloisite 30B Technical data sheet

SOUTHERN CLAY PRODUCTS / A SUBSIDIARY OF ROCKWOOD SPECIALTIES, INC.
PRODUCT BULLETIN/Cloisite®

Southern Clay Products, Inc.
1212 Church Street
Gonzales, TX 78629
Phone: 800-324-2891
Fax: 830-672-1903
www.scprod.com

Cloisite® 30B
Typical Physical Properties Bulletin

Description:
Cloisite® 30B is a natural montmorillonite modified with a quaternary ammonium salt.

Designed Used:
Cloisite® 30B is an additive for plastics and rubbers to improve various physical properties, such as reinforcement, CLTE, synergistic flame retardant and barrier.

Typical Properties:

Treatment/Properties:	Organic Modifier (1)	Modifier Concentration	% Moisture	% Weight Loss on Ignition
Cloisite® 30B	MT2EtOH	90 meq/100g clay	< 2%	30%

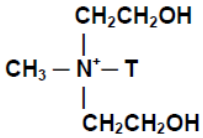

Where T is Tallow (~65% C18; ~30% C16; ~5% C14)

Anion: Chloride

(1) MT2EtOH: methyl, tallow, bis-2-hydroxyethyl, quaternary ammonium

Typical Dry Particle Sizes: (microns, by volume)

10% less than:	50% less than:	90% less than:
2µm	6µm	13µm

Color: Off White

Density:

Loose Bulk, lbs/ft^3	Packed Bulk, lbs/ft^3	Density, g/cc
14.25	22.71	1.98

X Ray Results: d_{001} = 18.5Å

For additional information or technical assistance contact Southern Clay Products, Inc. toll free at 800-324-2891.

Dimer fatty acid based polyamides Technical data sheet

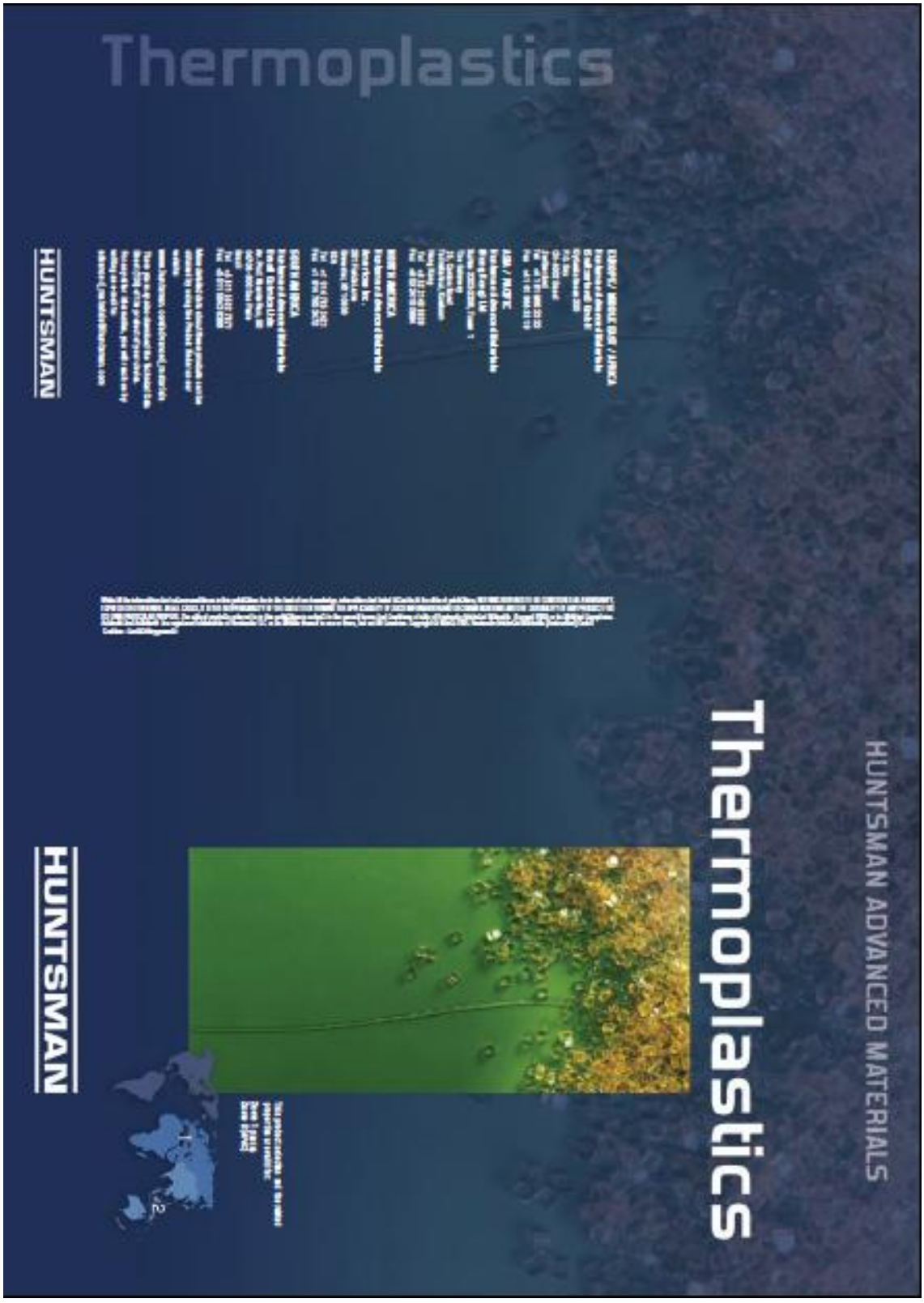

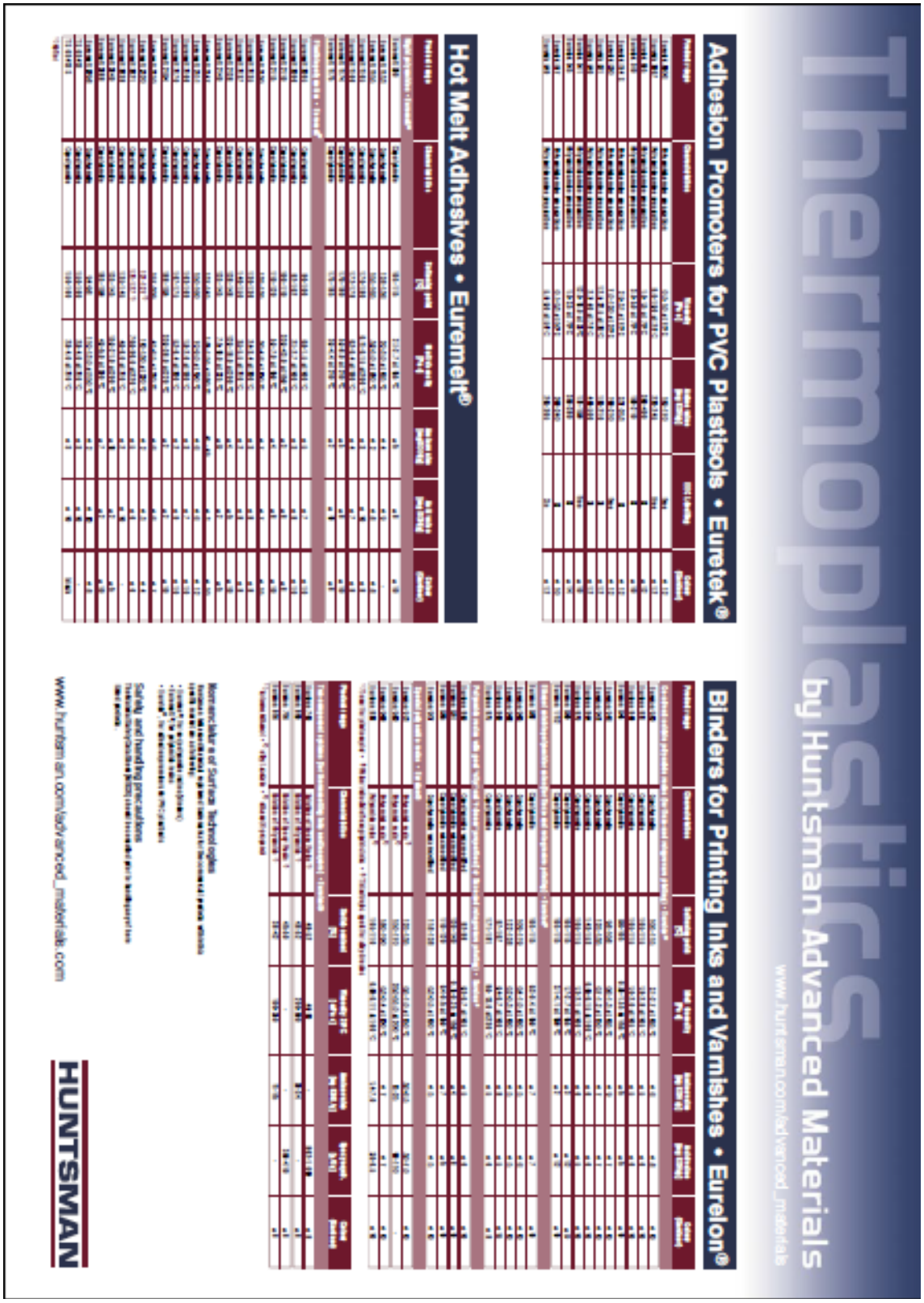

Polyamide 11 resin Technical data sheet (Rilsan BESNO P20 TL)

RILSAN® BESNO P20 TL

Rilsan® BESNO P20 TL is a polyamide 11 produced from a renewable source. This natural grade is plasticized and designed for extrusion.

MAIN CHARACTERISTICS

Property	Typical Value	Unit	Test Method
Nature & Designation	**PA11-P, EHL, 22-005**		ISO 1874
Renewable Carbon (calculation)	**> 93**	%	ASTM D6866
Density	**1.04**	g/cm³	ISO 1183
Melting Point	**182**	°C	ISO 11357
Hardness (*)			
Instantaneous	**74**	Shore D	ISO 868
After 15 s	**64**	Shore D	
Tensile Test (*)			
Stress at Yield	**31**	MPa	ISO 527
Strain at Yield	**40**	%	
Stress at Break	**45**	MPa	
Strain at Break	**>200**	%	
Tensile Modulus (*)	**510**	MPa	ISO 527
Flexural Modulus (*)	**430**	MPa	ISO 178
Charpy Impact (*)			
Unnotched 23°C	**No break**	kJ/m²	ISO 179
Unnotched -30°C	**No break**	kJ/m²	
V-notched 23°C	**No break**	kJ/m²	
V-notched -30°C	**11**	kJ/m²	

(*) Samples conditioned 15 days at 23°C - 50 % R.H.

RILSAN® BY ARKEMA

RILSAN® BESNO P20 TL

MAIN APPLICATIONS

- Fluid transportation.
- Tubing for use in motor vehicle.

PROCESSING CONDITIONS

Conditions	Typical values
Extrusion temperature Melt Temperature (Min / Recommended / Max)	230°C / 250°C / 280°C
Drying (only necessary for bags opened for more than two hours) Time Temperature	4 - 8 hours 80 - 90°C

PACKAGING

This grade is delivered dried in sealed packaging (25 kg bags) ready to be processed.

SHELF LIFE

Two years from the date of delivery. For any use above this limit, please refer to our technical services.

See Safety Data Sheet for Health & Safety Considerations.

Arkema Specialty Polyamides
420, rue d'Estienne d'Orves
92705 Colombes Cedex - France
arkema.com – **rilsan.com**

ARKEMA
INNOVATIVE CHEMISTRY

Polyamide 11 resin Technical data sheet (Rilsan BESNO TL NB)

RILSAN® BESNO TL NB

Rilsan® BESNO TL NB is a polyamide 11 produced from a renewable source. This grade is designed for extrusion and it does not contain any optical brightener.

MAIN CHARACTERISTICS

Property	Typical Value	Unit	Test Method
Nature & Designation	**PA11, EHL, 22-010**		ISO 1874
Renewable Carbon (calculation)	**> 98**	%	ASTM D6866
Density	**1.02**	g/cm³	ISO 1183
Melting Point	**186**	°C	ISO 11357
Hardness (*)			
Instantaneous	**76**	Shore D	ISO 868
After 15 s	**71**	Shore D	
Tensile Test (*)			
Stress at Yield	**38**	MPa	ISO 527
Strain at Yield	**5**	%	
Stress at Break	**57**	MPa	
Strain at Break	**>200**	%	
Tensile Modulus (*)	**1280**	MPa	ISO 527
Flexural Modulus (*)	**1100**	MPa	ISO 178
Charpy Impact (*)			
Unnotched 23°C	**No break**	kJ/m²	ISO 179
Unnotched -30°C	**No break**	kJ/m²	
V-notched 23°C	**11**	kJ/m²	
V-notched -30°C	**12**	kJ/m²	

(*) Samples conditioned 15 days at 23°C - 50 % R.H.

RILSAN® BY ARKEMA

RILSAN® BESNO TL NB

MAIN APPLICATIONS

- Ski top layer.

PROCESSING CONDITIONS

Conditions	Typical values
Extrusion temperature Melt Temperature (Min / Recommended / Max)	**230°C / 250°C / 280°C**

Drying (only necessary for containers opened for more than two hours)	
Time	**4 - 8 hours**
Temperature	**80 - 90°C**

PACKAGING

This grade is delivered dried in sealed packaging (550 kg rigid containers) ready to be processed.

SHELF LIFE

Two years from the date of delivery. For any use above this limit, please refer to our technical services.

See Safety Data Sheet for Health & Safety Considerations.

TDS / 31916 / Janvier 2013 - ARKEMA. Société anonyme au capital de 614 937 940 euros - 445 074 685 RCS Nanterre

Arkema Specialty Polyamides
420, rue d'Estienne d'Orves
92705 Colombes Cedex - France
arkema.com – **rilsan.com**

ARKEMA
INNOVATIVE CHEMISTRY